Aston University

If you have discovered material in AURA which is unlawful e.g. breaches copyright, (either yours or that of a third party) or any other law, including but not limited to those relating to patent, trademark, confidentiality, data protection, obscenity, defamation, libel, then please read our Takedown Policy and contact the service immediately.

SOME ASPECTS OF THE DYNAMIC PERFORMANCE

OF

MACHINE TOOL STRUCTURAL JOINTS

by

SAMIR NABIH SHOUKRY
B.Sc., M.Sc.

A Thesis submitted for the Degree of

DOCTOR OF PHILOSOPHY

THE UNIVERSITY OF ASTON IN BIRMINGHAM

Faculty of Engineering

Department of
Production Technology and Production Management

DECEMBER 1980

The University of Aston in Birmingham December, 1980

SOME ASPECTS OF THE DYNAMIC PERFORMANCE OF MACHINE TOOL STRUCTURAL JOINTS

A Thesis submitted for the Degree of PhD

by

SAMIR NABIH SHOUKRY

S U M M A R Y

The work presented in this thesis is concerned with the dynamic behaviour of structural joints which are both loaded, and excited, normal to the joint interface.

Since the forces on joints are transmitted through their interface, the surface texture of joints was carefully examined. A computerised surface measuring system was developed and computer programs were written. Surface flatness was functionally defined, measured and quantised into a form suitable for the theoretical calculation of the joint stiffness.

Dynamic stiffness and damping were measured at various preloads for a range of joints with different surface textures. Dry clean and lubricated joints were tested and the results indicated an increase in damping for the lubricated joints of between 30 to 100 times.

A theoretical model for the computation of the stiffness of dry clean joints was built. The model is based on the theory that the elastic recovery of joints is due to the recovery of the material behind the loaded asperities. It takes into account, in a quantitative manner, the flatness deviations present on the surfaces of the joint. The theoretical results were found to be in good agreement with those measured experimentally. It was also found that theoretical assessment of the joint stiffness could be carried out using a different model based on the recovery of loaded asperities into a spherical form. Stepwise procedures are given in order to design a joint having a particular stiffness.

A theoretical model for the loss factor of dry clean joints was built. The theoretical results are in reasonable agreement with those experimentally measured.

The theoretical models for the stiffness and loss factor were employed to evaluate the second natural frequency of the test rig. The results are in good agreement with the experimentally measured natural frequencies.

KEYWORDS: Machine Tool Structures; Machine Tool Joints; Stiffness; Damping.

L I S T O F C O N T E N T S

		PAGE NUMBER
List of Tables		viii
List of Figures		ix
Acknowledgements		xiv
Declaration		xv
Nomenclature		xvi
CHAPTER 1	INTRODUCTION	1
CHAPTER 2	A REVIEW OF RESEARCH WORK ON THE INTERFACE BETWEEN MACHINE TOOL JOINTS	
2.1	Introduction	5
2.2	The static behaviour of machine tool joints	6
2.3	Dynamic behaviour of machine tool joints	12
2.4	Conclusions	15
CHAPTER 3	MEASUREMENT OF THE DYNAMIC STIFFNESS AND DAMPING OF MACHINE TOOL JOINTS	
3.1	Introduction	17
3.2	Some features of the measuring test rig	18
3.3	The test rig structure	19
3.4	Instrumentation	20
3.5	Calibration of instrumentation	22
3.5.1	Calibration of the charge amplifiers	22
3.5.2	Calibration of "B & K" accelerometers and load cells	23
3.5.3	Static and dynamic calibration of Kistler load cell	23
3.6	Methods of measurement	24
3.7	Data reduction	28
3.8	The effect of the material of the discs	29

		PAGE NUMBER
3.9	Static calibration of the test rig	31
3.10	Dynamic calibration of the test rig	31
3.11	Conclusions	32
CHAPTER 4	DESIGN OF TESTS ON JOINTS	
4.1	Introduction	33
4.2	Some factors which affect the joint behaviour	33
4.2.1	Joint preload	33
4.2.2	Surface topography	34
4.2.3	Viscosity of lubricant	35
4.2.4	Other variables	36
4.3	Specimens: material and shape	36
4.4	Method of manufacture	37
4.5	Specimens for the study of the effect of surface texture	38
4.6	Specimens for the study of the effect of area	39
4.7	Specimens for the study of the effect of planform shapes	39
4.8	Specimens for the study of the number of joints	40
CHAPTER 5	SURFACE TOPOGRAPHY: MEASUREMENT AND ASSESSMENT	41
Section 1	The measurement of surface texture	43
5.1.1	Introduction	43
5.1.2	The Talysurf output	44
5.1.3	Datum of measurement	45
5.1.4	Output manipulation	46
5.1.5	The digitisation unit	47
5.1.6	Some considerations in the measuring setup	48
5.1.7	The measuring system	51
5.1.8	Software structure	52
5.1.8.1	The calibration program "GAM"	53
5.1.8.2	Roughness measuring program "SURFACE"	55
5.1.8.3	Waviness measuring program "FLAT"	55

		PAGE NUMBER
5.1.8.4	Subroutine "COVRT"	56
5.1.9	Some sources of error in the measuring system	57
5.1.9.1	Errors due to vibrations	58
5.1.9.2	The sylus tip dimensions	59
5.1.9.3	Digitisation errors	61
5.1.9.4	Calibration and verification of the measuring setup	63
Section 2	Assessment of surface texture	65
5.2.1	Introduction	65
5.2.2	Which surface texture parameters to measure and why?	66
5.2.3	Numerical analysis of surface roughness	73
5.2.3.1	Equation of mean line	74
5.2.3.2	Evaluation of the classical parameters	76
5.2.3.3	Evaluation of the height distribution	76
5.2.3.4	Evaluation of the slope	77
5.2.3.5	Width parameters	77
5.2.3.6	The peak radius and peak height distribution	77
5.2.4	The computer program	78
5.2.5	Waviness	80
5.2.5.1	The measurement and assessment of waviness	81
5.2.6	Conclusions	83
CHAPTER 6	EXPERIMENTAL INVESTIGATION INTO THE DYNAMIC PERFORMANCE OF FIXED JOINTS	
6.1	Introduction	84
6.2	Experimental procedures	86
6.3	Experimental results	88
6.4	Dynamic performance of joints	89
6.5	Mechanism of lubrication in fixed machine tool joints	94
6.5.1	Hole formation and its relation to the behaviour of lubricated joints	95
6.6	Influence of the planform shape	96
6.6.1	Experimental results	98

		PAGE NUMBER
6.7	Influence of lay direction	99
6.7.1	Experimental results	100
6.8	Characteristics of joints assembled in series	101
6.9	Influence of the apparent area of contact	103
6.9.1	Experimental results	104
CHAPTER 7	THE STIFFNESS OF JOINTS IN MACHINE TOOL STRUCTURES	
7.1	Introduction	108
7.2	Contact between machined surfaces	109
7.3	The nature of flatness measurement in relation to the peak height distribution	115
7.3.1	Contact between rough unflat surfaces	116
7.4	The general picture of contact in machine tool joints	117
7.5	A mathematical model for elastic recovery of machine tool joints	119
7.6	The effect of assuming circular contact spots	122
7.7	Stepwise procedures for estimating the stiffness of joints	123
7.8	Experimental analysis	124
7.9	Discussion and conclusions	125
CHAPTER 8	DAMPING IN DRY CLEAN JOINTS SUBJECTED TO DYNAMIC LOADS NORMAL TO THE JOINT INTERFACE	
8.1	Introduction	128
8.2	A brief literature survey	128
8.3	The effect of damping in joints on the damping of the assembly	130
8.4	A mathematical model for damping in dry clean joints	133
8.5	Discussion	137
CHAPTER 9	APPLICATION OF THE THEORETICAL ANALYSIS AND FUTURE WORK	
9.1	The use of joints data for the prediction of the natural frequency of machine structures	140

		PAGE NUMBER
9.2	The source of error in evaluating the stiffness of SH2 and SH4 joints	142
9.3	Future work	144
CHAPTER 10	CONCLUSIONS	148
References		154
Appendix I		160
Appendix II		168
Appendix III		170
Appendix IV		172

LIST OF TABLES

TABLE NUMBER	
1	The specifications of the test rig (41)
2	Cutting conditions for the specimens
3	Calibration of the surface measuring system
4	Results of surface texture analysis for ML1
5	Results of surface texture analysis for ML2
6	Results of surface texture analysis for ML3
7	Results of surface texture analysis for ML4
8	Results of surface texture analysis for SH1
9	Results of surface texture analysis for SH2
10	Results of surface texture analysis for SH3
11	Results of surface texture analysis for SH4
12	Results of surface texture analysis for SH5
13	Results of surface texture analysis for TN1
14	Results of surface texture analysis for TN2
15	Results of surface texture analysis for TN3
16	Results of surface texture analysis for TN4
17	Results of surface texture analysis for GN1
18	Results of surface texture analysis for GN2

LIST OF FIGURES

FIGURE NUMBER	
1	General characteristics of joints (14).
2	Influence of hardness on the unloading deflection characteristics (30).
3	Influence of components on damping of a lathe (33).
4	Frequency behaviour of equivalent system (34).
5	Stiffness versus frequency (29).
6	General view of the test rig.
7	Schematic systems representation.
8	The main feature of the rig (41).
9	Schematic view of the test rig.
10	The setup for testing joints.
11	Block diagram of the system.
12	Setup for calibration of charge amplifiers.
13	Setup for calibration of accelerometers.
14	Gain and phase error of charge amplifiers.
15	Gain and phase error of accelerometers.
16	Gain error of "B & K" force transducers.
17	Static calibration of Kistler load cell.
18	Gain and phase error of m method reference m_i method.
19	Correction of the material effect.
20	Static calibration of the test rig.
21,a	Effective stiffness of the auxiliary system.
21,b	Damping coefficient of the auxiliary system.
22	Dimensions of the specimens used for the study of the effect of surface texture.
23	Schematic view for the method of holding the specimens during machining.
24	Dimensions for the specimens for the study of the effect of apparent area of contact.
25	Specimens for the effect of planform shapes.
26	Dimensions of the specimens for the study of the effect of number of joints.
27	Simulated plastic contact of shot blasted surfaces (48).
28	Auxiliary socket connections (49).
29	Example of a set-up error in which the straight line datum is used.

FIGURE NUMBER

30	Skid errors (50).	
31	Surface texture measuring setup.	
32	Block diagram of the surface measuring system.	
33,a	Setup for checking the stylus dimensions.	
33,b	Profile records for stylii shapes.	
34	Replica of the stylii profiles shown in Fig 33,b.	
35	The effect of form errors on the state of loading on the joint.	
36	Archard's representation of surface roughness (64).	
37	Which sampling interval is suitable for the definition of peaks?	
38	Fitting a least squares mean line.	
39	Characterisation of roughness using amplitude height distribution.	
40	The measurement of waviness.	
41	Dynamic stiffness of dry and lubricated jointed column	ML1.
42	Loss factor of dry and lubricated jointed column	ML1.
43	Dynamic stiffness of dry and lubricated jointed column	ML2.
44	Loss factor of dry and lubricated jointed column	ML2.
45	Dynamic stiffness of dry and lubricated jointed column	ML3.
46	Loss factor of dry and lubricated jointed column	ML3.
47	Dynamic stiffness of dry and lubricated jointed column	ML4.
48	Loss factor of dry and lubricated jointed column	ML4.
49	Dynamic stiffness of dry and lubricated jointed column	SH1.
50	Loss factor of dry and lubricated jointed column	SH1.
51	Dynamic stiffness of dry and lubricated jointed column	SH2.
52	Loss factor of dry and lubricated jointed column	SH2.
53	Dynamic stiffness of dry and lubricated jointed column	SH3.
54	Loss factor of dry and lubricated jointed column	SH3.
55	Dynamic stiffness of dry and lubricated jointed column	SH4.
56	Loss factor of dry and lubricated jointed column	SH4.
57	Dynamic stiffness of dry and lubricated jointed column	SH5.
58	Loss factor of dry and lubricated jointed column	SH5.
59	Dynamic stiffness of SH2 contaminated with Hermetite.	
60	Loss factor of SH2 contaminated with Hermetite.	
61	Dynamic stiffness of dry and lubricated jointed column	TN1
62	Loss factor of dry and lubricated jointed column	TN1

FIGURE NUMBER

63 Dynamic stiffness of dry and lubricated jointed column TN2.

64 Loss factor of dry and lubricated jointed column TN2.

65 Dynamic stiffness of dry and lubricated jointed column TN3.

66 Loss factor of dry and lubricated jointed column TN3.

67 Dynamic stiffness of dry and lubricated jointed column TN4.

68 Loss factor of dry and lubricated jointed column TN4.

69 Dynamic stiffness of dry and lubricated jointed column GN1.

70 Loss factor of dry and lubricated jointed column GN1.

71 Dynamic stiffness of dry and lubricated jointed column GN2.

72 Loss factor of dry and lubricated jointed column GN2.

73 Comparison between the dynamic stiffness of SH4 and SH5.

74 Dynamic stiffness and loss factor of ML1 joint.

75 Dynamic stiffness and loss factor of ML2 joint.

76 Dynamic stiffness and loss factor of ML3 joint.

77. Dynamic stiffness and loss factor of ML4 joint.

78 Dynamic stiffness and loss factor of SH1 joint.

79 Dynamic stiffness and loss factor of SH2 joint.

80 Dynamic stiffness and loss factor of SH3 joint.

81 Dynamic stiffness and loss factor of SH4 joint.

82 Dynamic stiffness and loss factor of SH5 joint.

83 Dynamic stiffness and loss factor of TN1 joint.

84 Dynamic stiffness and loss factor of TN2 joint.

85 Dynamic stiffness and loss factor of TN3 joint.

86 Dynamic stiffness and loss factor of TN4 joint.

87 Dynamic stiffness and loss factor of GN1 joint.

88 Dynamic stiffness and loss factor of GN2 joint.

89 Effect of planform shapes on the dynamic stiffness of jointed columns.

90 Effect of planform shapes on the loss factor of dry jointed columns.

91 Effect of planform shapes on the loss factor of lubricated joints.

92 Influence of direction of lays.

93 Effect of number of joints in a fixed jointed column length.

94 The stiffness and loss factor of a single joint as the number of joints tested varies.

FIGURE NUMBER

95 Stiffness and loss factor of jointed columns (effect of the apparent area of contact).

96 Stiffness of jointed column versus preload in kp (effect of the apparent area of contact).

97 Effect of apparent area of contact on the dynamic stiffness of joints.

98 Stiffness of equivalent solid columns versus area.

99 Contact between a rough surface and a plane.

100 Contact between unflat surfaces.

101 $F^{\frac{1}{2}}(V)$ versus $F^{\frac{3}{2}}(V)$.

102 $F^{\frac{1}{2}}(V)$ versus $F_2(V)$.

103 Experimental and theoretical stiffness of ML1 joint.

104 Experimental and theoretical stiffness of ML2 joint.

105 Experimental and theoretical stiffness of ML3 joint.

106 Experimental and theoretical stiffness of ML4 joint.

107 Experimental and theoretical stiffness of SH1 joint.

108 Experimental and theoretical stiffness of SH2 joint.

109 Experimental and theoretical stiffness of SH3 joint.

110 Experimental and theoretical stiffness of SH4 joint.

111 Experimental and theoretical stiffness of SH5 joint.

112 Experimental and theoretical stiffness of TN1 joint.

113 Experimental and theoretical stiffness of TN2 joint.

114 Experimental and theoretical stiffness of TN3 joint.

115 Experimental and theoretical stiffness of TN4 joint.

116 Experimental and theoretical stiffness of GN1 joint.

117 Experimental and theoretical stiffness of GN2 joint.

118 Some results from reference (28).

119 Mean of loss factors of solid and dry jointed columns (Khoyi's results (41)).

120 Simulation of contact between roughness asperities.

121 Contact between two surface roughness asperities.

122 Theoretical and experimental loss factor for milled joints.

123 Theoretical and experimental loss factor for shaped joints.

124 Theoretical and experimental loss factor for turned joints.

125 Theoretical and experimental loss factor for ground joints.

FIGURE NUMBER	
126	Machined surfaces.
127	Natural frequency of the test rig with ML1 jointed column.
128	Natural frequency of the test rig with ML2 jointed column.
129	Natural frequency of the test rig with ML3 jointed column.
130	Natural frequency of the test rig with ML4 jointed column.
131	Natural frequency of the test rig with SH1 jointed column.
132	Natural frequency of the test rig with SH2 jointed column.
133	Natural frequency of the test rig with SH3 jointed column.
134	Natural frequency of the test rig with SH4 jointed column.
135	Natural frequency of the test rig with SH5 jointed column.
136	Natural frequency of the test rig with TN1 jointed column.
137	Natural frequency of the test rig with TN2 jointed column.
138	Natural frequency of the test rig with TN3 jointed column.
139	Natural frequency of the test rig with TN4 jointed column.
140	Natural frequency of the test rig with GN1 jointed column.
141	Natural frequency of the test rig with GN2 jointed column.
142	Dimensions of the stylus used for the repeated measurements of waviness (93).
143	Experimental and theoretical stiffness of SH2 joint after repeating the measurement of its flatness.
144	Experimental and theoretical stiffness of SH4 joint after repeating the measurement of its flatness.

A C K N O W L E D G E M E N T S

The author wishes to thank:

Professor R H Thornley, MSc Tech, PhD, DSc, AMCT, CEng, FIMechE, FIProdE, Mem JSME, for permitting this work to be carried out in the Department of Production Technology and Production Management of the University of Aston in Birmingham. Also for his help, guidance and encouragement as supervisor throughout the whole project.

The Egyptian Government for providing the financial support.

Mr E R Langton for his assistance with the electronic instrumentations and for the design and construction of the interface boards presented in Appendix III.

Finally, his wife for her understanding and for the active support in a good presentation of the work.

D E C L A R A T I O N

No part of the work described in this thesis has been submitted in support of an application for another degree or qualification of this or any other University or Institution of learning.

S. N. Loukas

N O M E N C L A T U R E

A_o	Nominal area of contact.
a_1, a_2	Acceleration of the mass blocks.
a_i	Area of any contact spot.
C	Viscous damping coefficient of the jointed column.
C_1, C_2	Equivalent viscous damping coefficients for the auxiliary system (symmetric system).
C_t	$= 2C + C_1$
E	Young's modulus of elasticity.
$\frac{1}{E'}$	$= \frac{(1 - \nu_1^2)}{E_1} + \frac{(1 - \nu_2^2)}{E_2}$
F	Dynamic load on the joint.
F_1, F_2	Exciting forces.
H'	Mean height of roughness peaks.
HQ	Standard deviation of peak heights (measured from a roughness sample).
H	The hardness of the joint surface.
K, τ	Stiffness and loss factor of the jointed column.
K_1, K_2	The stiffness of the springs of the test rig (symmetric system).
K_d, τ_d	Stiffness and loss factor for the jointed column under dry clean conditions.
K_J, τ_J	Stiffness and loss factor of the joint interface.
K_m, τ_m	Stiffness and loss factor of the material of the specimens.
$K_J + i\omega C_J$	Complex stiffness of the joint interface.
$K_m + i\omega C_m$	Complex stiffness of the equivalent solid.
K_t	$= 2K + K_1$
M_1, M_2	Masses of the upper and lower inertia blocks.
m_i	Apparent mass vector = F_1/a_1 or F_2/a_2

m	Apparent mass vector = F/a_1 or F/a_2
N	Number of joints.
NO.	Average number of zero crossings per unit length.
NP	Number of peaks per profile trace.
P	Applied pressure on the joint.
Q	Kurtosis of the amplitude distribution.
QF	Kurtosis of the flatness height distribution.
R	Mean radius of asperity peaks.
R_1, R_2	Peak radii of two roughness asperities in contact.
RA	Centre line average.
RP	Maximum peak height.
RQ	Root mean square value of roughness heights.
RQF	Standard deviation of flatness heights.
RT	Peak to valley height.
RV	Depth of valley.
r_i	Radius of contact spot.
SA	Mean absolute slope.
SG	Harmonic mean slope.
SK	Skewness of the amplitude distribution.
SKF	Skewness of flatness height distribution.
SQ	Root mean square slope.
u	Mean plane separation of the joint surfaces.
V	= u/σ
W	Load applied on the joint.
W'	Average wave length index.
W_i	Load carried by contact spot "i".
W_i	Compliance.
Y	= z/σ
z	Height of any roughness peak above the mean plane.

$\frac{1}{\beta}$	$= \frac{1}{R_1} + \frac{1}{R_2}$
λ_J	Total elastic deformation of the joint.
λ_i	Elastic deformation of any contact spot.
ψ	Specific damping capacity.
ξ	The number of roughness asperities per unit area.
σ	Standard deviation of flatness heights for the joint surfaces = standard deviation of peak heights for the joint surfaces.
$\phi(Z)$	Probability density function of peak heights = probability density function of flatness heights.
ν	Poisson's ratio.
ω_1, ω_2	First and second natural frequencies of the test rig.
ω	Exciting frequency.
μ	Coefficient of friction.

C H A P T E R 1

INTRODUCTION

The ever increasing demand for higher performance and better accuracy of a metal cutting machine tool led to the evolution of new and different concepts in the design of the machine structure. No longer is it acceptable to design the machine structure by only considering its static performance. As this is not the real working condition, modern design methods take into account the dynamic behaviour of the machine under various working conditions. Computers are no longer too expensive a tool which only large establishments can afford to install and use. They are becoming an indispensable aid to designers. This does not mean that the results obtained are fully satisfactory, since the common practice in computer aided design (as reported in reference 1) is to treat the complete machine tool as consisting of one piece of elastic material. Thus, the assumption made is that the connections between various machine elements are absolutely rigid for all degrees of freedom. This technique is basically wrong as the authors in (1) point out, but justified because of the following reasons:

1. There are relatively few reliable numerical values for the stiffness and damping of machine tool joints.

2. The form in which these data are available is largely unsuitable for direct use in computer aided design.

Taylor (2) reported that in modelling a machine structure consisting of a column and a cross rail complete with the tool box and ancillary equipment, an improvement of up to 39 per cent was obtained when the joints between the elements were assumed rigid. Thus, in 1965 Taylor was forced into making very rough assumptions (as he pointed out) about the stiffness of joints. Since then a great deal of research has been concentrated on the study of both the static and dynamic behaviour of joints and this basically led to a better understanding and appreciation of the properties of both fixed and movable joints. Nonetheless, the results of such extensive efforts did not seem sufficient to provide the basic information needed in order to compute or make estimates of the properties of joints which are accurate enough to be included in a computer simulation of machine tool structures. More recently, Yoshimura (3) reports that in order to include the joint properties in a model simulating a double column vertical lathe, he carried out actual experiments to measure the stiffness and damping of simulated joints. Such a technique is hardly suitable for application in a design office. It would seem then that the research into the behaviour of joints over the past two decades has not yet been crystallised in a simple enough form that can be used in estimating the properties under various conditions. Such a crystallisation of information could lead to:

1. A revolutionary improvement in the accuracy of prediction of the dynamic behaviour of the overall structure, not only for machine tool structures, but also in almost any metallic structure.

2. Optimisation of performance of an important element that could lead to up to 39% improvement in the static stiffness of the structure.

3. Functional design of joints which might result in some cost reduction.

In spite of the importance of joints, it is rather difficult to make an accurate theoretical prediction of their behaviour. A joint, whether intended to be fixed or movable, is the product of contact of two machined surfaces. If these surfaces were absolutely flat and smooth, the stiffness of the two jointed members could have been equal to their stiffness if they were solid. Unfortunately, surfaces are not only rough but their roughness is also random and moreover, they are always suffering from flatness deviations.

The inaccessibility of the region of metallic contact between surfaces makes it difficult to form a correct idea about the true area of contact, while the very high transmissibility of joints creates problems in measuring the stiffness and in particular the damping of the interface. The randomness of surface topography complicates the attempts of deriving a much needed theoretical expression which can accommodate a wide range of topography of the joint surfaces.

The work presented in this thesis seeks to examine and assess the normal dynamic characteristics of fixed machine tool joints. Whilst the theoretical and experimental results are mainly applicable to bolted joints where the stiffness in the normal direction is of importance, the theoretical expression derived for the stiffness is

also believed to be suitable for the computation of the stiffness of unfixed machine tool joints where the applied loads are much smaller.

An experimental study of some of the parameters which influence the dynamic characteristics of joints was carried out. Of these parameters, that of surface topography is perhaps the least understood. That is why special attention has been given to the description of the joint surfaces. Thus, together with the stiffness and damping measurements for every machined finish studied, 21 parameters are given to describe the surface texture; this includes quantisation of flatness deviations. The experimental study also includes data for lubricated joints as well as an investigation into the influence of some other parameters.

The theoretical investigation leads to mathematical formulae for the evaluation of the dynamic stiffness and loss factor of dry clean joints. The theoretical results are used to predict the natural frequency of the test rig and the results are compared to those measured experimentally.

CHAPTER 2

A REVIEW OF RESEARCH WORK ON THE INTERFACE BETWEEN MACHINE TOOL JOINTS

2.1 Introduction

A joint between two machine elements is defined as the region through which the forces are transmitted from one member to the other. This definition implies that the static and dynamic behaviour of a joint is primarily dependent on the characteristics of its interface. Thus a study into joint behaviour could be reduced to the study of contact between machined surfaces.

Contact in fixed machine tool joints is classified from other contact problems (e.g. friction, wear, electrical contact, etc.) by the unavoidable presence of flatness deviations on its surfaces and the range of loads applied to the joint.

What makes any study of the joint performance worthwhile is the scope by which the joint behaviour could affect the functional performance of the overall structure. In this respect, machine tool structures are very much affected by the behaviour of their joints. Cowley (4), after an extensive study of the static and dynamic behaviour of a plano-milling machine, concludes that if an accurate prediction of the dynamic characteristics of an actual machine structure is to be obtained by either computational or physical model techniques, it is of primary importance to simulate the machine joint characteristics as accurately as possible. He states that the

principle limitation to the computer aided design approach lies in the lack of fundamental information concerning the elastic behaviour of certain structural elements, bolted and sliding joints, foundation, etc.

Reshetov (5) states that contact displacements comprise of up to 90% of the total elastic displacement in units of the support type, knee type, brackets and tables, in spindle units, 30 to 40% and in slides, 40 to 70%. Other research workers (6 - 9) realised the importance of joints in their experimental and theoretical analysis of machine tool structures.

Research into the behaviour of machine tool joints branched into two main fields:

1. The static behaviour of joints where the study was directed towards examining the plastic and elastic deformation of the joint surface.

2. The dynamic behaviour of joints where the study was concerned with measuring the dynamic stiffness and damping properties of the joint interface.

2.2 The static behaviour of machine tool joints

Early researchers into the static behaviour of joints realised the fundamental dependence of the joint deflection upon the apparent pressure (10), through the empirical relations proposed. The condition of surface roughness was later studied by Kragelsky (11), Demkin (12) and Kragelsky and Demkin (13). The basic findings of those researchers

could be briefly summarised as follows:

1. The approach of machined surfaces is dependent on the apparent pressure applied and could be expressed in the form

$$\lambda_J = cP^{\alpha} + K \qquad 2.1$$

Where c, α and K are constants.

2. The joint deformation is dependent on surface roughness and waviness which also affects the true area of contact (13).

The applicability of the theoretical relations proposed was doubtful because the area of joints investigated was very small. It was also difficult to apply since the constants had to be found experimentally.

Thornley and Connolly (14 - 18) experimentally measured the deflection of machine tool joints formed from relatively large areas. In their work, when two surfaces were brought together, contact within the apparent area of contact took place over only a small fraction of the actual available area. As the applied load increased, plastic deformation progressed, and if the load was removed, the joints recovered elastically. The elastic recovery curves were congruent and the general characteristics of joints are as shown in Fig 1. The relation between the mean interface pressure and the joint deflection is non-linear for pressures below around 300 Kp/cm^2 and within this range of preload, the joint elastic deformation was found to fit into the relation

$$\ln P = m \lambda_J + c \qquad 2.2$$

where m and c are constants which are dependent on material properties and surface topography.

It follows from equation 2.2 that the stiffness of the joint is given by

$$K_J = mW \qquad 2.3$$

Although they emphasised that flatness deviations on joint surfaces seriously affect its static stiffness, they did not quantify their measured flatness deviations in a suitable form that could be related to the constant m. According to equation 2.3, the joint stiffness is independent of the apparent area of contact, contrary to what could be concluded from the theoretical relations used in (10 - 12), and also contrary to the findings of Levina (19) who maintains that the elastic deflection of joints is given by

$$\lambda_J = c'P^{m'} \qquad 2.4$$

where c' and m' are constants.

From equation 2.4, the joint stiffness is given by

$$K_J = \frac{A_o P^{(1 - m')}}{m' c'} \qquad 2.5$$

The dispute over the effect of the apparent area of contact is of fundamental importance. If the joint stiffness is dependent on the apparent pressure, then direct measurement of the stiffness should be carried out for samples subjected to the level of pressures experienced in machine tool joints, and the results are directly applicable to real joints. On the other hand, if equation 2.3 is correct, then the experimentally measured stiffness should be measured

for the same applied loads encountered in real joints, irrespective of the value of the apparent pressure.

Modern theories of contact appear to lead to the conclusion that the joint stiffness is dependent on the applied load and not the apparent pressure, a point which appears in the work of Greenwood (20) who was able to show theoretically that if an exponential approximation of the upper tail of the Gaussian distribution of asperity peaks (which is a reasonable approximation) was used in an elastic deformation model, the joint's elastic deformation would be obtained from

$$\ln P = c - \frac{d}{\sigma} \qquad 2.6$$

where c is a constant, σ is the standard deviation of peak heights and d is the separation between the mean planes of the joint surfaces.

It can be seen that equations 2.2 and 2.6 are very similar. Both show that the joint's elastic deformation is dependent on the logarithm of the mean interface pressure, and both would lead to the conclusion that the stiffness is dependent on the applied load.

An interesting conclusion could be reached by comparing equations 2.2 and 2.6, that is

$$m \propto \frac{1}{\sigma} \qquad 2.7$$

Almost the same conclusion was reached experimentally by Connolly and Thornley (17) where they made the following conclusion:-

> "For surfaces cut by single point tools (e.g. turned, shaped, planed), the m value was found to be approximately inversely proportional to the surface roughness measured in CLA."

The decisive effect of surface roughness upon joint behaviour was studied by Schofield (21 - 23) who described surface roughness using asperity shapes based on the shape of the bearing area diagram (24) and could be realised by a mathematical expression. He went on to show that the elastic recovery is given by

$$\lambda_J = c\sqrt{P}\, f \qquad 2.8$$

where c is a constant which depends on material properties and the shape given to the asperities, and f is the cutting tool feed rate. The above relation gives the joint deflection as a function of the tool feed rate, which could be taken as an expression for the number of asperities on the joint surfaces. A valuable conclusion obtained from the above work is that surface roughness is of secondary importance for joints which suffer from flatness deviations.

The educative nature of equation 2.8 is revealed when we try to compute the load carried by a single asperity and then integrate the result for all asperities on the surface, giving them a proper statistical distribution of peak heights, as will be shown in Chapter 7. The final expression is of the same form proposed by Greenwood (20) and this could be further reduced to a logarithmic-linear relation of the form of equation 2.2. It follows that the joint stiffness will be in this case dependent on the applied load. On the other hand, the joint stiffness derived directly from equation 2.8 shows that the stiffness is dependent on the apparent pressure. The conclusion that one could arrive at is that, the shape of the distribution of asperity heights is the origin of both the empirical expression in (16), that is, equation 2.2, and the dependence of the joint stiffness on load. Obviously, if one ignored the peak height distribution or gave it an

unrealistic linear form as in (25) and (26), the result would be an expression of the form suggested in (10) or (19).

The works cited so far were carried out for joints under dry and clean conditions. However, because this would not normally be the case in the ordinary workshop where joints could be contaminated with oil or grease, there has been some research work which examined the influence of contaminating layers on the normal static characteristics of machine tool joints. Connolly (27) found that the presence of grease or oil has no effect on the elastic recovery of rough machined surfaces, whilst for ground and lapped joints, its effect was more pronounced. He suggested that when the surfaces are under pressure the undulations of the rough surfaces are large enough to permit the escape of oil or grease, whereas in the case of smoother surfaces the oil or grease is liable to become trapped in pockets and will therefore influence the resulting static stiffness. Levina (19) reported that the stiffness of lubricated joints would be from 15 to 20 per cent higher than that for non-lubricated rough ground or scraped joints. On the other hand, for very smooth machined surfaces floating on thin oil film, the stiffness of lubricated joints was less than that of the non-lubricated. Thornley and Lees (28, 29) examined bonded joints and concluded that if the layer thickness of an adhesive film was limited to the same order of magnitude as the flatness deviation of the surface involved, the static stiffness of the joint could be increased to a value which is in close proximity to that of the equivalent solid. They also noted that the increase in static stiffness by bonding was dependent on the type and quality of the surface finish. The greater the surface stiffness before bonding, the less significant the increase in stiffness after bonding.

The joint behaviour is determined by the topography of its surface and the amount of preload applied. Nonetheless, other parameters related to material properties also have influence on the joint behaviour. The influence of hardness was examined in (30) and (31). For initial loading it was found that the surface hardness had considerable effect on the amount of plastic deformation experienced by the joint. The harder the joint surface, the less plastic deformation it undergoes. On unloading, the elastic recovery was also shown to be affected by the surface hardness. For all experiments carried out, it was found that the joint stiffness decreased as its surface hardness increased. As seen from Fig 2, the influence of hardness is most pronounced within the non-linear portion of the elastic unloading curves. That is, the surface hardness should appear in any expression describing the elastic deformation of joints within the range of preloads encountered in machine tools.

2.3 Dynamic behaviour of machine tool joints

The earliest known results on the dynamic characteristics of joints subjected to dynamic loads normal to the interface are owed to Reshetov and Levina (32). They reported that cast iron and steel joints showed similar values for the relative energy dissipation. They also found that the energy dissipation increased as the quantity and viscosity of lubricant increased, and that an increase in the applied pressure reduced the relative energy dissipation. Within the frequency range of 15 to 100 Hz they reported that the effect of frequency and amplitude were not significant. The dynamic stiffness of non-lubricated joints did not differ from their measured static stiffness. However, when the joints were lubricated, an increase in

dynamic stiffness by 1.5 to 2 times, depending on the quantity and viscosity of lubricant, was reported.

The significance of damping raised by the presence of joints in machine tool structures is fully illustrated in Fig 3, where the major part of damping results from the interface at joints. The interaction of the structure with the foundation may also produce considerable damping (33).

Corbach (34) studied the dynamic characteristics of static and movable joints. Regarding their behaviour in the absence of sliding motion, he found that an increase in joint preload increased its dynamic stiffness and reduced the loss factor*. As lubricant was introduced, both the joint stiffness and the loss factor increased. He reported that an increase in lubricant viscosity increased the stiffness, while the loss factor with more viscous oils was in most cases lower than that for the less viscous ones. Within the frequency range 20 to 300 Hz, the joint stiffness under dry clean conditions was reported to be frequency independent, whilst the loss factor increased linearly with frequency. When the joint was lubricated, he found that as the frequency increased from 20 to 300 Hz, the dynamic stiffness rose by up to 30%, whilst the loss factor generally changed slightly with frequency. To explain the effect of frequency, he proposed the model shown in Fig 4. From this model one could conclude that at a higher frequency range (say above 200 Hz) the joint stiffness and loss factor could be generally considered as frequency independent. This

*The loss factor is a measure of damping and is defined as the ratio of the quadrature to in phase stiffness components, that is:- $\gamma = \frac{\omega C}{K}$

conclusion could also be drawn from the results obtained by Thornley and Lees (29) for the dynamic stiffness of bonded joints as shown in Fig 5.

The results obtained by Andrew (35 and 36) show that the dynamic stiffness of lubricated joints rises very little with frequency within the range 30 to 270 Hz and is almost independent of frequencies above 180 Hz. The quadrature stiffness was found to increase continuously with frequency. Both the stiffness components were reported to increase with an increase in joint preload and lubricant viscosity. Similar results are also reported in reference (37).

Thornley (38 and 39) found that an increase in joint preload, lubricant viscosity or excitation frequency resulted in an increase in the dynamic stiffness of joints. As for the damping ratio, it decreases with increasing preload and increases with an increase in lubricant viscosity.

Dekoninck (40) reports that the loss of joint stiffness with increasing roughness of the joint faces is not very significant and that the use of a high quality adhesive may influence very favourably the joint stiffness.

Khoyi (41) reported that the main parameters which influence the dynamic stiffness and loss factor of a joint are the joint's apparent area, its surface roughness and the applied preload. An increase in joint preload increased the joint stiffness and reduced the loss factor. The frequency and amplitude of vibration were found to have no effect on either the dynamic stiffness or the loss factor.

A great deal of research work was carried out on bolted joints subjected to either bending moment or tangential forces (for example see references 42 to 45). Under such loading conditions the stiffness and damping characteristics are different from those when the joint is excited normal to its interface, which is the field of interest for this investigation. For this reason the survey presented in this Chapter is limited to works which deal with the latter type of loading.

2.4 Conclusions

A great deal of research work has revealed many aspects of the behaviour of bolted joints. Of those characteristics the most understood and fundamental property is the increase in the joint stiffness with increasing preload. However, the influence of many parameters, although qualitatively understood, is not yet quantitatively related to the joint behaviour. Of those, the least understood is the effect of surface texture.

Regarding damping in dry clean joints, it is universally agreed that its value is small. As to the question of how this damping arises, it remains to be answered. The enormous increase in damping as a result of lubricating the joint was illustrated in Andrew's experiment (36) where he found that when lubricating only some of the sliding and bolted joints of a knee type milling machine, the result was an improvement of 50% over the value of damping measured when the same joints were dry. On the other hand, doubts are thrown on the long-term stability of a lubricant layer between the interface of a bolted joint and whether an effective control on the type of lubricant could be made.

In general, both the stiffness and damping of bolted joints cannot be estimated by the designer, and the need still remains for a mathematical model which quantitatively relates various parameters to the joint's stiffness and damping. This could only be established with confidence if a wide range of experiments on joints were carried out to test the validity of such a model.

CHAPTER 3

MEASUREMENT OF THE DYNAMIC STIFFNESS AND DAMPING OF MACHINE TOOL JOINTS

3.1 Introduction

Due to the complexity of the mechanisms forming the behaviour of machine tool joints, it was realised that the first step towards a better understanding of those mechanisms is to carry out extensive tests in order to gather quantitative values for the dynamic stiffness and damping under various conditions and at different levels of variables. The experimental test rig, Fig 6, used in this investigation is based on a mechanism which enables the measurement of highly stiff elements to be carried out in isolation of extraneous effects normally encountered in this type of measurement. The principle of operation of the measuring setup is based on the idea that two exactly similar single degree of freedom systems could be transformed into one symmetrical two degrees of freedom system by joining the two masses of the parent systems by a spring (the joints under test, Fig 8,a) whose characteristics could be determined while the whole system is oscillating in a pure second mode. In this way the extraneous effects are minimised.

The test rig was designed and built by Khoyi (41) and was used in this investigation to produce the data for the stiffness and damping of joints. The present Chapter describes the test rig, the associated instrumentations, its calibration and the methods used for testing joints.

3.2 Some features of the measuring test rig

Due to the high transmissibility associated with the high stiffness of machine tool joints, the ideal conditions of massless and proportionally damped assembly needed for testing joints was not fully achieved in the past. The inevitable presence of various modes coupling made the process of data reduction limited to a rather small frequency band.

The system used in this investigation is basically a symmetrical two degrees of freedom system, Fig 7. It can be forced to vibrate in a pure mode, i.e. all points on the system could be forced to vibrate in or out of phase; furthermore, free vibrations exhibit simple harmonic motion. Those conditions were achieved by:

1. Observing the complete symmetry of the system.

2. The use of multi-point excitation which is generally necessary for pure mode excitation. The exciting system is such that the number of excitation points is equal to the number of degrees of freedom.

Thus measurement of the stiffness and damping of the specimens could be carried out under both conditions of forced and free vibrations. In the case of forced vibrations, tests could be carried out both at resonance and off-resonance frequencies. The first mode of vibration of the system gives values of the stiffness and damping of extraneous elements which may then be taken into account in the second mode to find the stiffness and damping of the joints under test.

The system has two sets of isolating springs which act as preloading devices to apply the required static preload on the joints under test. The springs also provide minimal transmission of load to and from the surroundings, hence minimal extraneous effects. A basic feature of the rig is that the size of vibration generators can be reduced considerably because of the amplifying effect of the mass blocks as resonance is approached. As Fig 8,b shows, the load amplification factor in the frequency range o to $\sqrt{2}\ \omega^2$ is always greater than unity. Depending on the damping ratio ξ this factor is reduced from 1 at $\sqrt{2}\ \omega^2$ to near zero as the frequency increases.

3.3 The test rig structure

The experimental setup is schematically shown in Fig 9. It consists of a steel frame (18), in which three vertical columns (13) are mounted. Three upper springs (4), (K_1 springs) are resting against the top plate (10) and acting as isolating springs for the upper inertia block (9), (M_1 mass). To prevent the upper mass block from falling, three soft springs (5) are placed against sleeves (19) mounted on each column. The lower inertia block (8), (M_2 mass) is mounted on three lower springs (3), (K_2 springs). Three hydraulic cylinders (17) are used to apply the required static preload on the specimen column. The hydraulic pressure is applied by a manual pump through a pipeline (16), to the hydraulic cylinders, which through their extended pistons (15), transmit the load to the top plate and through K_1 springs to the upper inertia block to the specimen column (20). The applied pressure is measured by a load cell (21) placed at the middle of the specimen column, or by measuring the deflection of K_2 springs. After applying

the load, locking nuts (11) are used to secure the top plate in position (see Fig 10). Dynamic load to the inertia blocks is applied via two electro magnetic exciters (1) and (2), and through their extended arms (12) and (14) to each mass; this load is measured by two piezoelectric load cells (6) and (7), whilst the amplitude of acceleration of the mass blocks is measured by two accelerometers mounted on each mass. The specifications of the rig are given in table 1.

3.4 Instrumentation

The system of instrumentation, Fig 11, enables the following features to be realised:

1. Pure sinusoidal exciting forces with high frequency stability and maximum control on both the amplitude and phase between the two exciting forces in order to realise and sustain pure mode excitation.

2. High accuracy and sensitivity in measuring both the amplitude and phase at any point within the system.

3. Ability to record decay curves.

The above requirements were satisfied by the use of two systems, one for exciting and controlling the mechanical system, and the other for measuring the resulting response. The two systems are linked at the frequency response analyser which produces the reference signal of the required frequency to drive the exciting and controlling system, and, at the same time, measures the response received from the accelerometers

and load cells composing the measuring system.

The exciting and controlling system consists of two electro-magnetic shakers driven by two power amplifiers. The amplifiers are driven by a variable phase oscillator which is locked to the frequency of the reference wave generated by the frequency response analyser (F.R.A.). The lock was made possible by aid of an external synchroniser which was built into the phase oscillator. This lock, once established, enabled the frequency from the F.R.A. to be varied over about 3 db, without affecting the stability or distorting the driving signal. A triggering control unit was built to enable cutting off the drive to the shaker units and simultaneously trigger the oscilloscope to record and store the damped oscillations. It also attenuates the input voltages to the shaker units equally.

The measuring system consists of two piezo-electric load cells fixed to each mass and measuring the exciting forces from the shakers. The static and dynamic loads are measured using a "Kistler" piezo-electric load cell, in its static mode a digital voltmeter was used to measure the static preload being applied to the specimen column. The acceleration of the mass blocks is measured using two accelerometers of relatively high sensitivity to enable using the maximum available gain on their charge amplifiers (10 v/g). Two oscilloscopes with storage facilities, each with two channels, were used to monitor the signals received from different transducers. A switch box enables routing any of the five recovered signals from the measuring transducers to any measuring or monitoring device within the system. The earth point on the measuring system was made at the oscilloscopes, the rest of the

instruments' terminals were floating, except for the power amplifiers which were earthed to the rack.

3.5 Calibration of instrumentation

The solartron frequency response analyser used is almost a substandard measuring instrument. A standard circuit supplied by the manufacturer is used to check that the tolerances on the measured response are maintained within the limits specified (± 0.1^{o} for phase and ± 0.1 db for amplitude). It was then possible to use the analyser in calibrating the high quality transducers used in this work.

3.5.1 Calibration of the charge amplifiers

The "B & K" conditioning amplifiers were calibrated by using a capacitor (1000 ± 1% PF) which was shunted across the input of the charge amplifier under calibration. The function of this arrangement was to enable the input of a known voltage to the capacitor which transforms every 1 mv into 1 PC input to the charge amplifier (C.A.). The C.A. was set to the sensitivity of the transducer to be used during actual tests. The input voltage at the required frequency was obtained by programming the F.R.A. while the output of the C.A. was measured by the analyser with respect to the input signal. The calibration arrangement is shown in Fig 12 and the results of calibration are plotted in Fig 14,a,b.

The "Kistler" charge amplifier has a built-in calibration circuit similar to the one mentioned above. This was used for its calibration. The results are shown in Fig 14,c.

The results of the calibration of the charge amplifiers indicated that they were functioning properly within the limits specified by the manufacturer. The "Kistler" charge amplifier showed an error of up to 4.6% for the gain settings of 1 and 2 MU/V and up to 2.5% for the setting of 5 MU/V. These settings were not used during the tests on joints. A magnification range of 10 MU/V was used for which the gain error is 0.8%.

3.5.2 Calibration of "B & K" accelerometers and load cells

The accelerometers were calibrated using a standard accelerometer in a back to back arrangement as shown in Fig 13. The results of this calibration are shown in Fig 15. During the period of the tests on joints the accelerometers were frequently checked using an accelerometer calibration table. This method of check based on the chatter-ball technique is only accurate within ± 5%, and was only used to check that the accelerometers did not suffer any damage.

The "B & K" load cells were calibrated using a mass block bolted to the load cell under calibration. The transducer was then subjected to an acceleration of 1 g at various frequencies and the force measured by the load cell due to the applied mass was recorded. The results of the calibration are shown in Fig 16.

3.5.3 Static and dynamic calibration of Kistler load cell

The static calibration of the Kistler load cell was performed on a "Denison" testing machine, and the results are shown in Fig 17. As for its dynamic calibration, the test rig was employed. The load cell was placed in the middle of a solid column and the required static preload was applied. A pure second mode was then excited and the

stiffness and loss factor were measured, once by using the Kistler load cell and the accelerometers (m method) and then by using the "B & K" load cells and the accelerometers (m_i method). By comparing the results obtained using both methods the error in gain of the load cell could be estimated. The results in Fig 18 also express the error in m method relative to m_i method.

3.6 Methods of measurement

The principle of operation of the test rig is given in detail in Appendix I. This section will briefly outline the procedures followed for measuring the dynamic stiffness and damping of joints.

After the specimen column under test was placed concentric with the lower mass block, the required static preload was applied and the platform (10) was securely locked in position. The specimen column arrangement is shown in Fig 19,b. The shakers were then connected to M_1 and M_2. For safety, the switches on the triggering and control unit (toggle switches) were initially set to "off" position, thus, short-circuiting the input terminals of the power amplifiers. Measurements were then carried out in the following sequence (41):

1. Search for the second natural frequency

   Before switching on the toggle switches, both the outputs from the analyser and the variable phase oscillator were set at zero. By employing the variable phase oscillator on its own, a single force, e.g. $\bar{F}_1$ with a very low amplitude was applied in search of the second natural frequency. In this way, it was possible to locate the natural frequency in the actual test without

having to adjust the frequency on the oscillator to sustain synchronisation during the actual test.

2. Pure mode excitation

The next step was to transfer control to the F.R.A. by appropriate programming of its generator as follows:

Frequency	: Close to 2^{nd} natural frequency (NF_2)
Output level	: 2 volts
Increment of frequency sweep	: 0.1 - 1 Hz
x input	: $\bar{F}_1$ or a_1
Y input	: $\bar{F}_2$ or a_2

With the measuring mode of the analyser set for the direct measurement of the ratio between exciting forces F_1 and F_2, the variable phase output on the oscillator was initially adjusted so that $y/x = 1$ and $\theta_y - \theta_x = 0$. The inputs to the analyser were then switched to measure a_1 and a_2. Fine adjustment on the oscillator was made until the acceleration ratio was 1 and 180^o for amplitude and phase respectively. During tests the tolerances permitted on symmetry were kept to within ± 5% for amplitude and a maximum of ± 3^o for phase difference.

Natural frequency excitation was then achieved by sweeping the frequency of excitation at small increments, while measuring the phase shift between the exciting force and resulting acceleration, until a phase shift of 90^o was realised. At this frequency, the test rig was vibrating at its 2^{nd} natural frequency. Final adjustments for the displacement amplitude level and conditions of symmetry were then made.

The measurement of specimen parameters were then carried out as follows:

(a) Resonance tests

I Forced vibration methods

i. m_1 method

The second natural frequency was recorded. This would directly render the stiffness as follows

$$K_t = M_1 \omega_2^2 = 118.5 \ (2\pi)^2 \ NF_2^2 \simeq 4678 \ (NF_2)^2 \quad N/m \qquad 3.1$$

With the inputs to the analyser set to measure $\bar{F}_i/a_i = m_i$, the display mode was changed into the real and imaginary components of the resultant vector (i.e. m_{iR}, m_{iI}) thus

$$C_t = - \omega_2 \ m_{iI} \qquad 3.2$$

$$\tau_t = \frac{C_t \ \omega_2}{K_t} = \frac{-m_{iI}}{118.5} \qquad 3.3$$

ii. m method

The Y input to the analyser was switched to measure $\bar{F}$ (the force within the specimen column), while the X input was measuring the acceleration, thus $m = \frac{\bar{F}}{a_i}$, the measuring mode being the real and imaginary components for the resultant vector. The specimen parameters were evaluated directly from

$$K = \frac{\omega_2^2}{2} \ m_R \qquad 3.4$$

$$C = \frac{\omega_2}{2} \quad m_I \qquad 3.5$$

$$\tau = \frac{\omega_2 C}{K} = \frac{m_I}{m_R} \qquad 3.6$$

II Free vibration method

The free-decay curves were obtained by cutting off the inputs to the shakers while triggering the storage oscilloscope to store the decay. Before starting the test, the acceleration signal (a_1 or a_2) was projected on the screen with amplitude magnification so that the signal occupied the full vertical length of the screen.

The number of cycles n made by the signal to decay from the full "a_o" to the minimum "a_n" measurable level were counted to give the value of damping from

$$\tau_t = \frac{1}{n\pi} \cdot \ln \frac{a_o}{a_n} \qquad 3.7$$

$$C_t = \tau_t \omega_2 M_1 \qquad 3.8$$

(b) Off Resonance Tests

i. m_i method

The required frequency of excitation was programmed and adjustment of the phase and amplitude of exciting forces were made to sustain pure second mode excitation. The

specimen parameters were calculated from

$$K_t = \omega^2 (M_1 - m_{iR}) = \omega^2 (118.5 - m_{iR}) \quad 3.9$$

$$C_t = - \omega m_{iI} \quad 3.10$$

$$\tau_t = \frac{C_t \omega}{K_t} = \frac{-m_{iI}}{M_1 - m_{iR}} = \frac{-m_{iI}}{118.5 - m_{iR}} \quad 3.11$$

ii. m method

By switching the analyser to measure the ratio between the force in the specimen column and the acceleration, the stiffness and damping of the specimen column could be found from

$$K = \frac{\omega^2}{2} m_R \quad 3.12$$

$$C = \frac{\omega}{2} m_I \quad 3.13$$

$$\tau = \frac{m_I}{m_R} \quad 3.14$$

The most important feature about this method is that direct measurement of the stiffness and damping of the specimen column could be made without the need to correct for the presence of the system parameters in the results.

3.7 Data reduction

The results measured using m_i method or free vibration method contain the effect of the test rig parameters. This should be extracted in order to render the required information about the

specimen parameters. The system parameters could be obtained from a separate test at the 1st pure mode to find K_1, C_1 and τ_1, thus

$$K = \frac{1}{2} (K_t - K_1) \qquad 3.15$$

$$C = \frac{1}{2} (C_t - C_1) \qquad 3.16$$

$$\tau = \frac{\omega C}{K} \qquad 3.17$$

The correction due to the auxiliary parameters amounted to very small values, specially for the stiffness (normally less than 1%). This is because of the very high stiffness of the jointed column compared to the stiffness of the system's springs. Fig 21, gives the values of the auxiliary parameters at various preloads.

3.8 The effect of the material of the discs

It has been shown in (41) that the maximum error 'e_{max}' which arises from neglecting the inertia of the discs could be estimated from

$$e_{max} \simeq \frac{N}{2} \cdot \frac{w}{W} \times 100 \quad \text{per cent} \qquad 3.18$$

Where N = number of joints, w = weight of one disc, and W = weight of the inertia block. As it can be seen, the expected error for a 10 disc jointed column and 0.1 Kg specimen is less than 0.5%, which is practically negligible. However, the effect of the stiffness and damping of the material of the discs had to be extracted in order to determine the stiffness and damping of the joint surface on its own. The effect of the discs' material could be found by

carrying out a separate test to measure the stiffness and damping of an equivalent solid, which is a solid column made of the same material as the joints and has the same dimensions as for the specimen column, Fig 19,a.

The model which represents the jointed specimen column is shown in Fig ,19,c. The receptance of the assembly is the sum of the receptances of two elements connected in series, thus

$$\frac{1}{K + i\omega C} = \frac{1}{K_m + i\omega C_m} + \frac{N}{K_J + i\omega C_J} \qquad 3.19$$

i.e.

$$\frac{N}{K_J + i\omega C_J} = \frac{1}{K + i\omega C} - \frac{1}{K_m + i\omega C_m} \qquad 3.20$$

By rewriting the above equation in terms of its real and imaginary components, the following set of equations is obtained

$$\frac{NK_J}{K_J^2 + \omega^2 C_J^2} = \frac{K}{K^2 + \omega^2 C^2} - \frac{K_m}{K_m^2 + C_m^2 \omega^2} \qquad 3.21$$

$$\frac{NC_J}{K_J^2 + \omega^2 C_J^2} = \frac{C}{K^2 + \omega^2 C^2} - \frac{K_m}{K_m^2 + C_m^2 \omega^2} \qquad 3.22$$

or in terms of the loss factor, these equations are further simplified to

$$\frac{N}{K_J (1 + \tau_J^2)} = \frac{1}{K (1 + \tau^2)} - \frac{1}{K_m (1 + \tau_m^2)} \qquad 3.23$$

$$\frac{N\tau_J}{K_J\ (1 + \tau_J^2)} = \frac{\tau}{K\ (1 + \tau^2)} - \frac{\tau_m}{K_m\ (1 + \tau_m^2)} \qquad 3.24$$

Thus, both K_J and τ_J could be found by solving the above set of equations.

3.9 Static calibration of the test rig

This calibration was carried out by applying the hydraulic pressure on a solid specimen column whilst measuring the load using the Kistler load cell (in its quasi-static mode) to obtain a direct reading of the applied preload on the specimen, and also measure the deflection of K_2 springs using a dial indicator, 0.0025 mm sensitivity. It was found that the relation between the preload W in Kp on the specimen, and the deflection of K_2 springs x in mm, fits the relation (41)

$$W = 0.25\ x^2 + 119.8\ x - 21.4 \qquad \text{kp} \qquad 3.25$$

The results of this calibration are shown in Fig 20. This offers the user an alternative method for measuring the joint preload should the use of a load cell become inconvenient because of the size or shape of the specimens.

3.10 Dynamic calibration of the test rig

This calibration aims at evaluating the auxiliary system parameters needed for equation 3.15 and 3.16 to obtain the specimen column parameters on their own. A solid specimen column was used and the required preload was applied. The test rig was then excited in its

first mode. Pure mode excitation was realised by forcing M_1 and M_2 to move completely in phase, a condition which was realised when the dynamic force $\bar{F}$ within the specimen column was almost zero. The test rig parameters were then evaluated as shown by equations 12.1 and 12.2 in appendix I.

The results of this calibration are shown in Figs 21,a, and 21,b. The system parameters (stiffness and mass), remained fairly unaltered as was reported in (41). The scatter of the viscous damping coefficient at higher preloads amounted to only ± 4.5% of its value found from the expression (41).

$$C_1 = 659 - 1.1\ x + 0.46\ x^2 \qquad 3.26$$

Whilst at lower preloads the above expression was in good agreement with the measured results.

3.11 Conclusions

The tests indicated that the test rig had an excellent degree of symmetry. During actual tests carried out on joints, it was always possible to achieve a pure second mode excitation within ± 5% for amplitude ratio and 3^{o} for phase difference.

The method of correction for the effect of the discs material also compensates for the presence of the load cell within the jointed column. Thus, the data reduced for the stiffness and damping of the single joint could be directly compared to the theoretical results obtained for the joint stiffness and damping from the information regarding its surface topography and material properties.

CHAPTER 4

DESIGN OF TESTS ON JOINTS

4.1 Introduction

The examination of the previous research work presented in Chapter 2 points towards the existing gap between the knowledge gathered from the experimental study of the behaviour of joints and the ability to produce a theoretical assessment for its stiffness. With this in mind it was decided that the present investigation should aim towards filling this gap by producing a reasonable theoretical model for the prediction of joint behaviour. This could then be employed by the designer to form some basis for the specifications made on the drawing. Therefore, plenty of experimental data should be provided in order to test the reliability of such a model.

4.2 Some factors which affect the joint behaviour

The experimental investigation presented in this work aims at studying some of the most important parameters that could influence the dynamic behaviour of joints. The parameters which were studied are:-

4.2.1 Joint preload

The results of tests carried out on actual machine tools (15), indicate that the majority of machine tool joints will be subjected to mean interface pressure which is very small when compared to the yield pressure of the material, i.e. 39 to 235 kp/cm^2. Thus it was decided that the present work should be carried out for joints loaded within

that range. The joint behaviour was examined at the following mean interface pressures:

20, 40, 60, 120, 160, 200 and 224 kp/cm^2.

These preloads would provide enough experimental points in order to properly describe the behaviour of the joint.

4.2.2 Surface Topography

The inability to manufacture smooth flat surfaces results in a reduction of the overall stiffness of jointed structures. Also, the difficulty in modelling the joint behaviour is a direct result of the difficulty in providing adequate description of its surfaces. Fortunately, the past ten years have seen the evolution of new methods and parameters for the characterisation of surface topography. The experimental work carried out in relation to this point was aiming at providing data for joints which have as a wide range of topography as possible. However, it was not precisely known which parameters in surface texture were most relevant to the joint behaviour. Moreover, no sufficient information was available on the relationship between various cutting conditions and the surface finish that could be achieved for the non-conventional texture parameters, i.e. radius of peaks, standard deviation of peak heights, etc. In choosing the cutting conditions for the specimens, use was made of the analysis in reference (46) in relation to turning. Nonetheless, such data seems to be insufficient on two counts. Firstly, they are not enough to exercise an efficient control on roughness (specially in case of operations other than turning). Secondly, there seems to be a general lack of information about flatness.

For the aforementioned reasons, it was decided that joints machined using a variety of cutting operations, under various cutting conditions, should be tested. The machining operations were:

1. Face milling : Joints having 1.893, 2.055, 0.850 and 2.373 μm CLA* were tested.

2. Shaping : Joints having 2.626, 5.286, 1.630, 4.728 and 1.802 μm CLA were tested.

3. Turning : Joints having 5.443, 2.604, 2.223 and 2.176 μm CLA were tested.

4. Grinding : Joints having 1.056 and 0.139 μm CLA were tested.

4.2.3 Viscosity of lubricant

Apart from testing the joints under dry, clean conditions, they were also tested when lubricated using the following set of oils:

1. Shell Tellus oil 15 : mid point viscosity at $40^{o}c$ = 15 cSt
2. Shell Tellus oil 23 : mid point viscosity at $40^{o}c$ = 22 cSt
3. Shell Tellus oil 71 : mid point viscosity at $40^{o}c$ = 220 cSt

In addition to the above mentioned lubricants, Shell Tellus oil 40 (100 cSt), simnia grease 0 (150 cSt) and a very heavy grease (its properties are not available) were tested.

*The values of CLA are the average for all the specimens in a specimen column in which all specimens are machined using the same operation and cutting conditions.

Because the use of lubricants in fixed joints as an aid to improve its dynamic behaviour is often objected to by doubts about the long-term performance of the lubricant layer, a test on the use of Hermetite as a layer between the joint interface was carried out. This involved testing the jointed column immediately after the application of Hermetite, and twenty days later another test was carried out to investigate the effect of time.

4.2.4 Other Variables

In addition to the above mentioned variables, the effect of apparent area of contact, number of joints in series, shape of the apparent area of contact, frequency and amplitude of vibration were also investigated.

4.3 Specimens: Material and Shape

All joints tested were manufactured of steel EN8. A circular form of the specimens was chosen for the following reasons:

1. It facilitates the inclusion of turning among other machining operations.

2. It eases the process of centring the specimens column onto that of the test rig, thus reducing the possibility of exciting unwanted modes during the dynamic tests.

The number of specimens in a jointed column was chosen to be ten. This number had to be large enough to lower the effective stiffness of the jointed column, yet, small enough to increase the frequency range of load amplification (Fig 8), and cut down the machining time

(41). The specimen column arrangement was as that shown in Fig 19,b.

4.4 Method of Manufacture

All groups of specimens were first parted off on a lathe. Their surfaces were then flash ground. This was mainly to standardise the condition of joint surfaces before producing the final required finish, since it was reported in (47) that the previous cutting operation could affect the shape of the peak height distribution for the next operation. (The peak height distribution was expected to have a significant effect on the stiffness of joints.)

The specimens were required to have a minimum amount of out of parallelism between their faces, as the presence of such an error would result in both non-axial loading of the specimens and deterioration in the ability to carry out pure mode excitation during the dynamic tests. Since out of parallelism error is mainly due to the way the specimens are held during machining, it was decided that all specimens should be held on a magnetic chuck (41).

The magnetic chuck was first secured on the machine table (on the machine spindle in the case of turning), shimmed and adjusted for minimum error of out of parallelism between the surface of the chuck and the tool holder, both in the direction of feed and perpendicular to that direction. A very small layer of the chuck surface was then machined (except in the case of shaping) to correct any further error which was left.

In order to increase the gripping force of the chuck magnet on

the specimen being machined, a fixture having the shape of a ring was manufactured and placed on the chuck. The specimen was to be placed on the chuck, and after applying the magnet, tightening screws were used to secure the specimen and the fixture into one body held by the chuck as shown in Fig 23. During machining of the specimens, a blast of air was used to drive the chip away from the surface being cut in order to prevent the possibility of chip interference.

4.5 Specimens for the study of the effect of surface texture

Every group of specimens (Fig 22) in a specimens column was marked off for angular position relative to each other. Each specimen was then secured on the chuck in a predetermined angular position with respect to the tool feed direction. The required finish was then produced according to the cutting conditions given in table 2. The specimen was then drilled, reamed and a recess was then made on the inner diameter to prevent the specimens making contact on the internal edge which might have suffered material rise during the cutting operation.

After machining, every specimens column was assembled on a mandrel, with the specimens having the same angular position relative to each other. The specimen column was then turned and cylindrically ground to the required outside diameter. Before dismantling the specimens they were remarked for angular position, then numbered for sequence.

Four specimens were surface ground on one side, and these were to be the ground ends of the specimens column facing both the mass

blocks of the test rig and the load cell in the middle of the column.

4.6 Specimens for the study of the effect of area

The successful study of the effect of area depends primarily on keeping the surface topography the same as the apparent area changes. For this reason it was decided that only one specimens column should be used for the study of this variable. A specimens column having the largest area under consideration (25.8 cm^2) was manufactured. The cutting operation was face turning. The cutting conditions were: 510 r.p.m. speed, 0.254 mm/rev for feed and 0.8 mm tool nose radius. These cutting conditions resulted in an average CLA of 1.83 μm. The machining procedures were the same as in 4.5.

After carrying the dynamic test for this column, the specimens were then mounted on a mandrel and the apparent area of the joints was reduced to 18.35 cm^2. Dynamic tests were again carried out for the new level of area after which the specimens area was reduced to 12.9 cm^2 and the dynamic tests were again carried out. The dimensions of the specimens for every stage of the experiment are given in Fig 24.

4.7 Specimens for the study of the effect of planform shapes

The effect of the shape of apparent area of contact was studied for three different shapes. The shapes chosen were square, triangular and circular as shown in Fig 25.

The specimens were first drilled and reamed, then parted off on a lathe. They were then flash ground on both sides. Every specimen

was located on the centre of the rotary table of an optical jig-boring machine, and the required shape was cut according to the dimensions in Fig 25. Before dismantling the specimen, a locating groove was machined on its side to facilitate assembling the specimens into a specimens column with all shapes aligned to each other.

The next operation was to give the shapes a ground finish while the other side of the specimen was face turned using the same cutting conditions in 4.6. During machining the surfaces of the specimens, attempts were made to minimise deviations in surface texture. This was done by machining a specimen of one shape followed by a specimen of another shape, and so on. Every group of specimens was then assembled on a mandrel and the outside diameter of the column was cylindrically ground to the final diameter specified. The specimens so produced had an average of 1.8 and 0.4 μm CLA for the turned and ground surfaces respectively.

4.8 Specimens for the study of the number of joints

By keeping the overall length of the specimens column constant while changing the number of joints within that length, it was possible to monitor the dynamic behaviour of the jointed column as the number of joints changes. 4, 8, 12 and 16 discs were examined. The dimensions of the specimens are given in Fig 26. The surface machining was face turning using the same cutting conditions in 4.7. The average value of roughness CLA was 1.78 μm.

C H A P T E R 5

SURFACE TOPOGRAPHY: MEASUREMENT AND ASSESSMENT

Given the undeniable role of surface topography in relation to contact problems, our concern in the present Chapter is two-fold:

1. How to measure surface topography.
2. Which parameters characterise surface topography.

Surface topography has been examined only through its significant role in deciding the state of contact between machined surfaces. Thus, no reference has been made with regards to its importance in a wide range of problems, both in engineering and other branches of science.

This Chapter falls into two sections:

Section 1 : Describes the measuring system established to facilitate the measurement and evaluation of machined surfaces.

Section 2 : By examining some of the key works which specifically dealt with the link between surface texture and contact problems, it was possible to form an idea about the way in which the surface could be assessed in a way most relevant to the study of joints (within the bounds of the state of knowledge). The next step was to describe the numerical evaluation of various parameters used in the assessment.

Before going into the details of the measurement and assessment of machined surfaces, it is necessary to clarify the difference between the terms 'TOPOGRAPHY' and 'TEXTURE'. According to the British Standards BS1134 : Part 1 : 1972, surface texture is defined as follows:

> "Surface texture. Those irregularities with regular or irregular spacing which tend to form a pattern or texture on the surface. This texture may contain the following components:
>
> (a) Roughness. The irregularities in the surface texture which are inherent in the production process but excluding waviness and errors of form.
>
> (b) Waviness. That component of surface texture upon which roughness is superimposed. Waviness may result from such factors as machine or work deflection, vibrations, chatter, heat treatment or warping strains."

The BS1134 does not define the term "Topography", but makes the following statement (Page 3 of BS1134 : Part 1 : 1972) under the heading 'scope':

> "This part of this British Standard relates to the topography of machined and self-finished surfaces ..."

The title of the BS1134 is: "Method for the Assessment of Surface Texture", and Part 1 is entitled "Method and Instrumentation".

Thus, in this investigation the term TOPOGRAPHY has been used to indicate the shape of any type of deviations from the nominal surface. The term TEXTURE means that part of topography which is actually measured and assessed in order to characterise Topography.

Section 1

The measurement of surface texture

5.1.1 Introduction

The dependence of a wide range of engineering problems on surface topography led to an increasing demand for a more comprehensive way in its assessment. Thus, the practice in surface roughness assessment can be classified under two categories:

1. The workshop practice.

2. The research practice.

In the workshop, a direct reading on the meter of the surface roughness measuring instrument is often used to assess the extent of roughness of the surface under consideration. An example for such a method of assessment is the widely used CLA value. The user is rather limited to whatever parameters are given by the meter, irrespective of the function of the component. Should any newly discovered parameter prove to be more useful, the user cannot simply use it without going into some expense to modify his instruments.

Because of the obvious limitations of the above method, researchers made use of digital computers (47). The measured profile is transformed into a digital form that could be stored in the computer memory or on a peripheral device. Thus, the researcher could have the choice of computing any new surface texture parameters, together with any classical ones, and in accordance with his exact specifications.

The versatility and powers of the digital technique were demonstrated by the ability to produce computer maps (48) that describe the development and change in the true area of contact at successive stages of plastic deformation of two rough surfaces as shown in Fig 27.

In the current work, use was made of the digital technique in order to enable the computation of surface parameters which were thought to provide a rather more adequate description of the surfaces of machine tool joints. The surface measuring system used consisted of a Talysurf* 4 which was linked to a Micro Nova computer. To establish the link, the output from the Talysurf was fed to an analog-to-digital converter which digitised the signal, and the output data was stored via the computer on diskettes. The successful establishment of this system requires some understanding of both the way the surface profile is produced using the Talysurf, and the way the analog-to-digital converter performs the digitisation process. The present section describes how the system was established.

5.1.2 The Talysurf output

The Talysurf is a stylus measuring instrument that operates in a similar manner to a gramaphone, where a sharp pointed stylus traces the profile of surface irregularities. The pick-up is an inductive transducer (49) connected in a bridge circuit in which the vertical movement of the stylus modulates a carrier wave form. The signal is amplified, demodulated and used to operate a recorder. This signal is

---

*The Talysurf is the trade name of Rank Taylor Hobson's surface roughness measuring instrument.

not normally available on a separate lead for special manipulation (e.g. digitisation or monitoring the output on an oscilloscope). After contacting the manufacturing company, it was suggested that the output could be branched from the auxiliary socket on the back of the electronic unit. A co-axial cable was permanently connected to positions P and EE shown in Fig 28. The output on this extra lead is symmetrical around the ground, ± 1 volt represents the full scale deflection on the graphical unit at any magnification. This output is the analogue of the stylus movement relative to a datum from which measurements are made.

5.1.3 Datum of measurement

The electrical signal from the pick-up represents the relative movement between the stylus and the pick-up body. In order that this signal be truly representative of the surface profile, the pick-up body must travel a path parallel to the general shape of the surface. The way to achieve this is to use a straight line datum against which the pick-up would travel in a straight line whilst the stylus tip follows the surface irregularities. The voltage output will then be proportional to the variation of heights of these irregularities with respect to the datum. This method involves tedious adjustment of the datum (particularly at higher magnification) in order to avoid set-up errors Fig 29. It might be relevant at this stage to point out that for production use it is customary to use a skid which carries the body of the pick-up and follows the general trend of the surface (the skid must have a large radius in comparison with texture spacing). The skid provides a serviceable datum only if roughness crests are close enough together. In Fig 30 it is shown how the vertical

movements of a skid traversing a periodic specimen can combine with those of the stylus, in phase, out of phase, or in an intermediate phase, giving the reading minimum, maximum or nearly correct value respectively (50). The skid system would not be generally suitable for digital techniques of measurement due to the following reasons:

1. The quantity measured by the stylus is the change in its vertical separation with respect to the skid. Thus, up and down movement of the skid will be reflected as a part of the profile being measured.

2. The skid acts as a mechanical high pass filter; thus the texture being recorded is not an exact duplicate of the actual surface profile.

3. The skid might cause surface damage.

For these reasons, a straight line datum was chosen as the datum from which measurements should be carried out.

5.1.4 Output manipulation

Perhaps the reason for the widespread use and popularity of the stylus instrument is the versatility of its output. The electrical signal could be plotted on graph paper or manipulated in one or more devices to yield many parameters describing the surface. Most important of all, it could be digitised and stored in digital form for immediate or later manipulation.

The computer which was made available for this work consisted of

16,000 words of user's memory; around 8,000 of those are occupied by the disk operating system, while the rest are available for the program and data storage. The machine has a dual floppy disk drive. The master drive would normally carry the operating system, while the second drive is available for making records of data and programs on diskettes. A Teletype is available as a means of communication between the user and the machine.

5.1.5 The digitisation unit

The computer is fitted with an analog-to-digital (A/D) interface board as a subsystem that enables the micro nova to read digitised data from an external analogue measuring device. It operates with voltage ranges of 0 to 5V, 0 to 10V, ± 5V and ± 10 Volts, which are hardware selectable, and provides data with a resolution of 12 bits. The subsystem employs a multiplexer allowing software selection of one of sixteen input channels. As only one channel sampling was required, channel zero was software selected and used for all subsequent sampling.

Sampling is performed on the pulse of an internal clock generated by an R/C integrated circuit square-wave oscillator. The "R" is a multi-turn potentiometer with screw-drive adjustment for controlling the sampling rate. The use of this clock would involve the connection of a frequency counter to monitor its pulse rate frequency. As the board could be software instructed to accept the commands of an external clock, a solartron crystal controlled digital frequency analyser, whose generator output could be programmed to any required

frequency (from 0.1 Hz to 9.999 kHz) was used as an external clock source. The square-wave generated by the analyser, being symmetrical about the ground, was fed into an integrated circuit interface (shown in appendix III), which translates it to the logic level required for the external clock option on the A/D board. This frequency source enabled the sampling rate to be both rapidly changed and accurately controlled.

Because the output level of the signal from the Talysurf was ± 1 volt, thus, incompatible with the voltage levels acceptable to the A/D board, an interface unit had to be built in order to transform the ± 1 V range into 0 to 10 V. The details of the interface circuit are shown in appendix III. Within the interface unit, the output from the Talysurf was first multiplied by 5 and then added to 5 V to give the required range of 0 to 10 V.

5.1.6 Some considerations in the measuring setup

The discussion in 5.1.3 has been based upon the assumption that the pick-up would travel against a stationary specimen. A gearbox unit available within the Talysurf system provides a constant speed drive of the stylus pick-up. The maximum traversing length that could be made in this way is limited to 11 mm. This traversing distance is adequate for roughness measurements provided that the computer could be instructed to start sampling shortly after the pick-up starts its motion (to avoid any transients and to ensure that no sampling has been carried out while the stylus was stationary). Sampling should also stop shortly before the pick-up reaches the end of its traversing

length for the same reasons as before. Such procedures are possible only if:

1. The stylus speed is very slow, i.e. 3 mm/min so that the motion of the stylus could be manually started via the gearbox, shortly before an order is given to the computer to start sampling. The overall sampling time must be safely estimated so that the machine stops sampling before the pick-up reaches the end of its traverse length.

OR -

2. A control unit could be made to fit on the gearbox unit so that the stylus would start motion after receiving a signal from the computer. Sampling would then start and terminate before the pick-up stops.

The first option above was not suitable for the following reasons:

1. The human coordination with the machine would be difficult to achieve, and it was expected that such a method would result in a large number of redundant measurements (due to loss of concentration).

2. The time taken in making a single roughness trace would be as large as 3.66 minutes and this is added to the time needed to set up the datum and the specimen.

3. The distance over which measurement could be made cannot be much more than 9 mm, since almost half a minute should be allowed to the operator between manually starting the gearbox and giving the instruction to the computer to

start sampling.

The implementation of the second option (although necessary for any similar system) was not considered economical in view of the temporary nature of the measuring setup.

Both options referred to above, also suffered from the limitation regarding the maximum traversing length (11 mm) which was only suitable for the assessment of surface roughness. Should waviness be measured using the same apparatus, some means had to be devised in order to extend the length of the trace. Fortunately, an air-supported measuring carriage of the type "Talytron S 150", manufactured by FAG company specially to permit larger traces to be made using the Talysurf was available. By aid of the air-supported carriage, the workpiece can travel under the stylus whilst the pick-up body is held firmly without any movement (see Fig 31). When travelling all its way of 150 mm, the carriage deviation from nominal is not more than 0.1 µm. The carriage is driven by a synchronous motor at speeds varying from 0.3 mm/min to 300 mm/min. Its movement is free from friction and vibrations according to the manufacturer's specifications.

This method of measurement appeared to be most suitable for making roughness and straightness traces using the same apparatus. As the datum from which measurements are made is now created by the table motion, the error of 0.1 µm over 150 mm was not objectionable, since the measured data would contain also set-up errors, these errors would then be taken care of during processing. Other objections for the use of an air-bearing table could arise from:

1. The fact that the measuring datum is created by the table motion, means that any vibrations will be included in the measured profile.

2. The accuracy of the table speed.

As for the first objection, measurement of the noise level from the floor and table were equal to the level from the floor only (i.e. with the table off). The table speeds could only be checked using higher quality apparatus (51) which were not available, and it was assumed that its speeds were correct. In general, any argument regarding the table speed could be as well applied to the Talysurf gearbox speeds.

N.B. Taylor Hobson market the Talytron table as an accessory to their advanced Talysurf range.

5.1.7 The measuring system

The hardware elements of the measuring system consisted of an air-supported measuring carriage which enables the specimen to travel under a stylus attached to a Talysurf 4 pick-up. The demodulated signal from the pick-up, being ± 1 V, is fed into an A/D converter through an interface unit which transforms its voltage range into 0 to 10 V.

A software program is used to control the A/D converter, manipulate the sampled data and synchronise the operator's interference according to the following procedures:

1. The operator switches on all instruments, sets up the

sampling rate and loads the main program.

2. The operator then sets up the specimen to ensure that the movement of the stylus is kept within the range of the chart all through the length of traverse.

3. The operator gives the computer the information requested by the program, starts the table motion and presses carriage return "CR" on the Teletype. The computer will then start sampling and when finished, informs the operator who can then stop the table motion and attend to the setting up of a new specimen. Meanwhile, the computer will carry out the necessary manipulation of data, reload the main program and wait for the operator's information.

Fig 31 is a general view of the measuring system and Fig 32 is a block diagram for the overall system.

5.1.8 Software structure

The operating program consists of a main routine written in a high level language (FORTRAN). The routine reserves a common array in memory where the digitised samples could be sequentially stored. It starts by setting all the array elements to zero. The program then requests some information from the operator depending on the type of measurement. After receiving the operator's order to start sampling, the program delivers the control to a subroutine "COVRT" which is the means of communication between the A/D converter and the computer. After all samples have been made and stored in the common array, "COVRT" delivers the control back to the main program which informs

the operator and carries out data manipulation. Three such operating programs were written:

5.1.8.1 The calibration program "GAM"

During the operation of "GAM" the Talysurf output was simulated by a precision DC voltage source which could be set up to produce any voltage between ± 0.9999 V. The program "GAM" would then enable the computer to measure five samples (to simulate an array of profile informations), and print them out. Comparison between the known input and the computer output leads to:

1. Verifying the correct functioning of the logic of the software structure as described in 3.1.8.

2. Verifying the correct functioning of the sampling subroutine "COVRT".

3. Checking on possible errors in both the interface unit and the A/D converter board.

The following is a flow chart for "GAM":

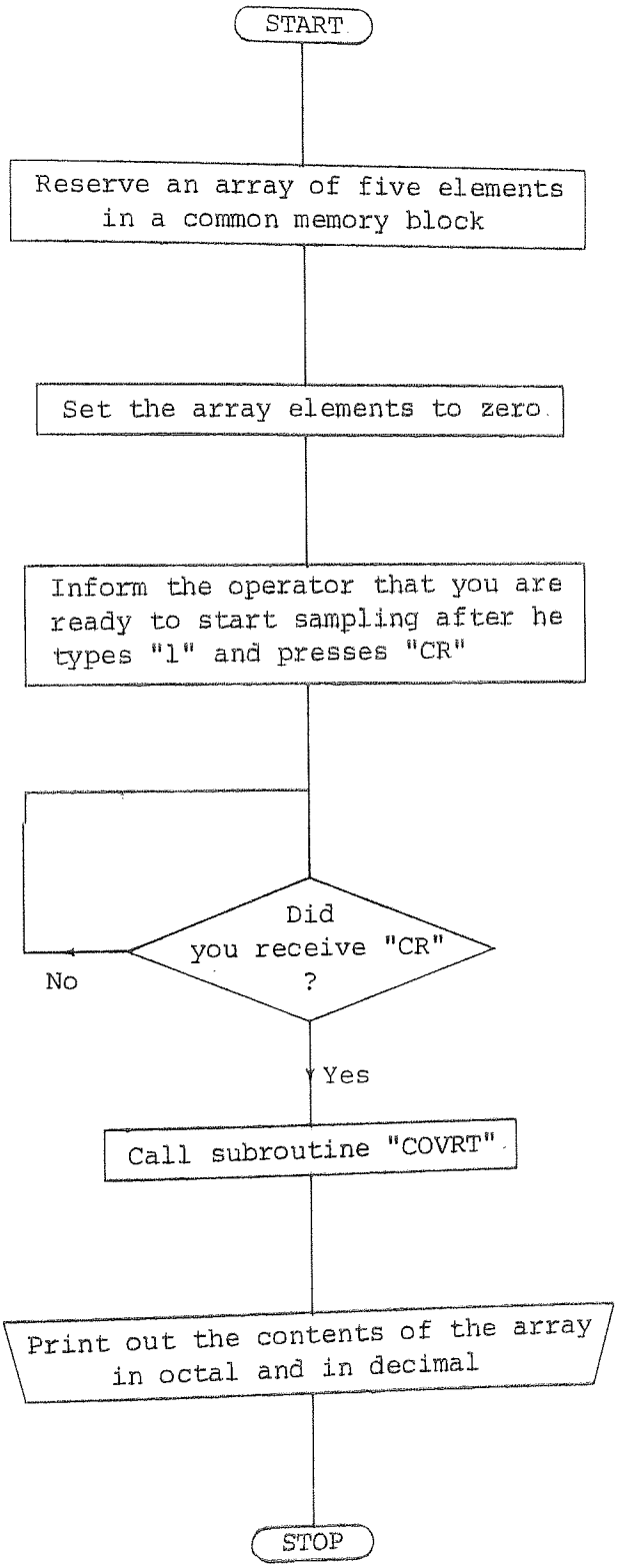
START
Reserve an array of five elements in a common memory block
Set the array elements to zero
Inform the operator that you are ready to start sampling after he types "1" and presses "CR"
Did you receive "CR" ?
No
Yes
Call subroutine "COVRT"
Print out the contents of the array in octal and in decimal
STOP

5.1.8.2 Roughness measuring program "SURFACE"

The program "SURFACE" creates and initialises a 3,200 locations array in a common area in the computer memory. The program then requests the following items of information:

1. The specimen name.
2. Talysurf magnification (vertical magnification).
3. Number of samples per cut-off length.
4. Sampling length in microns.

Having received the requested information, it interprets the "CR" (pressed after the reply to the last request) as an order to start sampling. Control will then be transferred to "COVRT" which will carry out the digitisation of the surface roughness profile by measuring 3,200 samples at the specified sampling interval and storing the measured samples in the common array. When sampling ends, "SURFACE" will first inform the operator, then opens a disk file and names it after the specimen. On the file, it writes the vertical magnification, number of samples per cut-off, the sampling length in microns and then all the sampled data in sequential order. The storage of roughness samples on a disk file was needed because it was not possible to include the assessment of roughness in the same program due to memory limitations.

5.1.8.3 Waviness measuring program "FLAT"

The program "FLAT" creates and initialises a 150 location array and asks for the following information:

1. Waviness trace number.

2. Talysurf magnification.

"COVRT" will sample the profile as before and when it finishes, "FLAT" will give the message "Sampling Ended" and carry out the assessment of the waviness trace as will be described in 5.2.5. It then prints out the results and stops. Control is then delivered to a computer macro which instructs the computer to load the program again for the next waviness measurement.

5.1.8.4 Subroutine "COVRT"

On calling "COVRT", the A/D converter board will be set up according to the instruction "SETUP : 17,000", that is:

1. Sets itself in data channel mode, i.e. the sampled data is transferred to the computer memory automatically after each conversion.

2. Carries out a conversion every time the external clock pulses.

3. The signal to be sampled is supplied on a single ended channel.

4. The signal to be sampled is supplied on channel number zero.

The setting up also includes:

1. Loading the work counter with the two's complement of the number of conversions to be triggered (instruction "COUNT").

2. Loading the memory address counter with the starting address of the memory block selected to store the results.

After establishing the setting up, the board will start sampling every time the external clock pulses. This process continues until all the samples have been measured. The routine will start adjusting the numbers stored in every word into a meaningful form to the computer. The reason for this is that the A/D board produces 12 bits numbers which are ill-positioned in the 16 bits computer word. To correct this the program loops on the number of samples shifting every word four places. When this process ends "COVRT" delivers the control back to the main program.

Complete listings of the programs: "GAM", "SURFACE", "FLAT" and the subroutine "COVRT" are given in Appendix IV.

5.1.9 Some sources of error in the measuring system

The fact that the measuring system consists of high quality instrumentation calls for extreme care during the use of these instruments. The temperature and humidity control in the laboratory provides protection for both workpiece and instrument against violent thermal changes that could seriously affect the values being measured. One should always remember the fact that when dealing with a fraction of a micron, any error, although negligible under ordinary conditions, could be significant.

The following are some of the sources of errors pursued wherever the facilities and knowledge permitted.

5.1.9.1 Errors due to vibrations

The Talysurf with its high magnification and low stylus force is effectively a seismic instrument (52). It feels and records vibrations transmitted through the floor to both the specimen and the stylus. This calls for its protection against vibrations. In order to check the level of vibrations recorded by the Talysurf, the stylus was lowered to contact a stationary workpiece. When the recorder pin was in the middle of the chart, the electrical output of the instrument was monitored on an oscilloscope. As the scale on the screen was increased it was possible to estimate the number of milli-volts induced by vibrations. As the magnification on the electronic unit increased, the amplitude of the output on the screen increased linearly.

It was found that the Talysurf in its normal position (mounted on a wooden bench) and during the normal working hours, gave between 50 to 60 mV at magnification 5000. Thus, it became clear that even with 50 mV error, the measured profile would contain an error of 7.5% on the account that it would normally occupy one third of the chart. As expressed earlier, the error linearly increases with magnification while the output range of ± 1 V is constant irrespective of magnification. Thus, it could be said that under no circumstances a magnification higher than 20,000 should be employed while the machine is at this position, since the error due to vibrations could almost be 0.25 V, i.e. 12.5% of the full scale. It should also be mentioned that outside working hours this error reduces to around 20 mV and even lower. This appears to be dependent on the amount of activities in and outside the building.

It was decided that the Talysurf should be moved to a rigid table, and for this purpose a large surface plate was used as shown in Fig 31. The level of vibrations monitored at the new position was around 20 to 30 mV at magnification 5,000. During the actual measurements, magnifications higher than 10,000 were never employed.

5.1.9.2 The stylus tip dimensions

In any stylus measuring instrument the measured profile will not be an exact representation of the true surface profile. Distortion of the measured profile due to the finite stylus tip dimensions is always present to some extent. The stylus acts as a low-pass filter. Thus, it limits the sensible measurement of very short wave lengths (53, 54). Various arguments (55) relating the tip dimension to sampling interval are possible. Since sampling intervals within the stylus dimensions are highly correlated, it is advised that sampling should only take place at intervals greater than the stylus size. Or, since the stylus dimension approximates to a filter cut-off, the Nyquist rate, which is about half that size, could be used as the sampling interval. Difficulties over such choices are usually compounded by inadequate knowledge of the stylus dimensions; even if its manufactured form is known, the initial use would cause some change of the shape and thus its effective size. Reason (50) describes how the stylus could be checked by using a specimen having fine calibrated V-grooves that the stylus cannot fully enter and comparing the meter reading (CLA) with the reading written on the specimen. This method will indicate a worn stylus but says nothing about its dimensions.

The exact profile of the stylus could be measured using a microscope, but it is not practical since the stylus has to be dismantled from the instrument. A sharp edge which traces the stylus could be employed in order to obtain a record of the shape of the stylus. A razor blade could be used (56) as it has a small radius of about 0.1 μm and a steep flank angle of almost 80°. It has been found (56) that when such an edge traces a stylus of curvature larger than 1 μm and a flank angle between 30 - 40°, the trace obtained will be representative of the stylus tip dimensions. This method was employed in the manner described below (see Fig 33,a).

A razor blade was firmly mounted between two steel blocks close to its edge (about 0.5 mm below the top edge) in order to guard the blade against bending under the stylus force. The blade was permitted to travel under the stylus with the aid of the Talytron table which was set at its lowest speed of 0.3 mm/min, thus offering a horizontal magnification on the chart which could be found from

$$\text{Horizontal magnification} = \frac{\text{Chart speed}}{\text{Table speed}} = \frac{305}{0.3} = 1016$$

The vertical magnification of the Talysurf was set at 1,000 so that the resulting traces (shown in Fig 33,b) suffered minimum distortion.

Fig 34,a, shows the profile of the stylus normally attached to the Talysurf, and which would have been used in this investigation if this check was not carried out.

Fig 34,b, shows an almost unused stylus (the recess stylus)

which was used for the roughness measurements in this work.

Comparison between Figs 34,a, and b, reveals that the stylus shown in "a" has suffered a significant amount of wear which might seriously affect the measurement. When the worn stylus was used to measure the CLA value for a standard roughness sample, the computed reading was 16% lower than the one obtained using the unworn stylus. It is clear that the profiles measured using the worn stylus will be distorted. Thus, its peak curvature, slope, peak count and height distribution will be different from those measured using a sharp stylus, depending on the nature of roughness of the surface being measured. The CLA meter reading using a worn stylus cannot be accepted as a reliable reading even when the meter was calibrated using a worn stylus. Measurement of the same component using a different machine will almost certainly result in a different value of CLA.

5.1.9.3 Digitisation errors

Errors due to digitisation could be either errors in the sampling interval or due to quantisation. The former could arise from errors either in the Real-time clock or in the speed of traverse.

$$\text{Sampling interval} = \frac{v \times 10^3}{60 \times f} \quad \mu m$$

Where: v = traverse speed in mm/min

f = clock frequency in Hz

Due to the high quality of the instrumentation used, no equipments were available for calibrating either the Talytron table speeds or the

frequency generated by the frequency analyser. On the other hand, there was no evidence that such errors were present. When a standard workpiece was measured using the system described earlier, the CLA reading did not deviate more than 1.14% compared to the value written on the workpiece.

Quantisation is a term which refers to the accuracy at which a sample is measured. The sensitivity of the A/D converter is related to the number of bits used by the board to measure the samples. It could be easily found from

$$\text{the A/D converter sensitivity} = \frac{\text{the range in volts}}{2^{B}} \quad \text{volts}$$

Where B is the number of bits of the A/D board excluding the sign bit whenever applicable.

Thus, for a voltage range of 0 to 10 V and 12 bits A/D board, the above equation gives

$$10 \times 10^{3} \times \frac{1}{2^{12}} = 2.44 \text{ mV}$$

This value represents 0.488 mV change in the output of the Talysurf. It can be seen that whenever the stylus experiences a displacement resulting in a change in the output voltage less than 0.488 mV, then this change cannot be properly quantised by the A/D board resulting in what is known as quantisation error. In general, A/D converters having ten or more bits are suitable for this kind of application (at 10 bits, the full scale of the chart is divided into 1024 parts).

5.1.9.4 Calibration and verification of the measuring setup

Calibration of the interface - A/D converter arrangement was carried out as follows:

A standard DC voltage source was used to input a known level of voltage into the input terminal of the interface. The program "GAM" was employed and a print-out for the digitised signal as measured by the computer was obtained.

For an input voltage X to the interface, the output Y is given by

$$Y = 5(1 + X) \qquad \text{volts}$$

The computer reading L should be

$$L = \frac{4096}{10} (1 + X)5$$

The maximum value of error was found to be less than 1.5% of full scale reading. The errors were mainly due to the necessary addition of the interface and take the form of a DC off-set which would have no consequence on the measured profile. The variable component of error was indeed very small, i.e. less than 0.1%. The results of this calibration are given in table 3.

The successful running of the program "GAM" indicated that the programming policy adopted was correct, and it also verified that the important routine "COVRT" was functioning satisfactorily.

So far, checking and calibration of various elements of the measuring system has been described. The next step was to check the overall system in a real measurement. This check could only be made by

measuring some known quantity and comparing the results. For this purpose, a standard workpiece of 0.87 μm CLA was measured using "SURFACE". The digitised profile was processed as will be described in the next section. It was found that the CLA reading computed digitally was 0.88 μm which was the average of 5 measurements. The error of 1.15% was considered small and well within the permissible instrumentation error.

Now that the measuring system is fully prepared, work could progress towards the more difficult task of assessing the profiles being measured. This will be fully examined in the next section.

Section 2

Assessment of surface texture

5.2.1 Introduction

Because roughness is a direct consequence of the cutting tool action, its assessment and control represent an effective way by which the machining process can be studied. This explains why roughness was that part of surface topography which received the most attention, while waviness, which is neither observed by the eye nor is directly related to cutting conditions, remains unspecified.

The well known classification of texture into roughness, waviness and form errors has no functional justification. Mathematically, however, a profile which contains the overall spectrum is classified as a non-stationary function, which is rather difficult to assess (57). On the other hand, since the only medium through which loads on joints are transmitted is their surface topography, there is no doubt that texture with all its components will determine the mode and extent of deformation.

A flat surface might contain form errors in the sense that the component might be slightly bowed and/or its top is not parallel to its base. Out of parallism might change the type of loading on the surface, i.e. a joint which was assumed to be subjected to pure normal loads would experience a tangential component of loading as shown in Fig 35. In fact, there appears to be no such term as "pure normal loads"; the degree of normality will depend on form errors on both mating surfaces.

Holding the specimens on a magnetic chuck during machining was the means by which attempts were made to minimise out of parallism between the surfaces of the specimen. Form errors of other types have been integrated into waviness, similar to the practice used with circular components where form errors are integrated with waviness and the product is termed out of roundness.

5.2.2 Which surface texture parameters to measure and why?

Early work in contact assessment aimed at reaching a rational explanation for Amontons' law of friction which stated that the friction force was proportional to the load and independent of the apparent area of contact. Holm (58) emphasised the crucial fact that when surfaces come into contact the true area of contact is small and the pressure over this area is high. Bowden and Tabor (59) argued that because surfaces contain asperities having small radius of curvature, the true area of contact arose from plastic deformation of their tips. This area is given by $\frac{W}{H}$, where H is the hardness of the softer metal. Adhesion, which occurs between plastically deformed asperities, was then responsible for the friction force which arose from shearing the junctions. Thus, the force of friction must be proportional to the area of contact which is, in turn, proportional to the load. It can be seen that surface roughness was introduced to ensure that the deformation was plastic (60), apart from that it has no effect on the true area of contact.

The observance of asperity persistence (61), and the failure of the above theory to explain how plastic deformation could be sustained between surfaces where rubbing took place, led Blook (62) to suggest

that under certain conditions surfaces could make elastic contact, provided that

$$\frac{h}{\ell} < \frac{2}{\pi} \frac{H}{E'}$$

Where h is the peak to valley height of asperities and ℓ is their spacing.

This work lead Halliday (74) to examine surface slopes using electron microscopy. He concluded that Block's criteria for elastic deformation should be modified to

$$m < k \frac{H}{E'}$$

Where m is the average surface slope and k is a constant.

Since then, surface texture started to play a much greater roll in the study of contact and wear problems. The elastic theory of contact, though successful in explaining some of the observed behaviour during wear tests, failed to arrive at a proportionality between load and true area of contact, which is necessary for the explanation of the law of friction.

It was Archard (64) who pointed out that although plastic flow could be expected to occur on the first few passes of two contacting parts in relative motion, it would not continue indefinitely; some equilibrium state would occur when the asperities could support the load elastically. Using a model of spherical protuberances as shown in Fig 36, he showed that as the model contains more small scale of size asperities, the relation between area and load became nearer to direct

proportionality. The importance of Archard's work was in pointing out that the source of deficiency in theoretical approaches was not the assumption of elastic deformation, nor was it the modelling with spherical peaks, but the way surface texture was presented in the model. As the representation of texture in the model became nearer to the actual surface, the load became more proportional to the area of contact and Amontons' law could be explained using a purely elastic model.

Thus, it became known that for any reliable study of contact problems, the classical parameters, like the CLA or the peak to valley height, were inadequate for the establishment of a coherent contact theory. Ling (65) explored the use of a probability distribution function for the heights of surface asperities having conical shapes. Pesante (66) proposed an assessment of surface roughness using the amplitude density function and the bearing area diagram. He went on to show how the shape of the bearing area diagram and the amplitude density function changed with the machining operations.

Reason (67) suggested the use of a consolidated surface waveform obtained from the bearing area diagram. He also suggested that the crest spacing should be taken into account by drawing the consolidated profile with a crest spacing nominally equal to that of the orignal profile. Schofield and Thornley (22, 23) used Reason's idea in a theoretical and experimental investigation of machine tool joints. Moreover, they extended the model to accommodate the presence of flatness deviations on the surface (24). They found that the more random the surface, the less reliable the model.

The impact of the introduction of digital techniques for measuring machined surfaces, appears in the work of Greenwood and Williamson (68), who were among the first to use this technique. By examining the shape of the peak height distribution for many machined surfaces they came to the conclusion that even surfaces which do not have Gaussian distribution of heights appear to display Gaussian distribution of peak heights. They went on to build a model of the surface (typical of those produced by finishing operations) which consisted of spherical asperities having the same radius of curvature (the average of the radii of asperities measured from the profile) and a Gaussian distribution of peak heights (description of their theory is given in Chapter 7).

A first look at a surface profile trace will reveal that it contains various scales of size peaks. In (68) a peak was defined when the central ordinate of a set of three was higher than the other two. But this definition suffers from a serious drawback (69) because it is dependent on the sampling interval at which the profile was digitised. If the sampling interval is 1.5 μm, a peak will occupy only 3 μm on the horizontal scale. Thus, peaks which occupy more than that might not be considered (see Fig 37).

Whitehouse and Archard (53) argued that the Greenwood-Williamson (G - W) model was over simplified because it took no account of the existence of superposed asperities of different sizes. They went on to show that the sampling interval will affect the computed mean radius of curvature. They proposed that the surface profile could be treated as a random signal. The profile was then assumed to have a Gaussian distribution of height and an exponentially decaying

autocorrelation function. The sampling interval at which the autocorrelation function decays to 0.1 of its original value (its value at very small sampling intervals) was defined as the interval at which the ordinates of the digitised profile will be statistically independent. Thus, curvatures measured using this interval would reveal the main structure of the profile, while shorter sampling intervals would reveal only the fine scale structure. Onions and Archard (70) extended the above approach into a theory of contact and arrived at essentially the same results as for G - W theory.

The dissatisfaction with the use of a single parameter in describing surface roughness led Spragg and Whitehouse (71) to propose a two parameter way for the specification of surface finish. The existing CLA would be combined with an average wave length parameter which they called "average wave length index".

An alternative approach in describing random surfaces was presented by Longuet-Higgins (72). Nayak (73) pointed out that this approach could be used in the description of a class of machined surfaces which are isotropic and have Gaussian distribution of heights. The theory (known as the random theory) simply states that all the information necessary for the analysis of a random isotropic and Gaussian surface are contained in the power spectral density (PSD) of a surface profile measured in an arbitrary direction. The higher order surface statistics (slope and curvature) are dependent on the first three even moments of the PSD. The zero moment is the variance of the profile heights, the second moment could be obtained by counting the number of zero crossings of the profile with its mean line and the fourth moment from counting the number of peaks. The theory was used

by Nayak (74) in a study of plastic contact and by Bush (86) in a study of the elastic contact.

According to Williamson (76) surfaces which have Gaussian distribution of their roughness heights, arise from cumulative machining processes such as spark erosion. Turning, shaping and milling (which are the types of machining operations examined in this work) are processes that create surfaces which are definitely non-Gaussian, yet, the distribution of peak heights is often closely Gaussian. This class of surfaces will not produce an exponential autocorrelation function as the model in (53) requires, nor do they have Gaussian distribution of heights as the random theory requires.

In the specific problem of contact in machine tool joints, flatness deviations will always be present. Such surfaces are difficult to treat using the random theory because their profiles are classified as non-stationary. Greenwood and Williamson (77) emphasise that it is not correct to ignore waviness except in the ideal experiment of bringing together two parallel nominally flat surfaces. It is also most certainly incorrect to ignore any overall curvature that might be present on the surface as form error.

Apart from the analysis in (23), no consideration was given (by the theoretical approaches) to the real form of flatness errors on joints' surfaces. More recently, however, Thomas and Syles (78) suggested that since shorter wavelengths on the surfaces of joints would suffer plastic deformation, the surface profile should be filtered to eliminate these wavelengths. They futher suggested that it should be filtered to eliminate any wavelengths that are longer than twice the

longest dimension on the joint surface. The remaining part of the profile was then assumed to have a Gaussian distribution of heights and an exponentially decaying autocorrelation function. They then combined the random theory with the G - W theory to arrive at an expression for the stiffness of joints.

The above method of treatment pays no attention to the physical characteristics of contact in machine tool joints. Apart from the questions that could be raised about the validity of the assumptions concerning the shape of surface profile after filtering, the basic objection to the above approach is that this part of roughness which was filtered is the major source (if not the only source) of elastic behaviour of joints (see references 14, 16, 21 and 79). Furthermore, very small roughness asperities could persist and resist plastic deformation (80); thus, instead of being crushed, they display elastic behaviour which cannot be ignored.

Stout (81) suggested that the skewness and kurtosis of the height distribution are useful in predicting the functional behaviour of the surface (no experimental evidence was given). Whitehouse (82) argues that those parameters are not discriminant between widely different machining operations. In addition to providing the experimental evidence, he gives two alternative parameters based upon fitting a beta function to the amplituded distribution. His experimental results seem to confirm his argument; nonetheless, more experimental confirmation about the usefulness of these parameters, specially their relation to functional behaviour, is still awaited.

Considering the specific problem of contact in machine tool joints, the choice of texture parameters which might be useful in describing the joint surfaces should be made along the following guidelines:

1. Together with the classical roughness parameters, a complete specification of height distribution is necessary.

2. The autocorrelation function might not be useful for a particular class of machined surfaces; nonetheless, past experience tells us that a width parameter should be included.

3. For the study of contact behaviour, the above survey reveals that information regarding slopes, peak curvature, number of peaks and peak height distribution could prove to be useful.

4. There is an urgent need to define, measure and assess waviness in a form which permits its inclusion into any mathematical model describing the joint stiffness.

5.2.3 Numerical analysis of surface roughness

The system described in section 1 was employed in digitising roughness traces and storing every trace on a disk file. Every roughness trace consisted of 3,200 samples, two independent traces per specimen were made, one on every face. Since a jointed column consisted of 10 specimens (see Chapter 4), the average roughness information was obtained from 16 independent roughness traces represented by 51.2×10^3 samples. For every specimen column tested, there was a

separate diskette which contained information about surface roughness of every specimen within the column. The full pattern of the numerical assessment of roughness will emerge from the following procedures.

5.2.3.1 Equation of mean line

The digitised profile contains unwanted long wavelengths which have to be removed. It will also contain some residual tilt due to the lack of alignment of the straight line datum. This misalignment has the effect of introducing a slope across the width of the chart (linear trend) and although every possible effort was made to properly align the specimen, any amount left should be removed before the assessment begins.

During the normal operation of the Talysurf, a 2 RC filter specified by the national standards is used to remove long wavelengths and to fit a mean line to the measured signal. The British standards (83) also specify that a least squares mean line might, alternatively, be used within a specified sampling length (equivalent to the filter cut-off). The least squares mean line was used in this work (it was also used in (51)) for various types of machined surfaces. The equation of the mean line could be derived as follows:

Referring to Fig 38, let:

N = number of samples per cut-off length

x_i = the height of ordinate "i" with respect to the datum line

y_i = the corrected height of the profile

m, h = slope and intersection of the least squares mean line

t = sampling interval

$$y_i = x_i - imt - h \qquad 5.1$$

The coefficients m and h are obtained by minimising the sum of squares of equation 1, and for this sum to be minimum we have

$$\frac{\partial \Sigma y_i^2}{\partial m} = 0 = \sum_{i=1}^{N} ix_i - mt \sum_{i=1}^{N} i^2 - h \sum_{i=1}^{N} i \qquad 5.2$$

$$\frac{\partial \Sigma y_i^2}{\partial h} = 0 = \sum_{i=1}^{N} x_i - mt \sum_{i=1}^{N} i - \sum_{i=1}^{N} h \qquad 5.3$$

By solving equations 5.2 and 5.3 we obtain

$$mt = \{12 \sum_{i=1}^{N} ix_i - 6(N + 1) \sum_{i=1}^{N} x_i\} / N(N^2 - 1) \qquad 5.4$$

$$h = \frac{1}{N} \sum_{i=1}^{N} x_i - \{\frac{N + 1}{2}\} mt \qquad 5.5$$

Equations 1, 4 and 5 were used to compute the corrected profile heights y_i.

All surface roughness parameters were measured with respect to the least squares mean line over a sampling length of 0.8 mm. Every profile had to contain at least five sampling lengths, in line with BS1134 recommendations.

5.2.3.2 Evaluation of the classical parameters

The following parameters were evaluated:

RT = Peak to valley height

RP = Maximum peak height

RV = Maximum valley height

RA = Centre line average

$$RA = \frac{1}{N} \sum_{i=1}^{N} |Y_i| \qquad 5.6$$

5.2.3.3 Evaluation of the height distribution (see Fig 39)

Three parameters were used to evaluate the height distribution, these were:

1. The standard deviation.

$$RQ = \left(\frac{1}{N} \sum_{i=1}^{N} Y_i^2\right)^{\frac{1}{2}} \qquad 5.7$$

2. The skewness.

This is a measure of the profile symmetry about the mean line (Fig 39,c).

$$SK = \frac{1}{(RQ)^3} \frac{1}{N} \sum_{i=1}^{N} Y_i^3 \qquad 5.8$$

3. The kurtosis.

This is a measure of the sharpness of the distribution (Fig 39,d).

$$Q = \frac{1}{(RQ)^4} \frac{1}{N} \sum_{i=1}^{N} y_i^4 \qquad 5.9$$

5.2.3.4 Evaluation of the slope

The slope of the profile at any point was measured according to a seven point analysis using the following equation (46)

$$\frac{dy}{dx} = \frac{1}{60t} \{y_{i+3} - 9y_{i+2} + 45y_{i+1} - 45y_{i-1} + 9y_{i-2} - y_{i-3}\} \qquad 5.10$$

The absolute mean slope, root mean square slope and the geometric mean absolute slope were computed.

5.2.3.5 Width parameters

The average wavelength index was computed from (84)

$$W' = 2\pi \frac{RA}{SA} \qquad 5.11$$

It was also decided to count the number of zero crossings "NO.", which is defined as the number of times the profile crosses the mean line per unit length. The number of zero crossings was employed in the program to estimate an appropriate sampling interval over which a roughness peak was defined and its radius was assessed.

5.2.3.6 The peak radius and peak height distribution

The sampling interval for the definition and computation of peak radius was found by considering the number of zero crossings of

the profile. The average distance between peaks was computed from the average number of samples between two consecutive up-crosses. The sampling interval t' for peak evaluation was taken to be between $\frac{1}{8}$ to $\frac{1}{16}$ of the average distance between peaks. The peak curvature was estimated using three point analysis according to

$$\frac{1}{R} = \frac{d^2y}{dx^2} = \frac{1}{t'^2}\{y_{i+1} - 2y_i - y_{i-1}\} \qquad 5.12$$

The peak height was taken to be the height of the central ordinate (i.e. y_i). The mean peak heights above the mean line and the standard deviation of heights around the mean were computed. The total number of peaks "NP" per profile (according to the peak definition by equation 5.12) was counted.

5.2.4 The computer program

The following is a flow chart for the computer program "FIGR3" which was used to compute roughness parameters. The input to the program is the name of the file carrying the digitised profile. The names of all such files for a specimen column are themselves given as a data file called "INDEX". No other input is requested by the program. The output results are stored in an output file called "RESULTS". This will contain the results computed for each profile on its own as well as the arithmetic mean, variance, maximum and minimum for each parameter over the specimen column. The program "FIGR3" is also listed in Appendix IV.

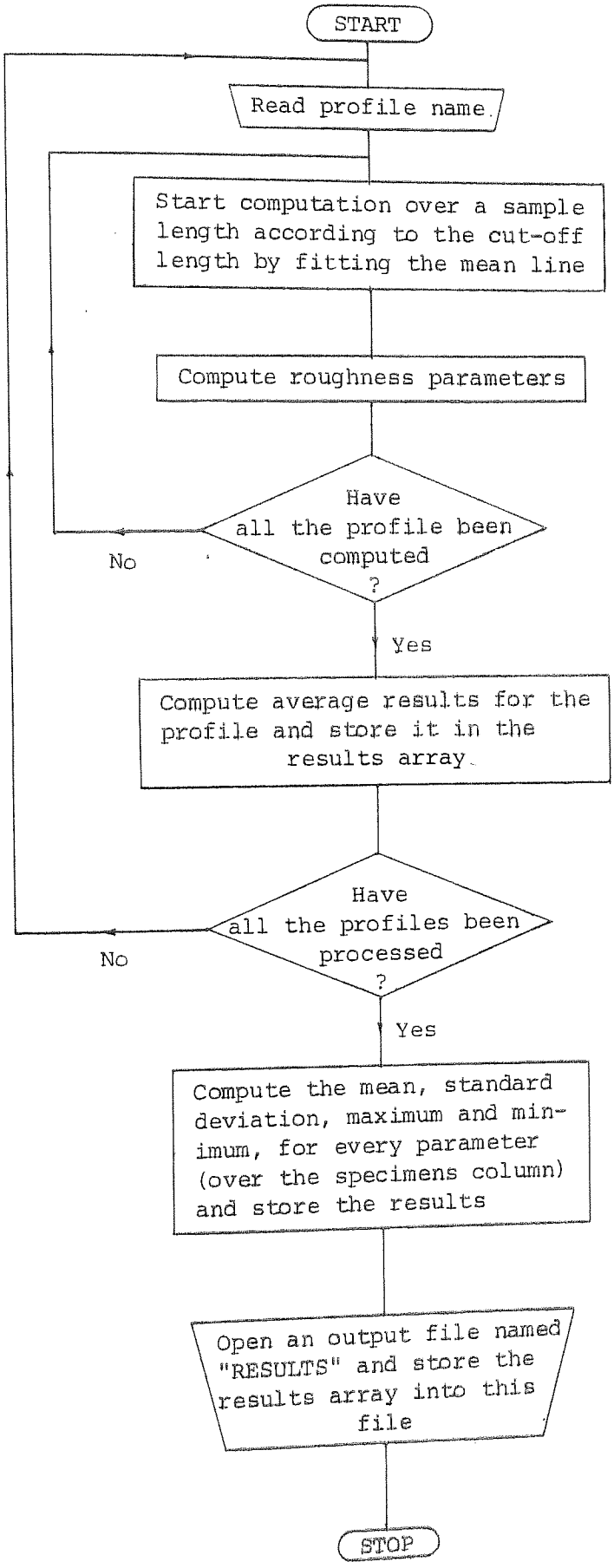
START
Read profile name.
Start computation over a sample length according to the cut-off length by fitting the mean line
Compute roughness parameters
Have all the profile been computed ?
No
Yes
Compute average results for the profile and store it in the results array.
Have all the profiles been processed ?
No
Yes
Compute the mean, standard deviation, maximum and minimum, for every parameter (over the specimens column) and store the results
Open an output file named "RESULTS" and store the results array into this file
STOP

5.2.5 Waviness

The only technical paper fully devoted to the study of waviness is that by Reason (93). He offers two different definitions of waviness as follows:

> "Waviness as seen in a profile graph can often be appraised both as an undulation of the mean line, and as an undulation of a line drawn through the more prominent crests. It is thus possible to speak of a mean line waviness and a crest line waviness."

The definition of waviness as being the undulation of the peak line has a considerable potential regarding the present study of machine tool joints. As it has already been mentioned, the G - W model requires the characterisation of a peak height distribution for the surfaces in contact. This could then lead to the determination of the pressure-deflection relation for the joint interface, from which the stiffness of the joint could be computed.

The peak height distribution was always thought of as being characterised using the data obtained from a short surface roughness profile trace. Thus, the way the peak height distribution is characterised limits the applicability of the contact theory to surfaces which suffer no flatness error. Such surfaces are not representative of the surfaces of machine tool joints. Common sense suggests that in order to extend the applicability of the G - W model to include surfaces with flatness error, the peak height distribution should be obtained from an unfiltered surface roughness profile which covers the longest dimension on the surface. But the measurement of such a long roughness profile is not a practical solution, since no roughness instrument which measures more than a few centimetres exists.

A practical alternative is, however, possible by considering a functional definition of waviness. That is, if we define waviness as the undulations of a line drawn through the more prominent roughness peaks, then the peak height distribution could simply be obtained from a waviness trace measured using a blunt stylus. The stylus will travel over the highest roughness peaks measuring waviness. The waviness profile so measured could then be characterised by its height distribution which is, in this case, the peak height distribution for the surface.

The definition of waviness as such extends the applicability of the G - W model to make it suitable for all sizes of contacting surfaces. On the other hand, the contact theory offers the method of characterising the waviness profile. The full pattern of the contact theory will emerge in Chapter 7.

5.2.5.1 The measurement and assessment of waviness

Before going into the details of measurement, it is necessary to emphasise the relation between surface flatness and waviness. Flatness is the three dimensional measurement of waviness on a nominally flat surface. In this way, every waviness trace could be considered as a sample taken out of the parent population, that is flatness. A practical way in which flatness of surfaces could be measured was first suggested by Thornley et al (14). Nonetheless, this approach was not used in the course of this work due to technical complications. The measuring system described earlier was used to measure waviness from which an estimation of the flatness height distribution was found.

A stylus of a flat circular tip (0.4 mm diameter) was mounted in a chatter arm which itself was mounted on the Talysurf stylus pick-up body as shown in Fig 40. The specimen was mounted on the Talytron table and the adjustment was made to align the path of the stylus to be parallel to the straight line datum of measurement. Any residual misalignment will be reflected on the profile as a linear trend which has to be removed by fitting a straight least squares mean line across the profile. The equation of the mean line and the fitting procedures are similar to those given in 5.2.3.1; the only difference is that the sample length covers the overall length of the profile. In this way, any form errors in the shape of general curvature on the surface are treated as waviness.

Every trace was digitised at 0.2 mm sampling interval, 150 samples per trace were taken and the height distribution was characterised by computing the standard deviation "RQF", skewness "SKF" and kurtosis "QF" with respect to the least squares mean line.

For every specimen surface two perpendicular waviness traces were measured. Thus, 32 waviness traces were obtained for every specimen column. The arithmetic mean of the parameters computed for all traces were considered representative of the flatness height distribution parameters of an average single specimen surface. It can be seen that the same technique of averaging was also used with roughness information. This technique is valid for the following reasons:

1. All the specimens within a specimen column were machined of the same material, same cutting conditions, on the same machine and the same day. Thus, it is expected that their

surfaces should display the same texture provided that the tool wear was observed.

2. The measurements of the stiffness and damping were to be carried out for the assembly and the results would express the average of the stiffness and damping for the average texture of the specimens within that assembly.

The results of measurement for both roughness and waviness are given in tables 4 to 18.

5.2.6 Conclusions

1. Earlier theories of contact did not put too much emphasis on surface texture; nonetheless, modern theories have shown that texture is a major factor in deciding the state and extent of deformation.

2. A computerised surface measuring system was built in order to enable measuring both roughness and waviness.

3. The wear of the stylus tip could seriously affect the assessment of roughness.

4. Flatness was included in the characterisation of joint surfaces through the measurement of waviness.

5. It is possible to make a functional assessment of flatness by considering the theory of contact. In this sense, flatness of joint surfaces should be characterised by its height distribution.

CHAPTER 6

EXPERIMENTAL INVESTIGATION INTO THE DYNAMIC PERFORMANCE OF FIXED JOINTS

6.1 Introduction

When two mating surfaces are loaded normal to their interface, the resulting mean interface pressure - deflection relation takes the form shown in Fig 1. Although the general features of the joint behaviour are known, one could not arrive at quantitative values for either the stiffness or damping that are expected to arise from a certain joint under a known preload. For example, it is known that the stiffness of a dry joint will be very much affected by the flatness deviations on its mating surfaces, yet, given the amount of these deviations, one cannot make a quantitative assessment for the stiffness.

A great deal of uncertainty surrounds the acting mechanism of lubricant between fixed joints. In the absence of any relative motion between the joints' surfaces parallel to the interface, hydrodynamic lubrication (with all its branches) is simply ruled out because the relative velocity is zero. On the other hand, the absence of any externally applied pressure on the lubricant (in order to force the oil to flow in between the interface) rules out an analogy to the action in an externally pressurised bearing. One could say that there is no satisfactory explanation to the tremendous increase in stiffness and loss factor when introducing lubricant to the joint. Moreover, the available experimental data are not enough to make a reliable theoretical

prediction of behaviour within this field.

It is obvious that the main factor influencing the behaviour of a joint is the topography of its surfaces. Therefore, the present study should start by exploring its effect. Only when the effect of surface texture is well understood; could a solution be directed towards establishing a realistic mathematical model that can be used by the designer to design joints which possess much better characteristics relative to the present practice. The main problem is that surface topography is itself still in the process of characterisation. Admittedly, some essential parameters are known, yet a great deal of essential information is either not adequately described or completely uncharacterised.

In the course of this investigation, it became clear that the essence of the problem is the need to investigate the effect of surface texture on the dynamic behaviour of dry and lubricated joints. Other parameters might as well be considered, but not until the effect of texture has been explored. The experimental investigation presented in this section aims at:

1. Providing experimental data for a reasonably wide range of differently machined joints having different surface topographies, enough to provide the experimental backing to the theoretical models presented in Chapters 7 and 8.

2. Investigating the effect of the presence of a lubricant layer on both the stiffness and damping. This is an investigation into two areas:

(a) Studying the effect of oil viscosity while keeping surface texture constant.

(b) Studying the effect of different textures on the dynamic characteristics of lubricated joints.

3. Investigating some other parameters that might contribute to the joint behaviour, such as area, shape, direction of lays etc.

6.2 Experimental procedures

The specimens prepared for the study of the dynamic properties of dry and lubricated joints were described in Chapter 4. The measurements of their texture were carried out as shown in Chapter 5, and the results are given in tables 4 to 18. The experimental investigation concentrated on measuring the dynamic stiffness and loss factor for a range of preloads. Details of the methods of measurement have already been described in Chapter 3.

The specimens in the specimens column under test were first degreased and dryed, then assembled in the test rig in a predetermined order and relative position. Static load was applied to its maximum during the test (i.e. 2,800 kp), then reduced to almost zero. The load was then increased to its first test level (250 kp) and the measurement of the dynamic stiffness and loss factor proceeded. The loading sequence as such was chosen to establish what can be considered as a standard initial condition for the state of plastic deformation which took place during the first loading cycle. Thus, one could say that

all tests were carried out with initial plastic deformation limited to that which permits the joint to stand a preload of 224 Kp/cm^2 without any further plastic deformation.

To study the effect of introducing lubricant or other intermediate layers in between the joint surface, one should know precisely the stiffness and damping of the dry clean joint which has exactly the same texture and metallic contact configurations as the contaminated one. Thus, any change in stiffness and/or loss factor could be accurately attributed to the presence of the contaminating layer. In other words, the effect of surface texture has to be neutralised as the viscosity of lubricant increases from zero (i.e. dry clean) to its maximum desired level. The only way to approach this was by testing the jointed column under dry conditions, and again after the introduction of lubricant. Care had to be taken so as not to interchange the order of the joints in the stack or their relative position to each other in order to maintain the metallic contact configuration as constant as possible. By so doing, the results obtained were repeatable and consistent.

The specimens were first cleaned from any oil traces or dirt, then fully immersed in an oil bath of the required viscosity. Assembly of the joints actually took place while the joints were fully immersed in oil. Pressure was applied by hand on the joints' stack to ensure that metallic contact took place, after which the joints were lifted off the oil bath and placed on a vee block. The stack was then cleaned from oil on its outside and inside circumference. The jointed column was then positioned in the test rig and the load was applied to its maximum level during the test. As the load increased, the oil squeezed

out of the joints and this was again removed and the outside rim of the specimens column was cleaned. The load was then reduced to zero level, then increased to its first test level and the measurement proceeded as in the dry test.

The testing procedures as such exercised some control on the quantity of lubricant; that is, the quantity of oil that could be preserved by the joint under the highest preload. The application of static load to its highest test level re-establishes the initial conditions for the state of plastic deformation as in the dry test. The presence of cavitations within the oil layer is possible, but so is the case in a real machine tool joint where no arrangements are normally made to lubricate a bolted joint.

6.3 Experimental results

The results obtained for the various jointed columns tested under dry and lubricated conditions are shown in Figs 41 to 72. The most predominant feature that could be seen in these graphs is the increase in dynamic stiffness with increasing preload associated with decrease in the loss factor. The results also clearly demonstrate the tremendous effect of introducing lubricant into the joints, specially on loss factor and at lower preloads.

Tests were carried out at a constant amplitude of 0.2 μm. The stiffness and loss factor were first measured at the second natural frequency of the test rig. The frequency of excitation was then changed within a range of around one octave while keeping the amplitude constant. It was found that the variation of stiffness and loss factor

with frequency did not exceed the experimental error in either case of dry and lubricated joints. This conclusion is in line with both references (32) and (41). Corbach (34), who also observed the same behaviour, offered an explanation in terms of the model shown in Fig 4. In this model, as the frequency of excitation increases, say above 200 Hz, both the dynamic stiffness and loss factor for the lubricated joint become very little affected by the excitation frequency. The joint behaviour as such is dependent on the ratio between the viscous damping coefficient for the lubricant layer and the viscous coefficient for the dry joint. As this ratio increases (say above 50, as it is the case for most lubricated joints loaded normal to the interface) the dynamic behaviour of the joint becomes fully independent of excitation frequencies above 300 Hz. This is in agreement with the observations made in this work under exciting frequencies ranging between 300 to 800 Hz.

The effect of amplitude was also checked at the 2^{nd} natural frequency. When reducing the amplitude of excitation from 0.2 μm to 0.05 μm no change in the value of the stiffness or loss factor was observed.

6.4 Dynamic performance of joints

Chapters 7 and 8 are fully devoted to the study of the stiffness and loss factor for dry clean joints, both theoretically and experimentally. For this reason, the discussion in this section will be limited to the behaviour of lubricated joints.

In Fig 41, the dynamic stiffness of ML1 appears to be much more affected by the presence of lubricant than that for ML2 in Fig 43. That is, the dynamic stiffness of lubricated ML1 joints is generally larger than that for lubricated ML2 joints. On the other hand, the dry stiffness for ML1 joints is less than that for ML2. Comparison between the loss factor graphs in Figs 42 and 44 shows that whilst T15 results in the highest loss factor when used to lubricate ML1 jointed column, the highest loss factor for ML2 joints was obtained when the column was lubricated using T23. As the preload on ML2 increased, the use of T71 resulted in loss factor higher than that obtained using T23 oil. For both ML1 and ML2, the change in the value of loss factor with the change in oil viscosity becomes small as the preload on the joints increases.

ML3 in Fig 45, which shows the highest dry stiffness among the milled joints tested, appears to be very much affected when lubricated using oil of any viscosity. The lubricated stiffness for this column changes very little when the oil viscosity changes from 10 to 220 cSt. On the other hand, the results obtained for the loss factor, Fig 46, when ML3 was lubricated using T15 were nearly equal to those obtained when T23 was used. When ML3 was lubricated using T71, the loss factor was less than that obtained using T15 or T23. Again, at higher preloads the effect of oil viscosity on the loss factor becomes less apparent and the three types of lubricant result in almost the same loss factor for the jointed column. Contrary to ML3, ML4 in Figs 47 and 48 is very sensitive to changes in oil viscosity.

The pattern of behaviour for shaped (SH), turned (TN) and ground (GN) joints is very much similar to that observed for milled (ML)

joints. The results contain the following features:

1. The contamination of joints by lubricant results in an increase in its dynamic stiffness. Nonetheless, this increase appears not to be directly related to the dry stiffness of the joint.

2. With the exception of the results with T71 for GN2 jointed column in Fig 71, an increase in oil viscosity results in an increase in dynamic stiffness. This increase appears to be only dependent on surface texture.

3. An increase in joint preload results in an increase in the dynamic stiffness under lubricated conditions. On the other hand, associated with the increase in stiffness is a decrease in loss factor. This behaviour is very much consistent over all the joints tested.

4. The rate of decrease in loss factor reduces with the increase in preload. As a result of the decrease in loss factor, the effect of changing the viscosity of oil becomes less significant at higher preloads.

5. The behaviour of loss factor with oil viscosity clearly indicates that for every type of texture there will be an optimum viscosity of lubricant that results in the highest possible damping. The general trend is that rougher surfaces need more viscous oil to produce better damping characteristics (see the results for SH2 and SH4 in Figs 52 and 56 respectively). On the other hand, for smoother surfaces less viscous oils result in higher values of the loss factor (Figs 70 and 72 for GN1 and GN2 respectively).

6. The independence of the lubrciated stiffness from the stiffness measured under dry clean conditions is very well illustrated in Fig 73. This Figure combines the results obtained for two jointed columns (SH4 and SH5) that have almost the same dry stiffness, yet when lubricated they show wide differences in their dynamic stiffness for the same oil viscosity. A similar conclusion could be drawn by comparing the results of TN2 and TN3 when lubricated with T15 and T23. An important conclusion that could be reached is that the lubricated stiffness appears to be dependent on other texture parameters than those affecting the dry stiffness (see Chapter 7 for surface texture parameters which influence the stiffness of dry clean joints).

7. TN1 in Fig 61 and 62 was taken as a test case for how much the stiffness of the jointed column could be increased by changing oil viscosity. The dry stiffness measured for this column was the lowest among all joints examined in this work. As it can be seen in Fig 61, it was possible to improve the stiffness of the assembly to reach around 96% of that for the equivalent solid at the lowest preload of 20 kp/cm^2. It can also be seen in Fig 62, that while the stiffness was improving, the loss factor for the jointed column was deteriorating. Nonetheless, the loss factor was still much higher than that when the column was dry. The improvement achieved in the dynamic characteristics of this column is further appreciated when considering that the average value of CLA was 5.433 μm.

8. The idea of optimisation of oil viscosity is illustrated in Figs 65 and 66 for TN3 where the application of T41 resulted in the

same dynamic stiffness as T71 but with improved damping characteristics. When Simnia grease O (semifluid lubricant usually applied in gearboxes) was used, both stiffness and loss factor were lower than those achieved using T41. An interesting feature appears in Fig 66 where the slopes of the loss factor curves for T41 and T71 are almost equal at all preloads. The same observation could also be made for the results of T15 and Simnia grease O.

9. Hermetite, a commercially available material usually used for sealing fixed joints, was tested with SH2 (25 μm peak to valley height and 5.28 μm CLA). The results for this jointed column with other lubricants are shown in Figs 51 and 52, whilst the results when introducing Hermetite are shown in Figs 59 and 60. The jointed column was tested immediately after the application of Hermetite and the results indicated an improvement in stiffness over that obtained using T71, while the loss factor was below that for T71. The load was then lifted completely and without separating the joints the column was left to dry for 20 days, after which the specimen column was tested again. As it is shown in Figs 59 and 60, a tremendous increase in stiffness was achieved. This increase was associated with an equally tremendous drop in loss factor. Nevertheless, the loss factor was still much higher than that obtained for the dry clean joint. The results demonstrate that given enough time to dry, a jointed column contaminated with Hermetite could be as stiff as its equivalent solid and probably possesses much better damping characteristics. The above experiment appears to offer a cheap solution to the problem of loss of stiffness in fixed joints (at

least in the normal direction). The solution as such is economical as far as surface texture is concerned, and it would be interesting to see the performance of such a joint when excited tangentially.

N.B. When hermetite is used, it is necessary to ensure that matallic contact takes place; otherwise a severe drop in stiffness could be experienced.

10. The results presented so far were those measured for the jointed column. The stiffness and loss factor for a single joint could be obtained by carrying the correction for the effect of material using the results measured for the equivalent solid. However, it was not possible to carry out this correction for some of the tests on lubricated joints. The reason for this is that, as the stiffness of the jointed column becomes nearer to its value for the equivalent solid, the use of equations 3.23 and 3.24 becomes unreliable and results in large errors as was reported in (41). On the other hand, for future reference, those cases for which the correction could be carried out were corrected and the results are shown in Figs 74 to 88.

6.5 Mechanism of lubrication in fixed machine tool joints

In order to arrive at a satisfactory explanation for the results obtained for the dynamic stiffness and loss factor of lubricated joints, one has to explore what happens in between the joint surfaces. A possible method by which the introduction of oil could increase the joint stiffness is by trapping the oil so that the volume trapped could be pressurised. Once pressurised, it shares the applied load, thus,

reduces the joint deformation. But, where could oil be trapped, specially when the mating surfaces are both very rough and have a definite direction of lays (e.g. shaped surfaces)? It could be argued that surface asperities could be fully interlocked so that oil is trapped between gaps within the interlocking asperities. Such an argument is plausible only in the case of contact between two shaped surfaces with their lays parallel. If the lays are not parallel or the surfaces of the joint are manufactured by face turning, it is rather difficult to accept an explanation based on interlocking asperities.

Alternatively, one could argue that contact spots contain holes which are full of oil. Within these holes the oil could be trapped, thus influencing the joint behaviour. The presence of holes within the contact spots will be dependent on the small scale of size features present on the relatively larger roughness asperities.

The idea of the presence of holes within the spots of contact was first suggested by Greenwood (20). A mathematical expression for the density of holes was derived by Nayak (74), and more recently Sayles (86) reported that at low applied loads not all holes would be completely sealed off. This last remark is of importance in explaining the behaviour of loss factor with increasing preload on the joint, as will be shown in the next section.

6.5.1 Hole formation and its relation to the behaviour of lubricated joints

When two surfaces come into contact, the actual contact takes place over very small areas scattered over the apparent area. The metallic junctions formed when the applied load is very small could be

assumed solid junctions. As the load increases the true area of contact increases; and since surfaces are rough, one would expect that the junctions will not stay fully solid. They will contain holes which will be filled with oil.

Under small applied loads, not all holes will be completely sealed off (86). In fact the majority of holes will be open, thus permitting any trapped oil to be pumped in and out under vibrations. This could explain why the measured loss factor was large when the joint preload was small. If the hole opening (through which oil could be pumped in and out) is small enough to reduce the flow of lubricant, the oil within the hole could stand more pressure. Thus, the stiffness increases while the loss factor would decrease. As the preload continues rising, many holes tend to become closed, thus trapping whatever oil they may contain and causing the stiffness to continue rising while the loss factor drops. The rates at which the stiffness increases and the loss factor decreases (with increasing preload) are dependent on the rate at which sealed holes are formed; the latter rate might be reduced with increasing preload. Thus, the rate of increase in stiffness reduces, while the loss factor decreases at a slower rate.

6.6 Influence of the planform shape

The present experiment explores the possibility of improving the dynamic characteristics of joints by simply changing the joint planform shape while maintaining the apparent area of contact constant. In reference (87) this problem was studied in the case of dry clean joints.

It was found that the shape of the apparent area of contact had little influence on the static and dynamic stiffness of joints. The experimentally observed effect of shape was attributed to one or both of the following reasons:

1. That the relative position of the shape with respect to the displacement measuring transducer varied with the change in the planform shape. Hence, the circular joints tended to have more flexible mounting than the rectangular ones.

2. That flatness deviations which varied from joint to joint were also responsible for the observed change in stiffness with the change in planform shapes, whilst variations in surface roughness were reported to be the reason for varying static stiffness measured for various shapes.

A similar study was reported in reference (41) where only annular circular joints of the same area but different aspect ratio were examined. The experiments were free of the flexibility problem encountered in (87); however, flatness and roughness variations were thought responsible for the progressive significance of shape with increasing preload.

With the above problems in mind, the present experiment is a comparative study of the dynamic behaviour of three jointed columns having the same apparent area of contact (6.45 cm^2) but three different shapes, i.e. triangular, square and circular. The specimens were manufactured as was described in 4.7. The small apparent area of contact and the machining technique were thought to reduce the possibility

of variations in flatness deviations for the three jointed columns tested.

6.6.1 Experimental results

The success of the technique of machining adopted in the manufacturing of various shapes was reflected in the congruency of the measured dry stiffness and loss factor shown in Figs 89 and 90 for the three shapes tested. Thus, under dry clean conditions it is not expected that the shape of the nominal area of contact of the joint has any influence on its dynamic performance. These results support the theoretical treatment presented in Chapter 7, where the joint stiffness was found to be dependent on the flatness deviations on its surface, while it is much less sensitive to surface roughness parameters and almost independent of the apparent area of contact. The way in which spots of contact are distributed over the nominal area of contact is one which primarily preserves the static balance of the joint. This distribution can in no way affect the joint stiffness once a reasonable preload was applied, nor can it be altered by changing the shape of the apparent area of contact.

The set of shapes produced provided an ideal opportunity for testing the effect of shape for lubricated joints. The reason is that the three shapes have the same dry stiffness and loss factor. Hence, the configurations of contact for the three columns are almost the same. The three columns were tested when lubricated with Shell Tellus oil 23, and the results are shown in Figs 89 and 91. The two shapes which showed the highest dynamic stiffness were the square and the triangular planforms. The circular planform appears to be inferior to the others as far as the dynamic stiffness is concerned. As for the loss factor,

the three shapes result in very similar damping characteristics. Considering the way in which the lubricant could act in between fixed joints, one could not attribute the increase in stiffness only to the influence of the planform shape, and no firm conclusion could yet be reached regarding this point.

6.7 Influence of lay direction

The experiments reported in sections 6.2 and 6.4 were carried out for joints making contact with their lays parallel. In reference (16), it has been found that the angle between lays will have a negligible effect on the elastic deformation of joints. In reference (21), the influence of lay direction was further examined. The treatment was based on the reasonable assumption that the angle between lays would decide the number and area of contact spots, thus, affecting the amount of elastic recovery, and hence the joint stiffness.

To examine further this point, two of the jointed columns tested earlier, under dry clean conditions, and with their lays parallel, were retested following the same procedures mentioned in 6.2, but with the angular position between their lays at 90°. Care was taken so as to keep the order of joints within each specimen column the same as it was when the direction of lays was parallel. The tests were carried out for two shaped columns; these were SH3 and SH4 representing two levels of roughness. The former had 1.63 μm CLA, while the latter had 4.728 μm CLA. The results obtained were plotted in Fig 92, together with the results previously obtained when the lays were parallel.

6.7.1 Experimental results

When changing the direction of lays for SH3, the dynamic stiffness did not show any significant change with respect to its values when the lays were parallel. This behaviour, however, was different when testing SH4, which showed a significant increase in its dynamic stiffness when the angle between lays was 90°. As the preload was increased, the difference in stiffness reduced, and the dynamic stiffness measured for the perpendicular lays converged to the value measured for the parallel lays at higher preloads. It is interesting to notice that the same trend also appeared in the results obtained for SH3 in spite of the small difference between the dynamic stiffness measured in either case.

The resolution of the above experimental results could not only be made in terms of the change in lay direction without considering the actual condition of finish present on the joint surface. In an ideal situation, one would imagine surface roughness on shaped surfaces to be in the form of straight parallel ridges which are smooth in the lay direction. Such an ideal situation should theoretically show that the change in lay direction affects the joint stiffness. This picture, however, hardly exists in practice, even for a strongly anisotropic surface such as the shaped surface. A roughness peak traced in the direction of lays will always show peaks and troughs when traced in the lay direction. Added to this is the fact that flatness deviations are present in all directions on the surface. Thus when two shaped surfaces come into contact, the number of contact spots will be primarily dependent on the way the flatness deviations, present on both surfaces, are summed up to form a stable joint. This could explain the experimental results obtained for SH4, where the joint stiffness

increased when the angle between lays was 90^{o}. The increase in stiffness implies less flatness error, which is possible, and could be explained in terms of an increase in plastic deformation that took place. This is partly because the original flatness errors were high and partly because the surfaces were very rough. On the other hand, for the relatively smoother surfaces of SH3, the flatness errors were much less, and thus the possibility of a significant change in flatness deviations taking place is less. Hence, in this case, the change of the angle between lays has almost no influence upon the dynamic stiffness of the joint.

6.8 Characteristics of joints assembled in series

This section covers an investigation carried out to explore the influence of the number of joints in a fixed specimen column length upon the dynamic behaviour of the assembly. Any structure will normally be a composition of a number of structural elements joined together in series and/or in parallel. The overall stiffness of the structure is then expected to be very much influenced by the number of joints, their stiffness and damping characteristics. Testing a number of joints connnected in series has the advantage of reducing the overall stiffness of the assembly, and thus the deflection increases enabling better measurement of the response. The investigation explores the effect of adopting this technique on the results obtained for a single joint after carrying the proper compensation for the material effect.

Tests were carried out in which the dry stiffness and loss factor for 2, 6, 10 and 14 joints' stacks were measured under dry

clean conditions. All four columns had the same area of 16.02 cm^2 and the same overall length. The specimens were machined according to the conditions mentioned in 4.8. The stiffness and loss factor were measured at four preloading levels of: 250, 500, 1500 and 2,500 kp respectively. An equivalent solid was also manufactured and tested at the same preloading levels as above.

The results obtained for the various columns are plotted in Fig 93, from which it becomes clear that as the number of joints increases, the stiffness of the assembly decreases, while the loss factor shows little change. The results also confirm that the test rig is sensitive to the change of the column stiffness as joints are introduced, irrespective of the preload.

Fig 94 shows the results obtained for the single joint after carrying the proper correction for the effect of the discs material using the equivalent solid results. It appears that the results tend to converge to a fixed value per joint as the number of joints connected in series increases. The observed convergence could be explained in terms of averaging the surface integrity when testing a number of joints at once. Theoretically, surfaces machined of the same material, under the same cutting conditions, using the same machine, should be identical. Practically, however, variations in surface texture were observed even over the same specimen surface. Obviously, the variations could be much larger if there are many such surfaces. Thus, what appears in Fig 94 to be convergence, is in fact the average stiffness and loss factor for slightly different surfaces of 2, 6, 10 and 14 joints. This leads us to advise the designer to

exercise care when mixing different machined joints; for, a weak joint might affect the overall stiffness of the structure.

6.9 Influence of the apparent area of contact

The present experiment was carried out to examine the effect of the apparent area of contact on the joint stiffness. The basic requirement of this study is to minimise the possible change in surface topography as the area of joints changes. For this reason, a single stack of joints having the largest area under consideration (25.8 cm^2) was manufactured, as was described in 4.6. The experimental procedures for this study were as follows:

1. The specimens were first cleaned from oil traces, then assembled in a predetermined order and relative position. The stiffness and loss factor were then measured at four different pressure levels; these were 20, 40, 60 and 100 kp/cm^2.

2. The same specimens were then mounted on a mandrel and their apparent area was reduced to 19.35 cm^2. The stiffness and loss factor for the new jointed column were again measured at the same pressure levels as in step 1.

3. Following the same procedures in step 2, the column area was finally reduced to 12.9 cm^2 and the stiffness and loss factor were measured at the same apparent pressure levels.

For every column area measured, an equivalent solid having the same area was also tested at the same pressure levels as for the jointed

column.

6.9.1 Experimental results

The dynamic stiffness and loss factor for the three levels of area tested are shown in Fig 95. The small value of the loss factor did not show significant changes as the area changed. The dynamic stiffness of the jointed column increased with the increasing apparent area (for the same applied pressure). In Fig 96, the dynamic stiffness results were plotted versus the applied load. This showed that the stiffness for all levels of area tends to follow the same path, at least for lower levels of applied load. As the load increases, so does the difference between the stiffness of the three columns. One could also see from Fig 96 that when the preload is small, an increase in the apparent area of contact could reduce the stiffness.

Fig 97 shows the joints stiffness versus preload after correcting for the material effect. It appears that in spite of the machining and testing technique adopted, it was not possible to completely eliminate the change in flatness deviations as the area changed. Nonetheless, the 12.9 cm^2 joint and that having an apparent area of 19.35 cm^2 (50% increase in the apparent area) appear to have almost the same stiffness for the same applied load. The 25.8 cm^2 joint has the lowest stiffness of the set; this indicates the presence of slightly larger flatness deviations on this joint.

The extent by which any surface suffers from flatness deviations will depend on the size of its area. As the area increases, it is most probable that its flatness deviations will also increase. On the other

hand, it is well known that the joint stiffness is sensitive to flatness errors, and thus no firm experimental conclusion could be reached for the relation between the apparent area of contact and the stiffness of joints. The almost inevitable change in flatness deviation with the change in apparent contact area could mask any possible influence of area on the stiffness.

Fortunately, the influence of apparent area could be illustrated by considering the theoretical model which will be derived in the next Chapter. The model relates the joint's separation V (a direct measure of the joint's elastic deformation) to the applied load through the expression

$$W = C\, A_o\, \sigma^2\, F_2(V) \qquad 6.1$$

Where: C = Constant for the joint.

σ = Standard deviation of flatness height distribution.

$F_2(V)$ = An integral function of the separation.

The above equation shows that the joint's elastic deformation is dependent on the apparent pressure and not the applied load. The joint stiffness is given by

$$\frac{dW}{dV} = K_J = 2\, C\, A_o\, \sigma\, F_1(V) \qquad 6.2$$

By dividing equation 6.2 by equation 6.1, the joint stiffness can be expressed as

$$K_J = \frac{2}{\sigma}\, W\, \frac{F_1(V)}{F_2(V)} = \frac{2}{\sigma}\, W\, F_2^1(V) \qquad 6.3$$

Where $F_2^1(V) = \dfrac{F_1(V)}{F_2(V)}$

The joint stiffness could be found by first substituting in equation 6.1 to find the value of $F_2(V)$ then, from Fig 102, $F_1(V)/F_2(V)$ could be directly found. The joint stiffness is then evaluated from equation 6.3. Let us assume that when the joint's apparent area was A_1, $F_2(V)$ was 0.01. Thus from Fig 102, $F_2^1(V)$ is 1.385 and the stiffness of the joint is obtained from equation 6.3

$$K_{J_1} = \left(\frac{2}{\sigma} W\right) 1.385 = 2.77 \frac{W}{\sigma}$$

Assume that the joint area was increased to 10 A_1 while the applied load and flatness deviation were kept the same. Thus, $F_2(V)$ will be reduced to 0.001 and the joint stiffness is given by

$$K_{J_2} = \left(\frac{2}{\sigma} W\right) 1.685 = 3.37 \frac{W}{\sigma} \quad N/m$$

That is, an increase of only less than 22% in stiffness as a result of increasing the area 10 times. It could also be seen from Fig 102 that if the original value of $F_2(V)$ is small (say below 0.0002) a ten-fold increase in the apparent area could result in only 5% increase in the stiffness. Practically, however, this is not the case, since if we also make the assumption that with 10 times increase in area, the flatness deviation was increased by only 50%, then from equation 6.1

$$\frac{W}{C A_1 \sigma^2} = 0.01 \quad \text{, for the original area}$$

$$\frac{W}{C (10A_1)((1.5)^2\sigma^2)} = F_2(V) \quad \text{, for the new area}$$

i.e. $$F_2(V) = \frac{0.01}{22.5} = 0.00044$$

Thus from Fig 102, $F_2^1(V) = 1.8$

$$K_{J_2} = \left(\frac{2}{1.5\sigma} W\right) 1.8 = 2.4 \frac{W}{\sigma}$$

That is, the stiffness decreased by slightly less than 14% which clearly demonstrates how a large increase in the apparent area of contact is fully masked by the slight increase in flatness deviations.

N.B. The assumed 50% increase in flatness deviation is very much less than what one would expect when the area of a joint increases from, say, 0.01 m^2 to 0.1 m^2 or from 10 in^2 to 100 in^2.

The above numerical examples and the experimentally obtained results are both pointing towards one conclusion; that is, the designer is advised not to increase the apparent area of contact of joints unless it is necessary to do so. An increase in the joint apparent area could result in reducing the stiffness of joints, in addition to increasing the cost of machining.

The results obtained for the stiffness of the equivalent solid columns are plotted in Fig 98, against the column cross sectional area. The results in that Figure show that:

1. The test rig is sensitive to the change in the area of the equivalent solid (which is directly proportional to its stiffness since $K_{solid} = \frac{E.A}{l}$).

2. That there is an error estimated at ± 11% with respect to the stiffness of the largest column area. This level of error could be attributed to the presence of joints at the load cell and between the column and the test rig.

CHAPTER 7

THE STIFFNESS OF JOINTS IN MACHINE TOOL STRUCTURES

7.1 Introduction

The work presented in this Chapter is concerned with the study of the stiffness of dry clean machine tool joints. For such a study to be of practical use, it must offer the designer the means which enables him to estimate the joint stiffness, with a reasonable degree of accuracy, from the specifications he makes on the design drawings. On the other hand, these specifications should be practically possible to achieve and can be controlled by the manufacturer.

A theoretical model for the stiffness of dry clean joints is developed in this Chapter. The model is in line with the experimental observations made by Thornley and his team (14, 16, 17, 22 and 23). The theoretical results obtained using the model are compared to the following:

1. The theoretical results obtained using the model due to Greenwood and Williamson (68) after modifying it to account for the presence of flatness deviations on the joint surfaces.

2. The experimentally measured stiffness for a wide range of joints having different surface textures.

Finally, stepwise procedures are presented to the designer in order to

carry out the design for a joint having a particular stiffness.

7.2 Contact between machined surfaces

According to Thornley (38), when two nominally flat surfaces are brought into contact for the first time, surface roughness asperities suffer plastic deformation until the true area of contact is sufficient to support the load. In addition to the plastic deformation, there will also be some elastic deflection which results from the stresses set up in the bodies behind the contacting spots. If the applied load is reduced, the joint surfaces will move apart due to the elastic recovery. If the load is increased again, the joint will deform elastically until the apparent pressure reaches the level at which the previous plastic deformation was stopped. Any increase over this pressure level will cause additional plastic deformation and if the load is removed the joints will display elastic behaviour. The elastic deformation of joints was found (16) to be directly proportional to the logarithm of the mean interface pressure for pressures between 3 kp/cm^2 and 315 kp/cm^2, and was represented by the following empirical relation

$$\ln P = m \lambda_J + C \qquad 7.1$$

Greenwood and Williamson (68) presented a theoretical model for the elastic deformation of machined surfaces. The model is based on the following assumptions:

1. Surfaces are covered with spherical asperities whose summits have the same radius.

2. Summit heights vary randomly.

3. The contact between two rough surfaces could be considered as that between a single surface which is rough and a plane, as shown in Fig 99.

4. The apparent area of contact is large so that the individual contacts are dispersed and the forces acting through neighbouring spots do not influence each other.

The contact radius r_1 and the load W_i on a single contact spot was obtained (68) from the Hertzian equations (88) as

$$r_1 = \beta^{\frac{1}{2}} w_i^{\frac{1}{2}}$$

$$W_i = \frac{4}{3} E' \beta^{\frac{1}{2}} w_i^{\frac{3}{2}} \qquad 7.2$$

Where $\frac{1}{\beta} = \frac{1}{R_1} + \frac{1}{R_2}$ and,

$$\frac{1}{E'} = \frac{(1 - \nu_1^2)}{E_1} + \frac{(1 - \nu_2^2)}{E_2}$$

From Fig 99, w_i is given by

$$w_i = Z - u$$

Where u is the separation defined as the distance between the mean plane of the rough surface and the smooth plane.

The probability that a particular asperity has a height between Z and $Z + dZ$ is given by

$$\phi(Z)\, dZ$$

When the separation between the reference planes of the mating surfaces is u, the probability of making contact at any given asperity of height Z is then given by

$$\text{prob } (Z > u) = \int_u^\infty \phi(Z)\, dZ$$

The total number of asperities in contact = $A_o\, \xi \int_u^\infty \phi(Z)\, dZ$

The total load on the surface is then obtained (68) from integrating equation 7.2 for all asperities in contact, thus

$$W = \frac{4}{3} E'\, A_o\, \beta^{\frac{1}{2}}\, \xi \int_u^\infty (Z - u)^{\frac{3}{2}}\, \phi(Z)\, dZ \qquad 7.3.1$$

The above equation could be normalised for the standard deviation σ of the peak height distribution $\phi(Z)$, thus

$$W = \frac{4}{3} E'\, A_o\, \beta^{\frac{1}{2}}\, \xi\, \sigma^{\frac{3}{2}} \int_V^\infty (Y - V)^{\frac{3}{2}}\, \phi(Y)\, dY \qquad 7.3.2$$

Where $Y = \frac{Z}{\sigma}$ and $V = \frac{u}{\sigma}$

Greenwood and Williamson went on to show that if $\phi(Y)$ was given an exponential distribution, then $\phi(Y) = e^{-Y}$ and by substituting in equation 7.3.2 and integrating we obtain

$$W = \pi^{\frac{1}{2}} E'\, A_o\, \beta^{\frac{1}{2}}\, \xi\, \sigma^{\frac{3}{2}}\, e^{-V}$$

The above equation could be further reduced in the following manner

$$\frac{W}{A_o} = P = \pi^{\frac{1}{2}} E'\, \beta^{\frac{1}{2}}\, \xi\, \sigma^{\frac{3}{2}}\, e^{-V} = C\, e^{-V}$$

Where C = constant for the surface under consideration, thus

$$\ln P = \ln C - V = \ln C - \frac{u}{\sigma}$$

but u = separation = $\partial - \lambda_J$

where ∂ is a constant relating the elastic deformation to the separation, thus

$$\ln P = \ln C - \left(\frac{\partial}{\sigma} - \frac{\lambda_J}{\sigma}\right)$$

$$\therefore \quad \ln P = \frac{\lambda_J}{\sigma} + C'$$

which is the same form predicted by Thornley and Connolly, i.e. equation 7.1.

Experimentally measured peak height distribution (68) showed that it is a Gaussian distribution for most machined surfaces. Thus, $\phi(Y)$ was assumed to be Gaussian and the integral in equation 7.3.2 becomes

$$F_n(V) = \frac{1}{\sqrt{2\pi}} \int_V^\infty (Y - V)^n \, e^{-\frac{1}{2}Y^2} dY \qquad 7.3.3$$

The above integral was tabulated (89) for various values of n and separations V. Equation 7.3.2 is then reduced to

$$W = \frac{4}{3} E' A_o \beta^{\frac{1}{2}} \xi \sigma^{\frac{3}{2}} F_{\frac{3}{2}}(V) \qquad 7.4$$

The stiffness of the joint could be obtained by differentiating 7.3.1 with respect to the separation u, thus

$$K_J = \frac{dW}{du} = \frac{4}{3} E' A_o \beta^{\frac{1}{2}} \xi \frac{3}{2} \int_u^\infty (Z - u)^{\frac{1}{2}} \phi(Z) \, dZ$$

The above equation is again normalised for the standard deviation σ, thus

$$K_J = 2 E' A_o \beta^{\frac{1}{2}} \xi \sigma^{\frac{1}{2}} \int_V^\infty (Y - V)^{\frac{1}{2}} \phi(Y) \, dY \qquad 7.5.1$$

And for a Gaussian distribution of peak heights, the stiffness is given by

$$K_J = 2\,E'\,A_o\,\beta^{\frac{1}{2}}\,\xi\,\sigma^{\frac{1}{2}}\,F_{\frac{1}{2}}(V) \qquad 7.5.2$$

From equation 7.4 and 7.5.2, the stiffness of the joint is given by

$$K_J = \frac{3}{2}\,\frac{1}{\sigma}\,W\,F^{\frac{1}{2}}_{\frac{3}{2}}(V) \qquad 7.6$$

Where

$$F^{\frac{1}{2}}_{\frac{3}{2}}(V) = F_{\frac{1}{2}}(V)/F_{\frac{3}{2}}(V)$$

Greenwood and Williamson went on to show that the mode of deformation (elastic or plastic) is only dependent on the value of a plasticity index ψ which is given by

$$\psi = \frac{E'}{H}\quad(\frac{\sigma}{\beta})^{\frac{1}{2}}$$

Thus, contact between machined surfaces can take one of the following forms:

1. Surfaces having $\psi < 0.7$ will display pure elastic behaviour.

2. Surfaces having $0.7 < \psi < 1$ will display elastic - plastic behaviour.

3. Surfaces having $\psi > 1$ will have plastic contact even under the smallest applied loads. If such surfaces are loaded up to a limit and then unloaded, they will recover elastically and when reloaded the behaviour will be elastic provided that:

(a) The surfaces are not separated.

(b) The initial load which caused plastic deformation is not exceeded.

For surfaces which suffer plastic deformation during its first loading cycle (as it is the case for almost all machined surfaces) one cannot simply use the G - W model to describe their elastic recovery, without considering the changes that take place due to plastic deformation. That is, if surface asperities are plastically deformed, their peak radius will suffer a considerable change in order to satisfy the plasticity index condition for elastic deformation. It is also possible that the standard deviation of the peak height distribution may suffer some change.

Another limitation to the use of the above model is imposed by the need to know the radius of curvature. Firstly, there is no universally agreed definition for the scale of asperities that could be considered as significant to the contact. Secondly, the model could only be used for a joint which has been actually manufactured instead of one which is still in the process of design.

The model is based on the assumption that the elastic recovery of joints is only a result of the recovery of spherical asperity peaks. This is not in line with the experimental observations of Connolly and Thornley (16). Schofield (21) carried out experiments on model asperities and concluded that the elastic recovery is due to the recovery of the body material behind the asperities. This last point was further emphasised in (79).

7.3 The nature of flatness measurement in relation to the peak height distribution

The mechanism of the motion of a stylus intended to measure flatness deviations on a rough surface could be analogous to walking on a surface covered with pebbles. The feet (their elasticity apart) only feel the peaks of the highest rocks, and automatically sample the changes in their peak heights, say, with respect to a sea level datum. Almost the same happens with the stylus (of an instrument measuring waviness) when it travels over the rough surface. It samples the heights of roughness peaks and if the sample length is large enough and the waviness definition in section 5.2.5 was adopted, we will end up with a trace which gives a fair idea about the distribution of roughness peak heights over the surface. Naturally, in order to obtain a reliable statistical distribution, more than one trace has to be measured and the outcome is a statistical distribution which represents:

1. The flatness of the surface.

2. The peak height distribution of the surface.

The statistical distribution obtained in this way could then be used in equations 7.4 and 7.5.2, thus extending their applicability to surfaces that suffer from flatness deviations, i.e. typical machine tool joints surfaces. Throughout this Chapter the flatness distribution will be assumed Gaussian. The standard deviation of the Gaussian distribution will be taken equal to the standard deviation of waviness heights as was described in section 5.2.5.

7.3.1 Contact between rough unflat surfaces

Consider a normally loaded contact between two unflat surfaces as shown in Fig 100,a. Let the undeformed flatness heights measured from the mean plane on each surface be given by Z_1 and Z_2 when the distance between their mean planes is ∂. When deformed, their surfaces overlap and it was shown (89) that the study of contact between two rough surfaces could be approximated to a study of contact between a single surface which is rough (the sum surface) and a smooth flat plane. Thus, the combined deflection of two rough unflat surfaces could be approximately obtained from the intersection of the sum surface with a plane at a distance equal to the separation between the mean planes of the original mating surfaces as shown in Fig 100,b.

The sum surface is expected to have a Gaussian distribution of peak heights even when the individual surfaces are not exactly Gaussian. Within the context of this work, the mean of the standard deviation of waviness measurements made for all the specimens within a particular specimen column was taken to represent the standard deviation of the Gaussian distribution of flatness heights for a single surface within this jointed column. The standard deviation of peak heights on the sum surface could then be obtained from

$$\sigma = \sqrt{RQF_1^2 + RQF_2^2} = RQF\ \sqrt{2}$$

The value of RQF for every machined surface studied is given in tables 4 to 18.

7.4 The general picture of contact in machine tool joints

When two joint surfaces come into contact, and before applying any load, the flatness deviation on both surfaces will determine which parts on each surface will be loaded. As the load is applied and deformation starts, the flatness will overlap and (for simplicity) we will assume that all asperities within the overlapping regions will share some part of the load.

As the applied load increases, the loaded asperities will plastically deform forming spots of contact. The shape of area of contact spots could be of any form; however, for small applied pressures compared to the yield pressure of the material, the spots of contact will be small and they can be given one of the uniform shapes (e.g. circular, square, etc).

The plastic deformation of every asperity will be associated with elastic deformation of the body material behind it. Thus, if the increasing load was stopped and the load was reduced, the surfaces will display elastic recovery. The elastic recovery is not due to the elastic deformation of asperity peaks, it is only a result of the recovery of the material immediately behind the loaded asperities.

The above picture differs from that given by the theory in 7.2, where asperities are assumed to have spherical peaks. If the contact is initially plastic (because the initial mean radius R_o of asperity peaks is small and the value of the plasticity index is large), then, when the load is removed, the plastically deformed asperities are assumed to recover elastically. The shape of asperities after recovery

will still be spherical, but with a mean radius R_1, so that

$$R_1 > R_o$$

The new radius of asperities will be sufficient to cause the second loading cycle to be entirely elastic, provided that the initial loading limit was not exceeded. If this limit was exceeded, the peaks will suffer more plastic deformation. When the load is removed, they will recover elastically into a spherical form, but with radius R_2, so that

$$R_2 > R_1$$

Thus, the elastic recovery curves are not congruent which is contrary to the experimental evidence (14 and 79).

It is rather difficult to predict the new value of peak radius after plastic deformation. However, substitution in equations 7.4 and 7.5 with values of mean radius measured for the as made surfaces will have rather little effect on the accuracy of the results. This can only be explained in terms of the sensitivity of equation 7.6 to the value of β, because when the radius changes from, say, 50 μm to, say, 10^3 μm, $\beta^{\frac{1}{2}}$ will only change from 5 to 22.36 microns$^{\frac{1}{2}}$. This roughly corresponds to around 22% change in the value of the stiffness at relatively small separations, while at larger separations it can be less than 10%.

The picture of contact presented earlier in this section replaces the need to assume an asperity shape, by assuming that the contact spots will have a uniform shape. This is only to facilitate the derivation a mathematical model for the elastic recovery. On the other hand, that picture is in line with the experimentally observed behaviour for the

mechanism of elastic deformation of machine tool joints.

7.5 A mathematical model for elastic recovery of machine tool joints

It will be assumed that within the range of loads encountered in machine tool joints, the contact spots will have circular areas after suffering some initial plastic deformation. Immediately before the elastic recovery starts, the pressure on the contact spot will be equal to the yield pressure of the material. This, in turn, could be taken as equivalent to the Vickers hardness number of the material (21), after transforming its units into N/mm^2. Thus, the load W_i carried by a single contact spot having an area a_i is given by

$$W_i = H\, a_i = H\, \pi\, r_i^2$$

$$\therefore \quad r_i = \left(\frac{W_i}{\pi\, H}\right)^{\frac{1}{2}} \qquad 7.7$$

The radius r_i will be assumed constant for all the spots of contact.

Now, the elastic deformation due to asperity contact can be treated as that due to a uniformally distributed load over an area on a semi-infinite solid (21). For a circular contact spot, the solution is given by Timoshenko (88) as

$$\lambda_i = 2\, \frac{(1 - \nu^2)}{E}\, P\, r_i$$

And for two rough surfaces in contact

$$\lambda_i = \frac{2}{E'}\, \frac{W_i}{\pi\, r_i} \qquad 7.7.1$$

Substituting for r_i from equation 7.7

$$\therefore \quad \lambda_i = \frac{2}{\sqrt{\pi}} \frac{1}{E'} \sqrt{W_i} \sqrt{H}$$

$$\text{ie} \quad W_i = \frac{\pi}{4} \frac{E'^2}{H} \lambda_i^2 \qquad 7.7.2$$

λ_i could be expressed in terms of the separation u, thus (see Fig 100, b)

$$\lambda_i = Z - u$$

$$W_i = \frac{\pi}{4} \frac{E'^2}{H} (Z - u)^2 \qquad 7.7.3$$

But, since surface asperities have peak height distribution $\phi(Z)$, then equation 7.7.3 could be summed for all asperities in contact in the same manner followed for equation 7.2, i.e.

$$W = \frac{\pi}{4} \frac{E'^2}{H} A_o \xi \int_u^\infty (Z - u)^2 \phi(Z) \, dZ \qquad 7.8$$

Equation 7.8 could be normalised for the standard deviation σ,

$$\therefore \quad W = \frac{\pi}{4} \frac{E'^2}{H} A_o \xi \sigma^2 \int_v^\infty (Y - V)^2 \phi(Y) \, dY$$

Or, since $\phi(Y)$ is Gaussian, then from equation 7.3.3, the load - separation relation is obtained as

$$W = \frac{\pi}{4} \frac{E'^2}{H} A_o \xi \sigma^2 F_2(V) \qquad 7.9$$

Equation 7.9 relates the applied load to the resultant separation without the need to know the shape of asperities. The stiffness of the joint is given by

$$K_J = \frac{dW}{du} = \frac{\pi}{2} \frac{E'^2}{H} A_o \xi \int_u^\infty (Z - u) \phi(Z) \, dZ$$

$$\text{Or} \quad K_J = \frac{\pi}{2} \frac{E'^2}{H} A_o \xi \sigma \int_v^{\infty} (Y - V) \phi(Z) \, dZ$$

$$\therefore \quad K_J = \frac{\pi}{2} \frac{E'^2}{H} A_o \xi \sigma F_1(V) \qquad 7.10$$

From 7.9 and 7.10, the joint stiffness could be related to the applied load

$$K_J = \frac{2}{\sigma} W \frac{F_1(V)}{F_2(V)}$$

$$\text{Or} \quad K_J = \frac{2}{\sigma} W F_2^1(V) \qquad 7.11$$

It appears from comparing equations 7.9 and 7.4 that the peak curvature in the latter has been replaced by $\frac{E'}{H}$ multiplied by a constant dependent on the separation. To explain further this point, we equate 7.9 by 7.4

$$\therefore \quad \frac{\pi}{4} \frac{E'^2}{H} A_o \xi \sigma^2 F_2(V) = \frac{4}{3} E' A_o \xi \sigma^{\frac{3}{2}} \beta^{\frac{1}{2}} F_{\frac{3}{2}}(V)$$

$$\text{ie} \quad \beta^{\frac{1}{2}} = \frac{3\pi}{16} \frac{E'}{H} \sigma^{\frac{1}{2}} \frac{F_2(V)}{F_{\frac{3}{2}}(V)}$$

take $\frac{F_2(V)}{F_{\frac{3}{2}}(V)} \simeq 0.85$, thus

$$\beta^{\frac{1}{2}} = 0.5 \frac{E'}{H} \sigma^{\frac{1}{2}}$$

Substitution with reasonable values for $\frac{E'}{H} \sigma^{\frac{1}{2}}$ will reveal large curvatures, not normally predictable by direct measurement of roughness, yet, needed to explain the elastic behaviour of the surface. Equation 7.9, then, obviates the need for much more complex measurements (peak radius) which would not normally lead to a rational explanation of the elastic recovery of joints.

The second modification in equation 7.9 is the method by which ξ the density of asperities is determined. Since, we no longer need a definition for a peak, and since the elastic recovery is due to the recovery of the body material behind the asperities, ξ can be found from the profile chart by simply counting the number of zero crossings of the mean line with the profile (per unit length).

$$\xi = \left(\frac{NO.}{2}\right)^2 \qquad \text{asperities/unit area}$$

7.6 The effect of assuming circular contact spots

Schofield (21) found that for square contact spots (resulting from contact between parabolic cusps with 90° between lays), the load deflection relation is given by

$$\lambda_J = 1.12 \frac{1}{E'} \sqrt{H\ P}\ f \qquad 7.12.1$$

where f = tool feed.

According to the analysis in (21), the elastic deformation of a single asperity λ_i is equal to the elastic deformation of the joint (since all asperities have the same height). Thus, equation 7.12 could be written as

$$\lambda_i = 1.12 \frac{1}{E'} \sqrt{H\ P}\ f$$

but $P = \frac{W_i}{f^2}$, thus

$$\lambda_i = 1.12 \frac{1}{E'} \sqrt{H\ W_i}$$

$$\therefore \quad W_i = 0.797 \frac{E'^2}{H} \lambda_i^2 \qquad 7.12.2$$

Assuming that the asperities have a distribution of peak heights $\phi(Z)$, then equation 7.12.2 could be summed for all asperities in contact in the same manner as before, thus

$$W = 0.797 \frac{E'^2}{H} A_o \xi \int_u^{\infty} (Z - u)^2 \phi(Z) \, dZ$$

and normalising for the standard deviation σ

$$\therefore \quad W = 0.797 \frac{E'^2}{H} A_o \xi \sigma^2 F_2(V) \qquad 7.12.3$$

while the stiffness is obtained from

$$K_J = \frac{2}{\sigma} W F_2^1(V) \qquad 7.12.4$$

Thus, when assuming square contact spots we arrive at the same results with the value of the constant changing from 0.785 for circular contact spots to 0.797 for square ones.

7.7 Stepwise procedures for estimating the stiffness of joints

The theoretical analysis presented in sections 7.2 and 7.5 could be used in the following manner to calculate the joint stiffness:

1. Knowing the applied load, material properties and the values of surface texture parameters, either equation 7.4 or 7.9 is used in order to find the value of $F_{\frac{3}{2}}(V)$ or $F_2(V)$ respectively.

2. From either Fig 101 or Fig 102 the value of $F^{\frac{1}{2}}_{\frac{3}{2}}(V)$ or $F_2^1(V)$ could be obtained. Figs 101 and 102 were drawn from the tabulated values given in reference 89.

3. The joint stiffness could now be evaluated from either

equation 7.6 or 7.11, depending on the model used.

Because the stiffness of joints will affect the overall stiffness and natural frequency of the structure, it is important that the joints are accounted for during the design stage. The following is an attempt to supply the designer with standardised procedures to implement when designing a joint having a required stiffness:

1. Estimate the joint's preload and specify the standard deviation of flatness deviations.

2. From equation 7.11 calculate $F_2^1(V)$ and from Fig 102 find $F_2(V)$.

3. Use equation 7.9 to decide on the machining conditions, the joint apparent area, and material properties.

7.8 Experimental analysis

The theory developed in the previous sections was tested for actual joints and the results were compared with the joint stiffness directly measured. Four machining operations were considered: turning, milling, shaping and grinding. Within each operation, the cutting conditions were varied to give different textures as tabulated in tables 4 to 18. The average Vickers Hardness number for the joints machined using every operation was as follows:

Shaping	:	2.152×10^3 N/mm^2
Turning	:	2.142×10^3 N/mm^2
Milling	:	2.0152×10^3 N/mm^2

Grinding : 2.007×10^3 N/mm^2

The value of E' was 1.136×10^5 N/mm^2

The stiffness at eight levels of preloads within the range 250 kp to 2800 kp was computed.

For every joint tested, the values of stiffness computed using equation 7.6, and those computed using equation 7.11 were plotted together with those experimentally measured, as shown in Figs 103 to 117. It can be seen from these Figures that, for all joints tested, a reasonable (if not accurate) theoretical assessment of the joint stiffness could be made.

7.9 Discussion and conclusions

The analysis presented in this Chapter provides two equations for the evaluation of the stiffness of dry machine tool joints. The two equations are basically different in their physical implementations. Equation 7.6 is based on assuming that surfaces are covered with spherical asperities, whilst equation 7.11 does not lay restrictions on the shape of asperities, but, instead specifies a uniform shape for the contact spots. The numerical results for the joint stiffness obtained by using either theories are not, however, very different from each other and more importantly, they are in close agreement with those experimentally measured.

What appears to affect the joint stiffness most is the condition of flatness deviations on its surface. The condition of the surface

roughness plays a rather less important role in deciding the stiffness of the joint. The only roughness parameter which significantly affects the joint stiffness is the density of asperities ξ.

Whilst the elastic deformation of the joint will be dependent on the applied pressure, the joint stiffness is mainly dependent on the applied load. The apparent pressure will have no effect on the joint stiffness if the value of $F_2(V)$ is less then 3×10^{-5} while at larger values the apparent pressure will have very little effect on the stiffness.

According to equation 7.9, the harder the material of the joint, the greater will be the value of $F_2(V)$, thus the less the value of $F_2^1(V)$ and consequently the less the joint stiffness will be. This is in line with what could be concluded from Fig 2.

The main body of the experimental work carried out in this Chapter is related to strongly anisotropic surfaces, and since the results obtained using either theories agree with those experimentally measured, one could then expect that both equations for the stiffness will hold for most (if not all) machined surfaces.

Some joints showed an increase in the rate of the stiffness increase with preload, whereas the majority of joints displayed a decreasing or constant rate. The theoretical models show that this rate could be either constant or decreasing. A possible explanation for an increasing rate could be that the peak height distribution has suffered some change which, in turn, caused a change in its standard

deviation, leading to a change in the rate at which the joint stiffness increases with preload.

C H A P T E R 8

DAMPING IN DRY CLEAN JOINTS SUBJECTED TO DYNAMIC LOADS NORMAL TO THE JOINT INTERFACE

8.1 Introduction

A machine tool structure is required to have high dynamic stiffness and large damping capacity for its dynamic performance to be satisfactory. Dynamic stiffness is dependent on the properties of the structural elements and on the method of joining them. The damping capacity of the structure is slightly dependent on the material damping of the components; the greater contribution will be made by the damping in the interface which will impress itself on the overall damping of the machine structure.

The joint model as described in the previous Chapter will be subjected to an alternating load which is normal to the joint interface. This implies that unless the load (carried by every individual spot) is exactly normal to the area of the contact spot, there might be a shearing force component and ultimately two contacting asperities may slide over each other dissipating part of the energy. This is a source of energy dissipation which is primarily created by the presence of an interface.

8.2 A brief literature survey

Reshetov and Levina (32) carried out an investigation into the

damping of oscillations in dry flat joints formed from a stack of discs subjected to a static preload and a dynamic oscillatory force. They reported that the average value of relative energy dissipation for unlubricated joints was 0.15 (which is equivalent to 0.0238 loss factor). Andrew et al (35) reported that the damping in dry clean joints, excited normal to the interface, was negligible.

Thornley (38) carried out an extensive experimental study of the dynamic behaviour of joints. He reported that damping in dry clean joints was slightly larger than that measured for the equivalent solid. Unlike the experiments in references 32 and 35, where a stack of joints was tested at one time, Thornley's experiments comprised only one joint. He pointed out the dependence of damping on the joint preload and that rough surfaces have a slightly better damping ratio than smooth surfaces.

Lees (28), in a continuation of the experiments started in (38), found that the damping decreases when increasing the joint preload. He studied the effect of the number of joints assembled in series on the overall damping capacity of the assembly. Some of his results (see Fig 118) indicate that the damping ratio decreases as the number of joints increases and, in some cases, the damping ratio for the assembly is less than that for the equivalent solid. Lees reported that the introduction of a thin sheet of Butyl rubber at the joint interface resulted in a reduction in the overall damping of the jointed column. Although he attributed this observation to the reduction of the overall stiffness of the jointed column (as a result of elimination of metal to metal contact) he did not explain why the same trend happened when he

tested joints lubricated with Vitrea oil 75 which showed an increase in its stiffness.

Khoyi (41) observed the dependence of loss factor on the joint preload. He demonstrated in one of his graphs (see Fig 119) that the average of the loss factors measured for stacks of dry clean joints was less than that measured for their equivalent solids; Khoyi did not offer any explanation for such a trend.

8.3 The effect of damping in joints on the damping of the assembly

What, then, can one conclude from the investigations reported above? Most important of all, they show that in the absence of any externally applied force acting parallel to the interface, fixed joints will display some damping under normal dynamic loads. Furthermore, they point out its main features regarding preload and joint finish. Finally, the examination of the results presented in references 28 and 41 reveals that the damping measured for a stack of dry joints may be less than that measured for the equivalent solid.

The last conclusion could be explained in terms of the relationship between the stiffness and damping for the dry jointed column on the one hand, and their corresponding values for the equivalent solid on the other. A jointed column could be simulated by two complex springs (one represents the stiffness and damping due to the material of the joints and the other represents the stiffness and damping of the interfaces) connected in series as shown in Fig 19,c.

Thus

$$\frac{1}{K_d + i\omega C_d} = \frac{1}{K_m + i\omega C_m} + \frac{N}{K_J + i\omega C_J} \qquad 8.1$$

by writing 8.1 in terms of the stiffness and loss factor we get

$$\frac{1 - i\tau}{K_d\,(1 + \tau_d^2)} = \frac{1 - i\tau_m}{K_m\,(1 + \tau_m^2)} + \frac{N\,(1 - i\tau_J)}{K_J\,(1 + \tau_J^2)} \qquad 8.2$$

Splitting 8.2 into its real and imaginary components

$$\frac{1}{K_d\,(1 + \tau_d^2)} = \frac{1}{K_m\,(1 + \tau_m^2)} + \frac{N}{K_J\,(1 + \tau_J^2)} \qquad 8.3.1$$

$$\frac{\tau_d}{K_d\,(1 + \tau_d^2)} = \frac{\tau_m}{K_m\,(1 + \tau_m^2)} + \frac{N\tau_J}{K_J\,(1 + \tau_J^2)} \qquad 8.3.2$$

Multiplying 8.3.1 by τ_J and subtracting the result from 8.3.2

$$\frac{\tau_d}{K_d\,(1 + \tau_d^2)} - \frac{\tau_J}{K_d\,(1 + \tau_d^2)} = \frac{\tau_m}{K_m\,(1 + \tau_m^2)} - \frac{\tau_J}{K_m\,(1 + \tau_m^2)}$$

$$\frac{\tau_d - \tau_J}{K_d\,(1 + \tau_J^2)} = \frac{\tau_m - \tau_J}{K_m\,(1 + \tau_m^2)}$$

i.e.

$$\frac{K_m\,(1 + \tau_m^2)}{K_d\,(1 + \tau_d^2)} = \frac{\tau_m - \tau_J}{\tau_d - \tau_J} \qquad 8.3.4$$

It is known that the loss factor for the solid is normally very small, so that

$$K_m\,(1 + \tau_m^2) \simeq K_m$$

Similarly, for the jointed column, the measured value for τ_d is even smaller, thus

$$K_d (1 + \tau_d^2) \simeq K_d$$

On the other hand, assembling a large number of dry clean joints in series reduces the effective stiffness of the assembly far beyond that for the equivalent solid, and the result is that the ratio in equation 8.3.4 might be larger than unity so that

$$\tau_m - \tau_J > \tau_d - \tau_J$$

$$\therefore \quad \tau_m > \tau_d \qquad 8.3.5$$

That is, the loss factor of the equivalent solid is larger than that for the jointed column, which is in line with the experimental results obtained in this work (see Figs 42 to 72), as well as the earlier observations by Lees and Khoyi (see Figs 118 and 119).

The above relationships state that unless the product $K_d (1 + \tau_d^2)$ is made larger than that for the equivalent solid, the introduction of joints in a structure will generally result in harming its damping properties. This could be avoided by contaminating the joints with oil or other agents which have the property of increasing both the stiffness and damping of the assembly. They also demonstrate that the introduction of dissipative elements at the joint interface will not result in a significant improvement in the damping of the assembly unless the stiffness is increased or at least kept constant. This is in line with Lees' observation concerning the introduction of Butyl rubber in between the joint interface. Finally, it can be seen that if the joints were ignored in a study of the dynamic behaviour of

a structure, the results could be misleading. For this reason, it was thought that a simple mathematical expression developed for damping is needed to be complementary to the stiffness expression developed in Chapter 7.

8.4 A mathematical model for damping in dry clean joints

Contact between real surfaces will include asperities which developed contact spots parallel to the plane of the joint as well as others which are oblique to that plane. The latter will be named "oblique spots" and the former "in-plane spots". In Chapter 7, a mathematical expression for the joint stiffness was derived; in order to simplify the mathematical treatment it was assumed that contact between two rough surfaces could be reduced to a condition of contact between a single surface which is rough and a smooth flat plane. The single rough surface (being the sum of the two rough surfaces in contact) will have the property of transferring all oblique spots into "in-plane" spots as shown in Fig 120. In practice, however, under normally applied dynamic loads, oblique spots will experience tangential forces which will result in shear deformation and ultimately two asperities forming an oblique spot may slide over each other.

In deriving a mathematical expression for damping in normally loaded joints, the following assumptions will be made:

1. All contact spots will share the dynamic load F equally. Thus, if W_i is the dynamic load carried by a single contact spot and n is the number of contact spots, then

$$F = n W_i$$

2. That all "oblique spots" will slide over each other as a result of the dynamic load, so that the average amount of sliding will depend on the average slope of the surface roughness asperities.

3. That the measured amplitude of vibration U_o will reflect the amount of elastic deformation of the "in-plane spots".

4. An "oblique spot" will slide a distance (measured in the normal direction) equal to the difference between its component of elastic deformation (projected on to the normal direction) and U_o.

The notation shown in Fig 121 is defined as follows:

U = Elastic component of deflection (due to the dynamic load) of an oblique contact spot. U is measured normal to the plane of the joint.

h = Elastic component of deflection of an oblique spot. h is measured in a direction normal to the common tangent at the point of contact.

μ = Coefficient of friction.

α = The angle between the common tangent and the plane of the joint = mean absolute slope of surface roughness asperities.

From Fig 121, the normal component of the friction force per asperity

$$= - \mu W_i \cos \alpha \sin \alpha$$

$$= -\frac{1}{2}\mu W_i \sin 2\alpha \qquad 8.4$$

The energy dissipated per cycle could be obtained, approximately (90), from the work done by the friction force per cycle. Thus, for n asperities in contact

$$D_o \simeq 4 \int_o^{U_o - U} n \left(-\frac{1}{2}\mu W_i \sin 2\alpha\right) dU$$

$$= -2 n \mu W_i (U_o - U) \sin 2\alpha \qquad 8.5$$

For "in-plane" spots, the relationship between the load and elastic deflection is obtained from equation 7.7.2

$$W_i = C U_o^2 \qquad 8.6.1$$

$$\therefore \quad U_o = \left(\frac{W_i}{C}\right)^{\frac{1}{2}} \qquad 8.6.2$$

where $C = \frac{\pi}{4}\frac{E'}{H}$

For "oblique spots", the component of load which causes elastic deformation will be perpendicular to the common tangent at the point of contact. This component will cause elastic deformation h which is given by

$$W_i \cos\alpha = C h^2$$

but from Fig 121

$$h = \frac{U}{\cos\alpha}$$

$$\therefore \quad U = \left(\frac{W_i}{C}\right)^{\frac{1}{2}} \cos^{\frac{3}{2}} \alpha \qquad 8.7$$

From equation 8.6.2 and 8.7, the sliding distance (measured in the normal direction) is given by

$$U_o - U = \left(\frac{W_i}{C}\right)^{\frac{1}{2}} (1 - \mathrm{Cos}^{\frac{3}{2}}\alpha) \qquad 8.8.1$$

From equations 8.6.1 and 8.8.1

$$U_o - U = U_o (1 - \mathrm{Cos}^{\frac{3}{2}}\alpha) \qquad 8.8.2$$

Substituting from equations 8.6.1 and 8.8.2 into equation 8.5

$$\therefore \quad D_o = -2\, n\, \mu\, \mathrm{Sin}2\alpha\, (1 - \mathrm{Cos}^{\frac{3}{2}}\alpha)\, C\, U_o^3 \qquad 8.9$$

The maximum elastic energy stored per cycle (for the joint) is obtained from

$$V_o = \int_o^{U_o} n\, W_i\, dU$$

$$= \int_o^{U_o} n\, C\, U_o\, dU$$

$$\therefore \quad V_o = \frac{C}{3}\, n\, U_o^3 \qquad 8.10$$

The specific damping capacity is defined (91) as the ratio of the energy dissipated to the maximum strain energy per cycle, i.e.

$$\psi = \frac{-D_o}{V_o}$$

Thus, from equation 8.9 and 8.10

$$\psi = 6\, \mu\, \mathrm{Sin}2\alpha\, (1 - \mathrm{Cos}^{\frac{3}{2}}\alpha) \qquad 8.11$$

The loss factor for the joint is obtained from

$$\tau_J = \frac{\psi}{2\pi}$$

$$\therefore \tau_J = \frac{3}{\pi} \mu \, \mathrm{Sin}\, 2\alpha \, (1 - \mathrm{Cos}^{\frac{3}{2}} \alpha) \qquad 8.12$$

Equation 8.12 gives the loss factor for the dry clean joint in terms of the average slope α and the coefficient of friction μ. It does not predict the relation between the loss factor and preload which could be the result of ignoring other acting mechanisms of damping.

Experimental measurements of the loss factor were carried out for differently machined joints to test the validity of equation 8.12. The experimental procedures and the specimens were described in Chapters 3, 4 and 6; the absolute mean slope for each type of joints used was measured in the manner described in Chapter 5. The coefficient of friction μ was taken to be 0.6. The theoretical and experimental results are shown in Figs 123 to 127. The theoretical and experimental results are not in precise agreement with each other. This is firstly due to the presence of other damping mechanisms which are not considered in the theoretical model, and secondly because of the simplifying assumptions which were needed in order to derive the expression for the loss factor. However, having a simple means of assessing the damping in dry joints is better than ignoring it all together.

8.5 Discussion

The photographs shown in Fig 126 are for some machined surfaces as they appear when examined using the scanning electron microscope. They convey the idea that machined surfaces contain very small roughness

details which are not fully revealed on a profile graph. These small details could have a decisive effect on the damping characteristics of joints. A contact spot, as described earlier, will be normally formed from smaller spots of contact ("micro spots"), which arise from the contact between the small roughness details present on both mating surfaces. Although the load on a contact spot may be purely compressive, the "micro spots" could experience other forms of loading. Thus, the smaller roughness details within a contact spot might slide over each other, or experience cyclic plastic deformation (42). A contact spot might also contain holes which are filled with air; thus under vibration, the air is pumped in and out, giving rise to viscous damping.

It is then clear that a variety of damping mechanisms are acting together at any time, every mechanism contributing to the normal component of the damping force. It is possible that a particular damping mechanism becomes more predominant when a certain joint preload is reached; this will be dependent on the conditions of contact achieved at this particular preload. If the preload changes, the contact configurations might change and a completely different mechanism could then become predominant. This would then explain the experimentally observed dependence of damping on the joint preload.

The total value of damping in a dry clean joint is very small. This reduces the need for its precise assessment, and for most tests carried out equation 8.12 appears to give the lowest value of damping. This was valid for all joints apart from:

(a) ML3 joint, for which the damping measured for the jointed

column was so small that after correcting for the effect of material, the loss factor for the joint was negative, whilst its theoretical value was 2.5×10^{-4}.

(b) The loss factor for GN2 joints (Fig 125) was very high when compared with its value obtained theoretically, which was 0.9×10^{-4}. This could be explained in terms of the presence of viscous damping (due to the air trapped in between the joint interface as a result of the smoothness of the joint surfaces; CLA was 0.139 μm).

The experimental results in Figs 122 to 125 show that the loss factor initially reduces with increasing preload. As the preload continues rising, the loss factor shows (in many cases) an increase in its value. The increase in the value of the loss factor at higher preloads could be attributed to the progressive significance of the damping component due to the air pumped in and out of the holes. That is, as the joint preload increases, more holes tend to have a smaller opening; thus, the air dissipates more energy when pumped in and out.

CHAPTER 9

APPLICATION OF THE THEORETICAL ANALYSIS AND FUTURE WORK

9.1 The use of joints data for the prediction of the natural frequency of machine structures

The theoretically derived expressions (in Chapters 7 and 8) for the stiffness and loss factor of dry clean machined joints, are employed in this section to explore how accurately one could predict the natural frequency of a typical machine structure. This is an example of the way in which prior knowledge of data about joints could be useful to the designer.

In the present analysis the test rig (described in Chapter 3) has been chosen as an example of the machine structure under consideration. This is because it has a second natural frequency dependent on the stiffness of the jointed column, hence, provides a good example of a structure sensitive to joints. It has been shown in Appendix I that the 2nd natural frequency of the test rig is given by equation 11.3

$$\omega_2^2 = (K_1 + 2K)/M_1$$

Since K_1, the stiffness of the system springs, is small compared to the stiffness of the jointed column K, then K_1 could be ignored, and for the purpose of the present analysis, the second natural frequency f_2 of the test rig is given by

$$f_2 = \frac{1}{2\pi}\sqrt{\frac{2}{118.5}}\ \sqrt{K} = 2.0676 \times 10^{-2}\ \sqrt{K} \qquad \text{Hz} \qquad 9.1.1$$

Equation 9.1 shows that the accuracy of predicting the 2nd natural frequency will be dependent on how accurate the jointed column stiffness could be predicted. To give an example, we assume that the stiffness could be evaluated with e per cent error, thus

$$f_2 = 2.0676 \times 10^{-2}\ \sqrt{K_o\ (1 + \frac{e}{100})}$$

Where K_o is the true value of the stiffness.

The percentage error e_f in evaluating the frequency f_2 is then given by

$$e_f = (\sqrt{(1 + \frac{e}{100})} - 1)\ 100 \qquad 9.1.2$$

That is, if the error in stiffness evaluation is, say, 20%, the natural frequency could be obtained with an error less than 10%.

The jointed column model was shown to be composed of two units connected in series as shown in Fig 19,c. From equations 3.23 and 3.24 we have

$$\frac{1}{K\ (1 + \tau^2)} = \frac{N}{K_J\ (1 + \tau_J^2)} = \frac{1}{K_m\ (1 + \tau_m^2)} \qquad 9.2$$

$$\frac{\tau}{K\ (1 + \tau^2)} = \frac{N\ \tau_J}{K_J\ (1 + \tau_J^2)} + \frac{\tau_m}{K_m\ (1 + \tau_m^2)} \qquad 9.3$$

In equations 9.2 and 9.3, the stiffness and loss factor for the material effect were substituted by those obtained from the equivalent solid test. The stiffness and loss factor of joints (K_J, τ_J) were

those theoretically computed from equations 7.11 and 8.12 respectively. The stiffness of the jointed column was then obtained and the frequency f_2 was calculated using equation 9.1. Both the theoretically computed and the experimentally measured 2^{nd} natural frequency of the test rig were plotted in Figs 127 to 141.

The results show that in all cases studied a reasonable, if not accurate, prediction of the natural frequency could be achieved. The maximum error in predicting the natural frequency was that for SH2 column shown in Fig 132. This error ranged between -25% at the lowest preload to -10.15% at the highest preload.

Some cases show that over-estimation of the frequency could be made; however, even for those cases the theoretically computed frequency could be taken as the safe operating limit of the machine. The reason is that machine tool joints will always be contaminated with some lubricant, and this will increase the joint stiffness causing the natural frequency to rise. Thus, the final resultant is that the computed frequency will be very near to the actual natural frequency of the machine.

9.2 The source of error in evaluating the stiffness of SH2 and SH4 joints

The relatively high level of error, which occurred when computing the stiffness of SH2 and SH4 joints, calls for some additional consideration. It was thought that this error arose because of an over-estimation of the average value of the standard deviation of waviness height distribution. The reason is that those roughly shaped

joints had a rather open texture which permitted the stylus originally used in measuring waviness to also travel in between the adjacent roughness peaks, thus recording higher values. The same problem was reported in reference 16 when measuring flatness deviations on planed joints.

To examine further the above observation, it was decided to repeat the measurement of waviness for SH2 and SH4. The stylus dimensions were to be large enough to eliminate any possibility that the new stylus may measure a part of what could be considered as roughness. Since the standard stylus supplied with the Talylin model 1 instrument had much larger tip dimensions than the one originally used, it was decided to use it for the new measurements. The dimensions of the new stylus are shown in Fig 142. The chisel edge of the stylus was positioned perpendicular to the lay direction, and the measurement of waviness was made only in the direction of lays. As a result, the average standard deviation of waviness height distribution was reduced from 4.415 to 2.973 μm for SH2, whilst that of SH4 was reduced from 3.052 to 2.349 μm. The joint stiffness was again computed from equation 7.11 and the results for the new and old data were plotted together with the experimentally measured ones in Figs 143 and 144.

The level of error between the experimentally measured stiffness and the computed one was reduced for both joints indicating that we succeeded in pointing towards one of the sources of errors. This also illustrates the importance of correct assessment of flatness deviations in order to obtain reasonably accurate theoretical results.

It is also interesting to point out that for very smooth surfaces, a similar problem seems to occur, though in a reverse manner. That is, the standard deviation measured was less than its true value for the surface because the stylus used in measuring waviness was too large when compared with the spacing between adjacent roughness peaks. This point is partially reflected on the theoretical results of the smoothest surface examined in this work, i.e. GN2 shown in Fig 117. In this case it appears that a sharper stylus should be used. The sharpness of the stylus should, however, be carefully assessed in order not to create problems similar to the ones encountered with SH2 and SH4 joints.

In general, however, the method by which flatness deviations was measured and assessed in this work appears to be suitable for a wide range of machined finishes. The error is only expected to increase when the surface is either very rough or very smooth. Even then, the theoretical analysis in Chapter 7 appears to give a fair estimate for the joint stiffness, whilst if the aim is to evaluate the natural frequency of the structure, the error will be much smaller.

9.3 Future work

I Measurement of flatness deviations

A direct relation between flatness deviations on the joint surfaces and the joint stiffness was established in this work. It was also shown how functional assessment of flatness deviations could be made. However, the way in which flatness errors are measured is not satisfactory for the following reasons:

1. The stylus which acts as a mechanical filter for roughness is not yet standardised in either shape or dimensions.

2. The filtering properties of the stylus are not fully defined.

3. There is no instrument available which is specifically designed for flatness measurements.

It is then suggested that a study should be carried out on the properties of the stylus as a mechanical filter. The outcome of such a study would be a recommendation of a set of stylii shapes that could be used depending on the type of surface texture to be measured. It is also recommended that a new machine should be designed specifically to measure the flatness height distribution on machined surfaces. Such a machine could be linked to a microprocessor that would analyse the measured data and give the readings needed for the complete description of the distribution.

II Lubricated joints

1. The present investigation has revealed that for every machined finish, there is an optimum oil viscosity which appears to result in the highest loss factor of the assembly. It is then recommended to examine further this point in order to establish the type of relation that exists between the lubricant viscosity, surface texture and damping.

2. It has also been shown that a lubricated joint is generally superior to unlubricated ones. It is

interesting to examine the effectiveness of the lubricant layer in between bolted joints against time. It is also interesting to find some means for ensuring that a layer of particular lubricant is always present between the interface.

3. A theoretical model for the evaluation of the stiffness and damping of lubricated joints is needed. Such a model should take into account the nature of the surface topography of joints in order to reveal its relation to the stiffness and damping of the joint when lubricated with a particular oil viscosity.

III The applicability of the theoretical models for the stiffness and loss factor of dry clean joints should be tested for joints manufactured of materials other than steel. In particular, it would be interesting to investigate the dynamic behaviour of synthetic joints.

IV The theoretical model for the joint stiffness could be employed in a theoretical investigation into the deflection of beams on elastic foundation.

V Further tests of joints machined using machining operations other than those covered in this work is suggested in order to test the consistency of the theoretical models presented above.

VI The equations derived in this work could be employed in a computer-aided design program to test the accuracy of predicting the dynamic behaviour of an actual or model machine

tool structure. The theoretical results could be compared to those obtained by direct measurement.

CHAPTER 10

CONCLUSIONS

1. The dynamic stiffness of joints increases with an increase in the applied preload.

2. The increase in the preload applied on the joint results in decreasing the damping.

3. The introduction of an oil film in between the joint interface increases its dynamic stiffness.

4. The stiffness of lubricated joints increases with the increase in the applied load.

5. The rate of increase in the stiffness of lubricated joints with increasing applied preload reduces at higher preloads.

6. The dynamic stiffness of lubricated joints increases with an increase in the viscosity of lubricant.

7. The increase in the dynamic stiffness of a joint lubricated with a particular oil viscosity appears to be dependent on the surface roughness of the joint. Thus, the more rough the surface of the joint, the higher the viscosity of oil needed to cause a significant improvement in its dynamic stiffness.

8. The use of heavy grease as a contaminating layer could cause the dynamic stiffness of the jointed assembly to rise very near to the stiffness of the solid.

9. The introduction of Hermetite into the joint interface results in an improvement in the dynamic stiffness and loss factor of the joint.

10. As the Hermetite layer solidifies, the dynamic stiffness of the bolted assembly increases to almost the stiffness of the solid, while the loss factor reduces. The final value of the loss factor for the assembly is, however, higher than that for the equivalent solid.

11. The introduction of oil into the joint interface results in an enormous increase in damping.

12. The increase in the loss factor of a lubricated jointed assembly appears not to be directly proportional to the oil viscosity. An optimum oil viscosity is needed for the best possible improvement in the loss factor of the assembly.

13. For all tests carried out for lubricated joints the loss factor decreases as the joint preload increases.

14. The rate of decrease of loss factor with increasing preload tends to considerably reduce as the preload increases.

15. The shape of apparent area of contact has no effect on the dynamic characteristics of dry clean joints; however, for lubricated joints the circular joints displayed lower dynamic stiffness than that for the square or the triangular joints.

16. The change in the direction of lays appears to have no influence on the stiffness of joints, provided that this change does not result in a significant change in the overall flatness

deviations on the joint surface.

17. The frequency and amplitude of vibrations appear to have no influence on the dynamic stiffness and loss factor within the frequency range of the tests carried out.

18. An increase in the apparent area of contact results in an increase in flatness deviations on the surface of the joint; hence, a reduction in its dynamic stiffness.

19. It is important to ensure that all joints within a jointed assembly are nearly of the same quality, since the presence of a weak joint could reduce the overall stiffness of the assembly, particularly when the number of joints is small.

20. The loss factor of a dry clean jointed assembly may be less than that of an equivalent solid. This conclusion is also supported by theoretical reasoning.

21. The loss factor of a dry clean joint could be evaluated from

$$\tau_J = \frac{3}{\pi} \mu \sin 2\alpha \quad (1 - \cos^{\frac{3}{2}} \alpha)$$

22. The above expression gives a lower estimate for the loss factor of the joint.

23. Damping in dry clean joints arises from a variety of mechanisms, one of which is the friction between contacting asperities. The predominance of one particular mechanism over the others will depend on the exact contact configurations achieved at a particular level of preload.

24. The dynamic stiffness of dry clean joints could be computed from the relations

$$W = \frac{\pi}{4} \frac{E'^2}{H} A_o \xi \sigma^2 F_2(V)$$

$$K = \frac{2}{\sigma} W F_2^1(V)$$

25. The above expressions reveal that:

(a) The only roughness parameter which affects the joint stiffness is that of density of asperities.

(b) The stiffness of the joint is inversely proportional to the standard deviation of its flatness height distribution.

(c) The stiffness of the joint is very little affected by its apparent area of contact.

(d) The stiffness of the joint decreases with an increase in the hardness of its surfaces.

26. The above expression for the stiffness is based on the theory that the elastic recovery of the surface of the joint is due to the recovery of the body material behind the asperities.

27. While the elastic deformation of the joint is dependent on the apparent pressure, the stiffness is rather dependent on the applied load.

28. The above equations are suitable for the evaluation of the stiffness of strongly anisotropic surfaces as well as the stiffness of ground joints.

29. The origin of the empirical logarithmic - linear relation between the applied preload on the joint and its elastic deflection lies in the shape of the peak height distribution for the joint surfaces.

30. Another theory that explains the elastic recovery of joints in terms of the recovery of roughness peaks into a spherical form was also found suitable for the evaluation of the stiffness of joints provided that the peak height distribution is that obtained from flatness measurements.

31. The experimental and theoretical results using either theories agree with the results measured experimentally.

32. Stepwise procedures are given in section 7 in order to design a joint of a certain stiffness.

33. With joints taken into account, it is possible to evaluate the natural frequency of a structure with accuracy better than that for the evaluation of the stiffness of joints.

34. The experimental test rig offers a good tool for the measurement of the stiffness and damping of highly stiff joints. The agreement between the theoretical and experimental results offer confidence in both the test rig and the mathematical models developed.

35. The correction for the effect of material stiffness also compensates for the effect of the presence of the load cell and the end conditions of the jointed column under test. On the other hand, this correction could be impractical for highly

stiff joints.

36. The setup used to measure surface roughness and flatness proved to be useful in providing enough information about the surface topography of the joint. The information provided was reliable in covering the range of parameters needed to describe the behaviour of joints.

37. The statistical distribution of flatness heights offers an excellent representation of the peak height distribution for the surface.

38. A statistical distribution for surface flatness could be obtained by averaging the results obtained from measuring several independent waviness traces on the surface.

39. The definition of waviness as the undulations of a line joining roughness peaks could be a functional definition. Furthermore, the characterisation of waviness by the root mean square value of its heights bears direct relation to the joint stiffness.

40. The stylus of a surface roughness measuring instrument should be checked for wear as the results of measurements made using a worn stylus could be faulty.

41. The use of a razor blade to check the wear on the stylus proved to be a cheap, simple and reliable method of checking the stylus shape.

REFERENCES

1. HIJINK, J. A. W. and VAN DER WOLF, A. C. H., Survey on stiffness and damping of machine tool elements. Annals of the CIRP, Vol. 22, No. 1, 1973.

2. TAYLOR, S., A computer analysis of an openside planing machine, Int. MTDR Conf., 1965.

3. YOSHIMURA, M. and OKUSHIMA, K., Computer-aided design improvement of machine tool structure incorporating joint dynamics data. Annals of the CIRP, Vol. 28, No. 1, 1979.

4. COWLEY, A., Machine tool structures. Edited by KOENIGSBERGER, F. and TLUSTY, J. Pergamon Press, 1970, Ch. 2, pp 486 - 504.

5. RESHETOV, A. N., Machine tool design calculations. Machines and Tooling, Vol. XLll, No. 11, 1965.

6. HIJINK, J. A. W. and VAN DER WOLF, A. C. H., Analysis of a milling machine: computed results versus experimental data, Int. MTDR Conf., 1973.

7. SATA, T., YASUI, T., OKUBO, N., SUZUKI, M., KUROIWA, A., Measurement of dynamic behaviours of mechanical structure by means of double pulsed holography and its application. Annals of the CIRP, Vol. 25, No. 1, 1976.

8. TAYLOR, S., Computers and mechanical design. Computer Aided Design, Vol. 5, No. 3, 1973.

9. YOSHIMURA, M., Analysis and optimisation of structural dynamics of machine tools by a synthesis of dynamic rigidity program system. Int. MTDR Conf., 1976.

10. VOTINOV, K. V., The rigidity of machine tools. Leningrad Section, Machine Builders' Union (Lonitomash), Leningrad, 1940, (as reported in reference 11).

11. KRAGELSKY, I. V., Friction and wear. Butterworths, London, 1956, pp 30 - 59.

12. DEMKIN, N. B., Actual contact area of solid surfaces. USSR Acad. Sci. Publ. House, Moscow, 1962, (as reported in reference 11).

13. KRAGELSKY, I. V. and DEMKIN, N. B., Contact area of rough surfaces. Wear, Vol. 3, 1960.

14. THORNLEY, R. H., CONNOLLY, R., BARASH, M. M. and KOENIGSBERGER, F. The effect of surface topography upon the static stiffness of machine tool joints. Int. J. Mach. Tool Des. Res., Vol. 5, 1965.

15. CONNOLLY, R. and THORNLEY, R. H., The significance of joints on the overall deflection of machine tool structures. Int. MTDR Conf., 1965.

16. CONNOLLY, R. and THORNLEY, R. H., The static stiffness of joints between machined surfaces. M.T.I.R.A. report No. 13, 1966.

17. CONNOLLY, R., THORNLEY, R. H., Determining the normal stiffness of joint faces. Trans. ASME, J. Eng. Ind., No. 6, 1967.

18. THORNLEY, R. H., CONNOLLY, R., KOENIGSBERGER, F., The effect of flatness of joint faces upon the static stiffness of machine tool joints. Proc. Instn. Mech. Engrs., Vol 182 Pt 1, No. 18, 1967.

19. LEVINA, Z. M., Research on the static stiffness of joints in machine tools. Int. MTDR Conf., 1967.

20. GREENWOOD, J. A., The area of contact between rough surfaces and flats. Trans. ASME, J. Lub. Tech., Vol. 89, 1967.

21. SCHOFIELD, R. E., An investigation into the fundamental problems of the static stiffness of bolted joints. Ph.D. Thesis, UMIST, 1967.

22. SCHOFIELD, R. E. and THORNLEY, R. H., Calculating the elastic and plastic components of deflection of plane joints formed from machined surfaces. Int. MTDR Conf., 1971.

23. SCHOFIELD, R. E. and THORNLEY, R. H., Calculating the elastic and plastic components of deflection of joints formed from machined surfaces with flatness errors. Int. MTDR Conf., 1972.

24. SCHOFIELD, R. E. and THORNLEY, R. H., Mathematical expression of surface-finish characteristics. Proc. Instn. Mech. Engrs, Vol. 182, Pt 3K, 1967.

25. BACK, N., BURDEKIN, M., COWLEY, A., Review of the research on fixed and sliding joints. Int. MTDR Conf., 1972.

26. BURDEKIN, M., COWLEY, A., BACK, N., An elastic mechanism for the microsliding characteristics between contacting machined surfaces. J. Mech. Eng. Science, Vol. 20, No. 3, 1978.

27. CONNOLLY, R., The static stiffness of joint faces. M.Sc. Thesis, UMIST, 1965.

28. LEES, K., An investigation into some of the properties which influence the dynamic behaviour of joints loaded normal to the joint surface. M.Sc. Thesis, UMIST, 1970.

29. THORNLEY, R. H. and LEES, K., Some static and dynamic characteristics of bonded, machined joint faces. Int. MTDR Conf., 1972.

30. CONNOLLY, R. SCHOFIELD, R. E. and THORNLEY, R. H., The approach of machined surfaces with particular reference to their hardness. Int. MTDR Conf., 1967.

31. SCHOFIELD, R. E., The effect of hardness on the static stiffness of joint faces. M.Sc. dissertation, UMIST, 1965.

32. RESHETOV, D. N. and LEVINA, Z. M., Damping of oscillations in the couplings of components of machines. Vestnik Mashinostroyeniya, No. 12, 1956. (Translated from Russian).

33. BOLLINGER, J. G., Shock and vibration Handbook. Edited by HARRIS, C. M. and CREDE, C. E., McGraw-Hill, 1976, Ch. 40, pp 16 - 17.

34. CORBACH, K., Die Dynamische Steifigheit ruhender und beweglicher verbindungen an werkzeugmaschinen. Maschinenmarkt, Jg. 72, Nr. 79, 1966. (Translation UMIST, 1969).

35. ANDREW, C., COCKBURN, J. A. and WARING, A. E., Metal surfaces in contact under normal forces: some dynamic stiffness and damping characteristics. Proc. Instn. Mech. Engrs, Vol. 182, Pt 3K, 1967.

36 ANDREW, C., Damping in fixed joints. MTIRA Conf. on damping in machine tool structures, 1969.

37. PERA Report 198, Machine tool joints, 1969.

38. THORNLEY, R. H., A study of some parameters which influence the static and dynamic stiffness of joints in machine tool structures. Ph.D. Thesis, UMIST, 1969.

39. THORNLEY, R. H. and KOENIGSBERGER, F., Dynamic characteristics of machined joints loaded and excited normal to the joint face. Annals of the CIRP, Vol. 19, 1971.

40. DEKONINCK, C., Experimental investigation of the normal dynamic stiffness of metal joints. Int. J. Mach. Tool Des. Res., Vol. 9, 1969.

41. KHOYI, M. R. H., Some aspects of damping and dynamic characteristics of machine tool structural joints. Ph.D., Aston Univ., 1976.

42. SCHOFIELD, R. E., The damping effect of joints formed from machined surfaces - the state of the art. Int. MTDR Conf., 1972.

43. BURDEKIN, M., BACK, N., COWLEY, A., Experimental study of normal and shear characteristics of machined surfaces in contact. J. Mech Eng. Science, Vol. 20, No. 3, 1978.

44. TSUTSUMI, M. and ITO, Y., Damping mechanism of a bolted joint in machine tools. Int. MTDR Conf., 1979.

45. YOSHIMURA, M., Measurement of dynamic rigidity and damping property for simplified joint models and simulation by computer. Annals of the CIRP, Vol. 25, No. 1, 1977.

46. WHITEHOUSE, D. J., VANHERCK, P., BRUIN, W., LUTTERVELT, C. A., Assessment of surface typology nalysis techniques in turning. Annals of the CIRP, Vol. 23, No. 2, 1974.

47. WILLIAMSON, J. B. P., The microtopography of surfaces, Proc. Instn. Mech. Engrs., Vol. 182, Pt 3K, 1967.

48. SAYLES, R. S. and THOMAS, T. R., Three-dimensional roughness measurement with a stylus instrument. Microtecnic, No. 2, 1978.

49. RANK TAYLOR HOBSON, Talysurf 4, Operator's Handbook, Catalogue No. 216-17.

50. REASON, R. E., Progress in the appraisal of surface topography during the first half-century of instrument development. Proc. Int. Conf. on Met. & Properties of Eng. Surf., Leicester, 1979.

51. PETERS, J., VANHERCK, P., SASTRODINOTO, M., Assessment of surface typology analysis techniques. Annals of the CIRP, Vol. 28, No. 2, 1979.

52. THOMAS, T. R., Stylus instruments, lecture, Teeside Poly., 1978.

53. WHITEHOUSE, D. J. and ARCHARD, J. F., The properties of random surfaces of significance in their contact. Proc. Roy. Soc. London, A.316, 1970.

54. REASON, R. E., Measurement of surface topography and accuracy of stylus instruments. Proc. Int. Conf. on Surface Technology, Pittsburgh, 1973.

55. CHETWYND, D. G., The digitization of surface profiles. Proc. Int. Conf. on Met. & Properties of Eng. Surf., Leicester, 1979.

56. VORBURGER, T. V., TEAGUE, E. C., SCIRE, F. E. and ROSBERRY, F. W., Measurements of stylus radii. Proc. Int. Conf. on Met. & Properties of Eng. Surf., Leicester, 1979.

57. BENDAT, J. S. and PIERSOL, A. G., Random data: analysis and measurement procedures. Wiley-Interscience, 1956, Ch. 10, pp 344.

58. HOLM, R., Electric contacts Handbook. Springer-Verlag, 1958, Ch. 1, pp 8 - 10.

59. BOWDEN, F. P. and TABOR, D., Friction and lubrication of solids. Oxford University Press, 1954.

60 WHITEHOUSE, D. J., Surfaces - A link between manufacture and function. Proc. Instn. Mech. Engrs, Vol. 192, 1978.

61. MOORE, A. J. W., Proc. Roy. Soc. London, A.195, 1948. (As reported in reference 59.)

62. BLOK, H., Comments on the paper by WILSON, R., Proc. Roy. Soc. London, A.212, 1952, pp 480.

63. HALLIDAY, J. S., Surface examination by reflection electron microscopy. Proc. Instn. Mech. Engrs, Vol. 169, 1955.

64. ARCHARD, J. F., Elastic deformation and the laws of friction. Proc. Roy. Soc. London, A.243, 1957.

65. LING, F. F., On asperity distributions of metallic surfaces. J. Appl. Physics, Vol. 29, No. 8, 1958.

66. PESANTE, M., Determination of surface roughness typology by means of amplitude density curves. Annals of the CIRP, Vol. 12, No. 2, 1963.

67. REASON, R. E., The bearing parameters of surface topography, Int. MTDR Conf., 1964.

68. GREENWOOD, J. A. and WILLIAMSON, J. B. P., Contact of nominally flat surfaces. Proc. Roy. Soc. London, A.295, 1966.

69. WHITEHOUSE, D. J. and ARCHARD, J. F., The properties of random surfaces in contact. Symp. Surface Mech., Proc. ASME, 1969.

70. ONIONS, R. A. and ARCHARD, J. F., The contact of surfaces having a random structure. J. Phys. D., Vol. 6, 1973.

71. SPRAGG, R. C. and WHITEHOUSE, D. J., A new unified approach to surface metrology. Proc. Instn. Mech. Engrs, Vol. 185, 1971.

72. LONGUET-HIGGINS, M. S., The statistical analysis of a random moving surface. Phil. Trans. Roy. Soc. London A.249, 1957.

73. NAYAK, P. R., Random process model of rough surfaces. Trans. ASME, J. Lub. Tech., Vol. 93, 1971.

74. NAYAK, P. R., Random process model of rough surfaces in plastic contact. Wear, Vol. 26, 1973.

75. BUSH, A. W., GIBSON, R. D. and THOMAS, T. R., The elastic contact of a rough surface. Wear, Vol. 35, 1975.

76. WILLIAMSON, J. B. P., PULLEN, J. and HUNT, R. T., The shape of solid surfaces. Symp. Surface Mech., Proc. ASME, 1969.

77. GREENWOOD, J. A. and WILLIAMSON, J. B. P., Developments in the theory of surface roughness. Proc. 4th Leeds-Lyon Symp. on Tribology, 1977.

78. THOMAS, T. R. and SAYLES, R. S., Stiffness of machine tool joints: a random-process approach. Trans. ASME, J. Eng. Ind., Vol. 99, 1977.

79. SCHOFIELD, R. E. and THORNLEY, R. H., Reply on a query from ANDREW, C. Proc. Int. MTDR Conf., 1971, pp 95.

80. PULLEN, J. and WILLIAMSON, J. B. P., On the plastic contact of rough surfaces. Proc. Roy. Soc. London, A.327, 1972.

81. STOUT, K., How smooth is smooth? The Prod. Eng., May, 1980.

82. WHITEHOUSE, D. J., Beta functions for surface typologie? Annals of the CIRP, Vol. 27, 1978.

83. B S 1134: Part 1: 1972. Method for the assessment of surface texture.

84. WHITEHOUSE, D. J., The measurement and analysis of surfaces. Trib. Int., Vol. 7, No. 6, 1974.

85. REASON, R. E., Some approaches to the measurement of waviness. Proc. Int. MTDR Conf., 1965.

86. SAYLES, R. S. and THOMAS, T. R., Computer simulation of the contact of rough surfaces. Wear, Vol. 49, 1978.

87. THORNLEY, R. H. and LEES, K., The effect of planform shapes on the normal dynamic characteristics of metal to metal joints. Proc. Instn. Mech. Engrs, Paper C62, 1971.

88. TIMOSHENKO, S. and GOODIER, J. N., Theory of elasticity, McGraw-Hill, 2nd edition, 1951.

89. GREENWOOD, J. A. and TRIPP, J. H., The contact of two nominally flat rough surfaces. Proc. Instn. Mech. Engrs, Vol. 185, 1971.

90. DEN HARTOG, J. P., Mechanical vibration, McGraw-Hill, 2nd edition, 1956, Ch. 8, pp 362.

91. GOODMAN, L. E., Shock and vibration Handbook. Edited by HARRIS, C. M., and CREDE, C. E., McGraw-Hill, 1976, Ch. 36.

92. SALT, J. H., The selection of surface finish for engineering components. M.Sc. Thesis, Aston Univ., 1971.

93. TAYLOR-HOBSON, Talylin 1: Operating instructions, Catalogue No. 214 - 7.

A P P E N D I X I

EVALUATION OF THE EFFECTIVE PARAMETERS OF THE TEST RIG

The equations of motion for the system shown in Fig 7,a could be written in terms of the principle co-ordinates p_1 and p_2 as

$$a_1 \ddot{p}_1 + b_1 \dot{p}_1 + d_1 p_1 + b_{12} \dot{p}_2 = F_1 + A F_2 \qquad 1.1$$

$$a_2 \ddot{p}_2 + b_2 \dot{p}_2 + d_2 p_2 + b_{21} \dot{p}_1 = F_1 + B F_2 \qquad 1.2$$

where

$$x_1 = p_1 + p_2$$

$$a_1 = M_1 + A^2 M_2$$

$$b_1 = C_1 + A^2 C_2 + C (1 - A)^2$$

$$d_1 = K_1 + A^2 K_2 + K (1 - A)^2$$

$$b_{12} = C_1 + C_2 A B + C (1 - A) (1 - B)$$

$$x_2 = A p_1 + B p_2$$

$$a_2 = M_1 + B^2 M_2$$

$$b_2 = C_1 + B^2 C_2 + C (1 - B)^2$$

$$d_2 = K_1 + B^2 K_2 + K (1 - B)^2$$

$$b_{21} = b_{12}$$

For harmonic excitation of the upper and lower mass blocks at the same frequency, p_1 and p_2 will also be harmonic with the same frequency, thus

$$F_n = \bar{F}_n e^{i\omega t} \quad , n = 1,2$$

$$p_n = \bar{p}_n e^{i\omega t} \quad , n = 1,2$$

where $\bar{F}_n$ and $\bar{p}_n$ contain information about the phase and amplitude only.

Equation 1 could then be written as

$$(d_1 - a_1 \omega^2 + i \omega b_1) \bar{p}_1 + i \omega b_{12} \bar{p}_2 = \bar{F}_1 + A \bar{F}_2 \qquad 2.1$$

$$i \omega b_{12} \bar{p}_1 + (d_2 - a_2 \omega^2 + i \omega b_2) \bar{p}_2 = \bar{F}_1 + B \bar{F}_2 \qquad 2.2$$

In order that only a single mode appears at any given frequency, the amplitude and phase relations between forces should be adjusted as follows

at the first mode $\bar{p}_2 = 0$

i.e. from equation 2

$$[(d_1 - a_1 \omega^2) + i \omega b_1]\bar{p}_1 = \bar{F}_1 + A \bar{F}_2 \qquad 3.1$$

$$i \omega b_{12} \bar{p}_1 = \bar{F}_1 + B \bar{F}_2 \qquad 3.2$$

at the second mode $\bar{p}_1 = 0$

$$i \omega b_{12} \bar{p}_2 = \bar{F}'_1 + A \bar{F}'_2 \qquad 4.1$$

$$[(d_2 - a_2 \omega^2) + i \omega b_2] \bar{p}_2 = \bar{F}'_1 + B \bar{F}'_2 \qquad 4.2$$

where the prime indicates values measured at the second mode.

1. Evaluation of the specimen parameters using forced vibration methods

(a) Asymmetric condition

The first mode is realised when $\bar{p}_2 = 0$ or

$\bar{x}_1 = \bar{p}_1$ and $\bar{x}_2 = A\,\bar{p}_1$

take $\bar{x}_1 = \bar{p}_1 = x_1$ real

from equation 3

$$C_1 + (1 - A)^2\, C + A^2\, C_2 = (F_{1I} + A\, F_{2I}) / \dot{x}_1 \qquad 5.1$$

$$K_1 + (1 - A)^2\, K + A^2\, K_2 - \omega^2\, (M_1 + A\, M_2) = (F_{1R} + A\, F_{2R})/x_1 \qquad 5.2$$

$$C_1 + (1 - A)\,(1 - B)\, C + A\, B\, C_2 = (F_{1I} + B\, F_{2I}) / \dot{x}_1 \qquad 5.3$$

$$0 = F_{1R} + B\, F_{2R} \qquad 5.4$$

The second mode is realised when $\bar{p}_1 = 0$ or

$\bar{x}'_1 = \bar{p}_2$ and $\bar{x}'_2 = B\,\bar{p}_2$

let $\bar{x}'_1 = \bar{p}_2 = \bar{x}'_{1\text{real}}$, and from equation 4

$$C_1 + (1 - B)^2\, C + B^2\, C_2 = (F'_{1I} + B\, F'_{2I}) / \dot{x}'_1 \qquad 6.1$$

$$K_1 + (1 - A)^2\, K + B_2^2\, K_2 - \omega^2\, (M_1 + B\, M_2) = (F'_{1R} + B\, F'_{2R})\, x'_1 \qquad 6.2$$

$$C_1 + (1 - A)\,(1 - B)\, C + A\, B\, C_2 = (F'_{1I} + A\, F'_{2I}) / \dot{x}'_1 \qquad 6.3$$

$$0 = F'_{1R} + A\, F'_{2R} \qquad 6.4$$

we also have the eigenvector equations (41)

$$M_1 + A\ B\ M_2 = 0 \qquad 7.1$$

$$K_1 + (1 - A)\ (1 - B)\ K + A\ B\ K_2 = 0 \qquad 7.2$$

where

$$A = \frac{x_2}{x_1} = -\frac{F'_{1R}}{F'_{2R}} \qquad 7.3$$

$$B = \frac{x'_2}{x'_1} = -\frac{F_{1R}}{F_{2R}} \qquad 7.4$$

The set of equations 5.2, 6.2, 7.1 and 7.2 are not enough to determine the five parameters K_1, K, K_2, M_1 and M_2. The set 5.1, 5.3, 6.1, 6.3 cannot be of any use because equations 5.3 and 6.3 are in fact one equation and both represent a small difference (due to proportional distribution of damping or near symmetry condition) which is hard to measure accurately. Thus one more equation is required for each set to render the determinate. This was achieved (41) by one further measurement of force at the specimen column, i.e. $\bar{F}$ measurement in Fig 7,a. When such measurement is employed, only the second mode need be excited in order to determine the specimen parameters.

From Fig 7,a

$$K_1 - M_1\ \omega^2 = (F_{1R} + F_R)\ /\ x_1 \qquad 8.1$$

$$K_2 - M_2\ \omega^2 = (F_{2R} + F_R)\ /\ x_2 \qquad 8.2$$

$$C_1 = (F_{1I} + F_I)\ /\ \dot{x}_1 \qquad 8.3$$

$$C_2 = (F_{2I} + F_I)\ /\ \dot{x}_2 \qquad 8.4$$

The specimen parameters are immediately found from

$$K = F_R / (x_2 - x_1) \qquad 8.5$$

$$C = F_I / (\dot{x}_2 - \dot{x}_1) \qquad 8.6$$

F is positive in tension and negative in compression.

(b) Completely symmetric system Fig 7,b

This means that

$$K_1 = K_2,\ M_1 = M_2 \text{ and } C_1 = C_2$$

From equation 7 it follows that

$$A = 1 \text{ and } B = -1 \text{ and } b_{12} = 0$$

Thus at the first mode

$$x_2 = x_1 \text{ and } \bar{F}_2 = \bar{F}_1$$

and at the second mode

$$x_2' = -x_1' \text{ and } \bar{F}_2' = -\bar{F}_1'$$

equation 5 is reduced to

$$C_1 = C_2 = F_{1I}/\dot{x}_1 = F_{2I}/\dot{x}_1 \qquad 9.1$$

$$K_1 - M_1 \omega^2 = F_{1R} / x_1 = F_{2R} / x_1 \qquad 9.2$$

Equation 9 when used in the following equation (reduced from equation 6) would furnish the specimen parameters C and K at the second mode

$$2C + C_1 = F'_{1I} / \dot{x}'_1 = - F'_{2I} / \dot{x}'_1 \qquad 10.1$$

$$(K_1 - M_1 \omega^2) + 2K = F'_{1R} / x'_1 = - F'_{2R} / x'_1 \qquad 10.2$$

2. Evaluation of the specimens parameters using free vibration methods

This method requires uncoupled free vibration. That is, the system should possess complete symmetry, and the coupling term b_{12} due to damping in equation 2 is zero. Equation 2 is then reduced to

$$M_1 \ddot{p}_1 + C_1 \dot{p}_1 + K_1 p_1 = \frac{1}{2} (F_1 + F_2)$$

$$M_1 \ddot{p}_2 + (C + 2C) \dot{p}_2 + (K_1 + 2K) p_2 = \frac{1}{2} (F_1 - F_2)$$

The first mode is excited when $\bar{p}_2 = 0$, therefore

$$x_1 = \bar{p}_1$$

and from 7.4 and 5.1 : $F_1 = F_2$, thus

$$M_1 \ddot{x}_1 + C_1 \dot{x}_1 + K_1 x_1 = F_1 \qquad 11.1$$

Similarly, the second mode is excited when $\bar{p}_1 = 0$, therefore

$$x_1 = \bar{p}_2$$

and from 7.3 and 6.1 : $F'_1 = - F'_2$, thus

$$M_1 \ddot{x}'_1 + (C_1 + 2C) \dot{x}'_1 + (K_1 + 2K) x'_1 = F'_1 \qquad 11.2$$

Equations 11.1 and 11.2 represent two equivalent single degree of freedom systems as shown in Fig 7,c.

Generally the free vibration methods on their own will not be sufficient for the determination of the specimen parameters. However, if the system parameters M_1, C_1 and K_1 are known in advance (using free/forced vibration method), the specimen parameters could readily be found from the free vibration at the second mode, as follows

$$\omega_2^2 = (K_1 + 2K) / M_1 \qquad 11.3$$

$$\text{i.e.} \qquad K = \frac{1}{2} (M_1 \omega_2^2 - K_1) \qquad 11.4$$

$$C = \frac{1}{2} (\tau_2 \omega_2 M_1 - C_1) \qquad 11.5$$

where

$$\tau_2 = \frac{\omega_d}{\omega_2} \cdot \frac{\delta_2}{\pi} \simeq \frac{\delta_2}{\pi}$$

and δ_2 = logarithmic decrement.

3. Evaluation of the test rig parameters

The test rig parameters K_1, M_1 and C_1 could be evaluated at the first mode using forced/free vibration methods as follows from equation 9.2

$$K_1 - M_1 \omega^2 = \frac{F_{1R}}{x_1} = \frac{F_{2R}}{x_2} = m_{iR} \omega^2 \qquad 12.1$$

where $m_i = \frac{F_i}{x}$ = apparent mass vector.

By measuring m_{iR} at two close frequencies around the first natural frequency and substituting in equation 12.1, thus two equations are obtained which are sufficient to determine both the system mass M_1 and the spring stiffness K_1.

Measurement of the decay curves at the first natural frequency yields the logarithmic decrement δ, thus the damping constant (see Appendix II) could be found from

$$C_1 = \frac{\delta}{\pi} M_1 \omega_1 \qquad 12.2$$

APPENDIX II

RELATIONSHIPS BETWEEN VARIOUS MEASURES OF DAMPING

The following measures of damping are often used to describe the damping capacity for a single degree of freedom system with frequency independent parameters.

1. Viscous damping coefficient C

Viscous damping is the dissipation of energy that occurs when a particle in a vibrating system is resisted by a force that has a magnitude proportional to the velocity of the particle. The coefficient of proportionality C is called the damping coefficient and is the value of this force at unit velocity.

2. Damping ratio ξ

The damping ratio is the ratio of the damping coefficient C to the critical damping coefficient C_c. Thus

$$\xi = \frac{C}{C_c} = \frac{C}{2M\omega} = \frac{C}{2\sqrt{KM}}$$

3. Logarithmic decrement δ

The logarithmic decrement is the natural logarithm of the ratio of any two successive amplitudes of like sign in the decay curve; or to express the average for n cycles

$$\delta = \frac{1}{n} \ln \frac{x_1}{x_n}$$

$$\delta = \frac{2 \pi \xi}{\sqrt{1 - \xi^2}} \simeq 2 \pi \xi$$

4. Loss factor τ

The loss factor τ is a none dimensional measure of damping defined as the ratio of the quadrature to the in-phase stiffness components.

$$\tau = \frac{\omega C}{K} = \frac{C}{\sqrt{K M}} = 2 \xi \simeq \frac{\delta}{\pi}$$

5. *Specific damping capacity* ψ

The specific damping capacity is the ratio of the energy dissipated to the maximum available energy per cycle of vibrations.

$$\psi = \frac{-D_o}{V_o} = \frac{\pi \omega C x_o^2}{\frac{1}{2} K x_o^2} = 2 \pi \frac{\omega C}{K} = 2 \pi \tau$$

i.e. $\psi = 2 \pi \tau = 4 \pi \xi \simeq 2 \delta$

A P P E N D I X I I I

(a) Interface unit for the real time clock

The square-wave from the solaretron frequency response analyser was fed into the following interface in order to translate its voltage level to that accepted by the Analog-to-Digital converter board.

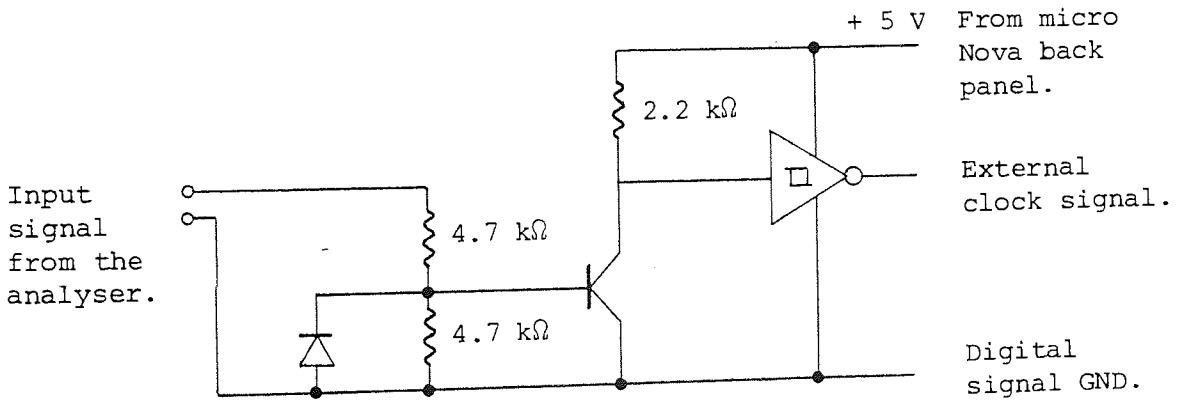

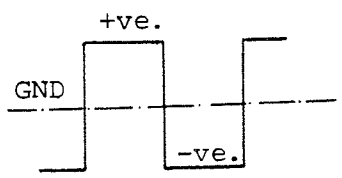

Input signal to the interface.

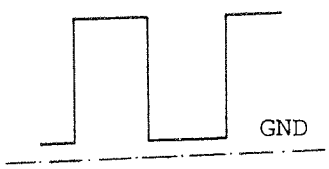

≃ 0.75 V

Output signal from the interface. (External clock signal.)

(b) Talysurf - A/D interface unit

The signal from the talysurf has a voltage range of ± 1 V. This signal is fed through the following interface unit in order to transform its range to 0 to 10 V which is acceptable to the A/D board.

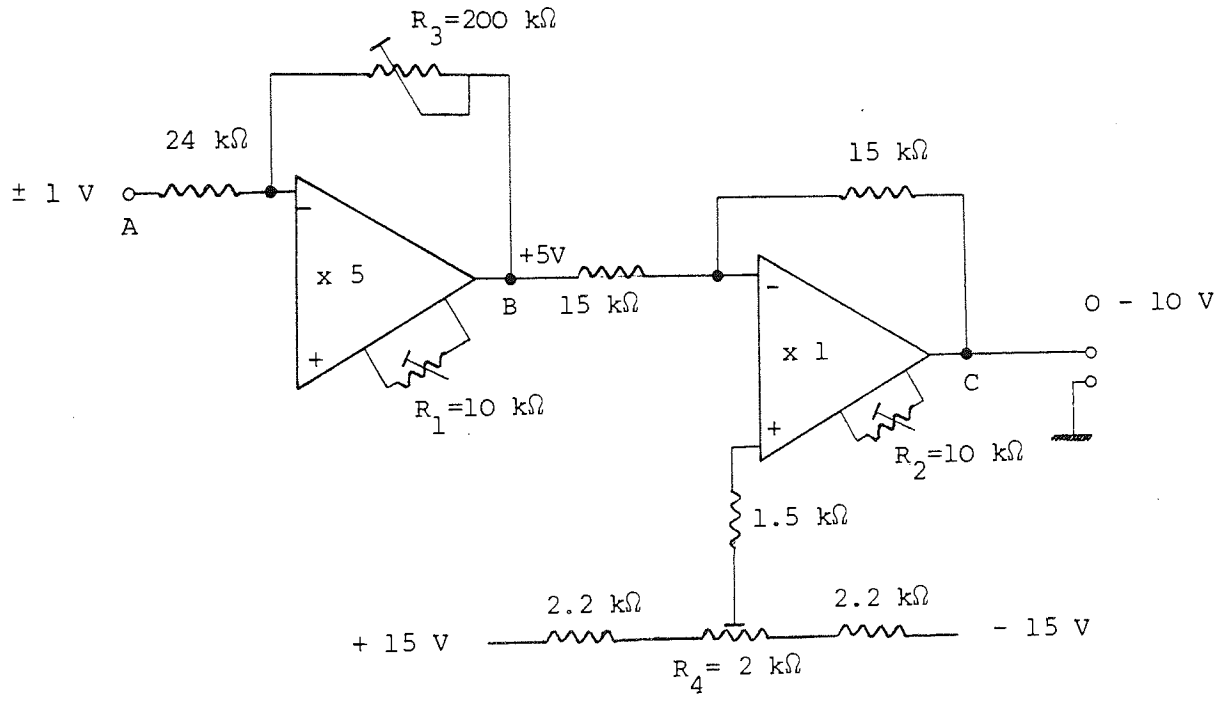

R_1 and R_2 : adjusted to give 0 V at C with 0 V at A.

R_3 : adjusted to give + 10 V at C with - 1 V applied at A.

R_4 : adjusted to give 0 V at C with + 1 V applied at A.

Note:- R_3 and R_4 will react against each other, and therefore it was necessary to repeat their adjustment until an optimum setting was achieved.

A P P E N D I X I V

(a) Program "GAM"

The following is a listing of the program "GAM" described in section 5.1.8.1.

```
      COMMON JON(5)
      DO 20 I=1,5
20     JON(I)=0
      WRITE(10)"   I AM READY TYPE 1 WHEN YOU ARE READY  "
      READ(11,19) IRE
19    FORMAT(I2)
      CALL COVRT
      WRITE(10,40) JON
40    FORMAT(5OI6)
      WRITE(10) JON
      END
```

(b) Program "SURFACE"

The following is a listing of the program "SURFACE" described in section 5.1.8.2.

```
      COMMON JON(3200)
      DO 20 I=1,3200
 20    JON(I)=0
      WRITE(10,60)
 60   FORMAT(" PLEASE TYPE SPECIMENT NAME (ONLY 2 LETTERS)  :",Z)
      READ(11,19) U
 19   FORMAT(S2)
      WRITE(10)"TALYSURF MAGNIFICATION"
      READ(11) AGN
      WRITE(10)"NO. OF SAMPLES PER CUT-OFF"
      READ(11) N
      WRITE(10)"TYPE SAMPLING LENGTH (MICRON), PRESS CR TO START"
      READ(11) SLN
      CALL COVRT
      WRITE(10)"********END OF SAMPLING********"
      CALL FOPEN(40,U)
      WRITE(40,70) AGN,SLN,N
 70   FORMAT(1X,2F7.1,I5)
      WRITE(40,50)(JON(I),I=1,3200)
 50   FORMAT(1X,10I5)
      CALL CLOSE(40,IER)
      END
```

(c) Program "FLAT"

The following is a listing for the program "FLAT" described in sections 5.1.8.3 and 5.2.5.1.

```
      COMMON J(150)
      N=150
      AN=N
       WRITE(10)"**TRACE NO."
       READ(11,30) U
 30    FORMAT(S6)
      DO 1 I=1,N
 1    J(I)=0.0
      WRITE(10)"**TALYSURF MAGNIFICATION"
      READ(11) AGM
      CALL COVRT
      WRITE(10)"**SAMPLING ENDED********"
      AGM=50000.0/(AGM*4096.)
      S1=0.0
      S2=0.0
      DO 2 I=1,N
      R=J(I)
      R=R*AGM
      S1=S1+R
      T=I
 2    S2=S2+(R*T)
      S5=((12.*S2)-(6.*(AN+1.)*S1))/(AN*((AN*AN)-1.))
      S6=(S1/AN)-(S5*(AN+1.)/2.)
      S1=0.0
      S2=0.0
      S3=0.0
      S4=0.0
      DO 3 I=1,N
      T=I
      R=J(I)
      R=R*AGM
      R=R-(S5*T)-S6
      S1=S1+R
      S2=S2+(R*R)
      S3=S3+(R*R*R)
 3    S4=S4+(R*R*R*R)
      S1=S1/AN
      S2=(S2/(AN-1.))-(S1*S1)
      S3=(S3/AN)/(S2*(S2**.5))
      S4=(S4/AN)/(S2*S2)
      S5=S2**.5
      WRITE(10) S1,S2,S3,S4,S5
      END
```

(d) Subroutine "COVRT"

The following is a listing of the subroutine "COVRT" described in section 5.1.8.4.

```
                .TITL    COVRT
                .ENT      COVRT
                .NREL
                .EXTU
.F1:
IA1:        0
.F2:            0
                .CSIZ     6200
                FS.=0
                FS.
COVRT:
                JSR       @.FARL
                JSR       @.FINI
                .F1
                .F2
START:
                NIOC    ADCV
                LDA     1,IA1
                STA     1,TEM
                SKPBZ     ADCV
                JMP       .-1
                LDA       0,COUNT
                DOC       0,ADCV
                LDA       0,TEM
                DOB       0,ADCV
                LDA       0,SETUP
                DOAS      0,ADCV
                 SKPBZ      ADCV
                 JMP        .-1
                STA         1,DEM
JUST:           LDA         0,@DEM
                MOVZR       0,0
                MOVZR     0,0
                MOVZR     0,0
                MOVZR     0,0
                STA       0,@DEM
                INC       1,1
                STA       1,DEM
                ISZ       NUMB
                JMP       JUST
                JMP       @.FRET
TEM:            0
COUNT:          171600
SETUP:          170000
DEM:            0
NUMB:           171600
                .END
```

(e) Program "FIGR3"

The following is a listing of the program "FIGR3" which was used to compute roughness parameters in accordance with the description given in section 5.2.3. A flow chart for the program is given in section 5.2.4.

```
      INTEGER Z,W
      DIMENSION R(400),RS(21),RES(21,20)
      DO 369 I=1,21
      DO 369 J=1,20
  369 RES(I,J)=0.0
C  FILE HANDLING
C  ************
      CALL OPEN(18,"INDEX",1,IER)
      READ(18,80) N5
   80 FORMAT(I3)
      DO 999 IK1=1,N5
      READ(18,60) U
      WRITE(10,99) U
      CALL FOPEN(40,U)
   99 FORMAT(1X,"**** FILE NAME  : ",S2)
   60 FORMAT(S2)
C
C  CALCULATIONS START HERE
C  **********************
      READ(40,50) AGM,SLM,N
   50 FORMAT(2F7.1,I5)
      AGM=50000.0/(AGM*4096.0)
      DO 17 I=1,21
   17 RS(I)=0.0
      NP=0
      RI=0.0
      RI2=0.0
      PI=0.0
      PI2=0.0
      M=3200/N
      DO 1 J=1,M
      READ(40,51)(R(I),I=1,N)
   51 FORMAT(10F5.0)
C  FILTERING OPERATION
C  *******************
      S1=0.0
      S2=0.0
      DO 2 I=1,N
      R(I)=R(I)*AGM
      S1=S1+R(I)
```

```
      T=I
      S4=R(I)*T
    2 S2=S2+S4
      AN=N
      S5=((12.*S2)-(6.*(AN+1.)*S1))/(AN*((AN*AN)-1.0))
      S6=(S1/AN)-(S5*(AN+1.)/2.)
      DO 98 I=1,N
      T=I
   98 R(I)=R(I)-(S5*T)-S6
C
C  BASIC PAREMETRS ARITHMATICS
C  ***************************
       S7=0.0
      S1=0.0
      S2=0.0
      S3=0.0
      S4=0.0
      SMAX=0.0
      SMIN=AGM
      DO 3 I=1,N
      IF(R(I).LT.SMIN) SMIN=R(I)
      IF(R(I).GT.SMAX) SMAX=R(I)
      T=R(I)
      IF(T.LT.0.0) T=-T
      S7=S7+T
      S1=S1+R(I)
      T=T*T
      S2=S2+T
      S3=S3+(T*R(I))
    3 S4=S4+(T*T)
C  CLASIC PARAMETERS  RT  RP  RV  RP/RT  RA  RQ  RQ/RA  SK  Q
C  ******************
      RS(1)=(SMAX-SMIN)+RS(1)
      RS(2)=SMAX+RS(2)
      RS(3)=-SMIN+RS(3)
      RS(4)=(SMAX/(SMAX-SMIN))+RS(4)
      S7=S7/AN
      RS(5)=RS(5)+S7
      S2=(S2/(AN-1.))**.5
      RS(6)=RS(6)+S2
      RS(7)=RS(7)+S2/S7
      RS(8)=RS(8)+((S3/AN)*(1./(S2**3)))
```

```
      RS(9)=RS(9)+((S4/AN)*(1./(S2**4)))
C  BETA FUNCTION PARAMETERS
C  ************************
      S3=(SMAX-AMIN)*S2*S2
      SMIN=-SMIN
      S1=((SMIN*SMAX)-(S2*S2))
      RS(10)=(SMIN*S1/S3)+RS(10)
      RS(11)=(SMAX*S1/S3)+RS(11)
C  SLOPE AND WAVE LENGTH     ARITHMATIC AND GEOMETRIC SLOPE
C  *********************     AVERAGE WAVE LENGTH INDEX
C                            NO. OF ZERO CROSSINGS
      S4=0.0
      S3=0.0
      S1=0.0
      SL2=0.0
      K=N-4
      DO 5 I=4,K
      S6=(R(I+3)-R(I-3))-(9.*(R(I+2)-R(I-2)))
      S5=(S6+(45.*(R(I+1)-R(I-1))))/(60.*SLM)
      SL2=SL2+(S5*S5)
      IF(S5.LT.0.0) S5=-S5
      IF(R(I-1).LT.0.0.AND.R(I+1).GT.0.0) S3=S3+1.
      S1=S1+ALOG10(S5)
    5 S4=S4+S5
      S4=S4/(AN-8.)
      RS(12)=RS(12)+S4
      S1=10**(S1/(AN-8.0))
      RS(13)=RS(13)+S1
      SL2=(SL2/(AN-9.))**.5
      RS(14)=RS(14)+SL2
      RS(15)=RS(15)+(6.2383185*S7/S4)
      RS(16)=RS(16)+(2.*S3)
      T=(AN-8.)/(S3*2.)
      V=(6.2831852*S7/S4)/(SLM*2.)
C
      DO 200 I=1,N
  200 R(I)=R(I)+SMIN
C
C  PEAK PAREMETERS      RADIOUS OF CURVATURE DISTRIBUTION
C  ***************      PEAK HEIGHT DISTRIBUTION AND
C                       NUMBER OF PEAKS
C
C
```

```
      T=T*2.0
      L=1
      K=T
      IF(K.GT.8) L=K/8
      W=2*L
      Z=3*L
      T=L
      T=SLM*SLM*T*T
      K=4*L
      K1=N-(4*L)
      DO 10 I=K,K1,L
      IEE=I
      IF(R(I).LT.SMIN) GO TO 10
      IM1=I-L
      IP1=I+L
      IF(R(I).LT.R(IM1)) GO TO 10
      IF(R(I).LT.R(IP1)) GO TO 10
C
C     THREE POINTS ANALYSIS :
      S6=T/(R(IP1)+R(IM1)-(2.*R(I)))
      IEE=IEE+L
C
C  PEAK PRAMETERS ARITHMATICS
C  **************************
      NP=NP+1
      S6=-S6
      RI=RI+S6
      RI2=RI2+S6*S6
      PI=PI+(R(I)-SMIN)
      PI2=PI2+((R(I)-SMIN)*(R(I)-SMIN))
      IF(IEE.GT.K1) GO TO 1
      I=IEE
   10 CONTINUE
    1 CONTINUE
      T=NP
      RI=RI/T
      RS(17)=RS(17)+RI
      RI2=(((RI2/T)-(RI*RI))**0.5)
      RS(18)=RS(18)+RI2
      PI=PI/T
      RS(19)=PI
      RS(20)=(((PI2/T)-(PI*PI))**.5)
      RS(21)=NP
      CALL CLOSE(40,IER)
      T=M
```

```
      DO 7 I=1,15
    7 RS(I)=RS(I)/T
      RS(16)=RS(16)/(SLM*3.2)
      DO 11 I=1,21
   11 RES(I,IK1)=RS(I)
  999 CONTINUE
      CALL CLOSE(18,IER)
C
C  ***********************************
C  SPECIMEN COLUMN DATA MANIPULATION
C  ***********************************
      DO 14 I=1,21
      SMAX=-10.0E 20
      SMIN=10.0E 20
      DO 12 J=1,16
      IF(RES(I,J).GT.SMAX) SMAX=RES(I,J)
      IF(RES(I,J).LT.SMIN) SMIN=RES(I,J)
   12 RES(I,17)=RES(I,17)+RES(I,J)
      RES(I,17)=RES(I,17)/16.0
      RES(I,19)=SMAX
   14 RES(I,20)=SMIN
      DO 16 I=1,21
      DO 15 J=1,16
   15 RES(I,18)=RES(I,18)+((RES(I,J)-RES(I,17))**2)
   16 RES(I,18)=((RES(I,18)/16.0)**.5)
      CALL OPEN(19,"RESULTS",3,IER)
      WRITE(19,109) SLM
  109 FORMAT(1X,F8.3)
      WRITE(19,19) ((RES(I,J),J=1,16),I=1,21)
   19 FORMAT(8(2X,F8.3))
      WRITE(19,18) ((RES(I,J),J=17,20),I=1,21)
   18 FORMAT(1X,F10.3,3X,F10.3,3X,F10.3,3X,F10.3)
      CALL CLOSE(19,IER)
      END
R
```

TABLE 1

THE SPECIFICATIONS OF THE TEST RIG (41)

Length of specimen (maximum preload)	$124.5 < \ell < 274.3$ (mm)
Maximum diameter of specimen	116.8 (mm)
Maximum preloading capacity	5 (ton.f.)
Maximum pump pressure	5.36 (MP_2)
Average rate of preloading - Isolating spring	127.5 (kp/mm)
Effective mass of inertia blocks	118.5 (kg)
Effective stiffness of auxiliary system	$K_1 = 121 + 1.114\ x$ (kp/mm) (x = deflection of lower mass block)
Effective loss factor of auxiliary system	$\tau_1 = 0.046 + 0.001\ x$
Average first natural frequency	16.3 (Hz)
Maximum load capacity of shaker system	22.7 (kp)
Overall size	1676 X 1118 X 737 (mm)
Overall weight	1134 (kg)

TABLE 2

CUTTING CONDITIONS FOR THE SPECIMENS

Milling

Specimens	Speed, r.p.m.	Feed, mm/min	Depth of cut, mm	Tool
ML1	180	158.75	0.254	Face milling cutter
ML2	295	158.75	0.254	with 6 throw away
ML3	895	212.725	0.254	tips having flat
ML4	500	558.8	0.254	cutting edges.

Shaping

Specimens	Speed, m/min	Feed, mm/st	Depth of cut, mm	Tool nose radius, mm
SH1	10.668	0.254	0.254	3.5
SH2	10.668	0.508	0.254	5.25
SH3	8.534	0.254	0.254	7.6
SH4	8.534	0.508	0.254	3.5
SH5	8.534	2.54	0.05	Straight cutting edge

Turning

Specimens	Speed, r.p.m.	Feed, mm/rev	Depth of cut, mm	Tool nose radius, mm
TN1	310	0.508	0.254	0.4
TN2	710	0.508	0.254	0.8
TN3	510	0.254	0.254	0.8
TN4	510	0.127	0.254	0.8

Grinding

Specimens	Wheel type	Depth of cut, mm	Wheel speed, r.p.m.
GN1	WA - 36 - JP 4V	0.0254	2850
GN2	6A - 100 - 18 V75	0.0127	2850

TABLE 3

CALIBRATION OF THE SURFACE MEASURING SYSTEM

Input Voltage	Computer Reading	Nominal Reading	Error
- 0.9999	0	0	0
- 0.9000	155	204.8	- 49.8
- 0.8	360	409.6	- 49.6
- 0.7	565	614.4	- 49.4
- 0.6	770	819.2	- 49.2
- 0.5	974	1024.0	- 50
- 0.4	1179	1228.8	- 49.8
- 0.3	1384	1433.6	- 49.6
- 0.2	1590	1638.4	- 48.2
- 0.1	1795	1843.2	- 48.2
0	2001	2048	- 49.0
0.1	2204	2252	- 48.0
0.2	2410	2457.6	- 47.6
0.3	2615	2662.4	- 47.4
0.4	2819	2867.2	- 48.2
0.5	3024	3072.0	- 48.0
0.6	3228	3276.8	- 48.8
0.7	3434	3481.6	- 47.6
0.8	3639	3686.4	- 47.4
0.9	3844	3891.2	- 47.2
0.999	4050	4096	- 46.0

It can be seen that the error is almost constant over the scale, thus, excluding the reading at - 0.999 V input, the error causes an almost constant DC shift of the signal which means that if the signal is kept within the upper 98% of the chart, the maximum error due to the interface and quantisation is $\frac{50 - 46}{4096} \times 100 = 0.097\%$.

TABLE 4

RESULTS OF SURFACE TEXTURE ANALYSIS FOR ML1
****

ROUGHNESS
****

	MEAN	ST. DEV.	MAXIMUM	MINIMUM
RT	10.411	0.561	11.186	9.351
RP	4.688	0.334	5.267	4.095
RV	5.723	0.316	6.371	5.167
RP/RT	0.454	0.016	0.479	0.423
RA	1.893	0.133	2.176	1.651
RQ	2.338	0.150	2.642	2.080
RQ/RA	1.238	0.014	1.264	1.218
SK	-0.185	0.098	-0.072	-0.377
Q	2.659	0.165	2.896	2.379
SA	0.127	0.006	0.139	0.117
SG	0.077	0.004	0.085	0.069
SQ	0.170	0.008	0.185	0.158
W'	93.113	6.638	116.127	85.747
NO.	37.666	2.035	41.562	32.500
R	46.405	7.835	63.581	35.382
H'	2.108	0.122	2.296	1.774
HQ	1.399	0.107	1.647	1.182
NP	317.062	18.636	351.000	287.000

SAMPLING LENGTH 4.00 MIC.

FLATNESS
****

RQF	1.184	0.204	1.853	0.807
SKF	-0.359	0.884	3.975	-1.609
QF	3.448	1.357	8.385	2.069

TABLE 5

RESULTS OF SURFACE TEXTURE ANALYSIS FOR ML2

****

ROUGHNESS

****

	MEAN	ST. DEV.	MAXIMUM	MINIMUM
RT	10.807	0.797	12.798	9.823
RP	4.567	0.584	5.916	3.786
RV	6.240	0.498	7.023	5.375
RP/RT	0.425	0.032	0.483	0.377
RA	2.055	0.138	2.400	1.895
RQ	2.524	0.171	2.966	2.346
RQ/RA	1.230	0.010	1.256	1.212
SK	-0.340	0.170	-0.084	-0.614
Q	2.661	0.221	3.175	2.349
SA	0.126	0.005	0.136	0.119
SG	0.073	0.005	0.082	0.065
SQ	0.171	0.007	0.183	0.159
W'	102.459	5.447	111.582	94.817
NO.	34.404	3.028	39.062	28.750
R	68.268	21.215	136.821	48.677
H'	2.198	0.209	2.785	1.968
HQ	1.331	0.155	1.643	1.149
NP	312.187	42.043	395.000	229.000

SAMPLING LENGTH 4.00 MIC.

FLATNESS

****

RQF	1.194	0.351	1.949	0.653
SKF	-0.724	0.338	0.270	-1.426
QF	3.768	0.999	6.708	2.505

TABLE 6

RESULTS OF SURFACE TEXTURE ANALYSIS FOR ML3
****

ROUGHNESS
****

	MEAN	ST. DEV.	MAXIMUM	MINIMUM
RT	5.335	1.942	8.517	2.653
RP	1.644	0.615	2.782	0.860
RV	3.691	1.347	5.836	1.659
RP/RT	0.316	0.025	0.376	0.268
RA	0.850	0.451	1.810	0.348
RQ	1.112	0.523	2.163	0.471
RQ/RA	1.344	0.072	1.455	1.205
SK	-1.272	0.336	-0.667	-1.846
Q	5.060	1.442	8.384	2.836
SA	0.066	0.019	0.097	0.036
SG	0.034	0.009	0.049	0.020
SQ	0.103	0.029	0.146	0.053
W'	74.726	20.136	117.258	50.184
NO.	45.732	10.624	62.656	29.844
R	99.724	22.458	140.786	64.171
H'	0.744	0.377	1.560	0.343
HQ	0.473	0.197	0.881	0.215
NP	528.062	94.703	686.000	319.000

SAMPLING LENGTH 4.00 MIC.

FLATNESS
****

RQF	0.544	0.179	1.308	0.352
SKF	0.157	0.646	2.902	-0.649
QF	3.237	1.074	6.100	2.124

TABLE 7

RESULTS OF SURFACE TEXTURE ANALYSIS FOR ML4
****

ROUGHNESS
****

	MEAN	ST. DEV.	MAXIMUM	MINIMUM
RT	12.122	1.675	15.812	9.527
RP	5.062	1.069	7.711	3.574
RV	7.060	0.717	8.299	5.953
RP/RT	0.414	0.032	0.485	0.376
RA	2.373	0.401	3.059	1.806
RQ	2.873	0.454	3.708	2.213
RQ/RA	1.220	0.019	1.257	1.186
SK	-0.457	0.156	-0.179	-0.680
Q	2.703	0.228	3.068	2.371
SA	0.108	0.008	0.122	0.088
SG	0.060	0.006	0.069	0.047
SQ	0.153	0.011	0.175	0.128
W'	138.363	21.003	175.461	108.762
NO.	24.424	3.944	31.094	17.812
R	148.739	47.589	272.360	89.881
H'	2.221	0.428	3.080	1.678
HQ	1.388	0.294	1.968	0.944
NP	229.937	54.468	335.000	128.000

SAMPLING LENGTH 4.00 MIC.

FLATNESS
****

RQF	1.699	0.544	3.294	0.850
SKF	-0.479	0.918	3.917	-1.626
QF	3.582	1.294	8.094	1.984

TABLE 8

RESULTS OF SURFACE TEXTURE ANALYSIS FOR SH1
****

ROUGHNESS
****

	MEAN	ST. DEV.	MAXIMUM	MINIMUM
RT	13.777	1.247	15.459	11.122
RP	6.872	0.873	8.025	5.381
RV	6.905	0.498	7.603	5.741
RP/RT	0.499	0.025	0.545	0.458
RA	2.626	0.340	3.157	1.942
RQ	3.171	0.389	3.789	2.372
RQ/RA	1.212	0.012	1.239	1.187
SK	-0.005	0.168	0.208	-0.302
Q	2.396	0.164	2.746	2.159
SA	0.166	0.008	0.179	0.155
SG	0.103	0.005	0.111	0.094
SQ	0.219	0.011	0.238	0.207
W'	98.852	13.658	119.263	71.477
NO.	34.531	5.133	48.125	28.750
R	34.794	6.981	52.519	20.911
H'	3.061	0.440	3.710	2.265
HQ	1.966	0.322	2.461	1.407
NP	276.937	55.723	381.000	191.000

SAMPLING LENGTH 4.00 MIC.

FLATNESS
****

RQF	1.475	0.315	2.305	0.928
SKF	-0.237	0.378	0.804	-1.214
QF	3.103	0.907	6.073	2.101

TABLE 9

RESULTS OF SURFACE TEXTURE ANALYSIS FOR SH2
****

ROUGHNESS
****

	MEAN	ST. DEV.	MAXIMUM	MINIMUM
RT	25.674	2.243	29.623	21.850
RP	12.095	1.241	14.905	10.008
RV	13.579	1.299	16.876	10.863
RP/RT	0.472	0.021	0.507	0.431
RA	5.286	0.567	6.533	4.433
RQ	6.381	0.629	7.703	5.409
RQ/RA	1.217	0.021	1.260	1.191
SK	-0.165	0.136	0.010	-0.488
Q	2.541	0.295	3.478	2.260
SA	0.177	0.008	0.192	0.164
SG	0.107	0.005	0.114	0.100
SQ	0.241	0.012	0.263	0.220
W'	187.323	18.779	227.441	160.504
NO.	18.779	2.382	23.594	15.156
R	81.980	21.424	134.561	53.682
H'	5.558	0.459	6.381	4.627
HQ	3.782	0.411	4.762	3.099
NP	126.000	22.603	170.000	99.000

SAMPLING LENGTH 4.00 MIC.

FLATNESS
****

RQF	4.415	1.077	8.638	2.691
SKF	-0.707	0.327	0.136	-1.364
QF	3.758	0.852	5.931	2.257

TABLE 10

RESULTS OF SURFACE TEXTURE ANALYSIS FOR SH3
****

ROUGHNESS
****

	MEAN	ST. DEV.	MAXIMUM	MINIMUM
RT	9.967	0.792	11.443	8.481
RP	4.327	0.383	4.954	3.631
RV	5.640	0.469	6.758	4.849
RP/RT	0.439	0.015	0.469	0.414
RA	1.630	0.179	2.064	1.331
RQ	2.043	0.212	2.548	1.680
RQ/RA	1.255	0.014	1.283	1.234
SK	-0.322	0.122	-0.113	-0.524
Q	2.970	0.238	3.587	2.708
SA	0.161	0.012	0.186	0.146
SG	0.100	0.008	0.116	0.090
SQ	0.211	0.016	0.245	0.191
W'	63.777	9.462	86.161	50.746
NO.	54.502	6.850	65.469	41.562
R	25.315	4.969	39.559	18.112
H'	1.859	0.198	2.249	1.506
HQ	1.162	0.127	1.336	0.936
NP	432.187	35.520	497.000	380.000

SAMPLING LENGTH 4.00 MIC.

FLATNESS
****

RQF	0.973	0.158	1.247	0.567
SKF	0.109	0.708	3.293	-0.649
QF	3.350	1.456	9.510	2.057

TABLE 11

RESULTS OF SURFACE TEXTURE ANALYSIS FOR SH4
****

ROUGHNESS
****

	MEAN	ST. DEV.	MAXIMUM	MINIMUM
RT	23.039	1.797	26.358	20.358
RP	11.453	0.766	12.991	10.422
RV	11.586	1.097	13.367	9.937
RP/RT	0.500	0.014	0.524	0.479
RA	4.728	0.530	5.772	4.128
RQ	5.707	0.587	6.846	4.980
RQ/RA	1.213	0.015	1.246	1.186
SK	0.044	0.082	0.187	-0.134
Q	2.360	0.123	2.595	2.139
SA	0.171	0.006	0.181	0.159
SG	0.104	0.004	0.112	0.097
SQ	0.232	0.010	0.249	0.217
W'	173.456	14.756	206.119	158.281
NO.	19.648	1.890	22.500	16.250
R	78.047	16.944	116.618	55.587
H'	5.342	0.629	6.809	4.591
HQ	3.627	0.262	3.980	3.215
NP	122.312	18.714	159.000	88.000

SAMPLING LENGTH 4.00 MIC.

FLATNESS
****

RQF	3.052	0.577	3.883	1.702
SKF	-0.444	0.259	0.121	-1.157
QF	2.980	0.581	4.452	2.030

TABLE 12

RESULTS OF SURFACE TEXTURE ANALYSIS FOR SH5
****

ROUGHNESS
****

	MEAN	ST. DEV.	MAXIMUM	MINIMUM
RT	10.310	1.091	12.183	9.182
RP	4.654	0.693	6.150	3.891
RV	5.656	0.498	6.657	4.970
RP/RT	0.450	0.023	0.499	0.419
RA	1.802	0.187	2.138	1.568
RQ	2.231	0.230	2.605	1.941
RQ/RA	1.241	0.010	1.262	1.219
SK	-0.261	0.127	-0.040	-0.474
Q	2.774	0.159	3.196	2.480
SA	0.142	0.007	0.156	0.130
SG	0.089	0.005	0.097	0.080
SQ	0.186	0.009	0.205	0.172
W'	78.670	6.024	91.058	65.943
NO.	43.867	3.002	50.000	37.031
R	30.249	3.816	40.391	24.640
H'	2.001	0.212	2.399	1.774
HQ	1.365	0.212	1.785	1.133
NP	371.312	27.642	423.000	319.000

SAMPLING LENGTH 4.00 MIC.

FLATNESS
****

RQF	2.049	0.963	4.555	0.722
SKF	-0.290	0.541	1.192	-1.169
QF	3.503	1.552	9.445	1.950

TABLE 13

RESULTS OF SURFACE TEXTURE ANALYSIS FOR TN1
****

ROUGHNESS
****

	MEAN	ST. DEV.	MAXIMUM	MINIMUM
RT	24.204	1.478	26.648	21.930
RP	15.014	1.043	16.713	13.309
RV	9.190	0.516	10.378	8.438
RP/RT	0.621	0.010	0.645	0.603
RA	5.443	0.395	6.075	4.828
RQ	6.412	0.485	7.155	5.665
RQ/RA	1.179	0.009	1.195	1.161
SK	0.651	0.064	0.753	0.493
Q	2.279	0.080	2.391	2.142
SA	0.212	0.012	0.234	0.193
SG	0.140	0.009	0.160	0.126
SQ	0.267	0.015	0.292	0.239
W'	160.211	4.978	169.381	152.157
NO.	17.500	1.094	19.687	15.938
R	33.013	8.517	60.733	25.266
H'	12.424	1.705	14.893	9.581
HQ	2.743	1.163	4.786	1.100
NP	24.312	2.256	29.000	22.000

SAMPLING LENGTH 2.00 MIC.

FLATNESS
****

RQF	2.109	0.208	2.904	1.802
SKF	-0.523	0.190	-0.212	-0.977
QF	2.540	0.363	3.773	2.117

TABLE 14

RESULTS OF SURFACE TEXTURE ANALYSIS FOR TN2
****

ROUGHNESS
****

	MEAN	ST. DEV.	MAXIMUM	MINIMUM
RT	12.708	1.334	14.828	10.902
RP	7.092	0.543	8.220	6.275
RV	5.616	0.866	7.018	4.328
RP/RT	0.567	0.025	0.609	0.520
RA	2.223	0.213	2.640	1.917
RQ	2.772	0.288	3.289	2.344
RQ/RA	1.248	0.020	1.282	1.207
SK	0.484	0.149	0.692	0.143
Q	2.793	0.117	3.023	2.577
SA	0.128	0.013	0.153	0.108
SG	0.077	0.007	0.092	0.065
SQ	0.177	0.018	0.209	0.150
W'	109.279	5.867	119.790	101.248
NO.	26.582	4.183	32.812	21.875
R	57.525	21.374	130.750	37.775
H'	3.418	0.532	4.334	2.578
HQ	2.464	0.244	2.935	2.001
NP	53.750	16.103	88.000	33.000

SAMPLING LENGTH 2.00 MIC.

FLATNESS
****

RQF	1.670	0.223	2.122	1.209
SKF	1.570	1.597	4.768	-0.620
QF	0.878	1.290	2.932	-0.873

TABLE 15

RESULTS OF SURFACE TEXTURE ANALYSIS FOR TN3
****

ROUGHNESS
****

	MEAN	ST. DEV.	MAXIMUM	MINIMUM
RT	11.966	1.585	15.647	9.502
RP	5.408	1.043	7.888	3.775
RV	6.558	0.667	7.821	5.462
RP/RT	0.451	0.035	0.506	0.390
RA	2.176	0.285	2.817	1.739
RQ	2.669	0.346	3.440	2.174
RQ/RA	1.228	0.018	1.270	1.207
SK	-0.235	0.183	0.014	-0.629
Q	2.627	0.293	3.604	2.337
SA	0.168	0.009	0.182	0.153
SG	0.102	0.007	0.113	0.088
SQ	0.226	0.011	0.242	0.210
W'	80.830	7.208	97.220	70.457
NO.	45.508	4.088	51.562	35.625
R	34.864	6.344	50.158	26.491
H'	2.399	0.366	3.081	1.781
HQ	1.525	0.306	2.109	0.974
NP	166.875	29.408	227.000	120.000

SAMPLING LENGTH 2.00 MIC.

FLATNESS
****

RQF	1.326	0.511	2.469	0.556
SKF	-0.336	0.461	0.471	-1.476
QF	3.367	1.107	6.571	1.945

TABLE 16

RESULTS OF SURFACE TEXTURE ANALYSIS FOR TN4
****

ROUGHNESS
****

	MEAN	ST. DEV.	MAXIMUM	MINIMUM
RT	11.914	1.893	15.661	9.811
RP	4.959	1.340	7.317	2.962
RV	6.955	0.837	8.682	5.706
RP/RT	0.412	0.059	0.485	0.288
RA	2.228	0.438	3.318	1.660
RQ	2.727	0.514	3.932	2.056
RQ/RA	1.229	0.024	1.284	1.188
SK	-0.454	0.376	-0.036	-1.302
Q	2.819	0.554	4.233	2.098
SA	0.173	0.021	0.209	0.127
SG	0.100	0.016	0.123	0.068
SQ	0.239	0.022	0.282	0.192
W'	80.558	13.352	108.062	63.819
NO.	46.914	6.922	59.687	37.187
R	44.016	21.429	88.262	20.925
H'	2.419	0.616	3.634	1.535
HQ	1.413	0.387	2.026	0.875
NP	194.750	47.499	274.000	121.000

SAMPLING LENGTH 2.00 MIC.

FLATNESS
****

RQF	1.263	0.406	2.617	0.704
SKF	-0.152	0.739	1.207	-2.547
QF	3.640	1.768	10.956	2.064

TABLE 17

RESULTS OF SURFACE TEXTURE ANALYSIS FOR GN1
****

ROUGHNESS
****

	MEAN	ST. DEV.	MAXIMUM	MINIMUM
RT	6.684	0.581	8.239	5.785
RP	2.965	0.258	3.525	2.543
RV	3.719	0.391	4.713	3.091
RP/RT	0.446	0.021	0.485	0.406
RA	1.056	0.096	1.259	0.910
RQ	1.310	0.123	1.586	1.151
RQ/RA	1.243	0.012	1.266	1.218
SK	-0.273	0.129	-0.015	-0.513
Q	2.855	0.252	3.465	2.542
SA	0.155	0.016	0.173	0.128
SG	0.095	0.011	0.109	0.079
SQ	0.206	0.020	0.231	0.172
W'	43.239	6.116	59.282	35.453
ND.	75.605	6.664	84.687	59.375
R	17.016	5.315	28.211	11.996
H'	1.140	0.092	1.352	1.008
HQ	0.749	0.088	0.986	0.656
NP	370.312	49.005	451.000	255.000

SAMPLING LENGTH 2.00 MIC.

FLATNESS
****

RQF	0.958	0.222	1.510	0.642
SKF	0.056	0.588	2.922	-0.614
QF	2.963	1.256	7.611	1.884

TABLE 18

RESULTS OF SURFACE TEXTURE ANALYSIS FOR GN2
****

ROUGHNESS
****

	MEAN	ST. DEV.	MAXIMUM	MINIMUM
RT	1.301	0.152	1.696	1.072
RP	0.479	0.134	0.891	0.338
RV	0.823	0.064	0.932	0.714
RP/RT	0.367	0.052	0.505	0.294
RA	0.139	0.024	0.187	0.111
RQ	0.185	0.027	0.243	0.154
RQ/RA	1.336	0.039	1.400	1.262
SK	-0.965	0.393	-0.178	-1.646
Q	5.958	1.501	8.887	3.621
SA	0.047	0.005	0.058	0.041
SG	0.029	0.004	0.035	0.025
SQ	0.064	0.007	0.078	0.057
W'	18.344	1.508	21.044	16.027
NO.	162.012	13.264	180.313	140.313
R	34.640	4.875	41.111	26.742
H'	0.155	0.029	0.211	0.124
HQ	0.100	0.023	0.160	0.074
NP	650.937	33.767	712.000	601.000

SAMPLING LENGTH 2.00 MIC.

FLATNESS
****

RQF	0.633	0.172	0.927	0.335
SKF	-0.416	0.506	0.605	-1.240
QF	2.891	1.164	8.207	1.566

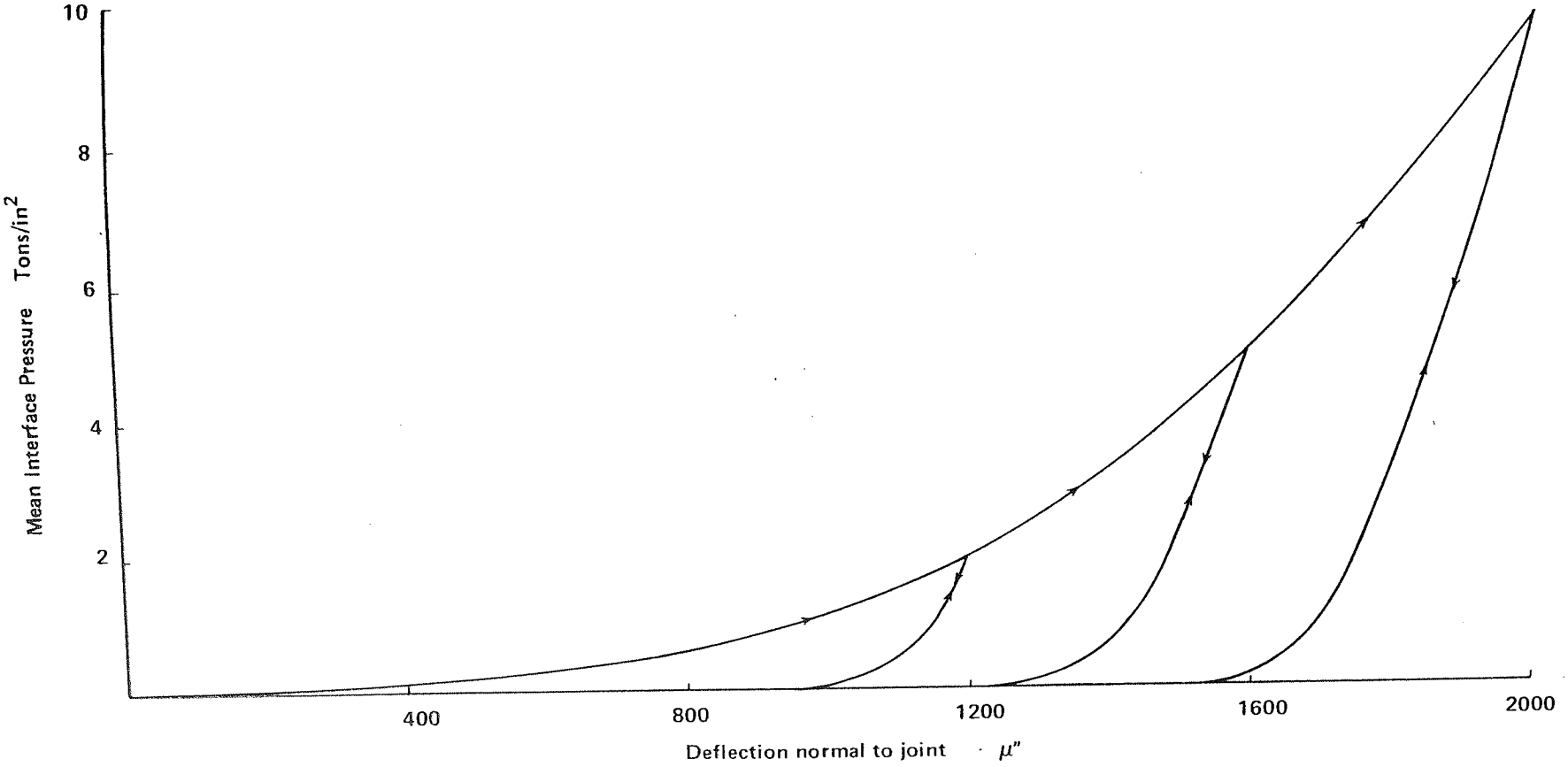

Fig. 1 General characteristics of joints [14]

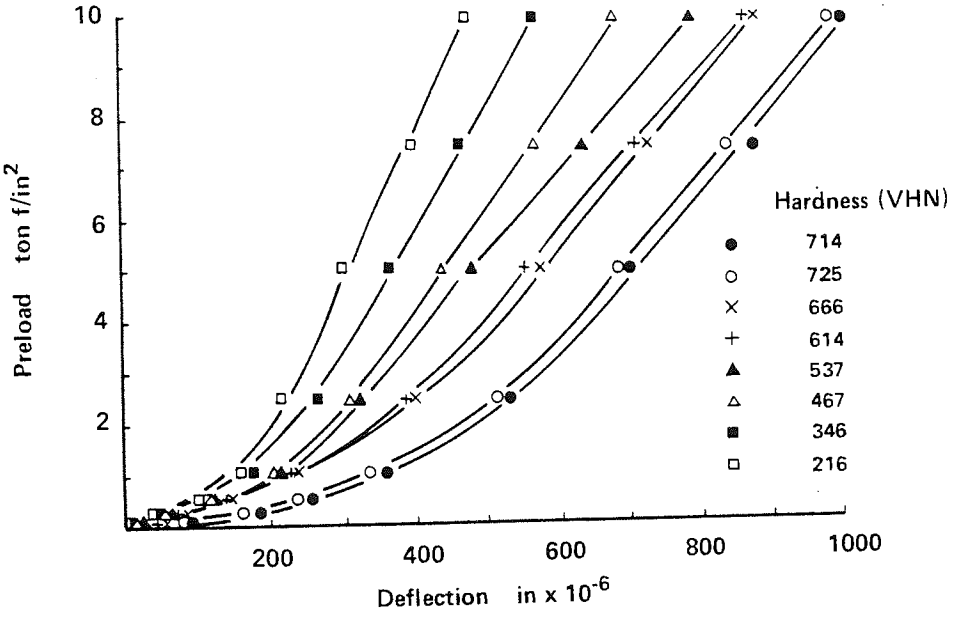

Fig. 2 Influence of hardness on the unloading deflection characteristics[30]

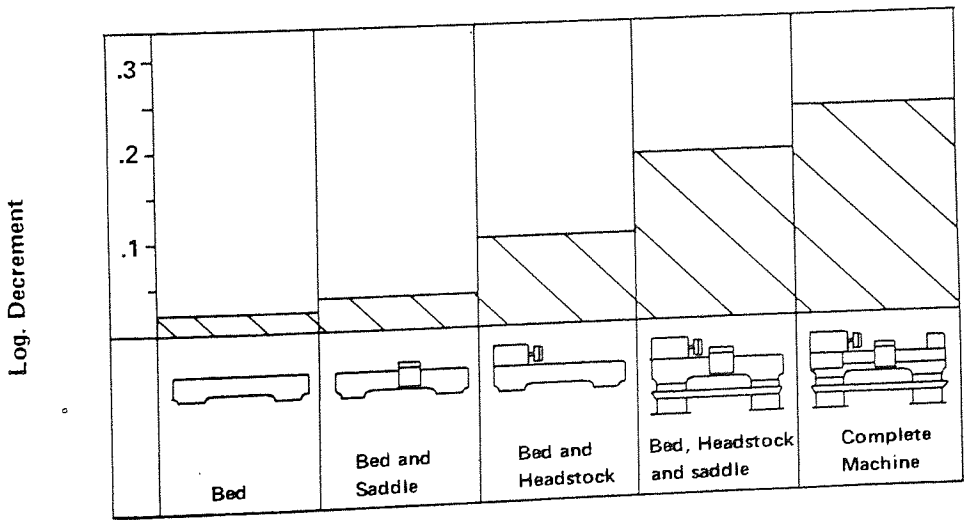

Fig. 3 Influence of components on damping of a lathe[33]

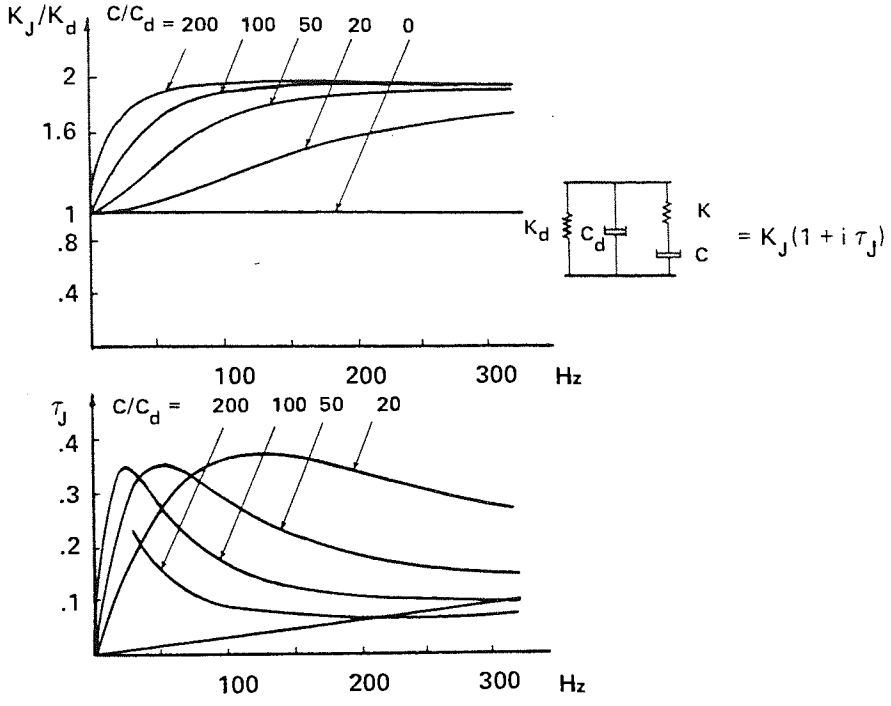

Fig. 4 Frequency behaviour of equivalent system[34]

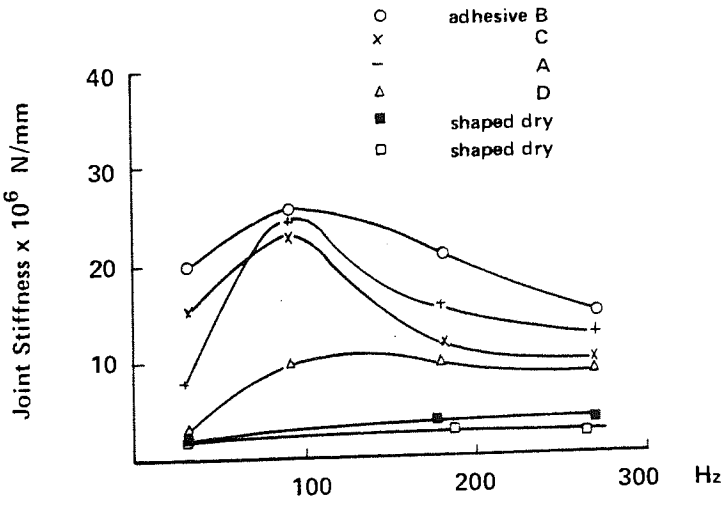

Fig. 5 Stiffness versus frequency[29]
(preload 1890 x 10^3 N/m^2)

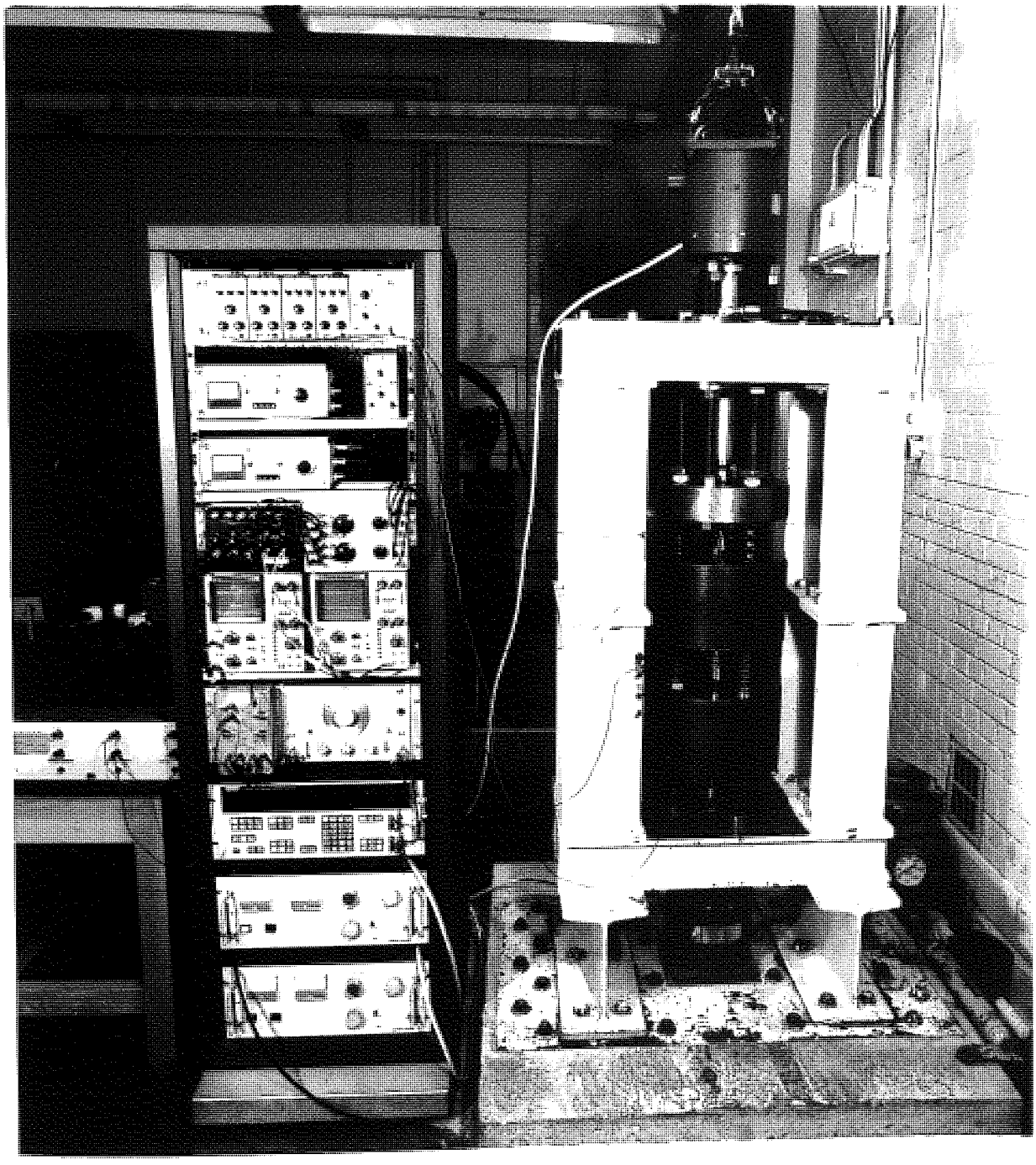

Fig. 6 General view of the test rig

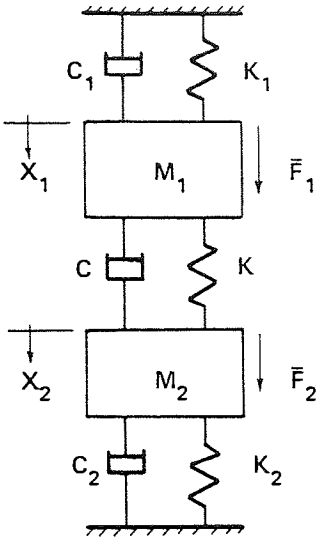

a. Two degrees of freedom system

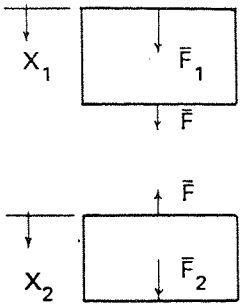

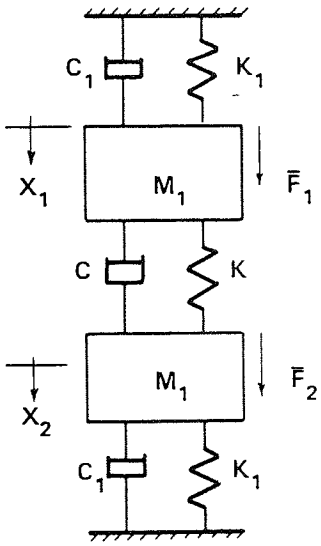

b. Symmetric T.D.F.S.

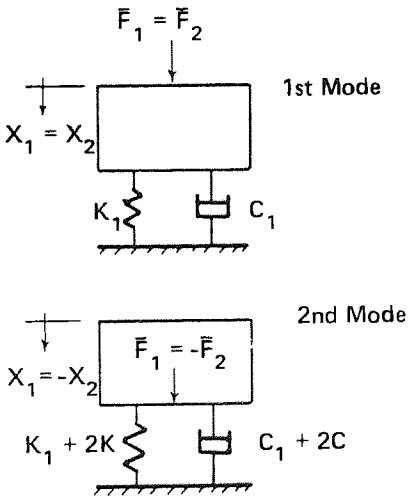

c. Equivalent systems

Fig. 7 Schematic systems representation

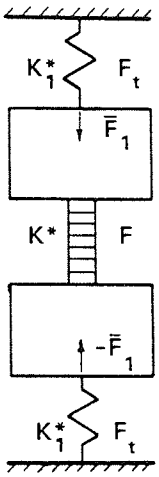

a. Test rig representation
(K^* = complex stiffness)

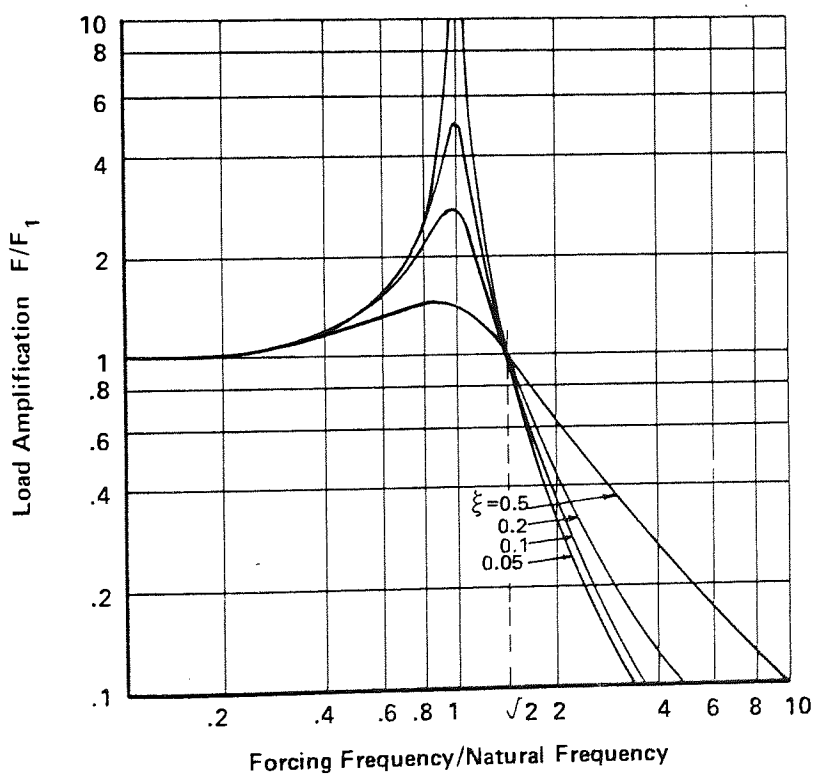

b. Transmissibility with frequency independent parameters
($\omega_2 \gg \omega_1, \xi_2 \gg \xi_1$)

Fig. 8 The main feature of the rig[41]

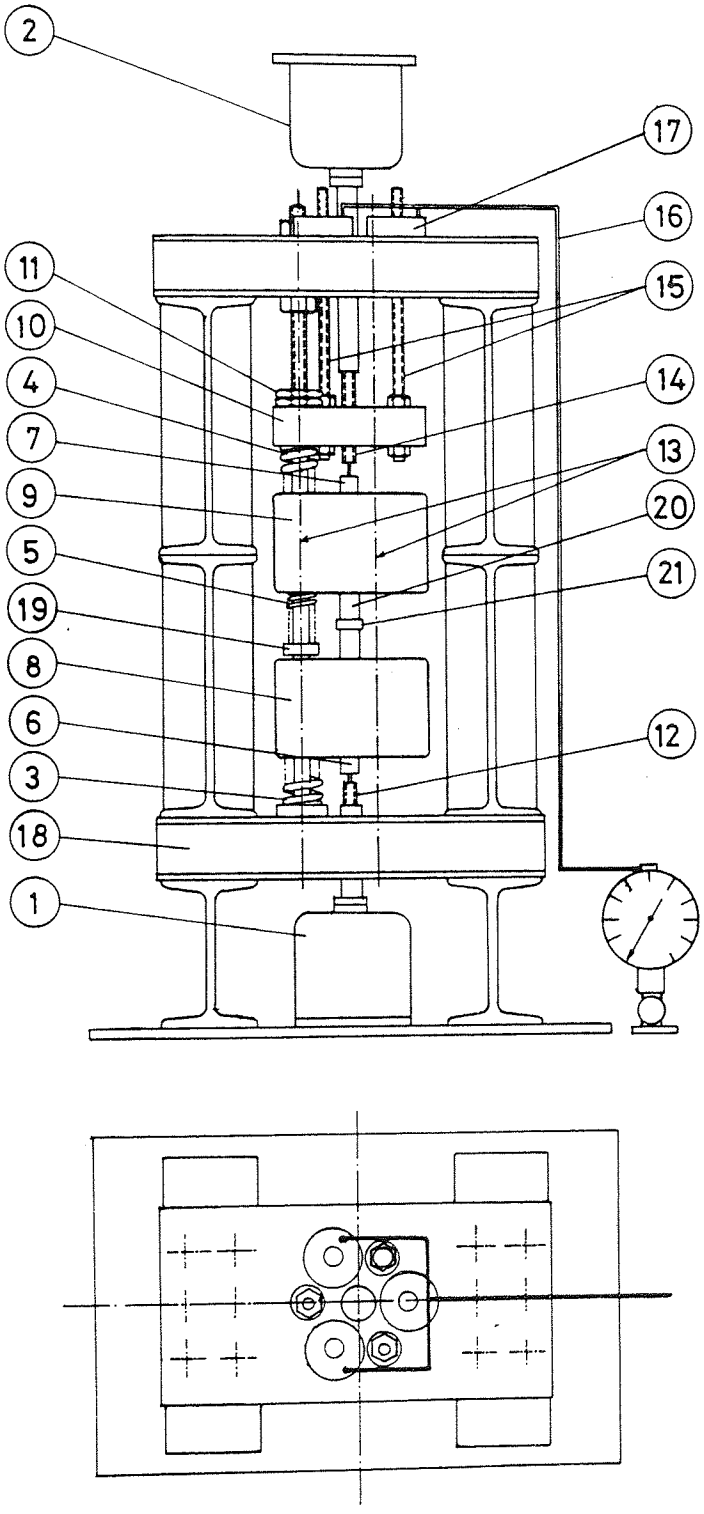

Fig. 9 Schematic view of the test rig

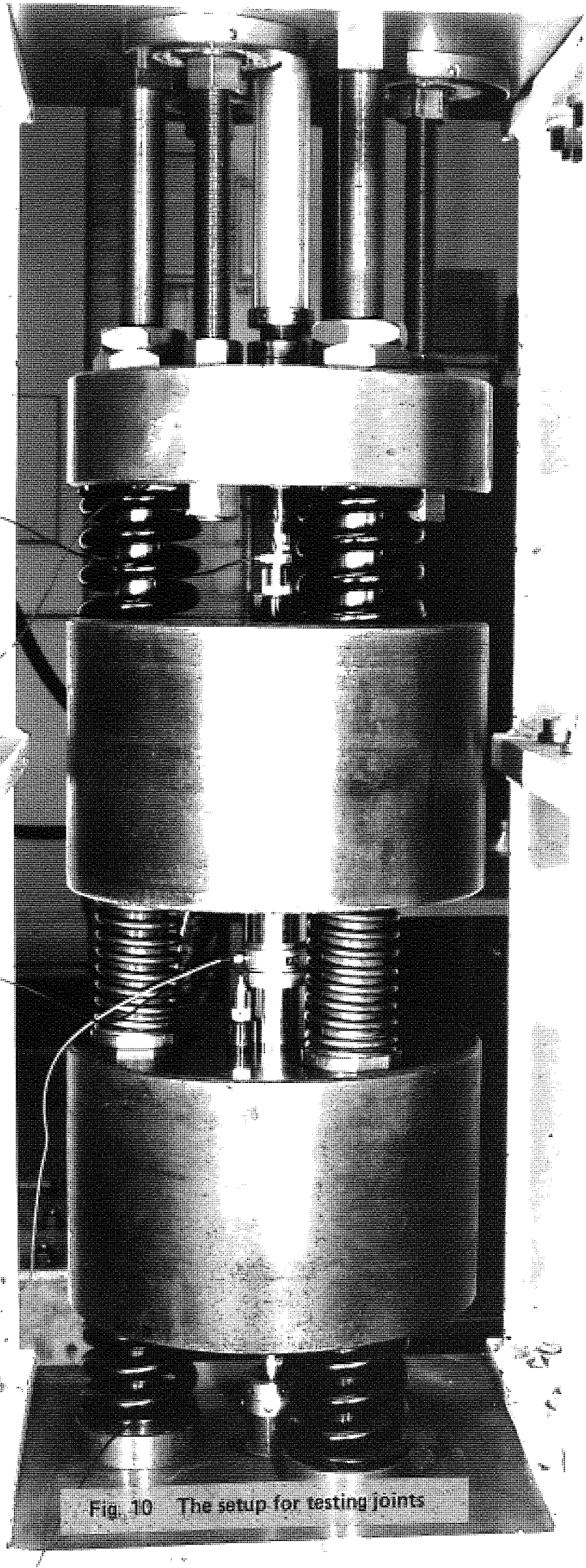

Fig. 10 The setup for testing joints

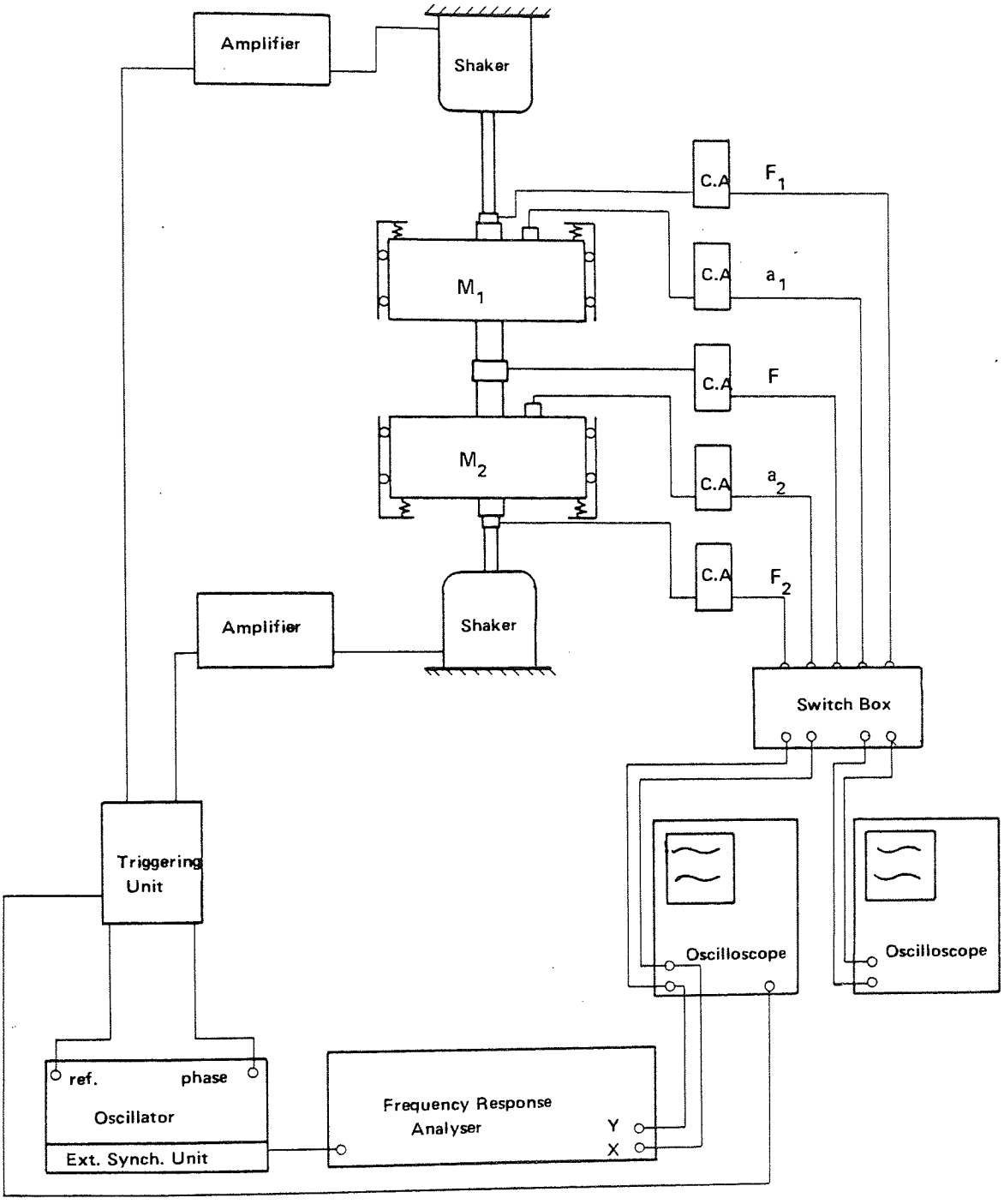

Fig. 11 Block diagram of the system

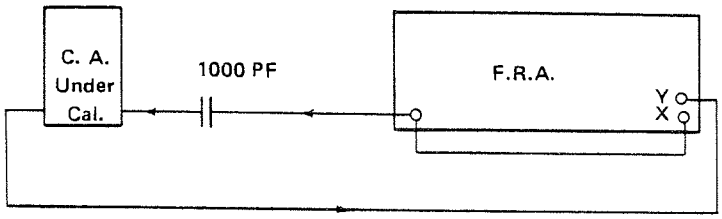

Fig. 12 Setup for calibration of charge amplifiers

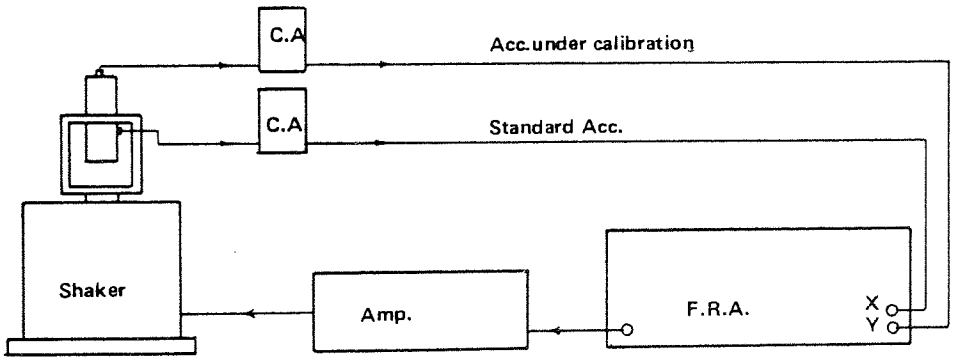

Fig. 13 Setup for calibration of accelerometers

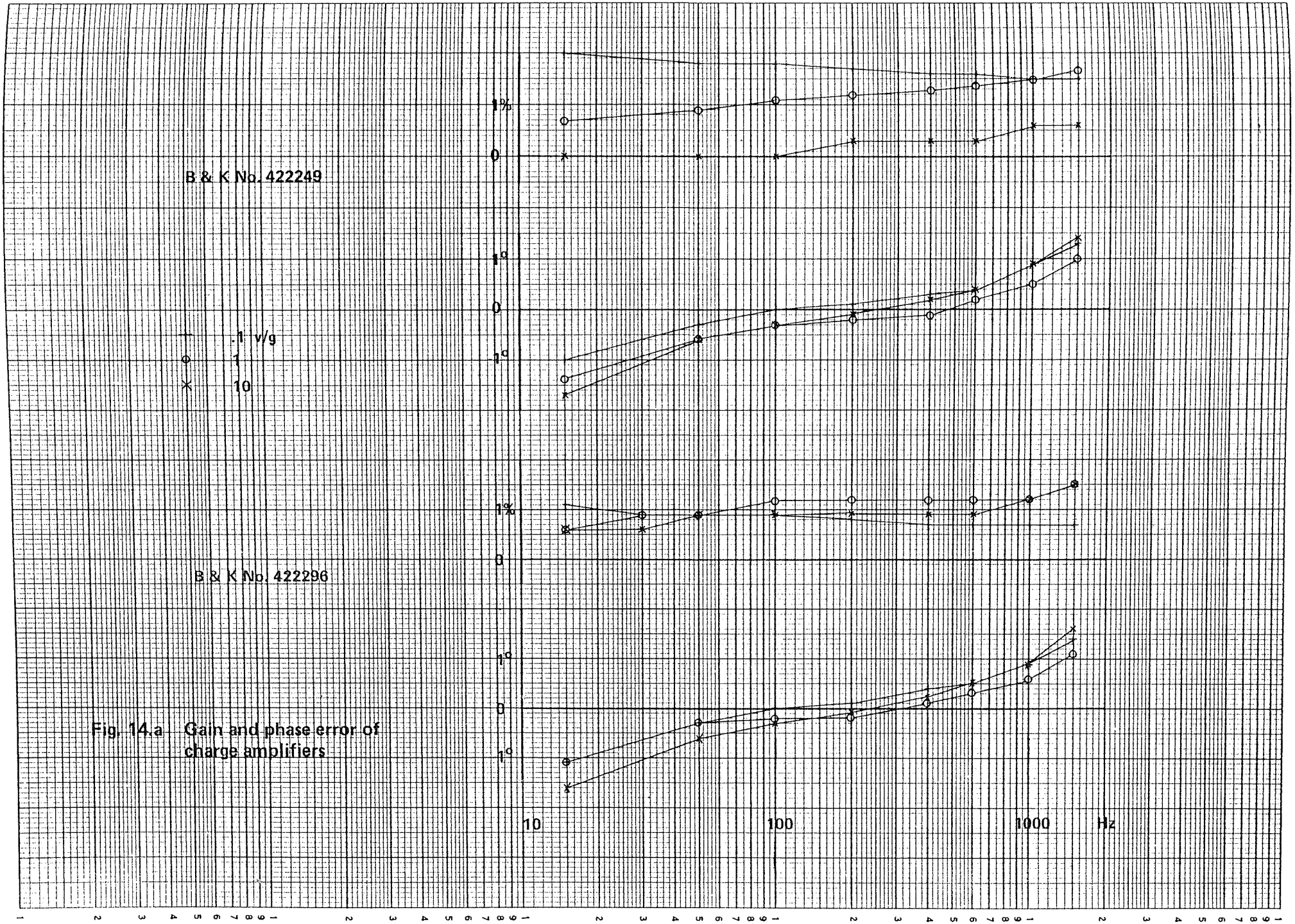

Fig. 14.a Gain and phase error of charge amplifiers

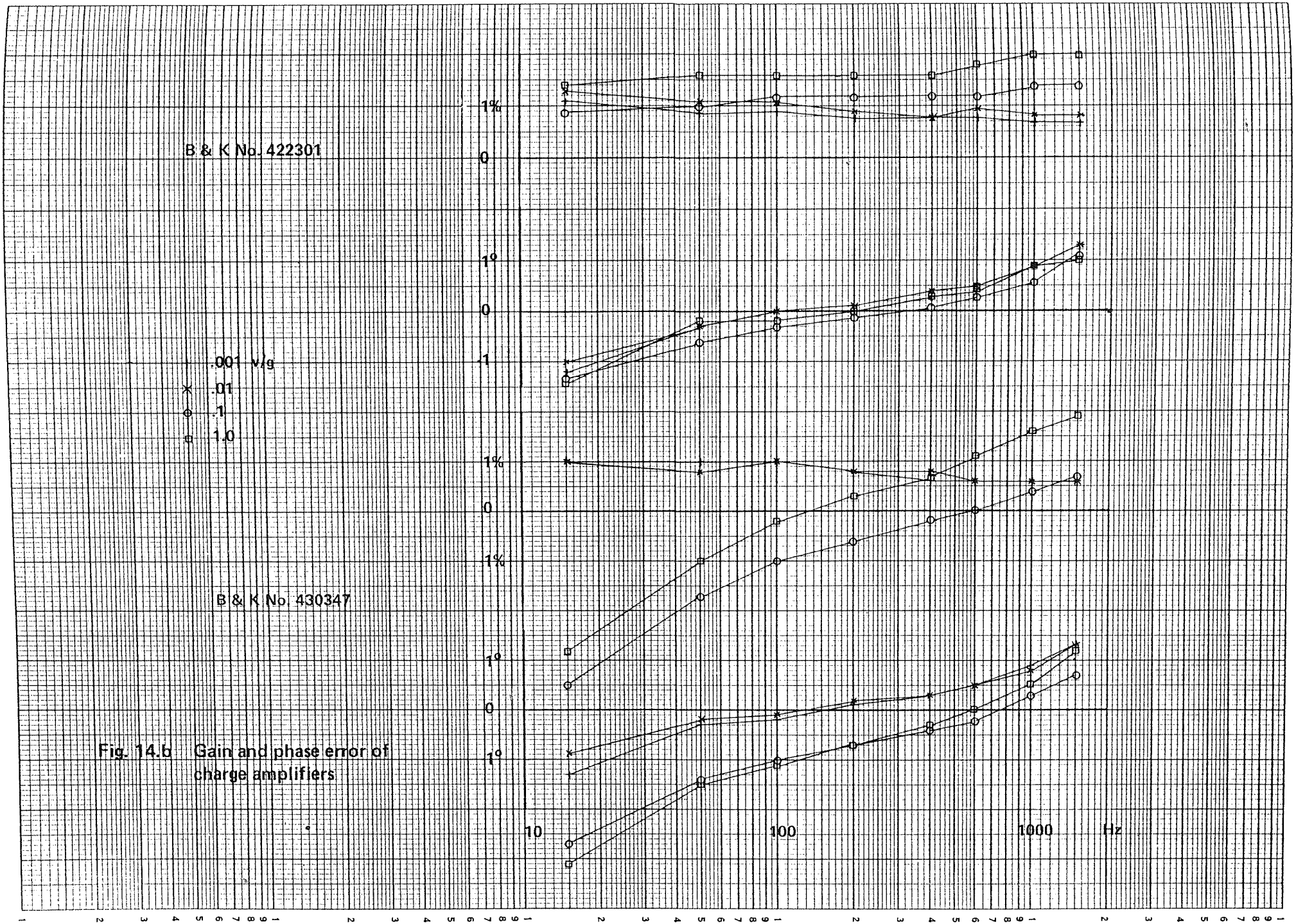

Fig. 14.b Gain and phase error of charge amplifiers

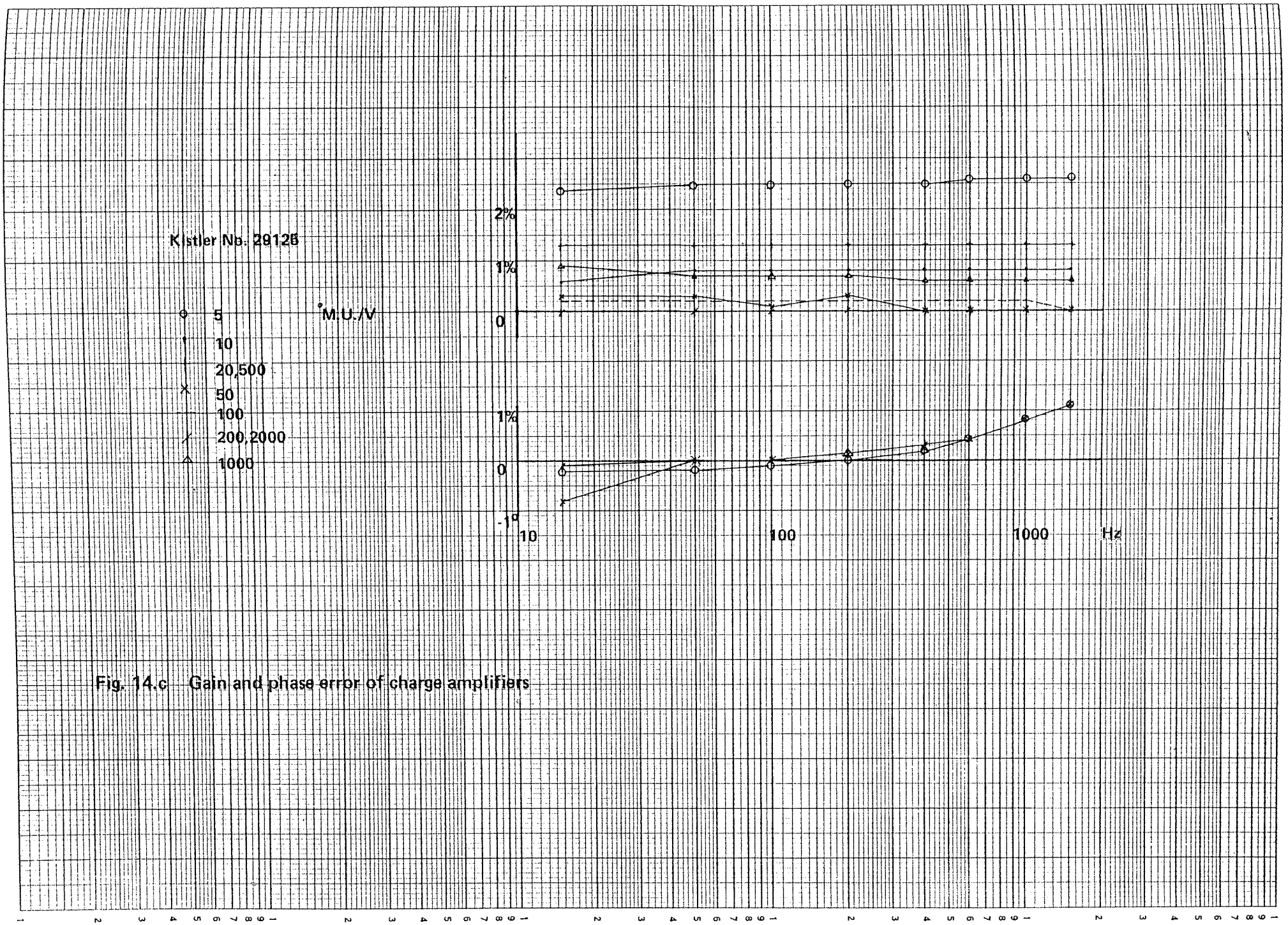

Fig. 14.c Gain and phase error of charge amplifiers

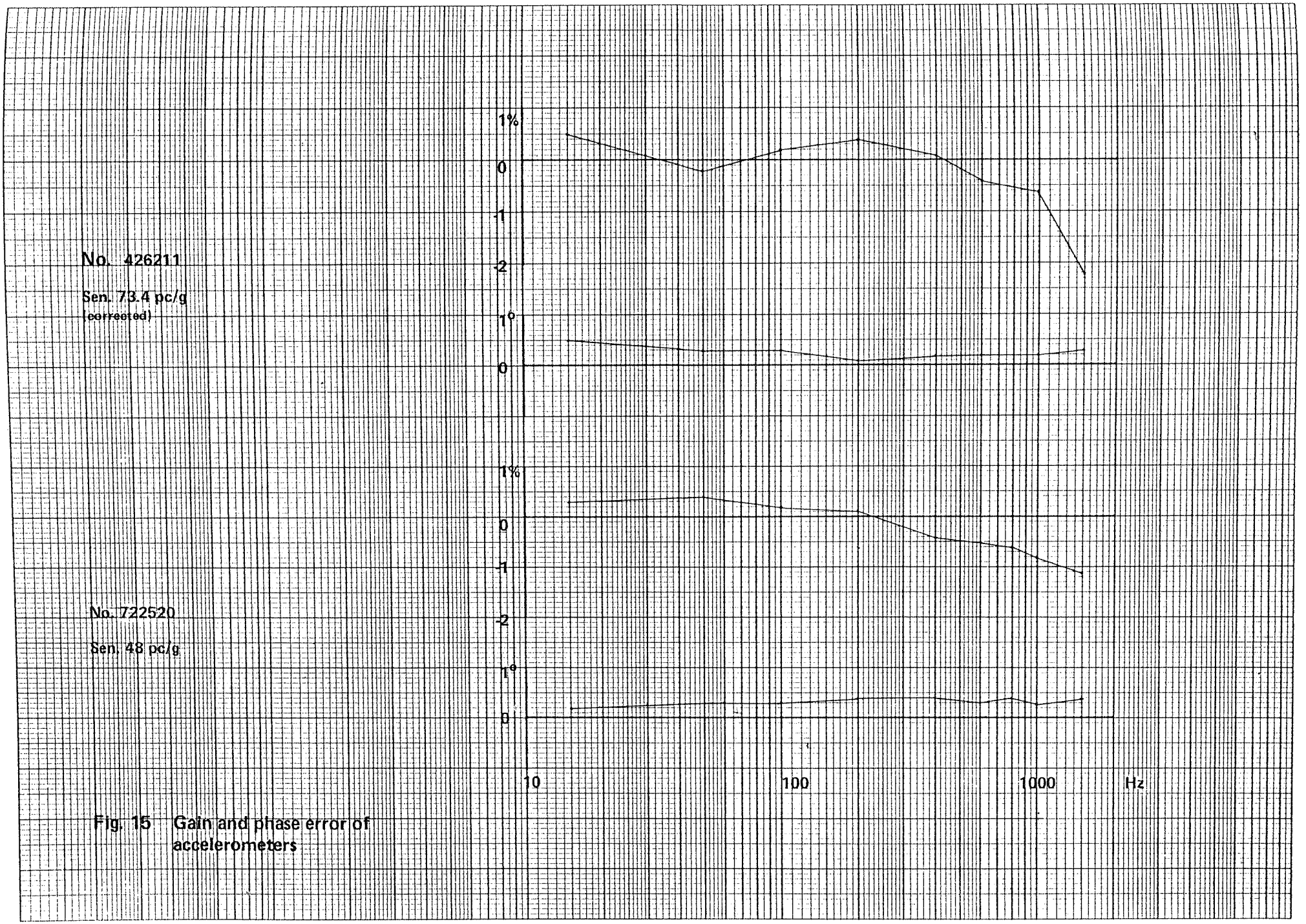

Fig. 15 Gain and phase error of accelerometers

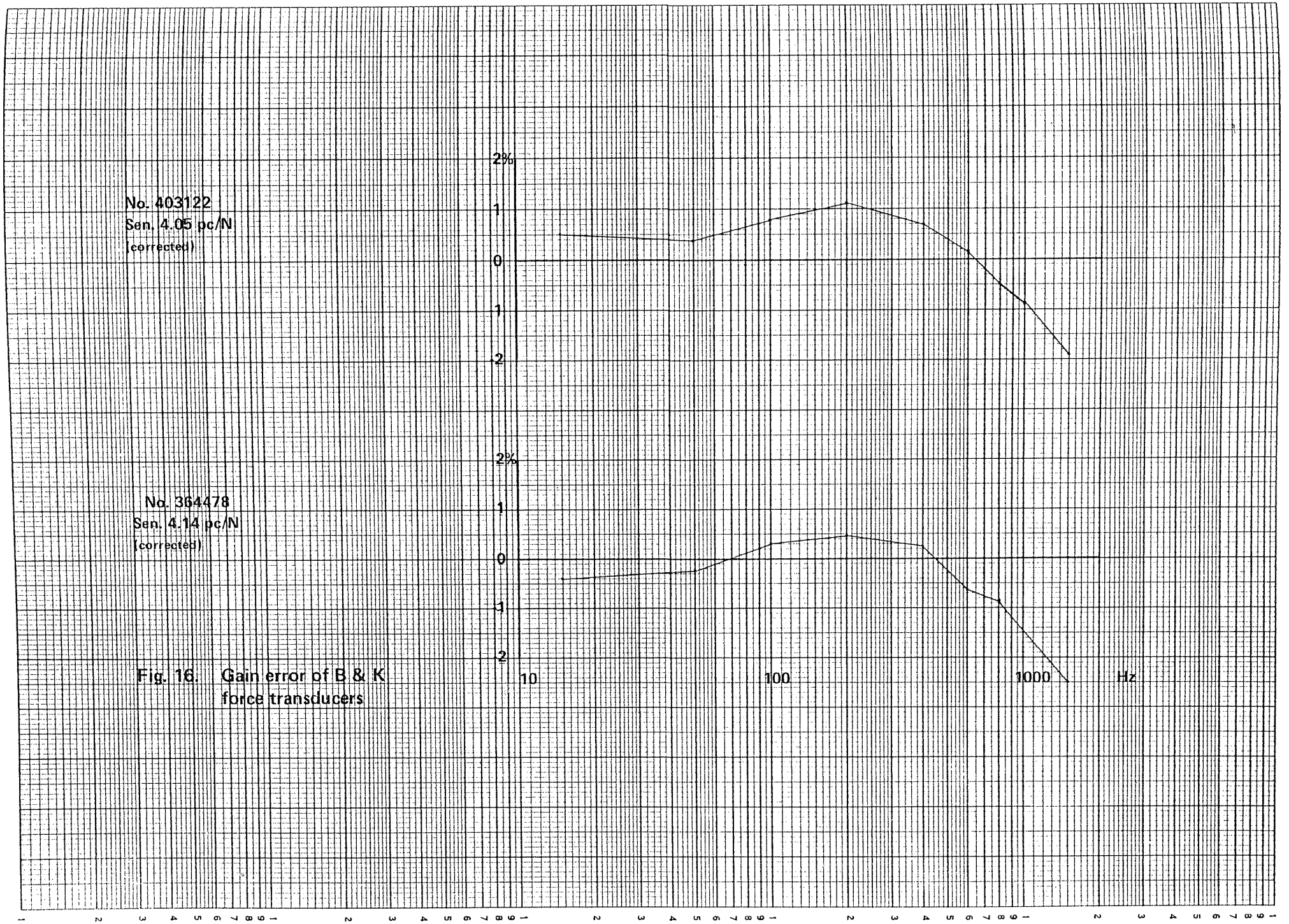

Fig. 16. Gain error of B & K force transducers

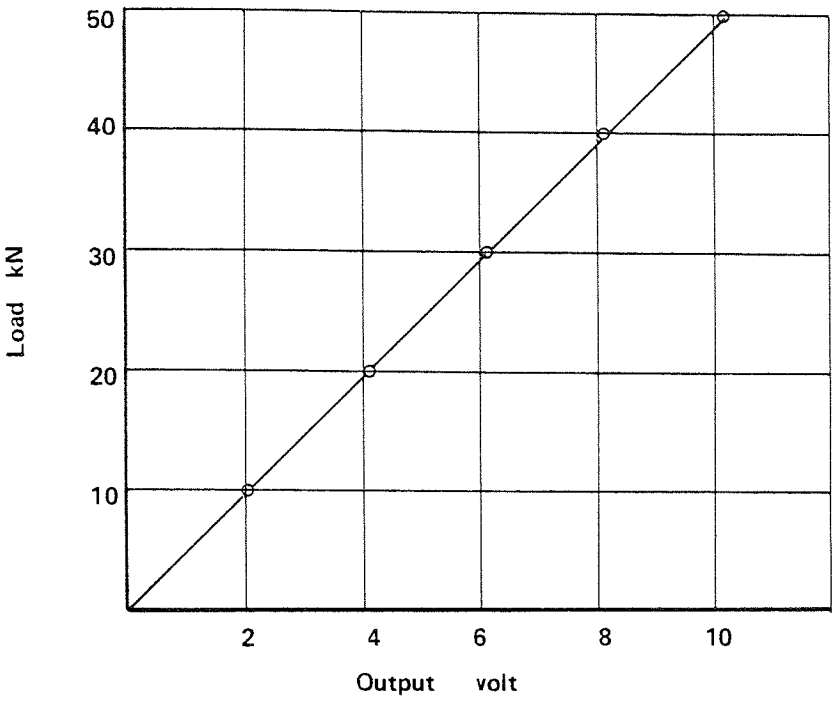

Fig. 17 Static calibration of Kistler load cell

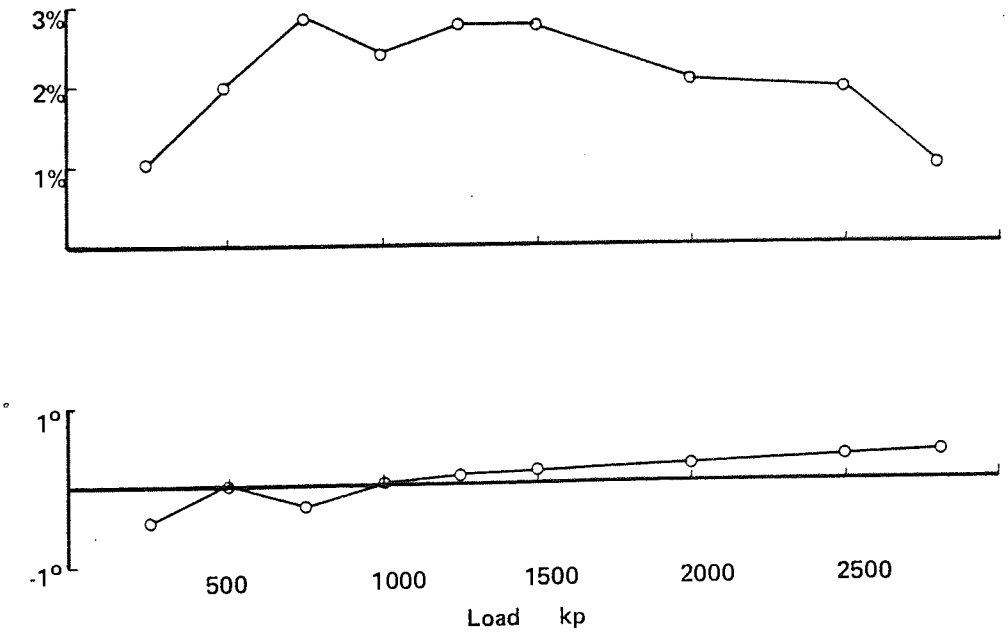

Fig. 18 Gain and phase error of m method reference m_i method

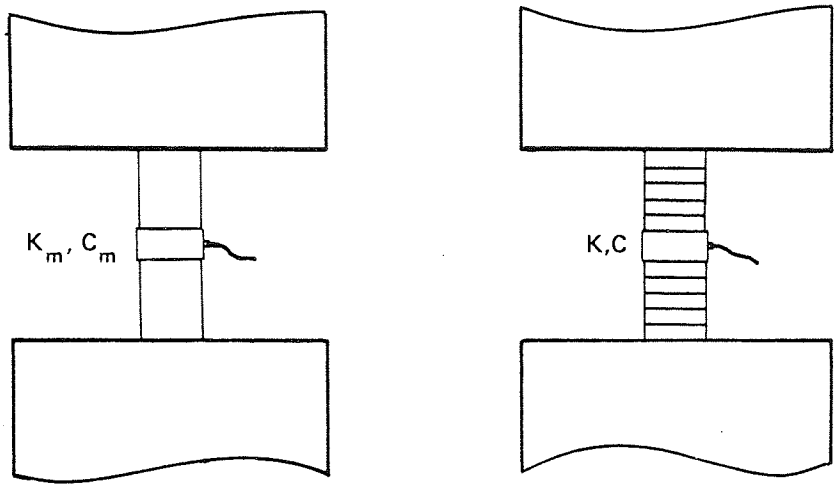

a. Equivalent solid

b. Jointed column

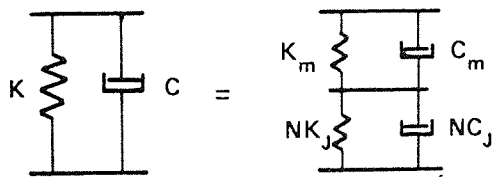

c. Jointed column model

Fig. 19 Correction for the material effect

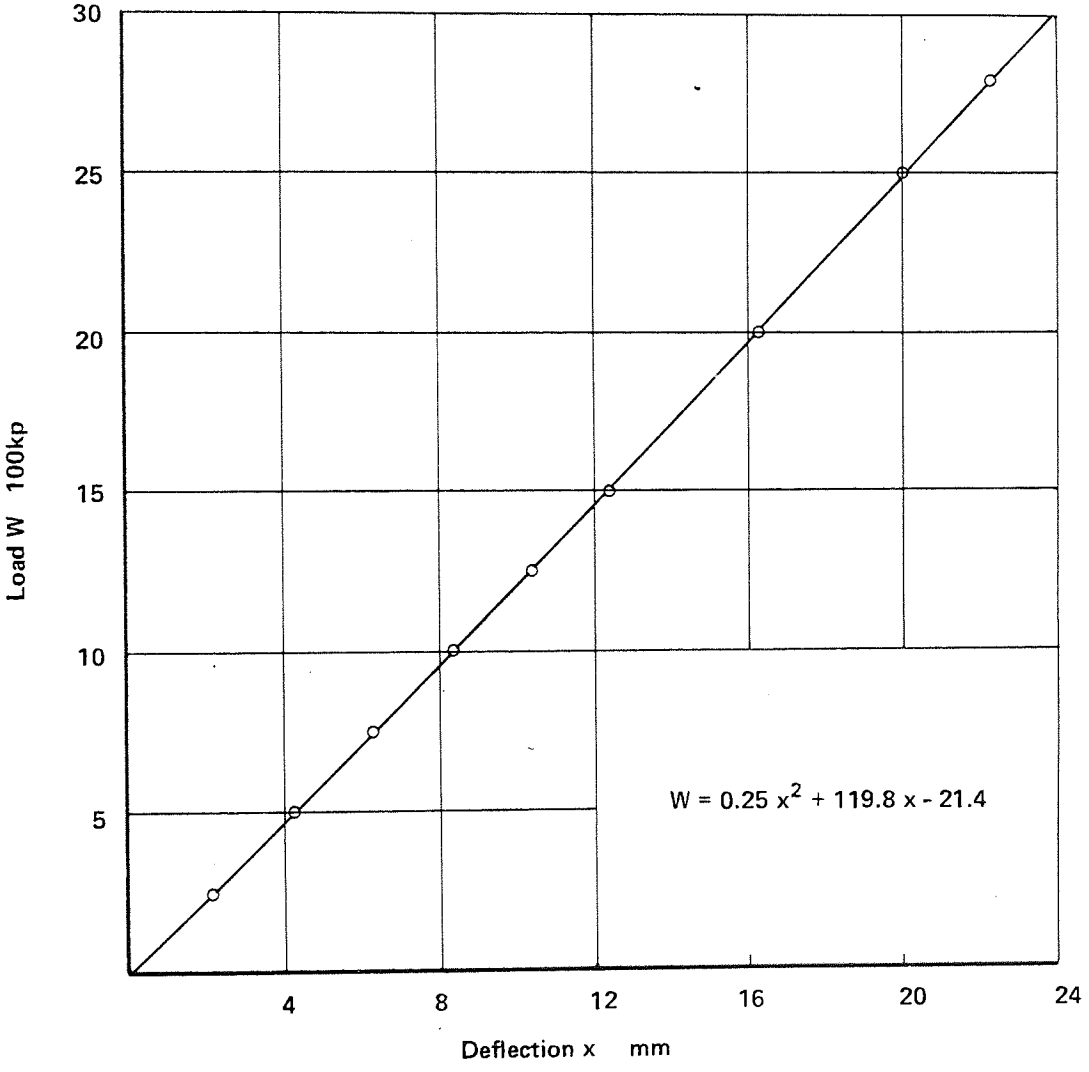

Fig. 20 Static calibration of the test rig

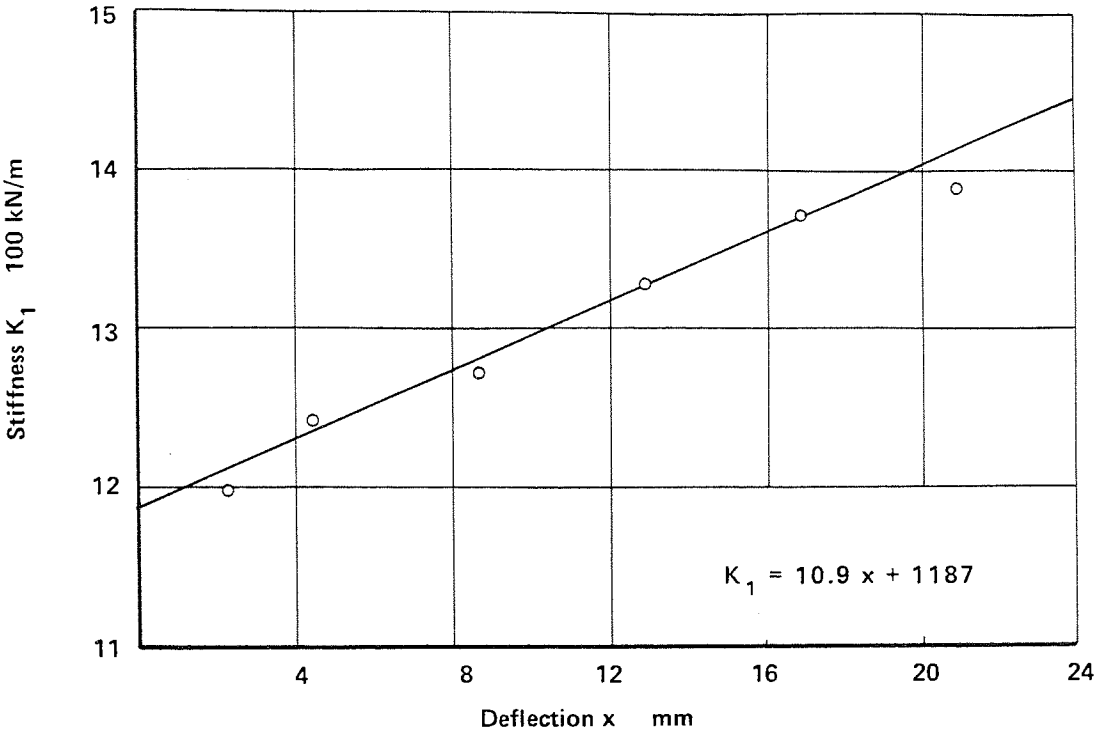

Fig. 21.a Effective stiffness of the auxiliary system

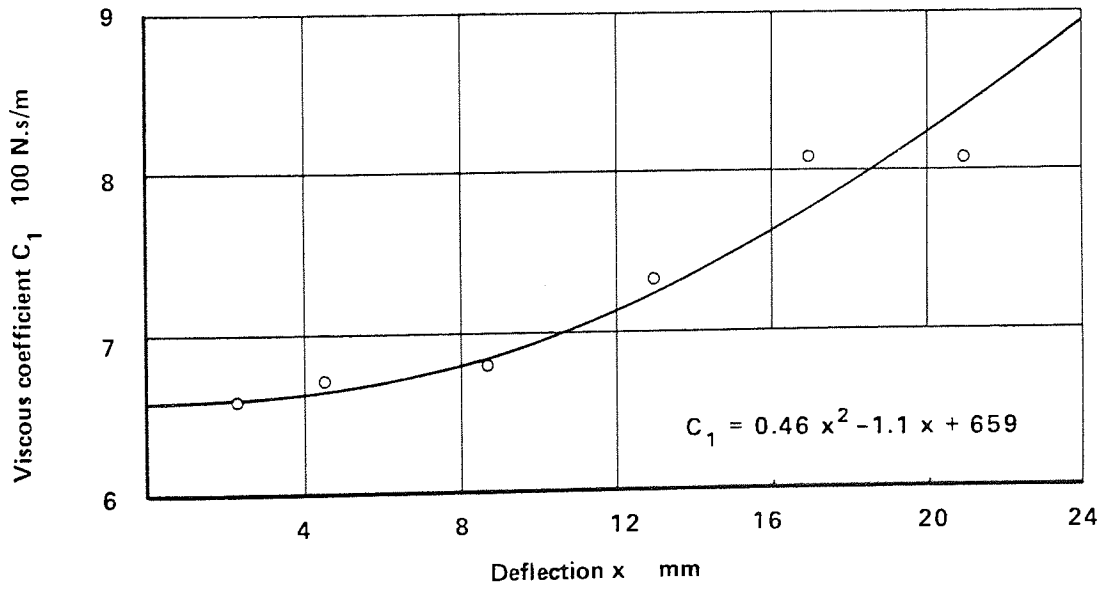

Fig. 21.b Damping coefficient of the auxiliary system

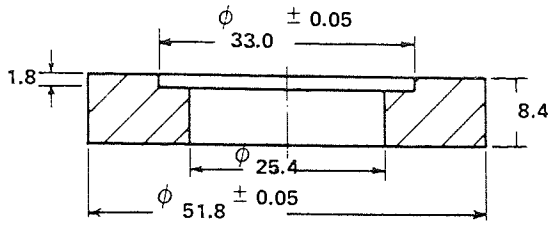

Material: Steel EN8

Tolerances unless otherwise specified ± 0.1

Dimensions in mm

Fig. 22 Dimensions of the specimens used for the study of the effect of surface texture.

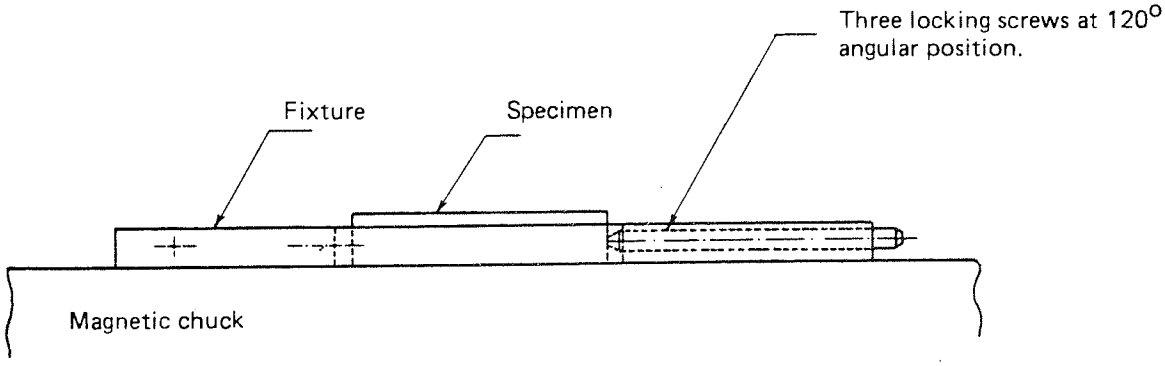

Fig. 23 Schematic view for the method of holding the specimens during machining.

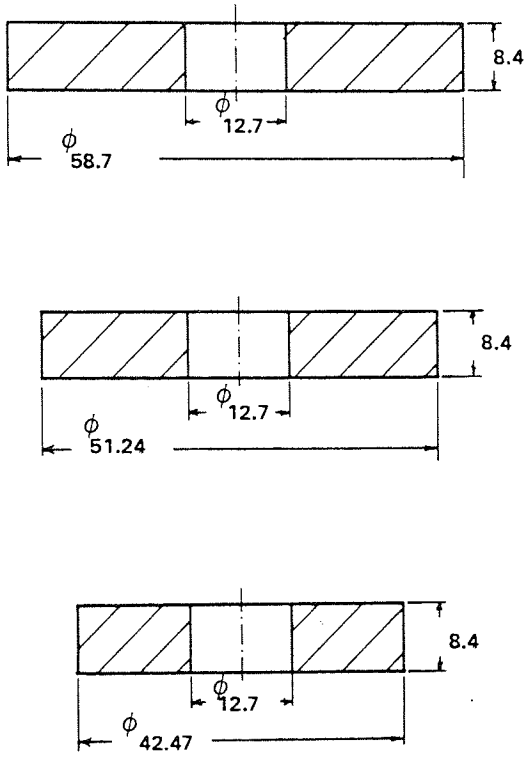

Material: Steel EN8

Tolerances: ± 0.05 mm

Dimensions in mm

Fig. 24 Dimensions of the specimens for the study of the effect of apparent area of contact

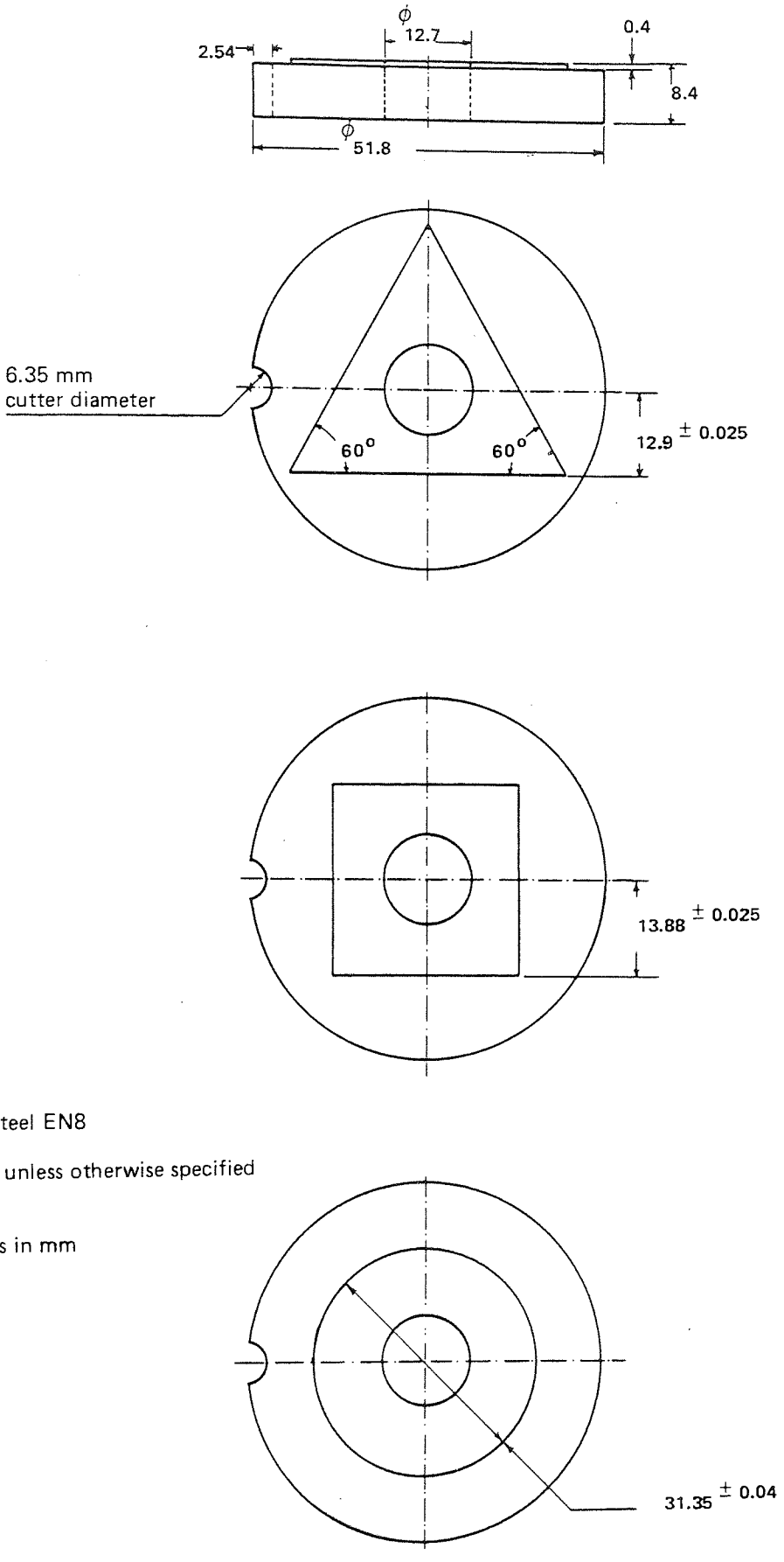

Material: Steel EN8

Tolerances unless otherwise specified
± 0.05

Dimensions in mm

Fig. 25 Specimens for the effect of planform shapes

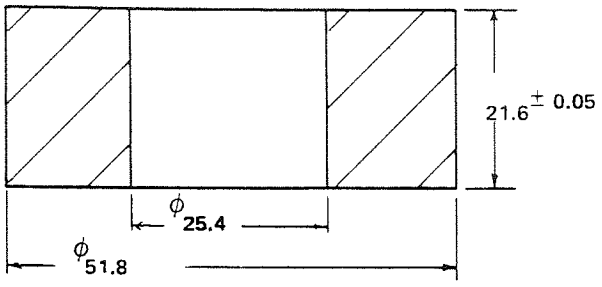

(a) 4 Discs

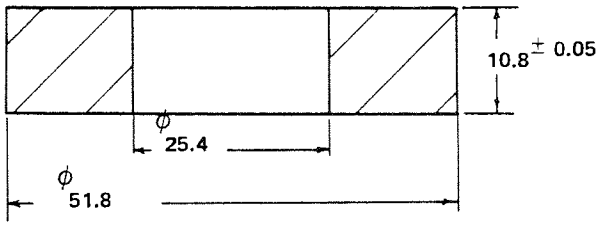

(b) 8 Discs

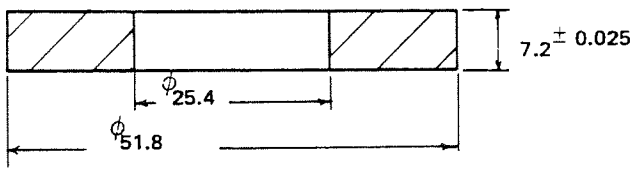

(c) 12 Discs

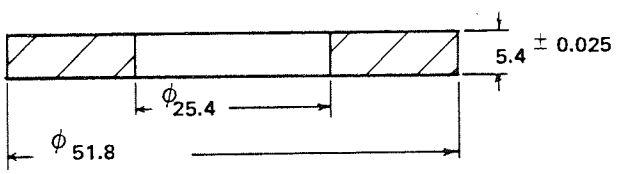

(d) 16 Discs

Material: Steel EN8

Tolerances on diameters ± 0.05 mm

Dimensions in mm

Fig. 26 Dimensions of the specimens for the study of the effect of number of joints

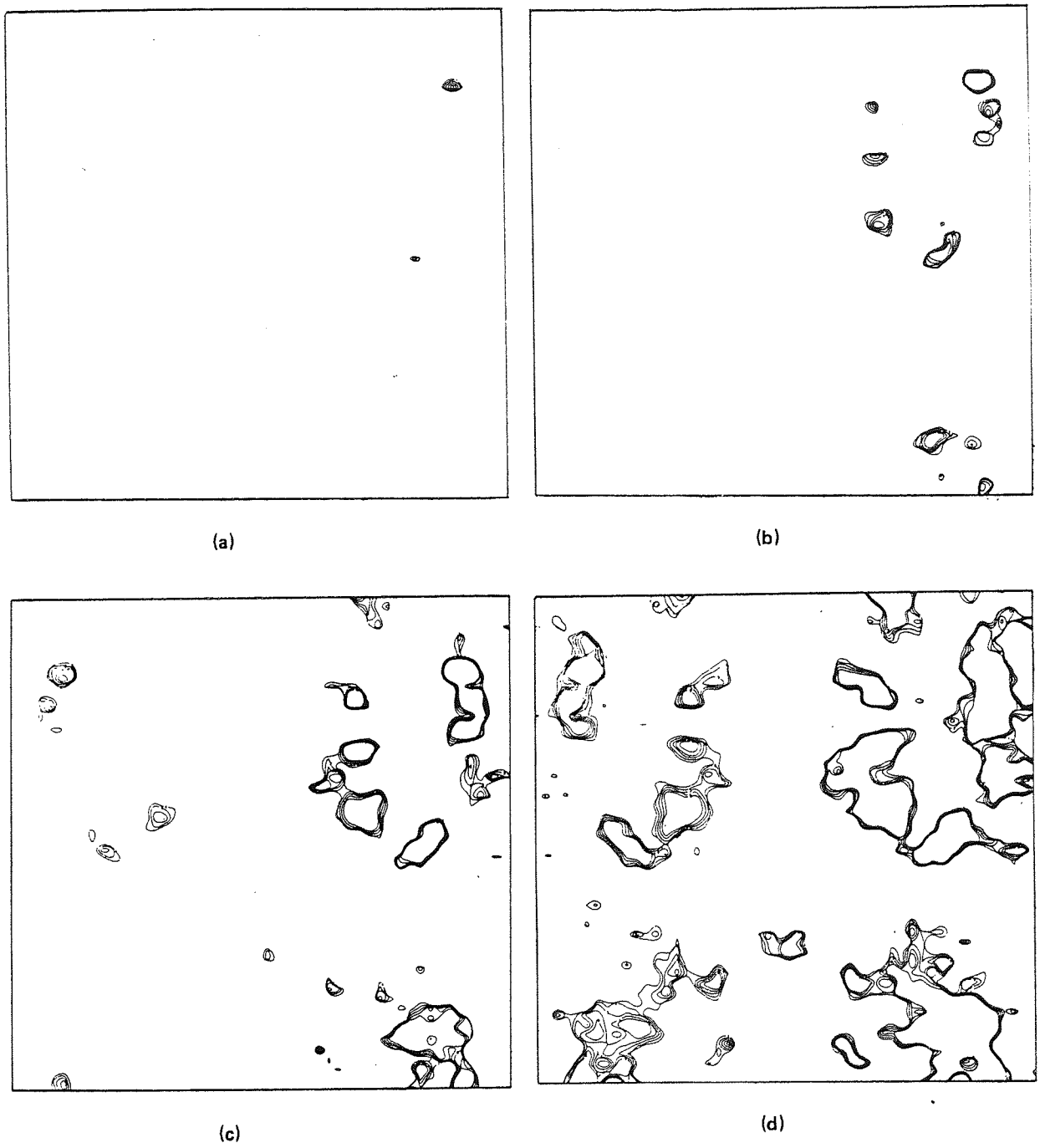

Fig. 27 Simulated plastic contact of shot blasted surfaces.

RMS Roughness 15 μm

Nominal area = 2 x 2 mm, Contours at vertical intervals of 2.5 μm

Mean plane separation: (a) 59 μm; (b) 44 μm; (c) 29 μm; (d) 14 μm
[After Sayles and Thomas (48)]

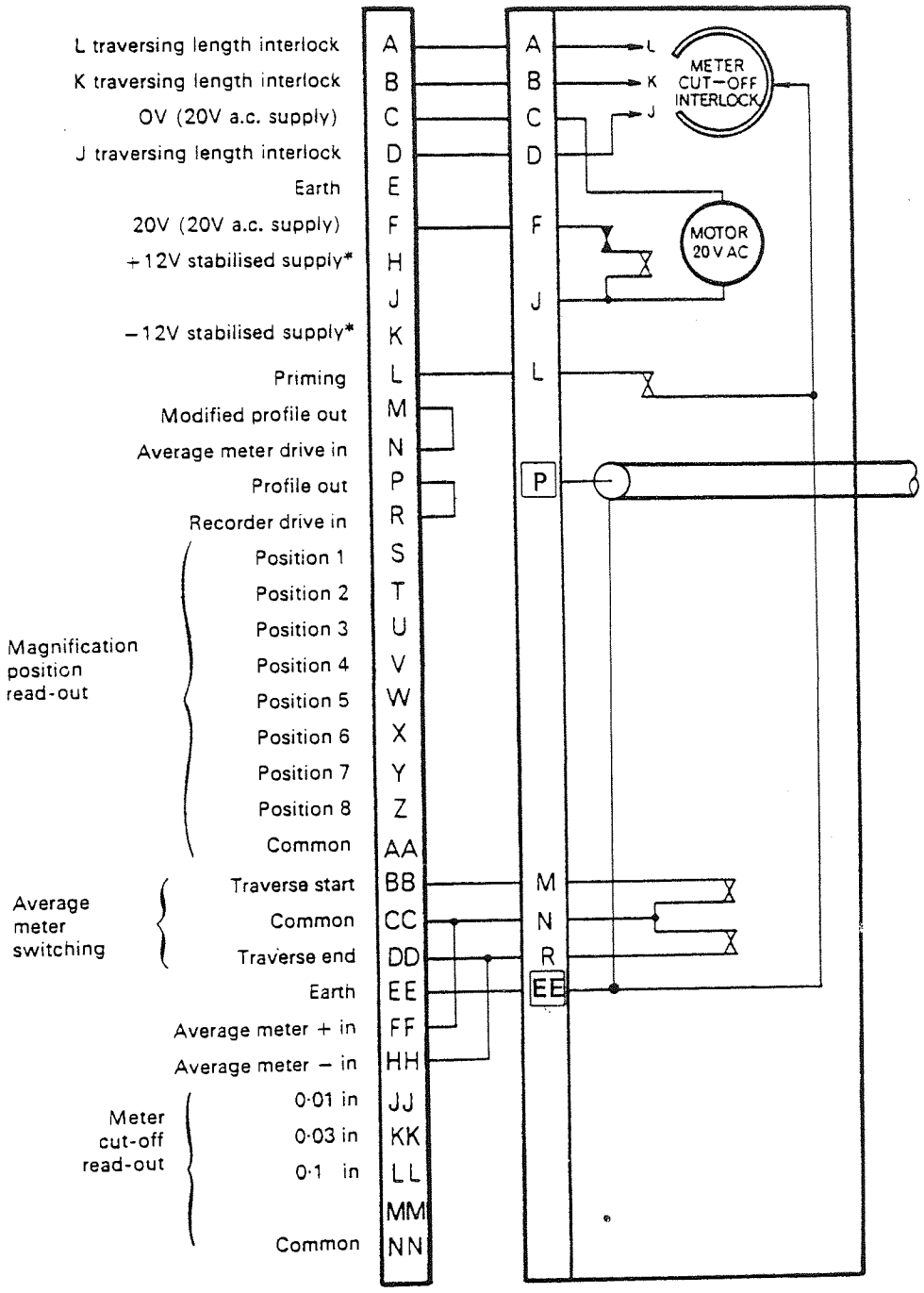

Fig. 28 **Auxiliary socket connections** [49]
(The profile signal is obtained via a co-axial cable fitted to positions P and EE)

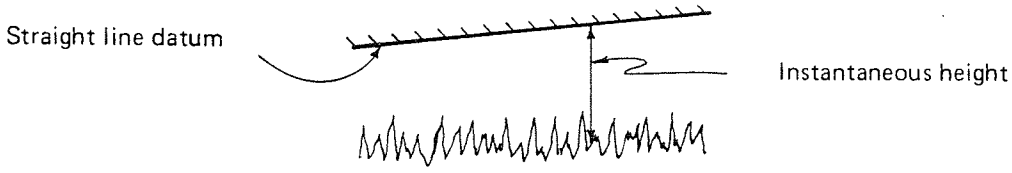

Fig 29 Example of a set-up error in which the straight line datum is used.

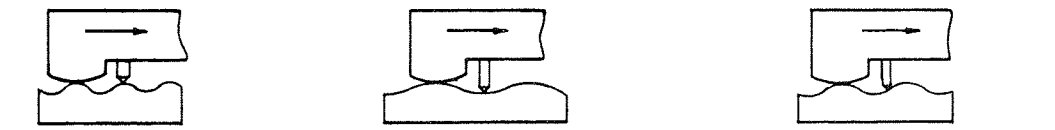

Fig. 30 Skid errors[50]

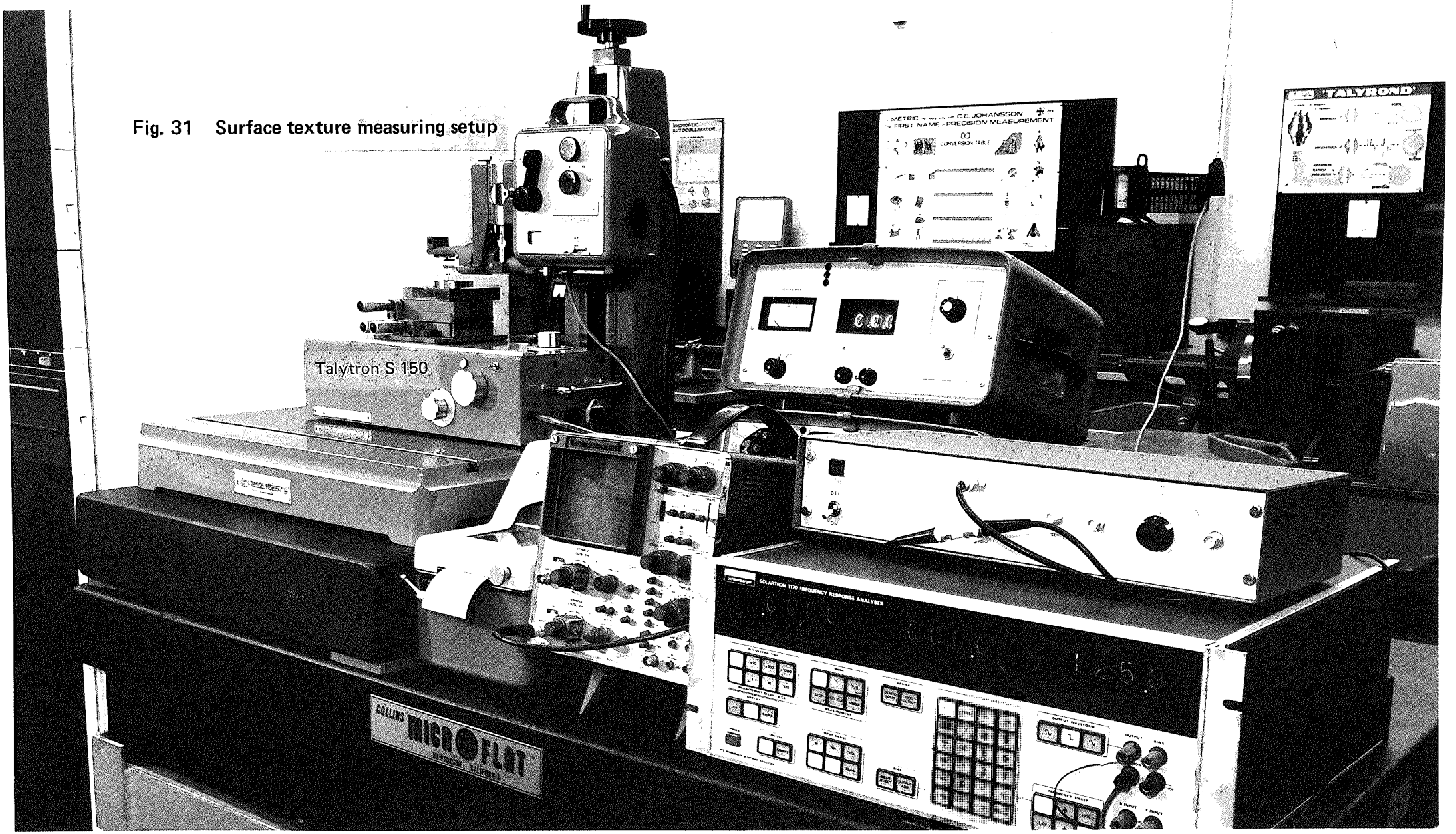

Fig. 31 Surface texture measuring setup

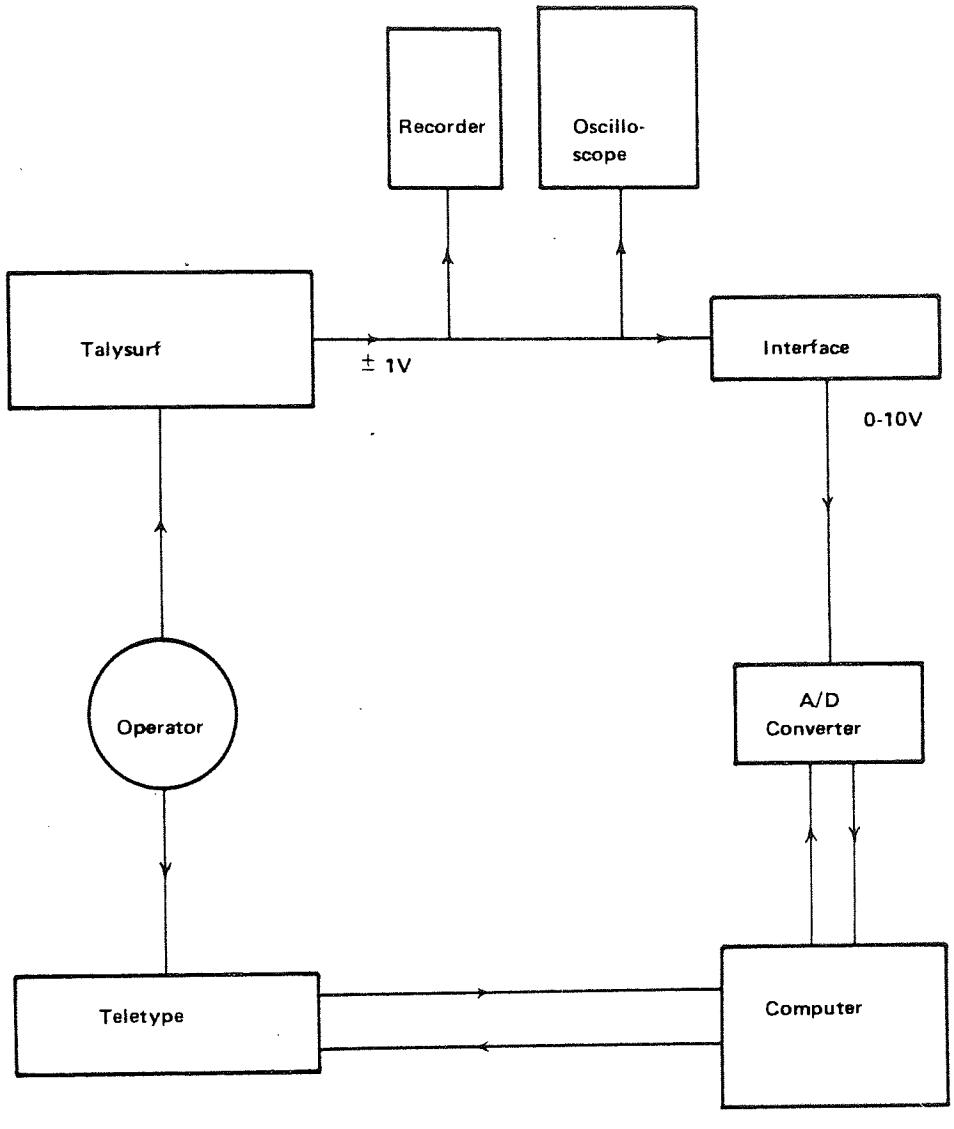

Fig. 32 Block diagram of the surface measuring system.
(the arrows indicate the direction of flow of information)

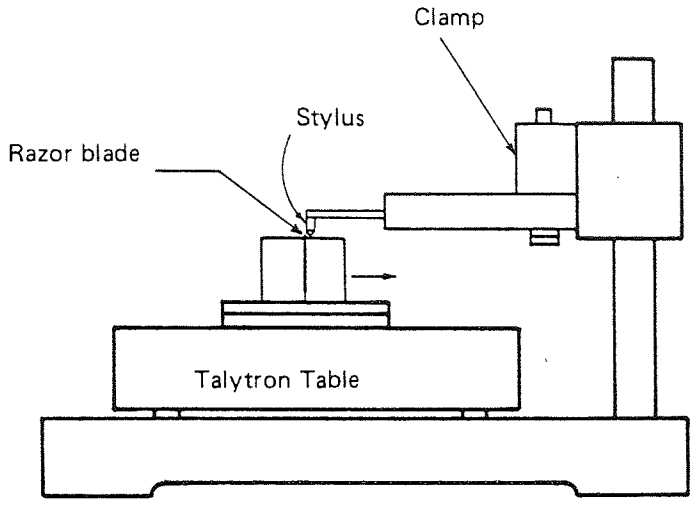

Fig. 33.a Setup for checking the stylus dimensions

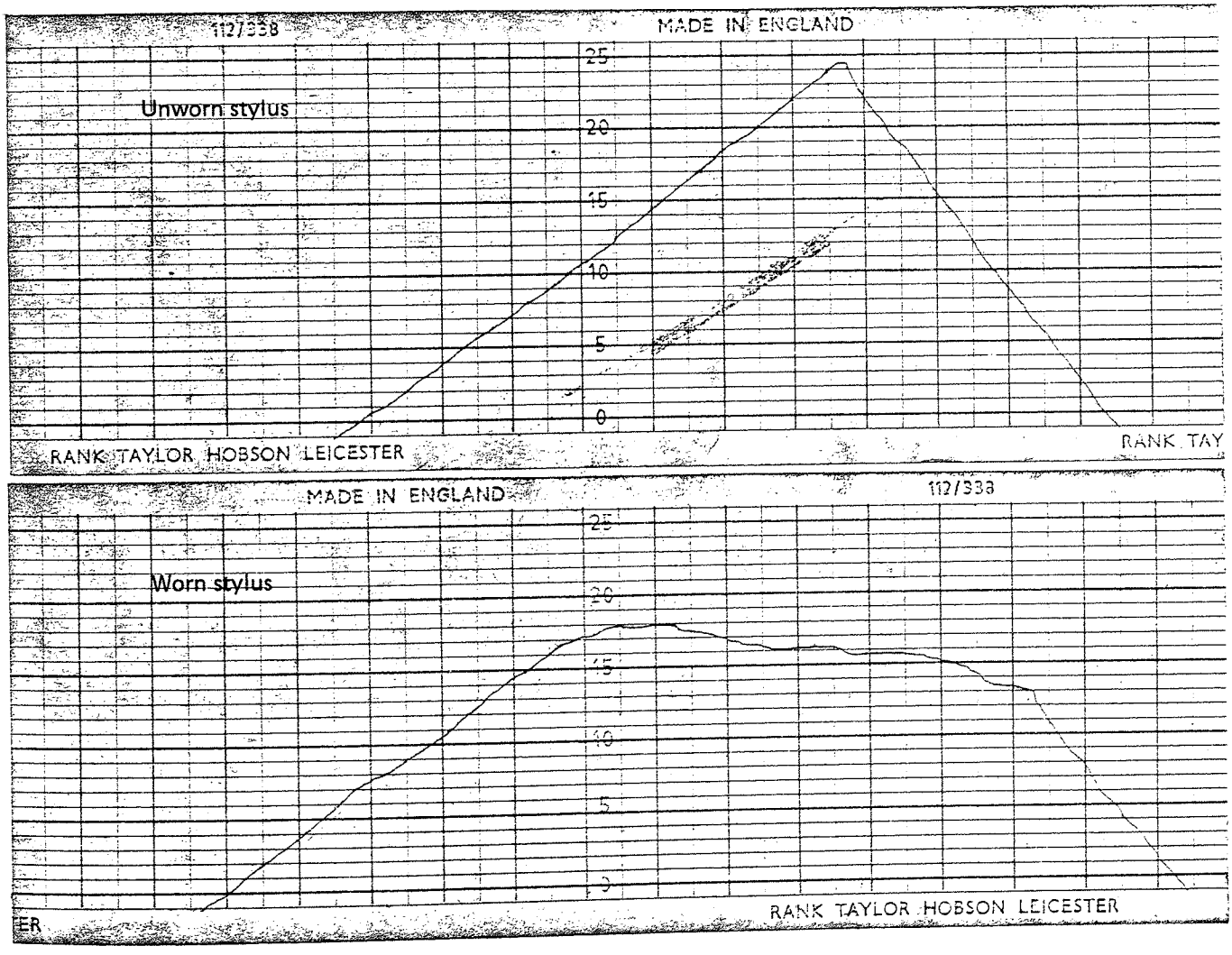

Fig. 33.b Profile records for stylii shapes
horizontal magnification = vertical magnification = 1,000

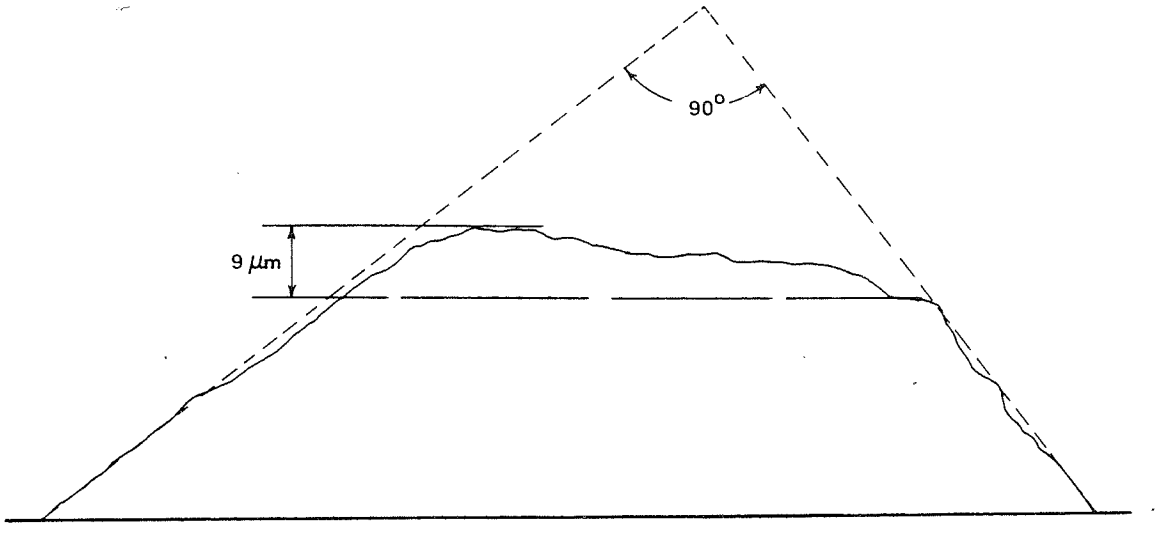

(a) Worn Talysurf stylus
(The dotted line is to illustrate the extent of wear)

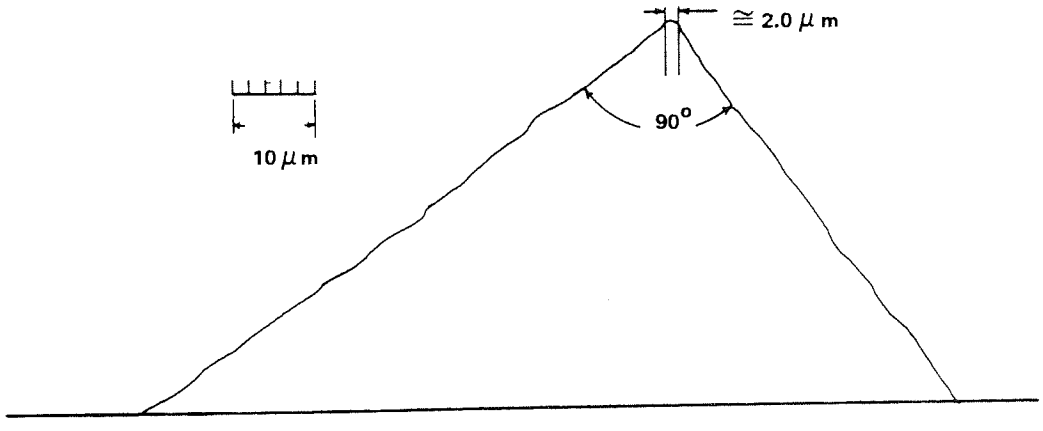

(b) Unworn stylus
(This is the profile of the stylus used for roughness measurements carried out in this work)

Fig. 34 Replica of the stylii profiles shown in Fig. 33.b.

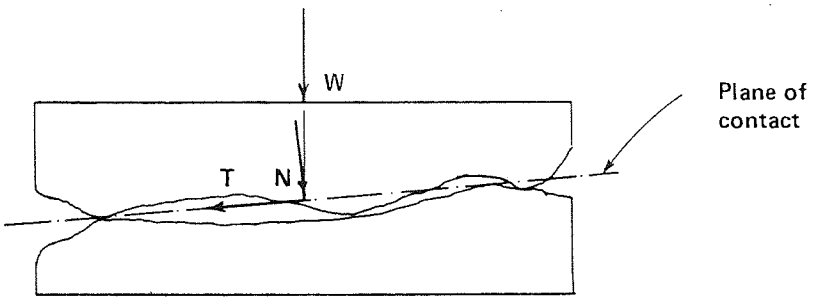

Fig. 35 The effect of form errors on the state of loading on the joint
(N & T are the normal and tangential components of the applied load W)

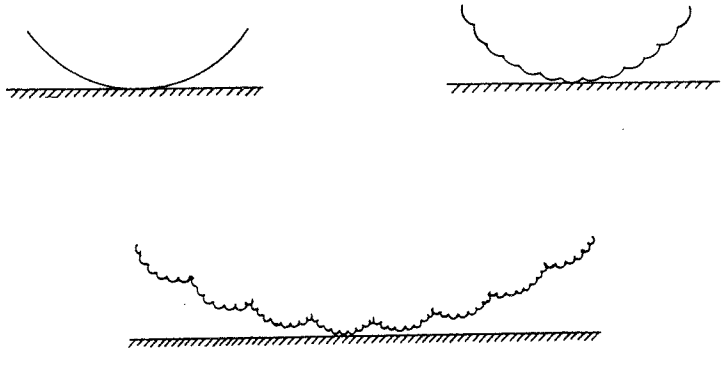

Fig. 36 Archard's representation of surface roughness[64]

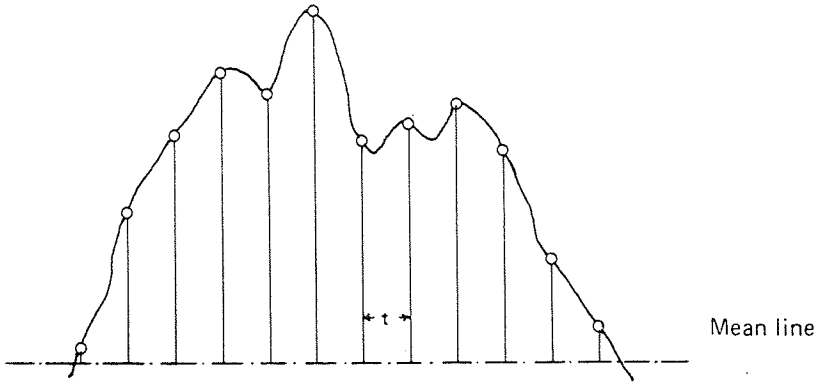

(a) Sampling at interval 't':
3 points analysis counts 4 peaks

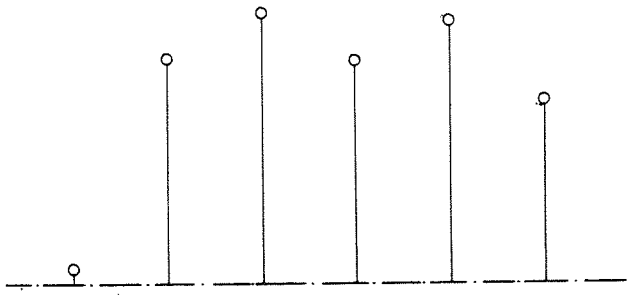

(b) Sampling at interval '2t':
3 points analysis counts 2 peaks

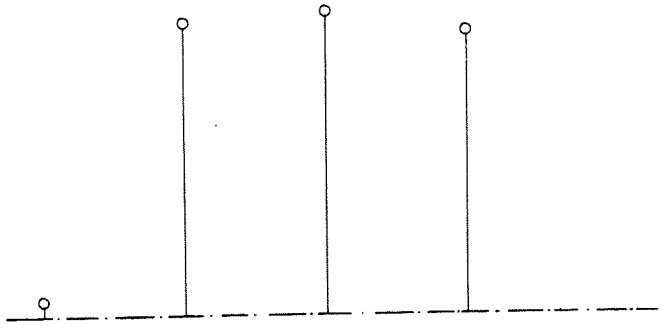

(c) Sampling at interval '3t':
3 points analysis counts 1 peak

Fig. 37 Which sampling interval is suitable for the definition of peaks?

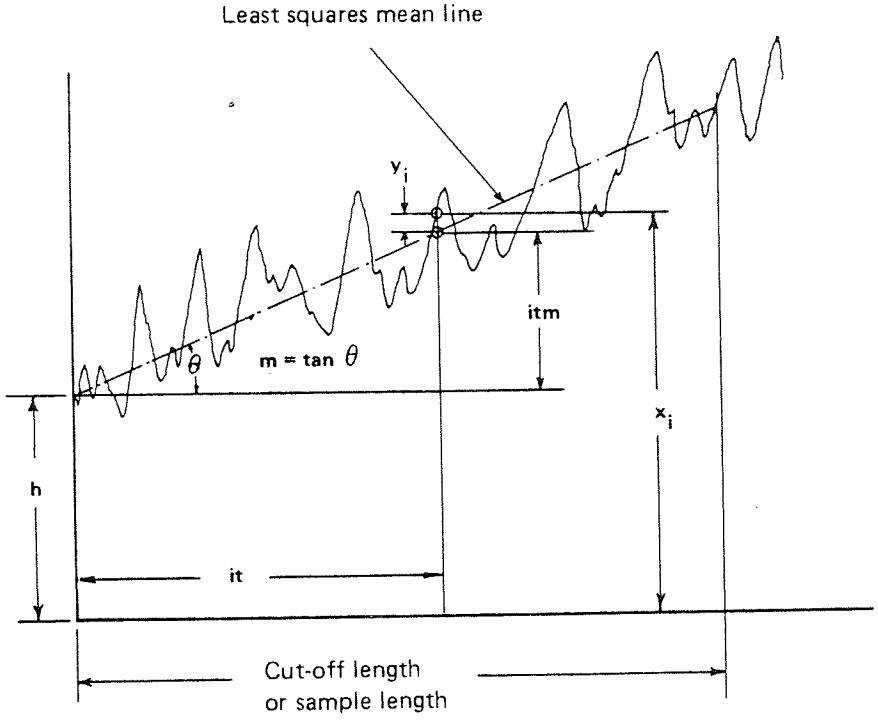

Fig. 38 Fitting a least squares mean line.

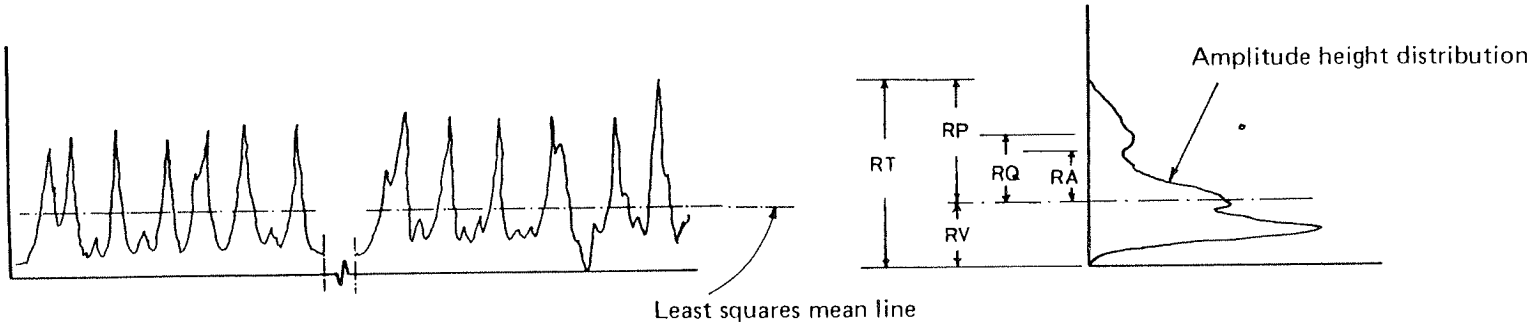

a. Roughness profile

b. Amplitude sensitive parameters

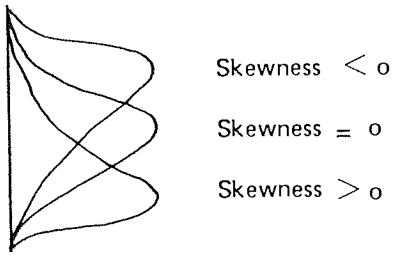

c. Skewness of the distribution

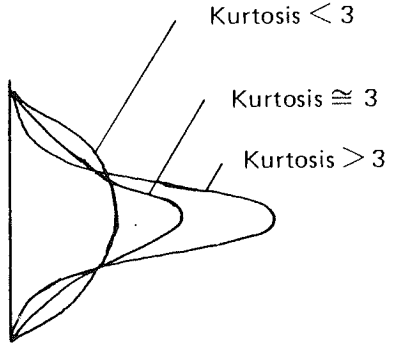

d. Kurtosis of the distribution

Fig. 39 Characterisation of Roughness using amplitude height distribution.

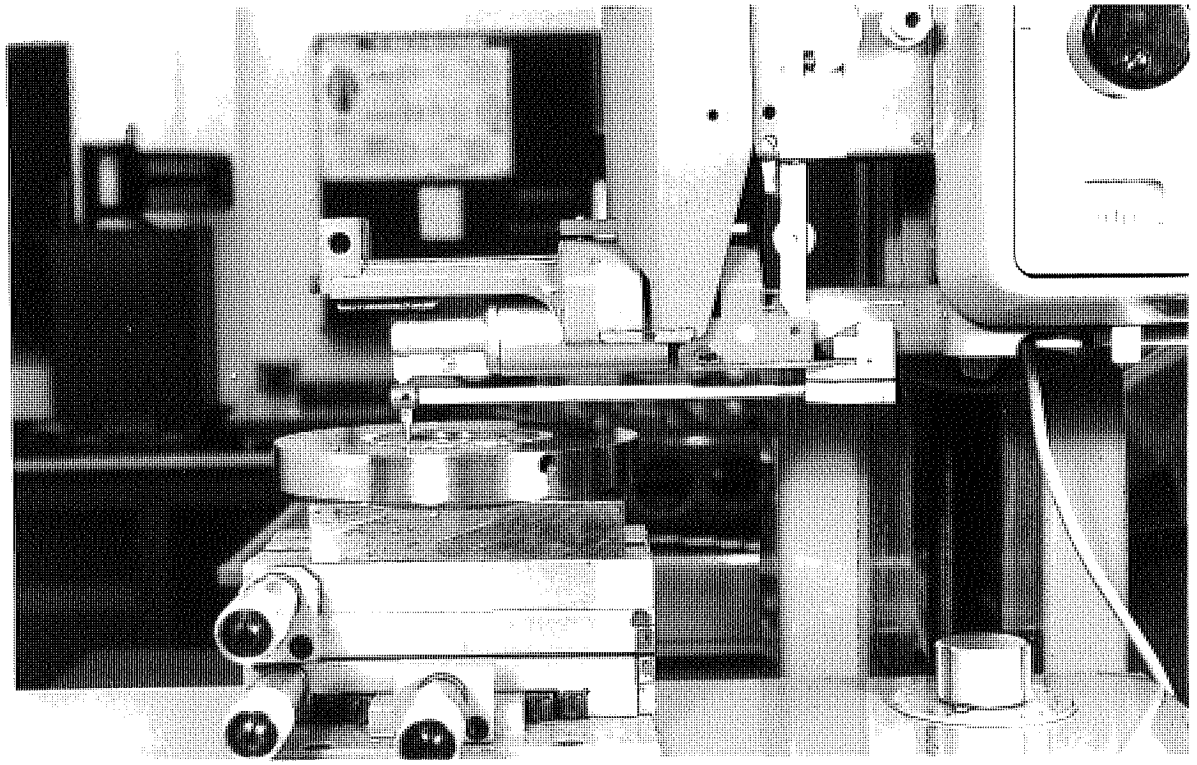

Fig. 40 The measurement of waviness

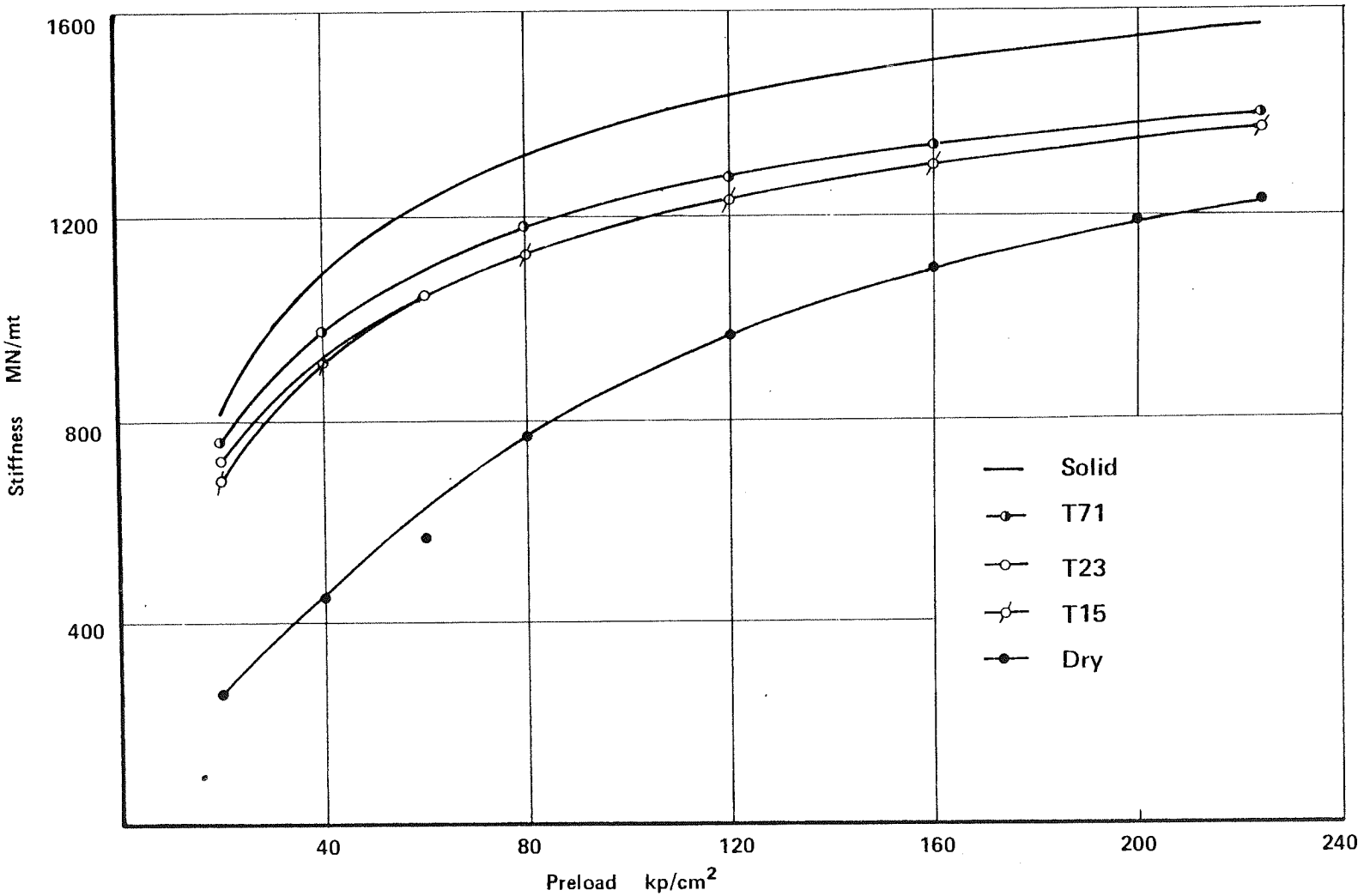

Fig. 41 Dynamic stiffness of dry and lubricated jointed column ML1 (Milled)

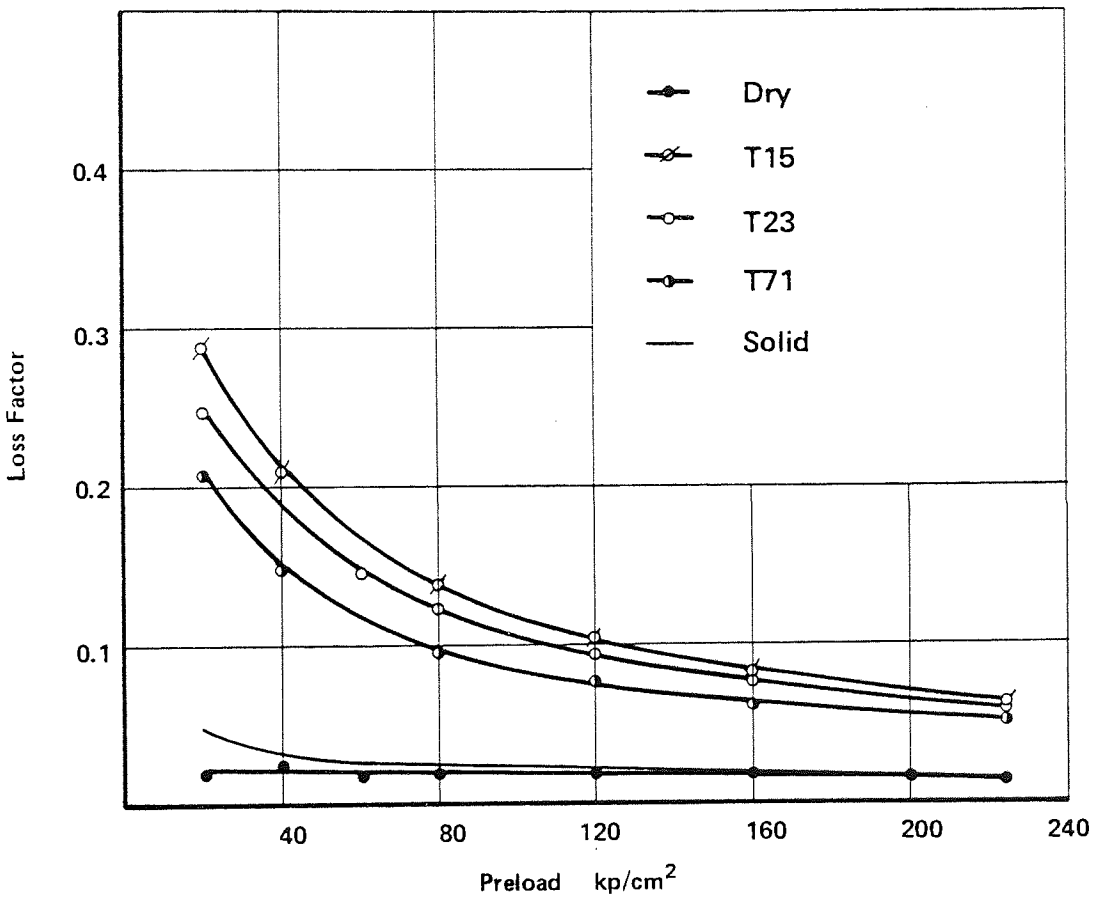

Fig. 42 Loss factor of dry and lubricated jointed column ML1

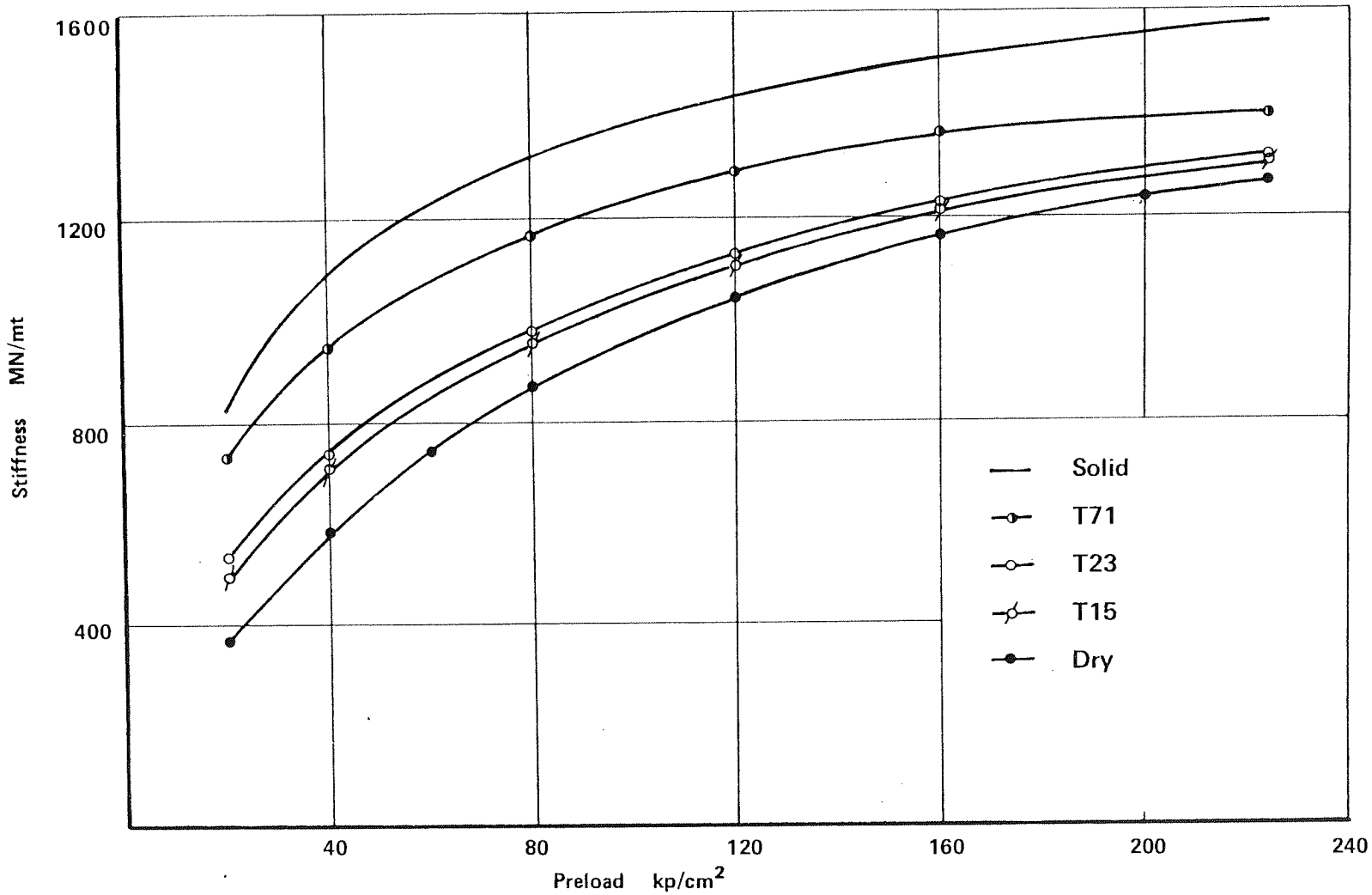

Fig. 43 Dynamic stiffness of dry and lubricated jointed column ML2

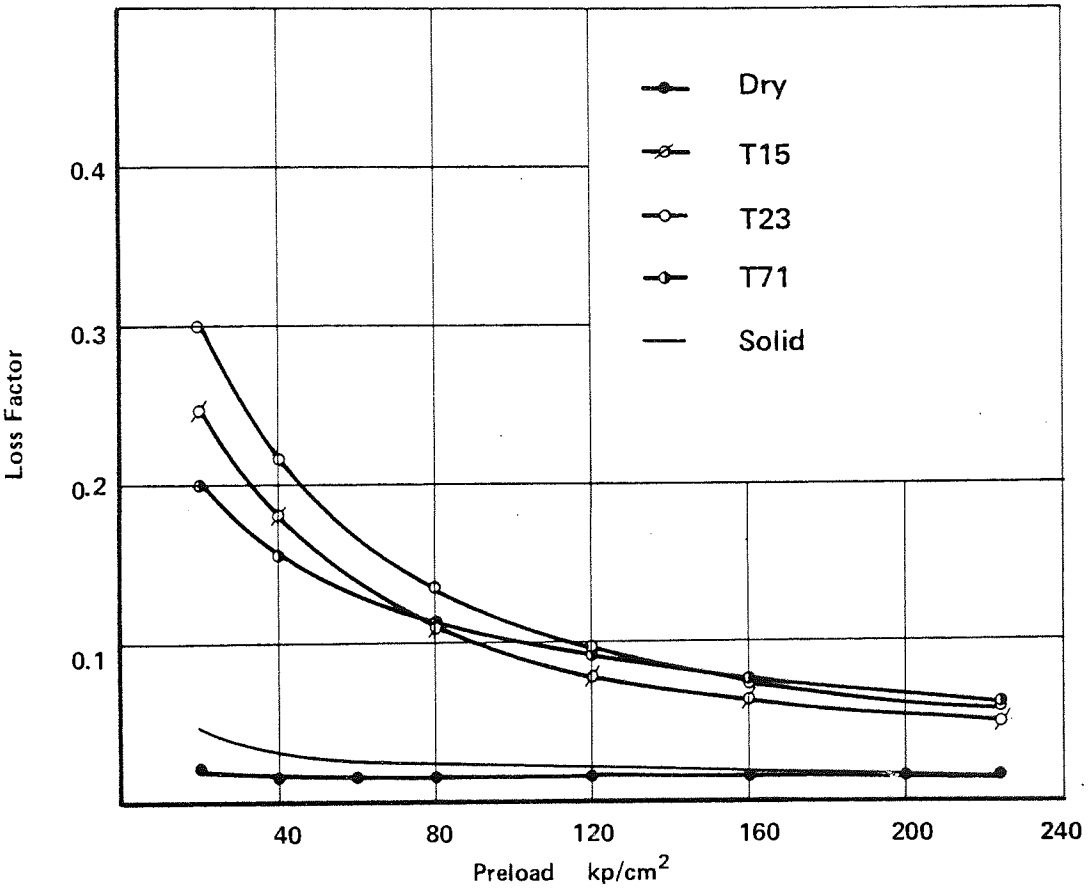

Fig. 44 Loss factor of dry and lubricated jointed column ML2

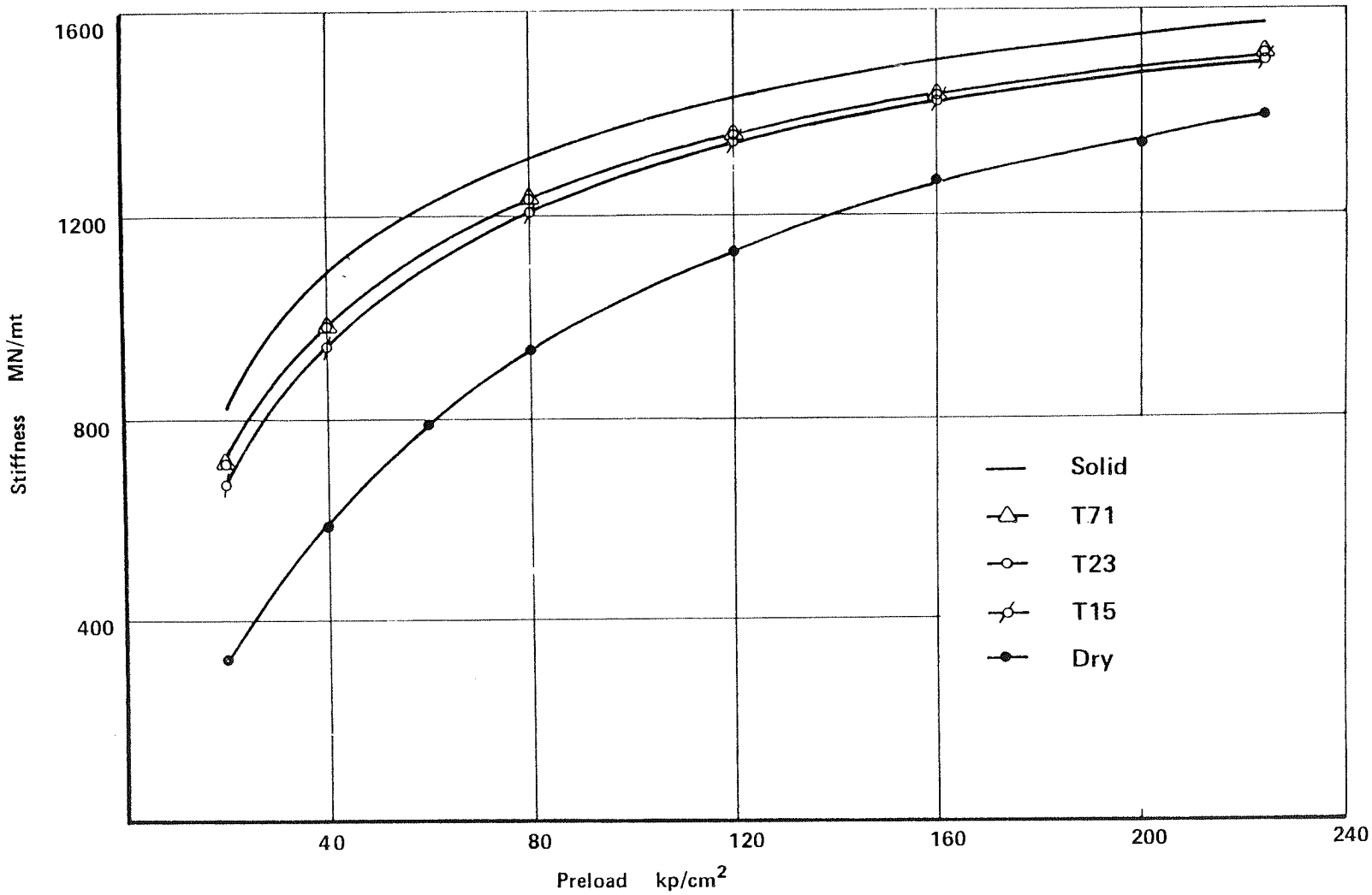

Fig. 45 Dynamic stiffness of dry and lubricated jointed column ML3

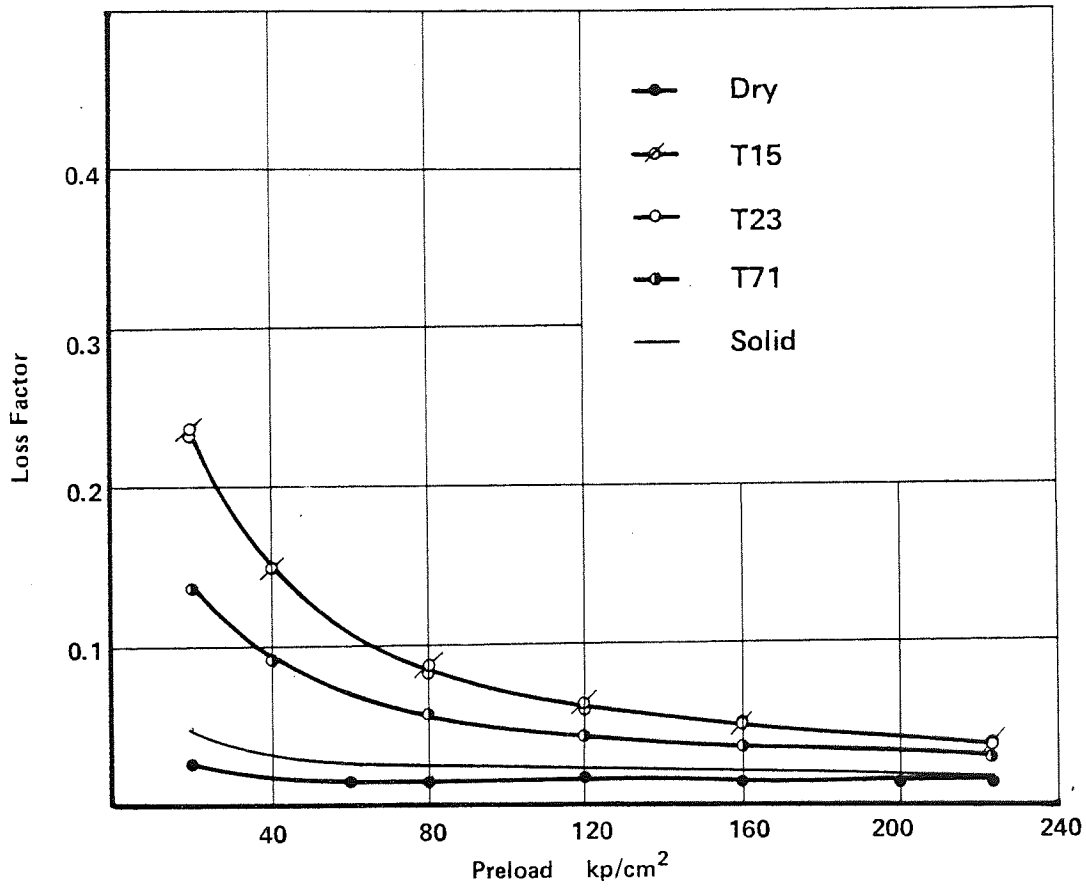

Fig. 46 Loss factor of dry and lubricated jointed column ML3

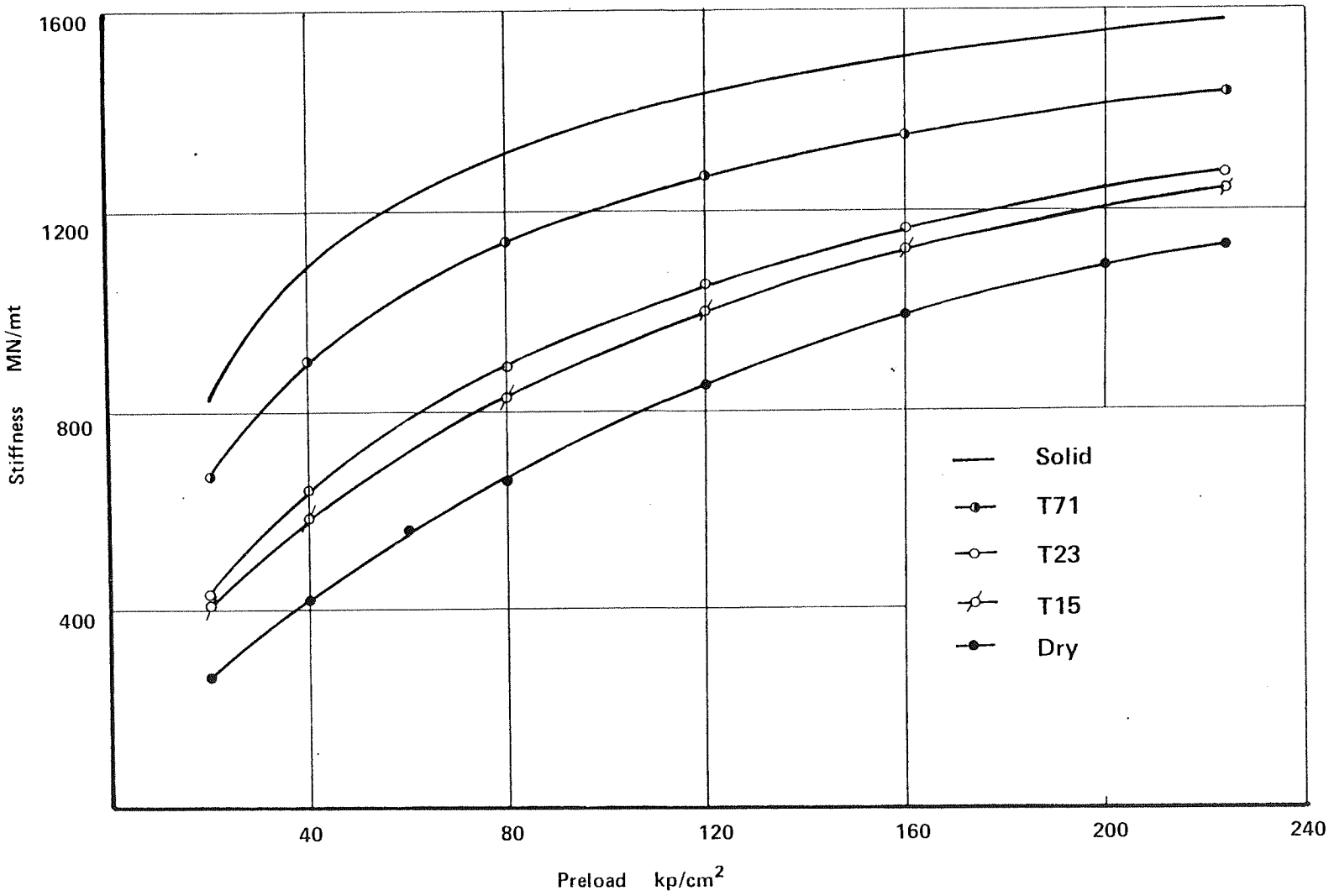

Fig. 47 Dynamic stiffness of dry and lubricated jointed column ML4

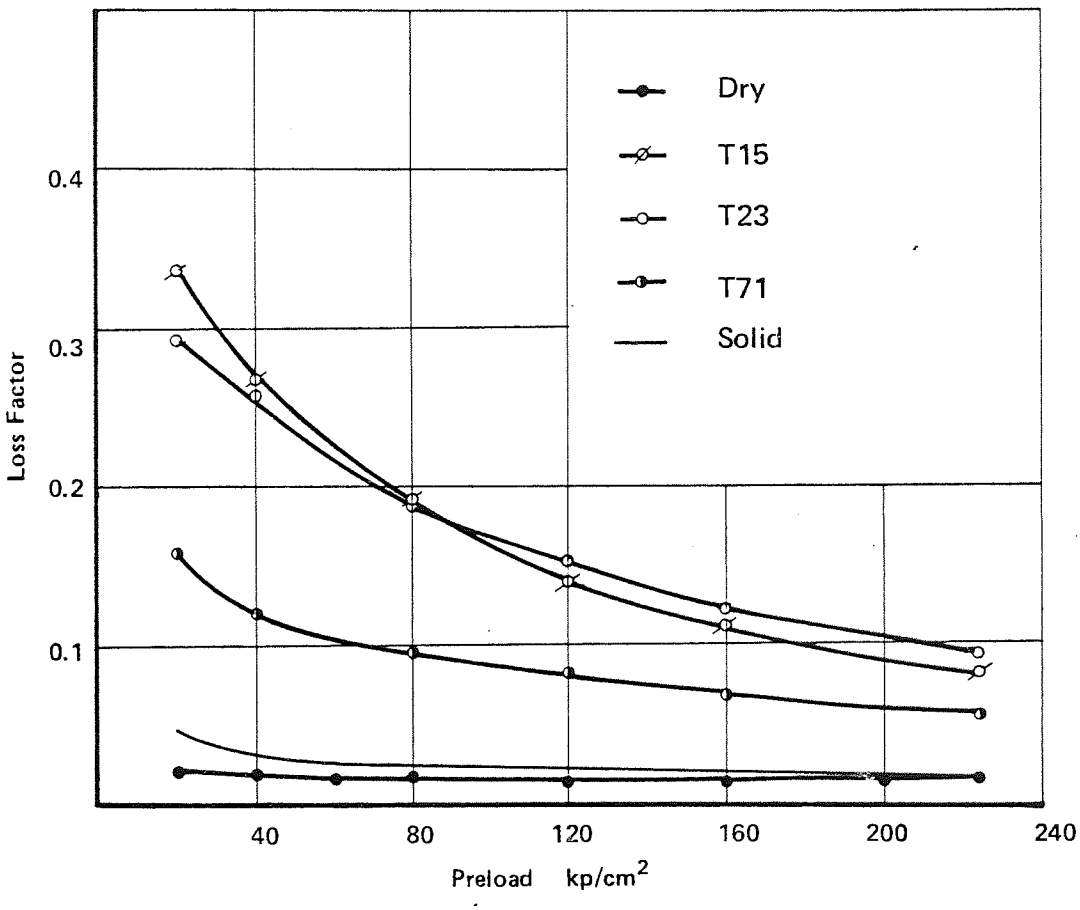

Fig. 48 Loss factor of dry and lubricated jointed column ML4

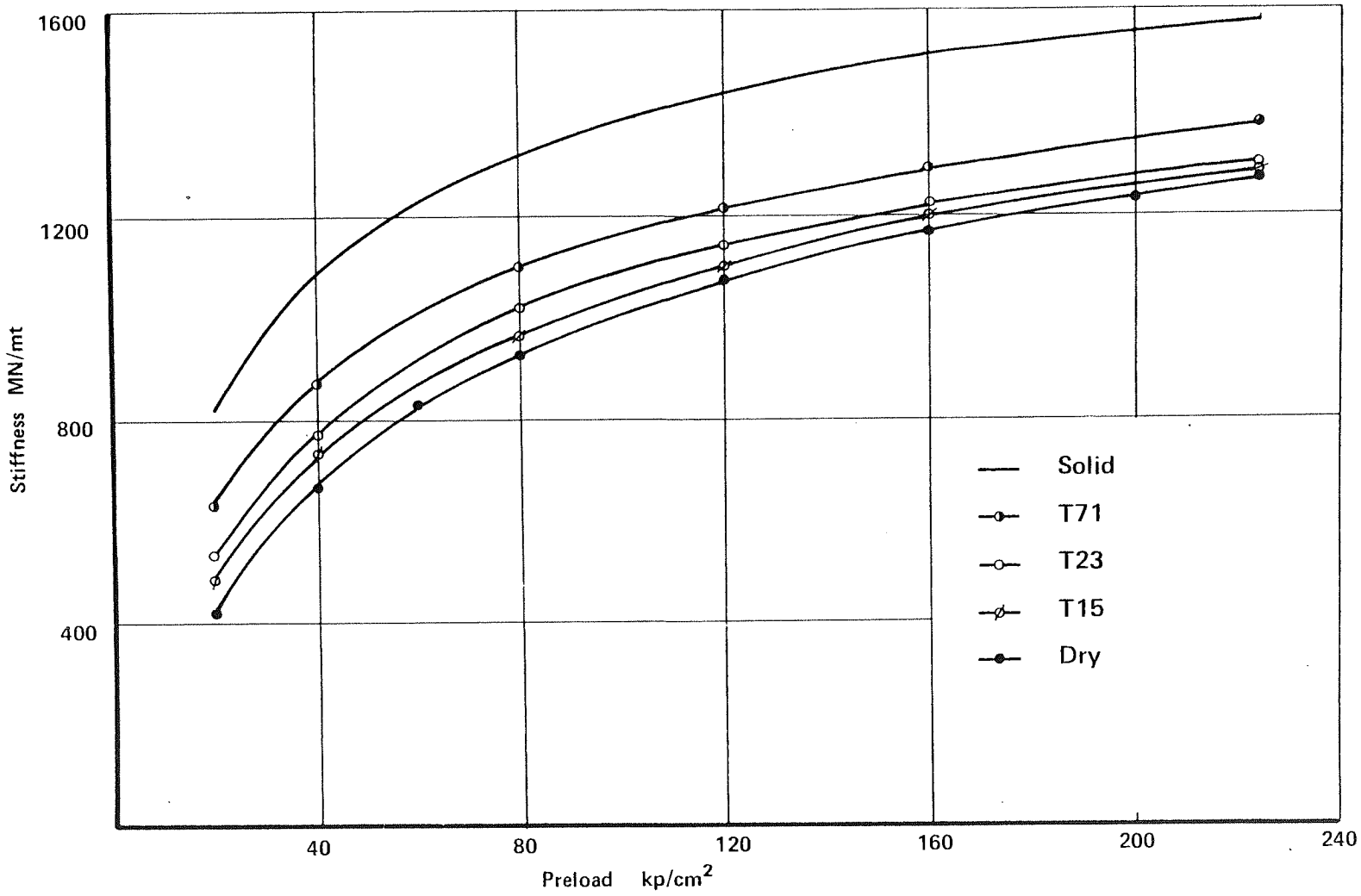

Fig. 49 Dynamic stiffness of dry and lubricated jointed column SH1 (shaped)

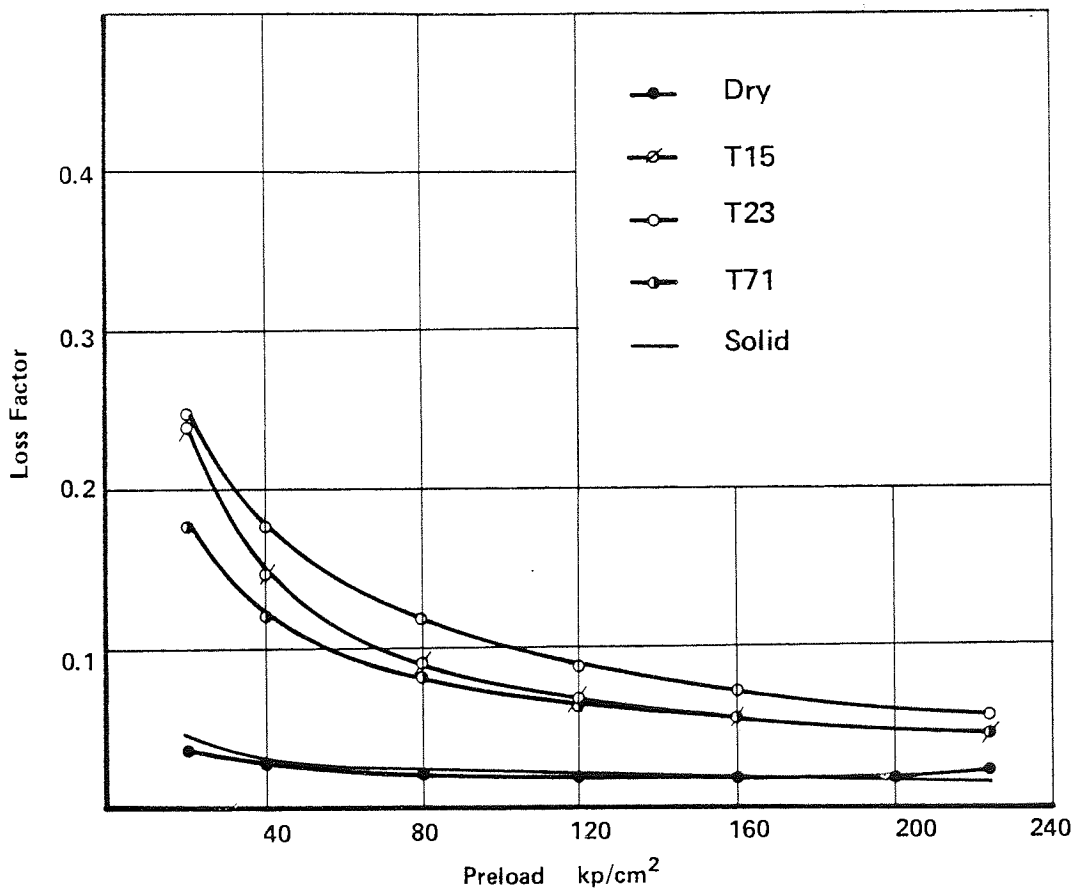

Fig. 50 Loss factor of dry and lubricated jointed column SH1

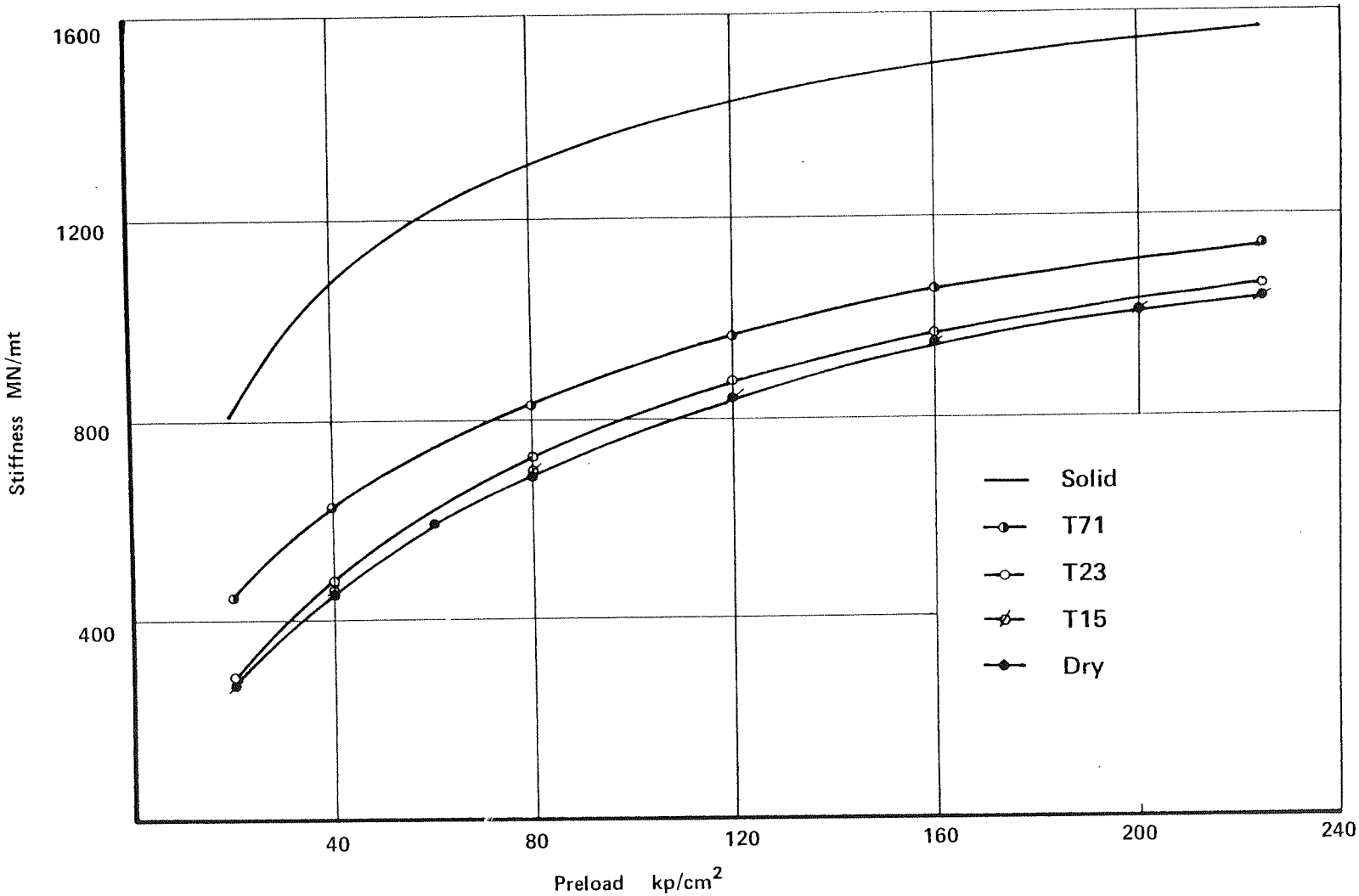

Fig. 51 Dynamic stiffness of dry and lubricated jointed column SH2

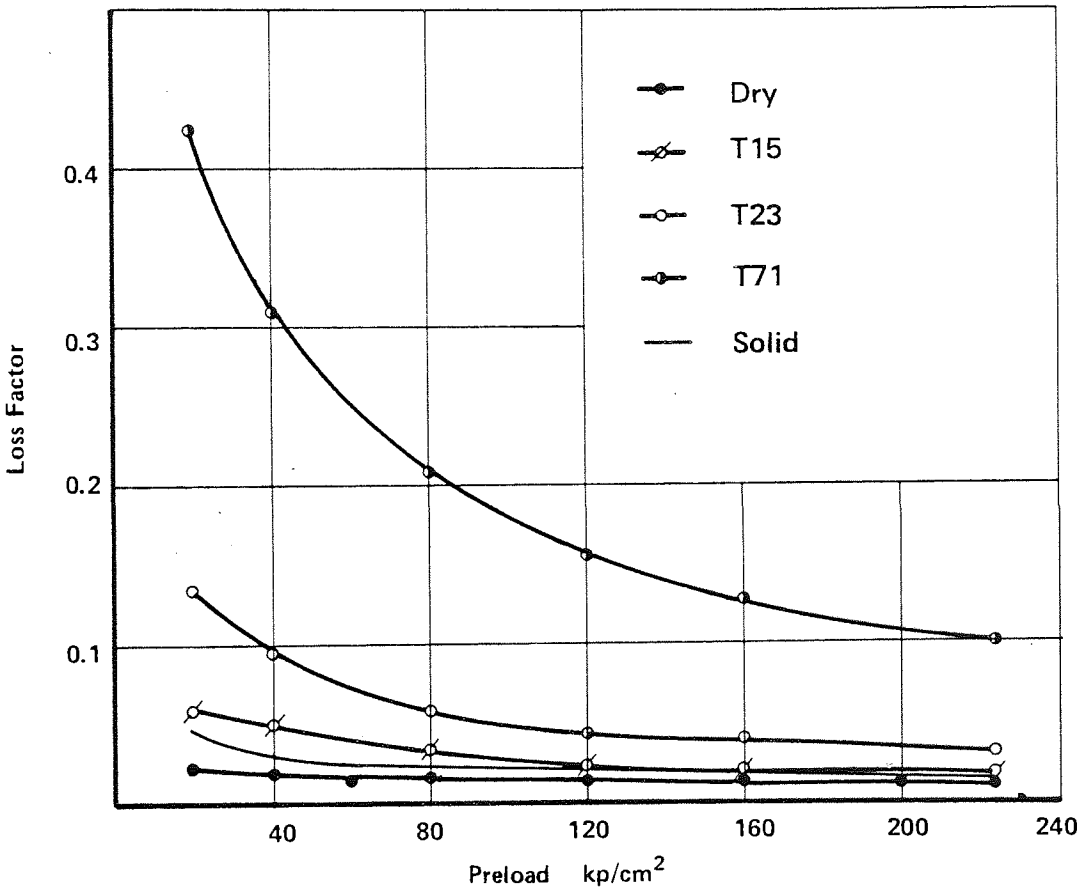

Fig. 52 Loss factor of dry and lubricated jointed column SH2

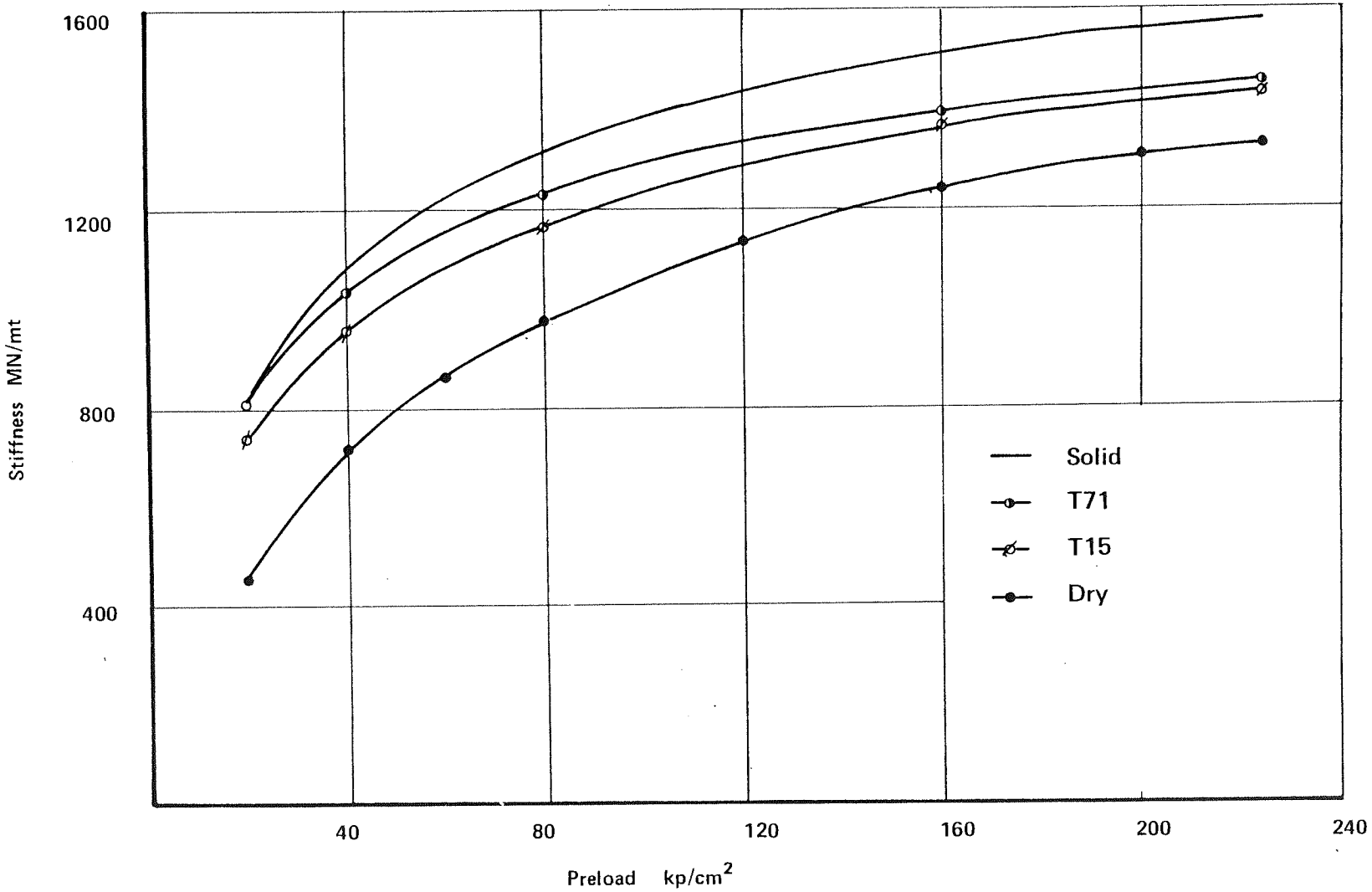

Fig. 53 Dynamic stiffness of dry and lubricated jointed column SH3

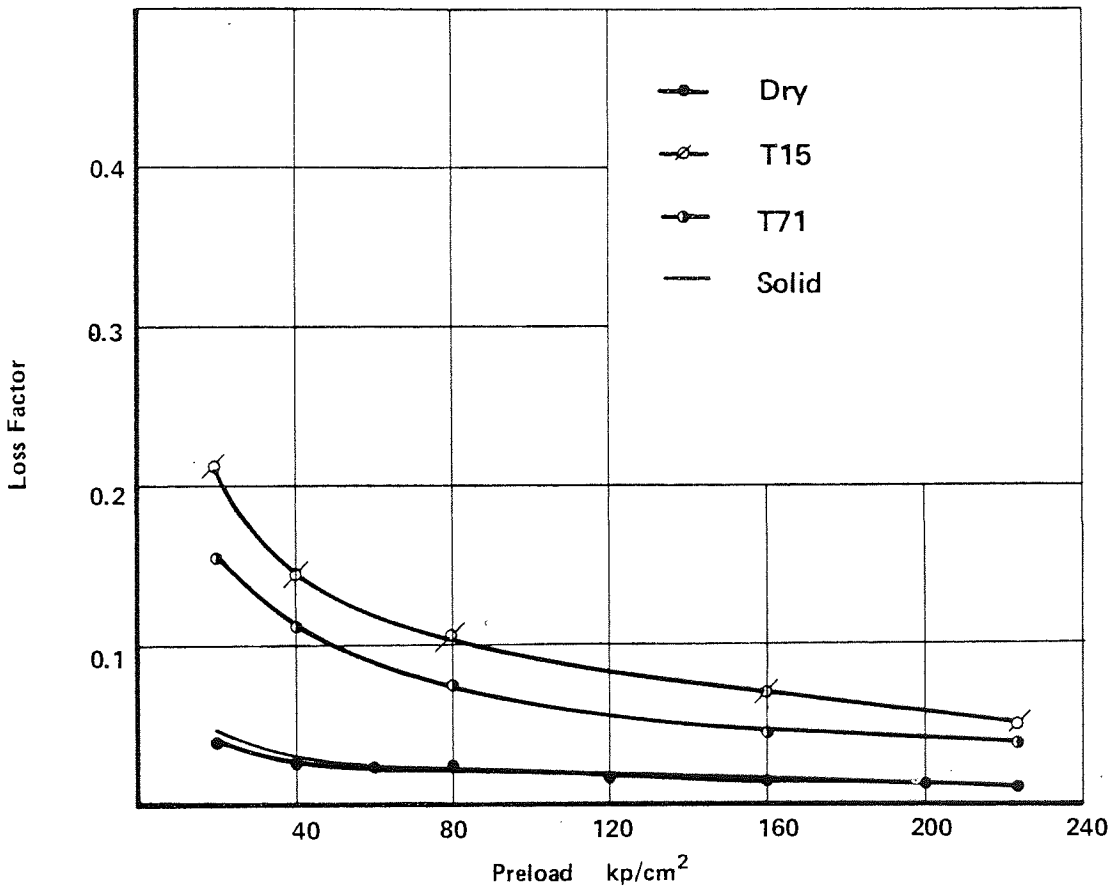

Fig. 54 Loss factor of dry and lubricated jointed column SH3

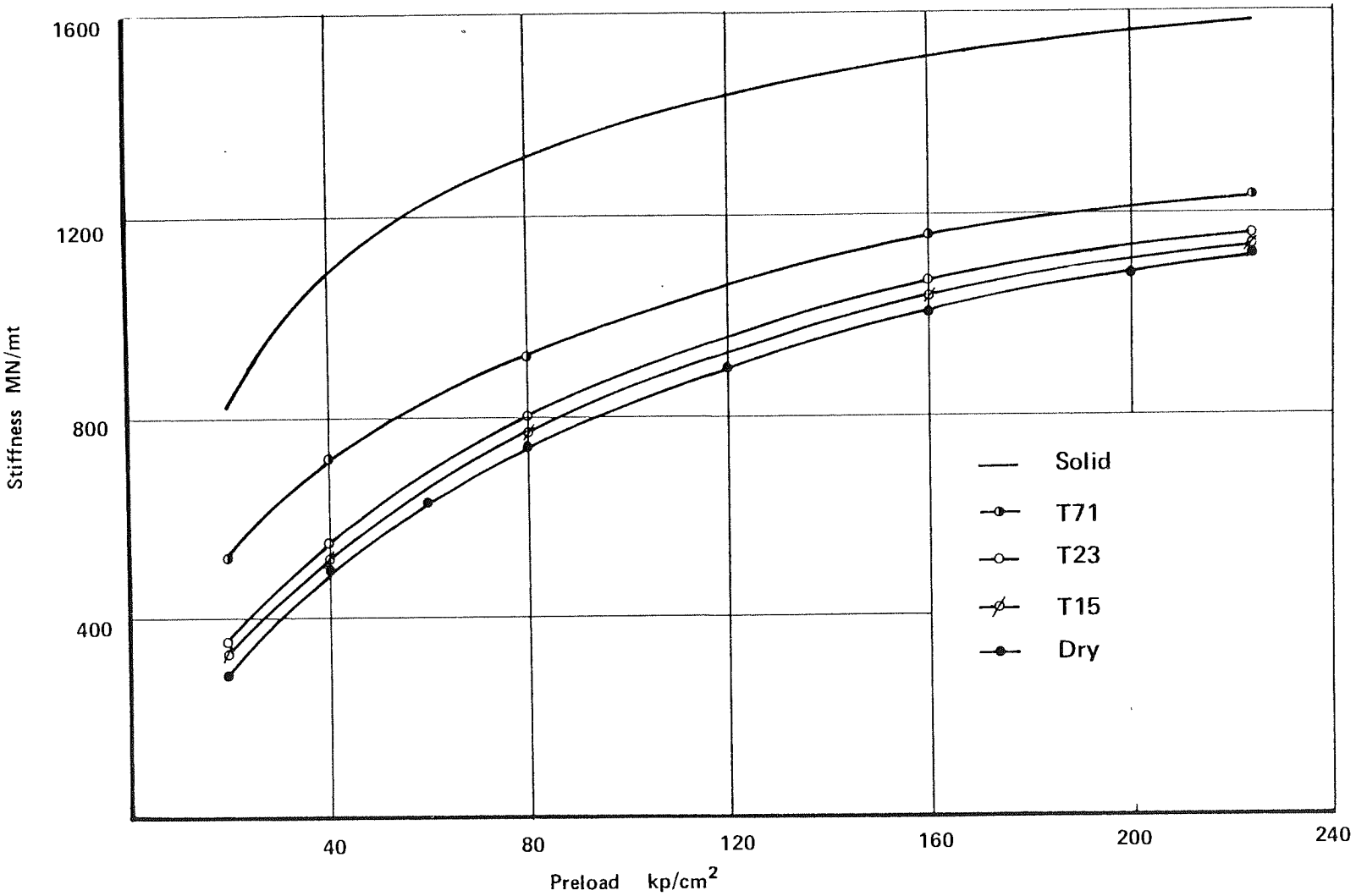

Fig. 55 Dynamic stiffness of dry and lubricated jointed column SH4

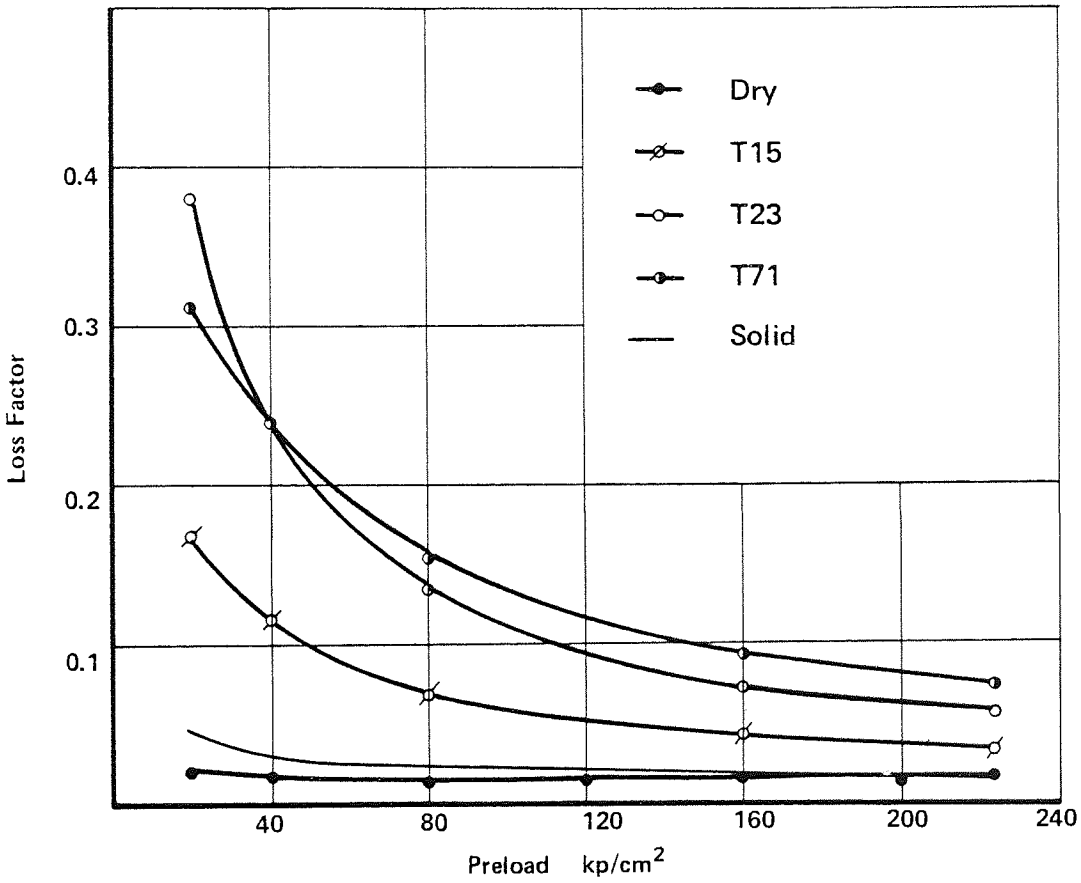

Fig. 56 Loss factor of dry and lubricated jointed column SH4

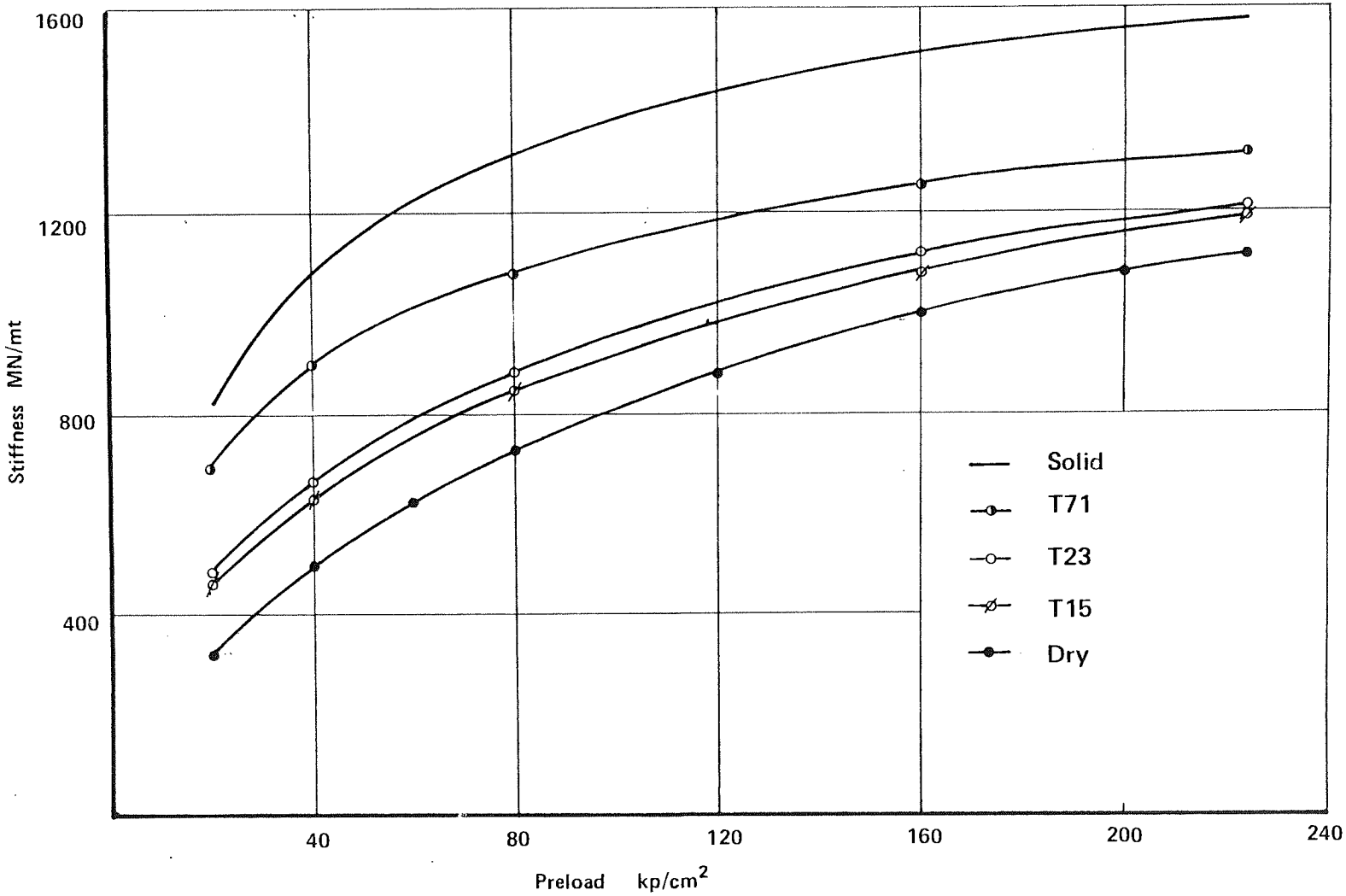

Fig. 57 Dynamic stiffness of dry and lubricated jointed column SH5

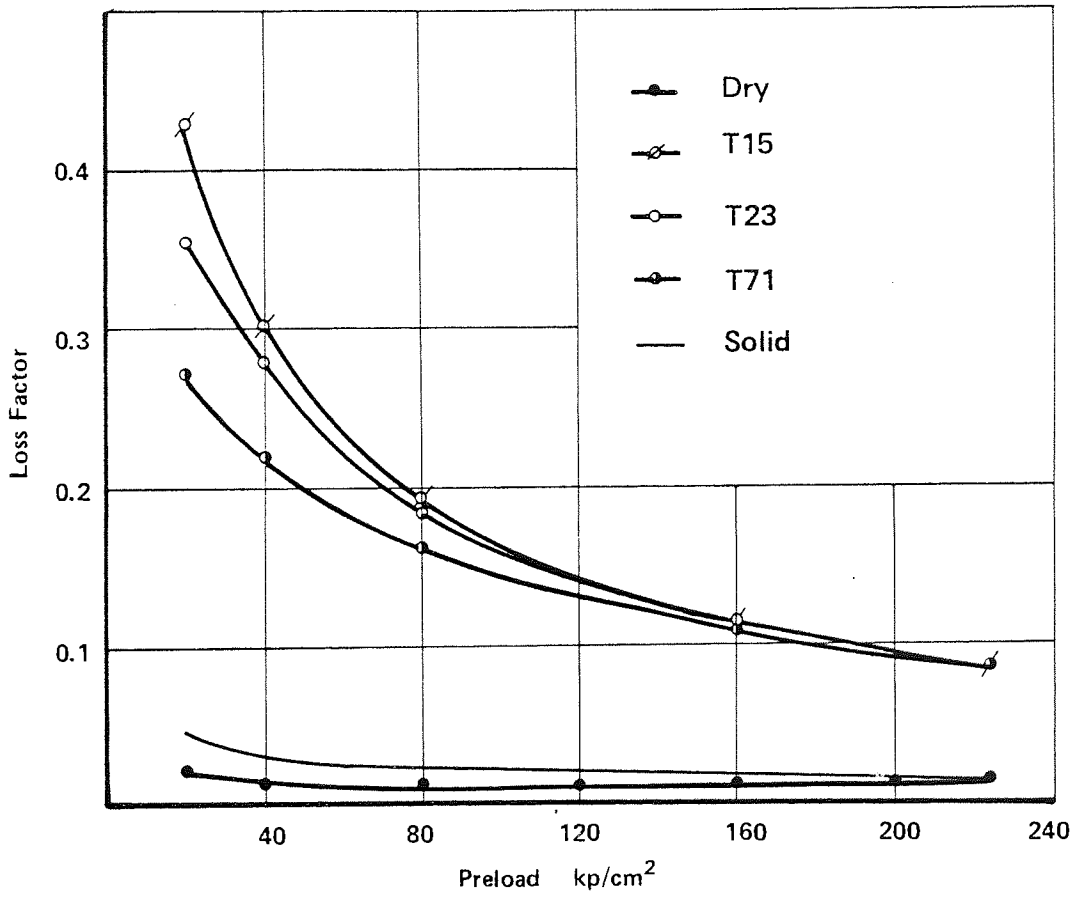

Fig. 58 Loss factor of dry and lubricated jointed column SH5

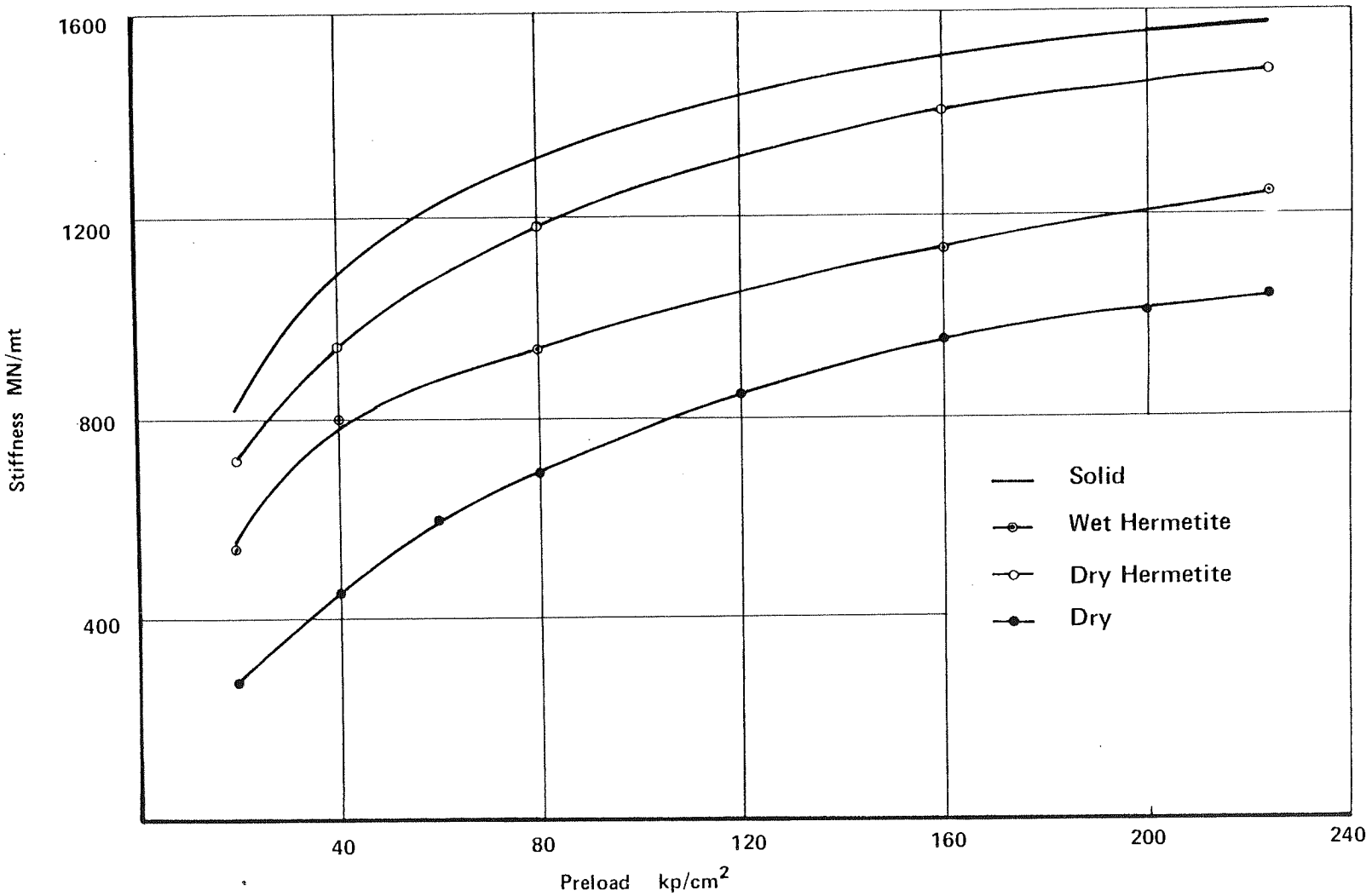

Fig. 59 Dynamic stiffness of SH2 contaminated with Hermetite

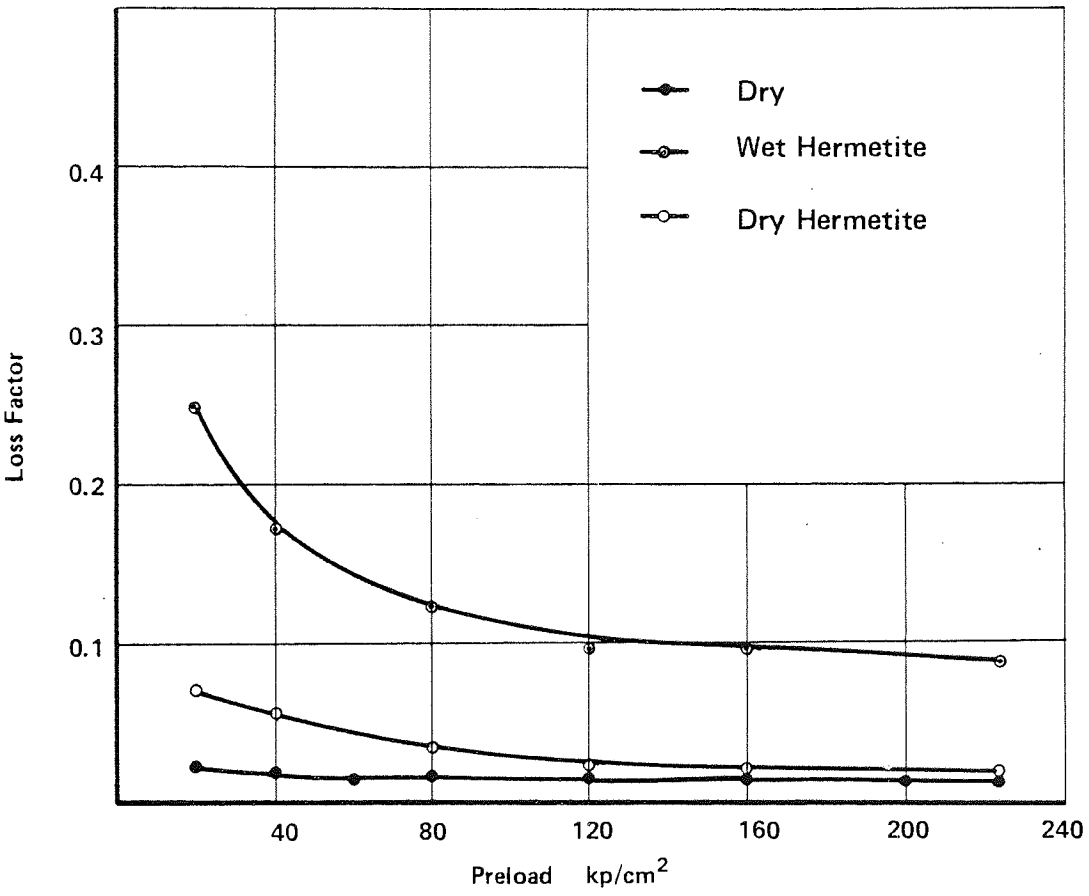

Fig. 60 Loss factor of SH2 contaminated with Hermetite

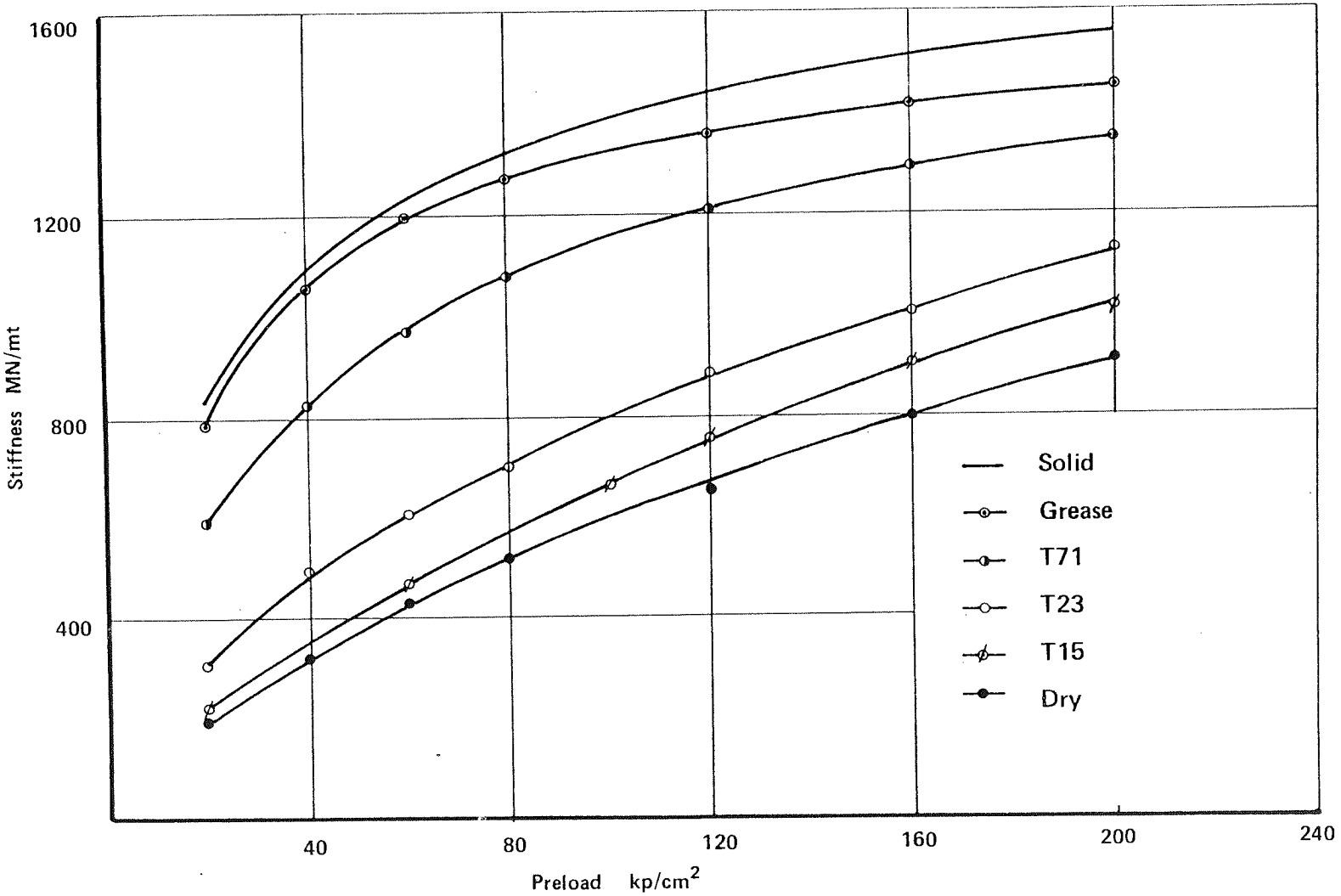

Fig. 61 Dynamic stiffness of dry and lubricated jointed column TN1

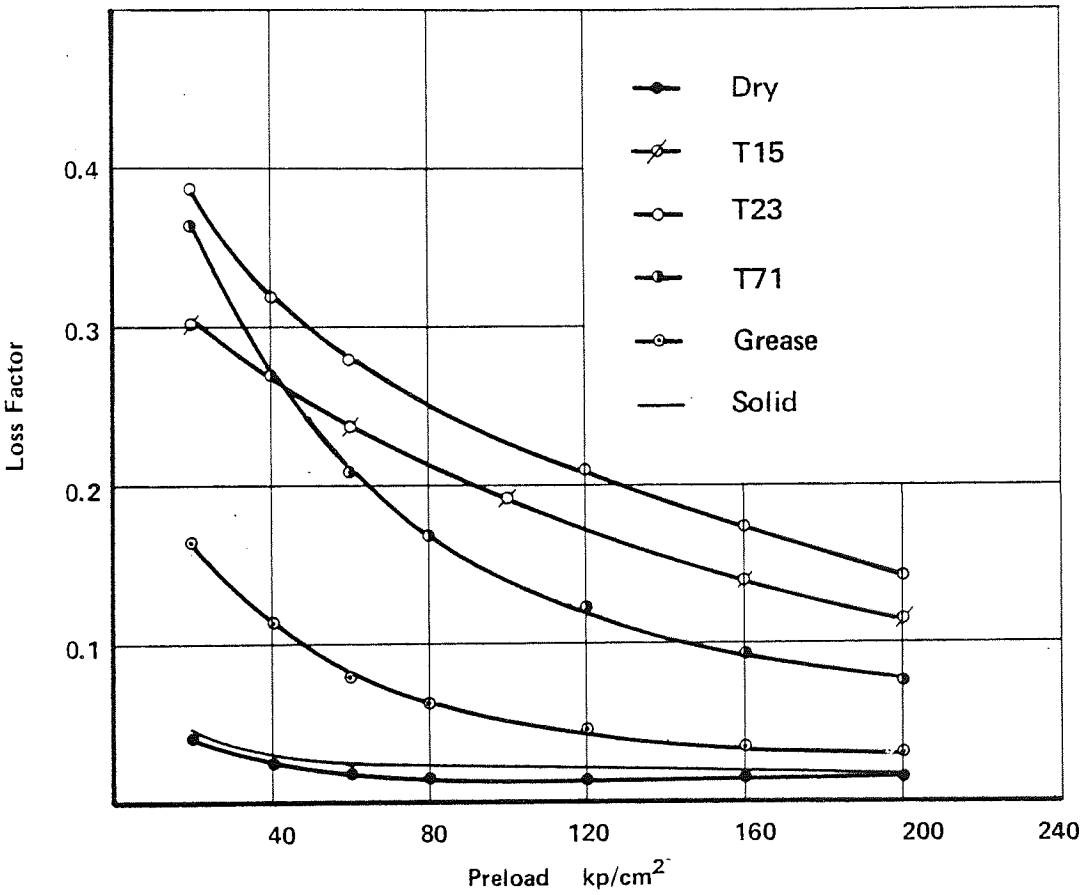

Fig. 62 Loss factor of dry and lubricated jointed column TN1

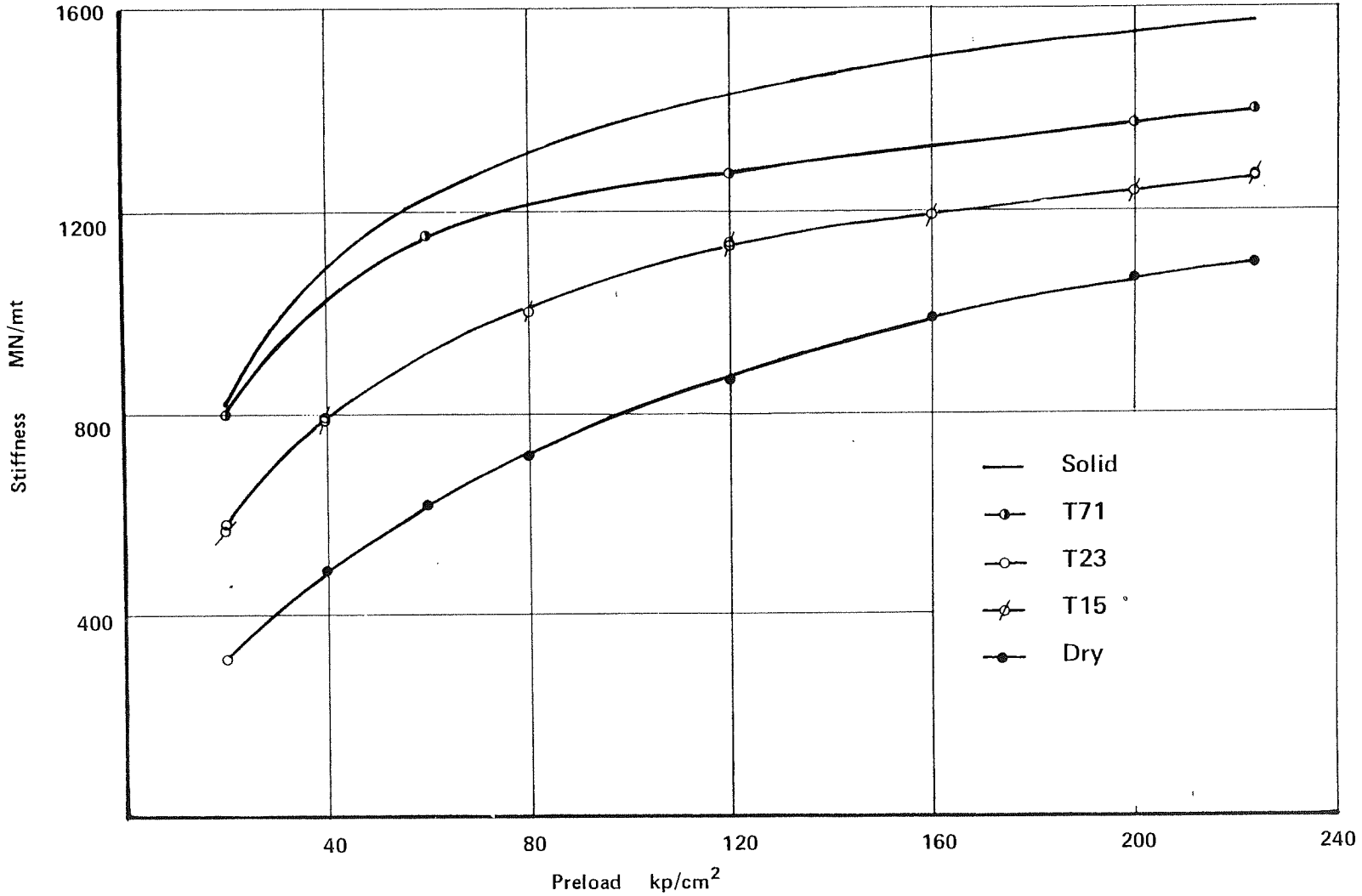

Fig. 63 Dynamic stiffness of dry and lubricated jointed column TN2

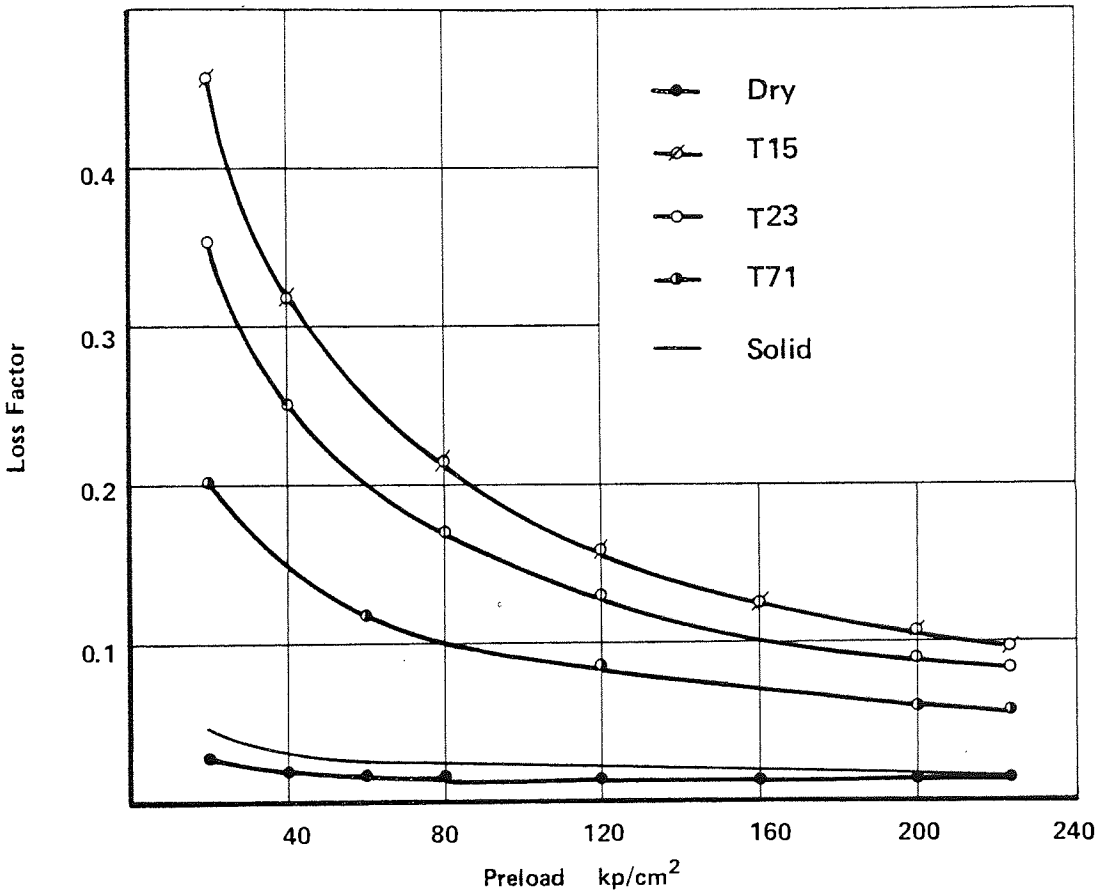

Fig. 64 Loss factor of dry and lubricated jointed column TN2

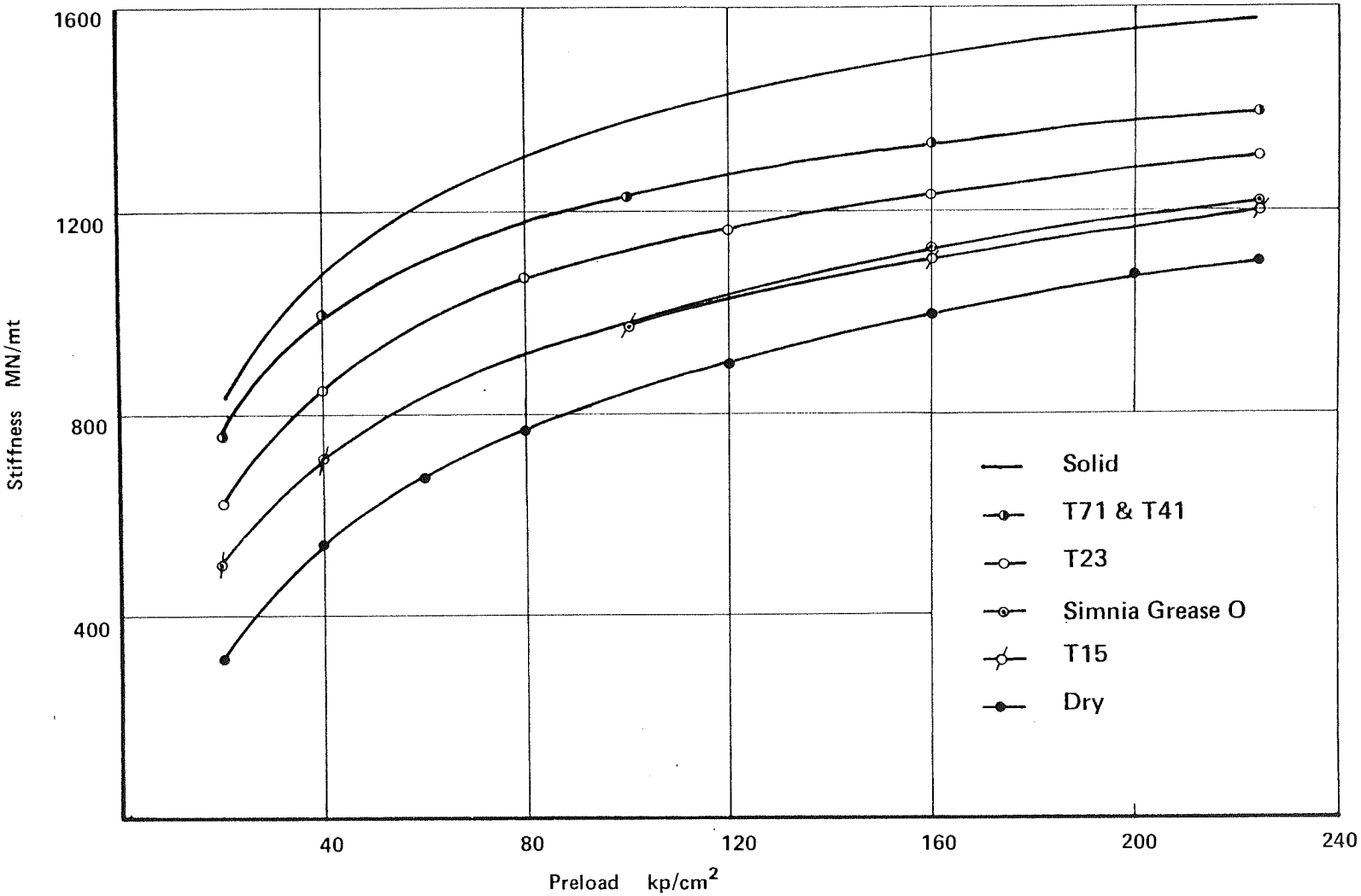

Fig. 65 Dynamic stiffness of dry and lubricated jointed column TN3

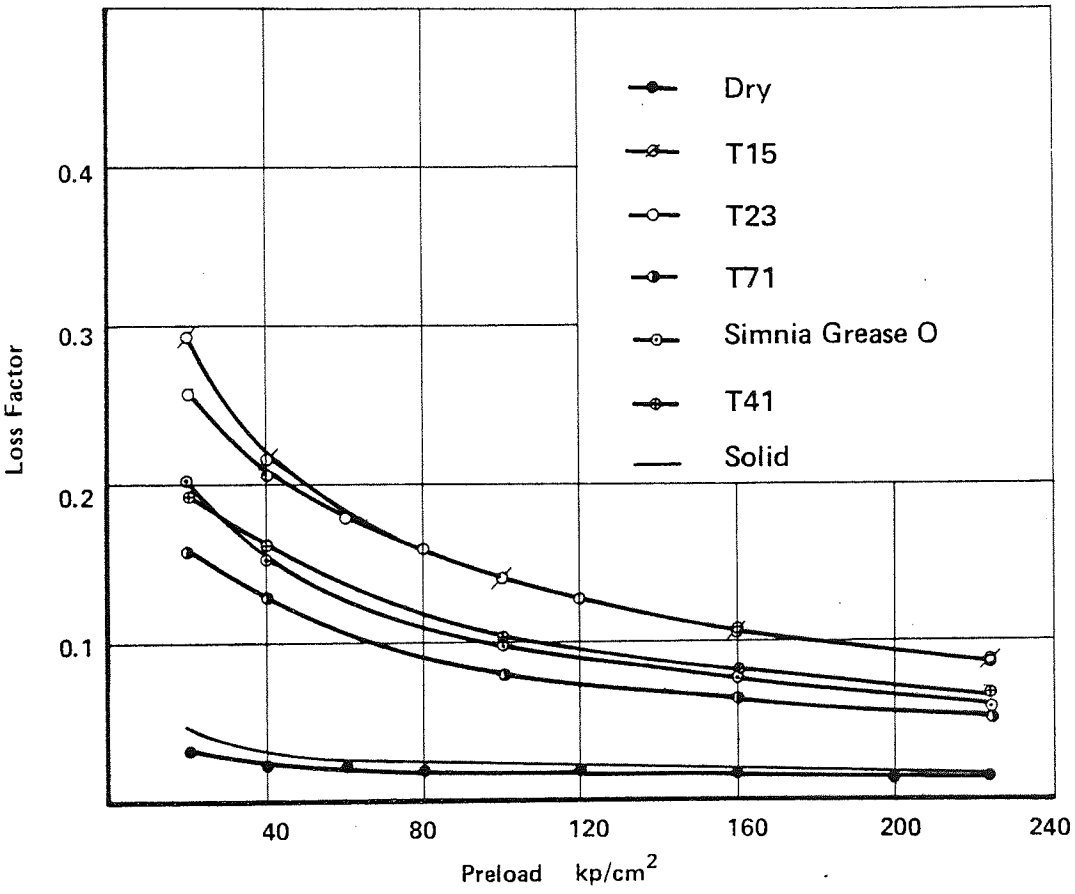

Fig. 66 Loss factor of dry and lubricated jointed column TN3

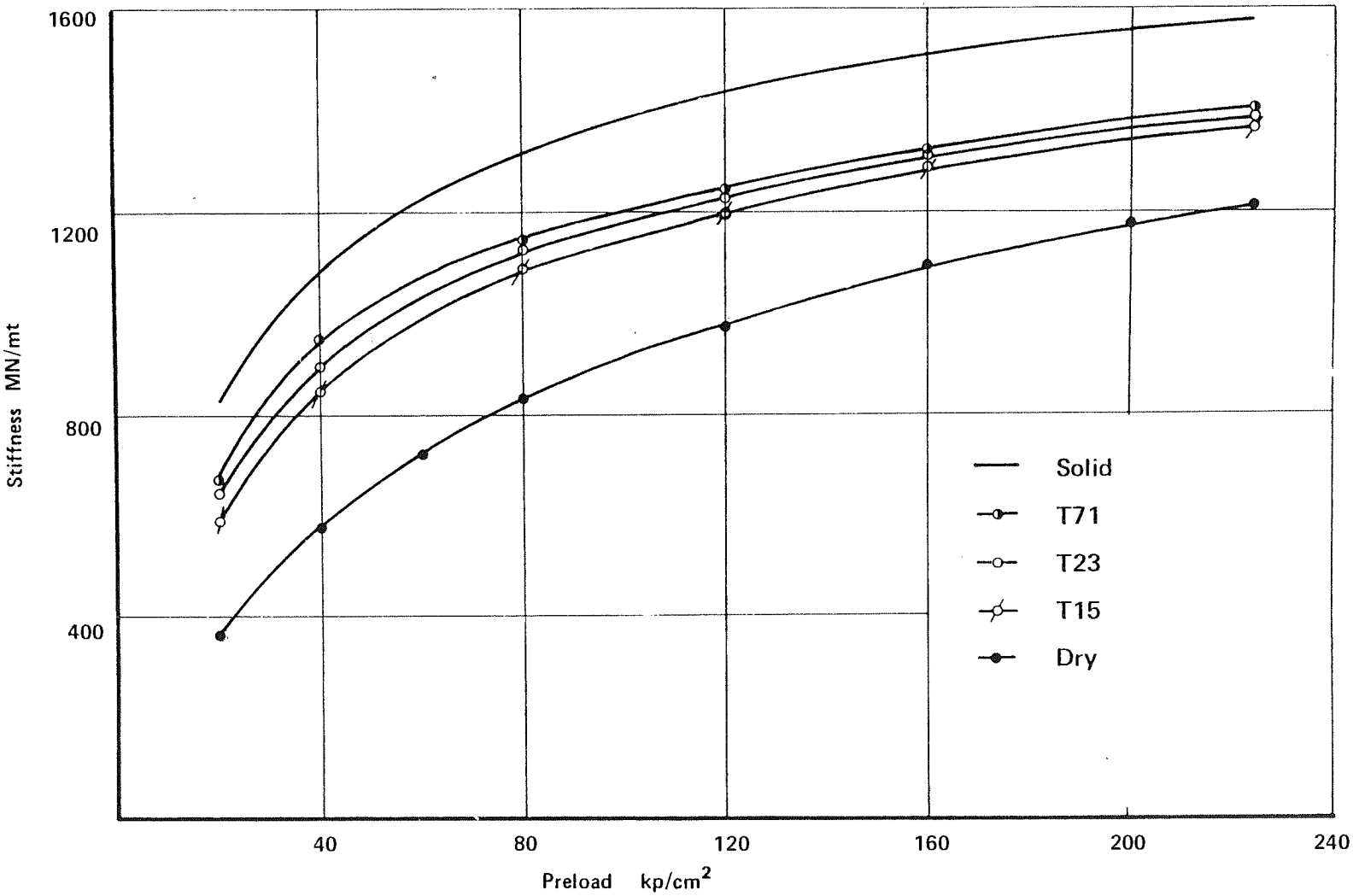

Fig. 67 Dynamic stiffness of dry and lubricated jointed column TN4

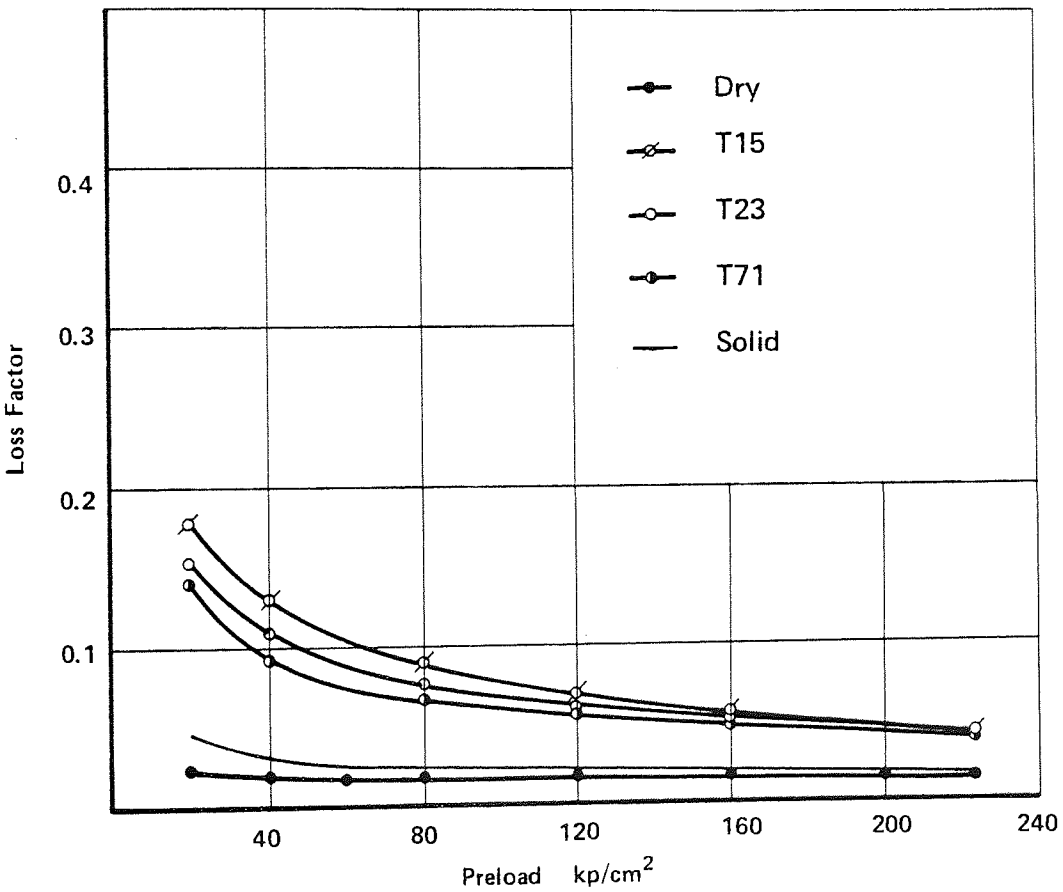

Fig. 68 Loss factor of dry and lubricated jointed column TN4

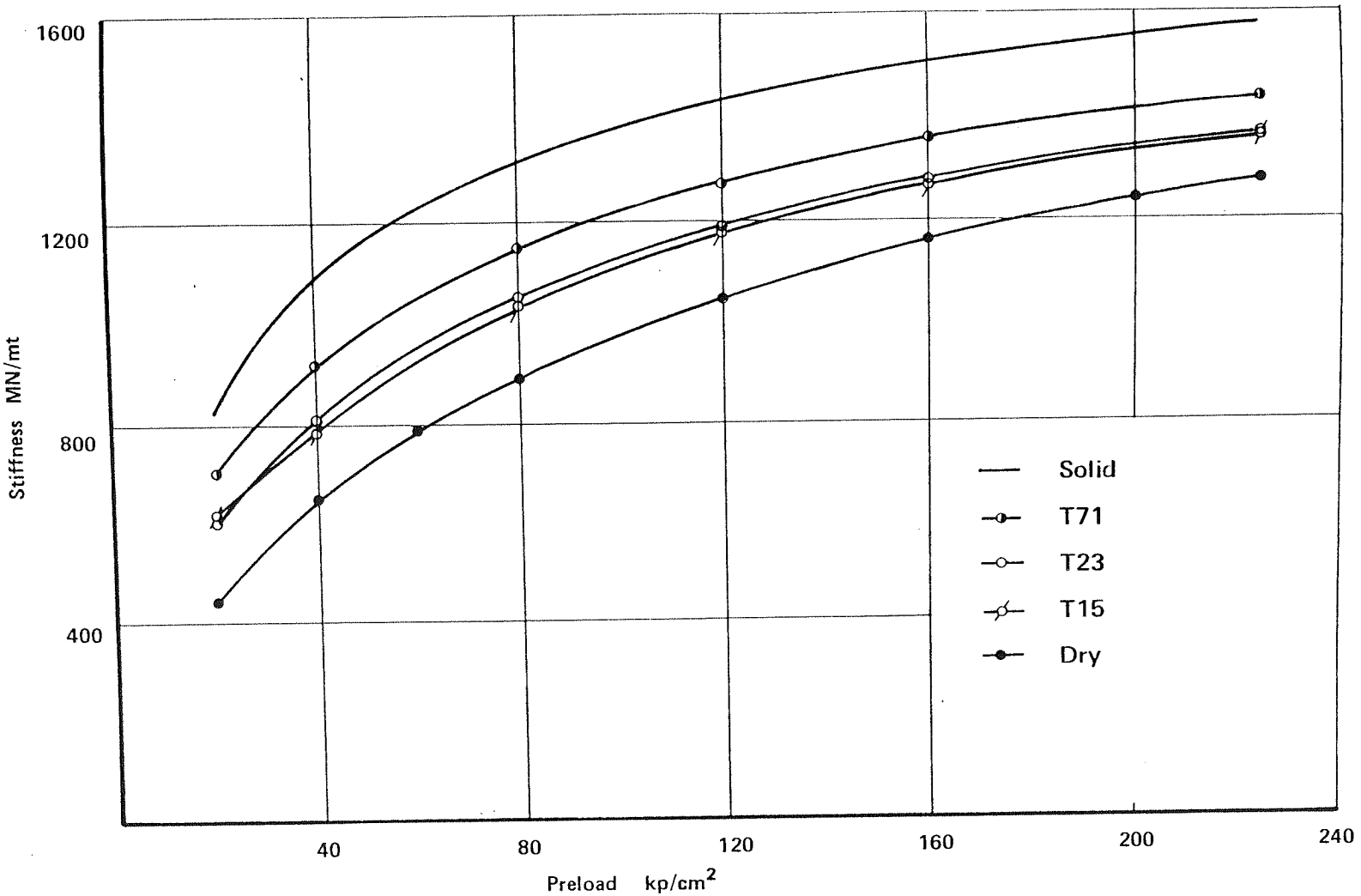

Fig. 69 Dynamic stiffness of dry and lubricated jointed column GN1 (Ground)

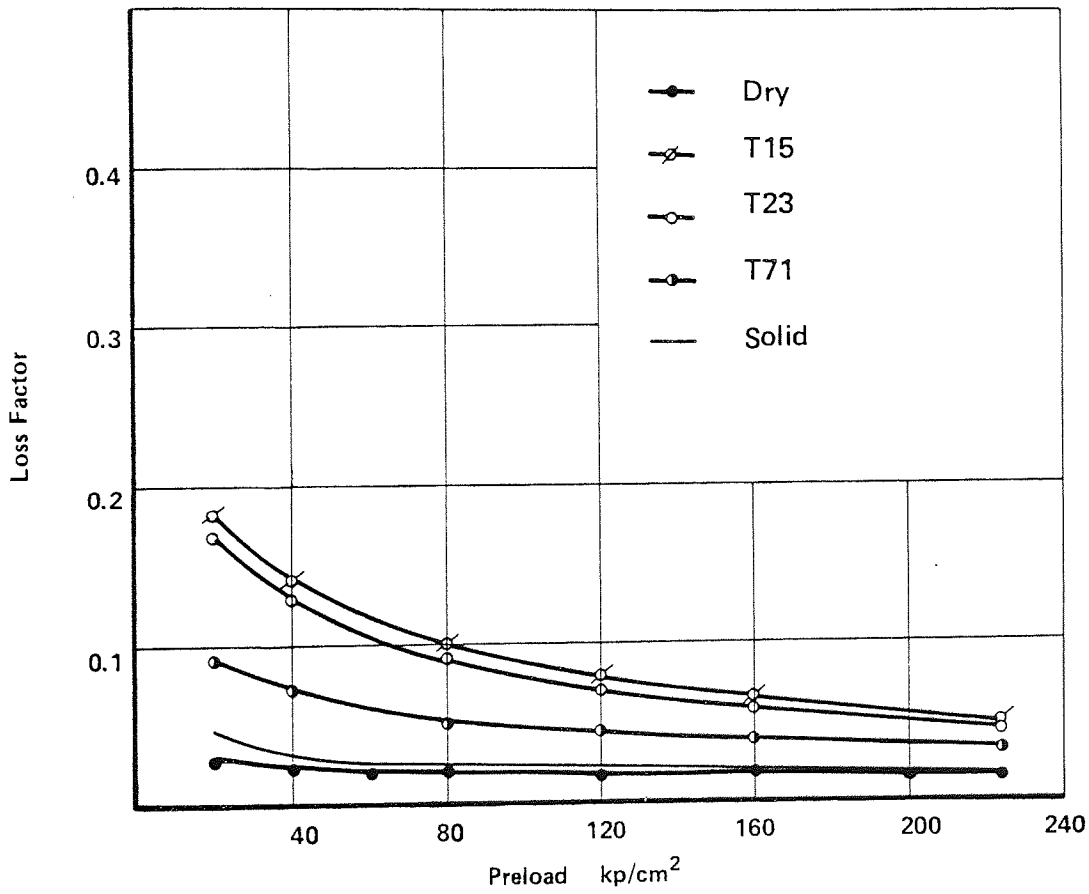

Fig. 70 Loss factor of dry and lubricated jointed column GN1

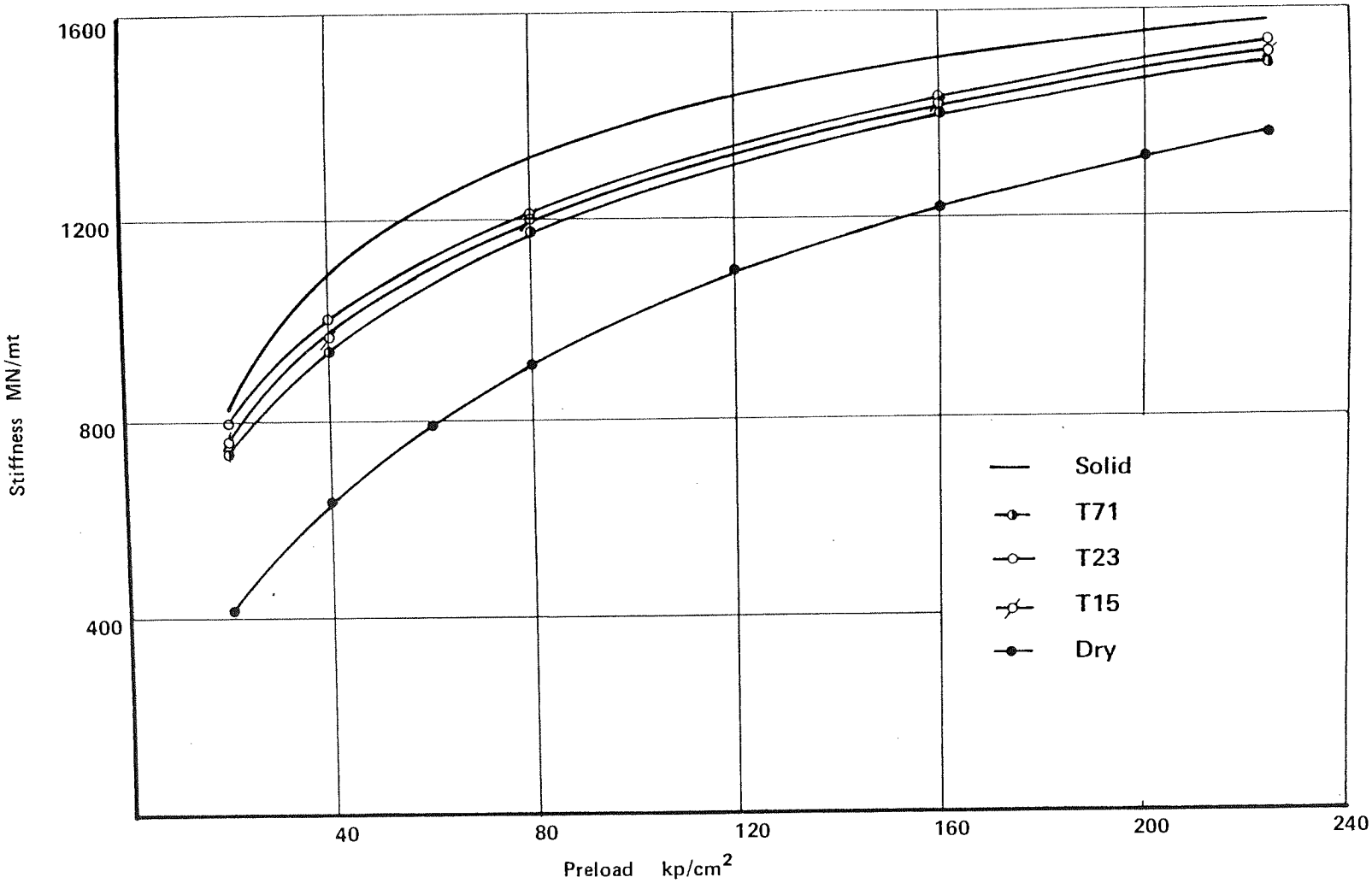

Fig. 71 Dynamic stiffness of dry and lubricated jointed column GN2

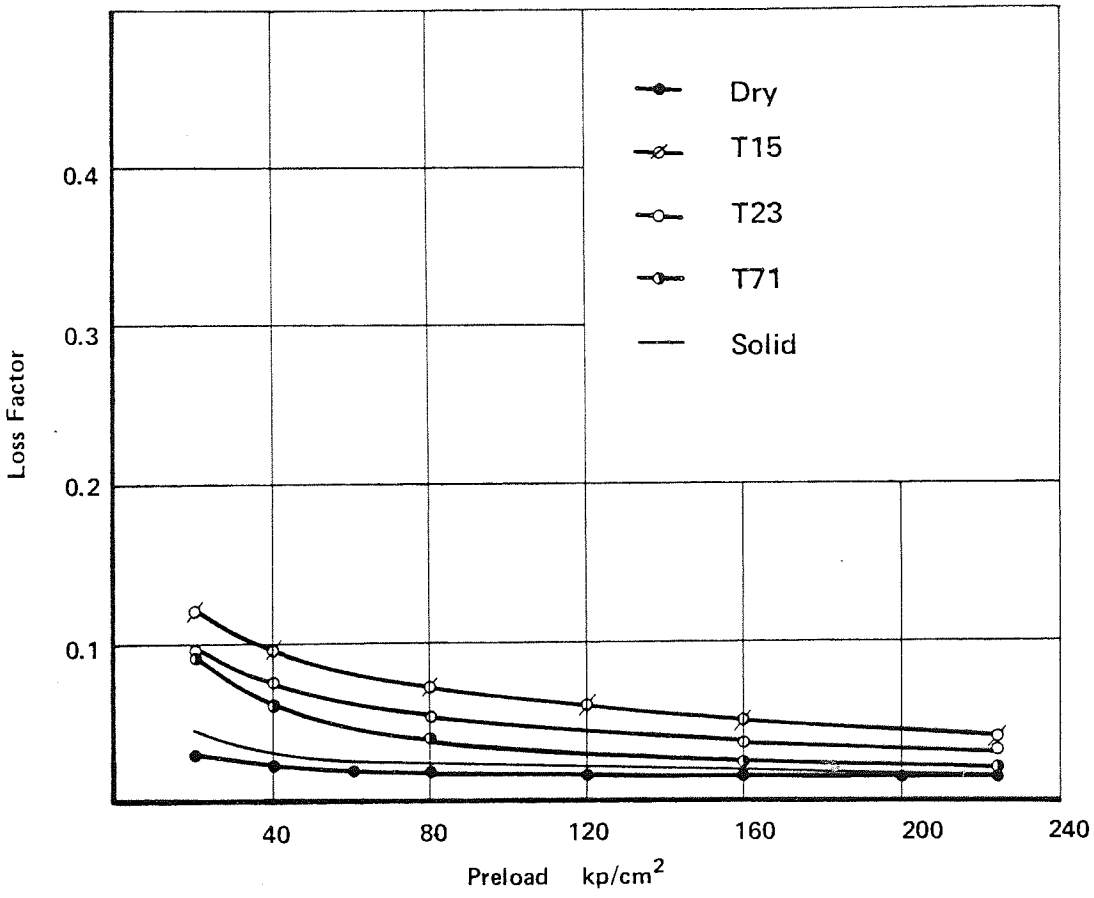

Fig. 72 Loss factor of dry and lubricated jointed column GN2

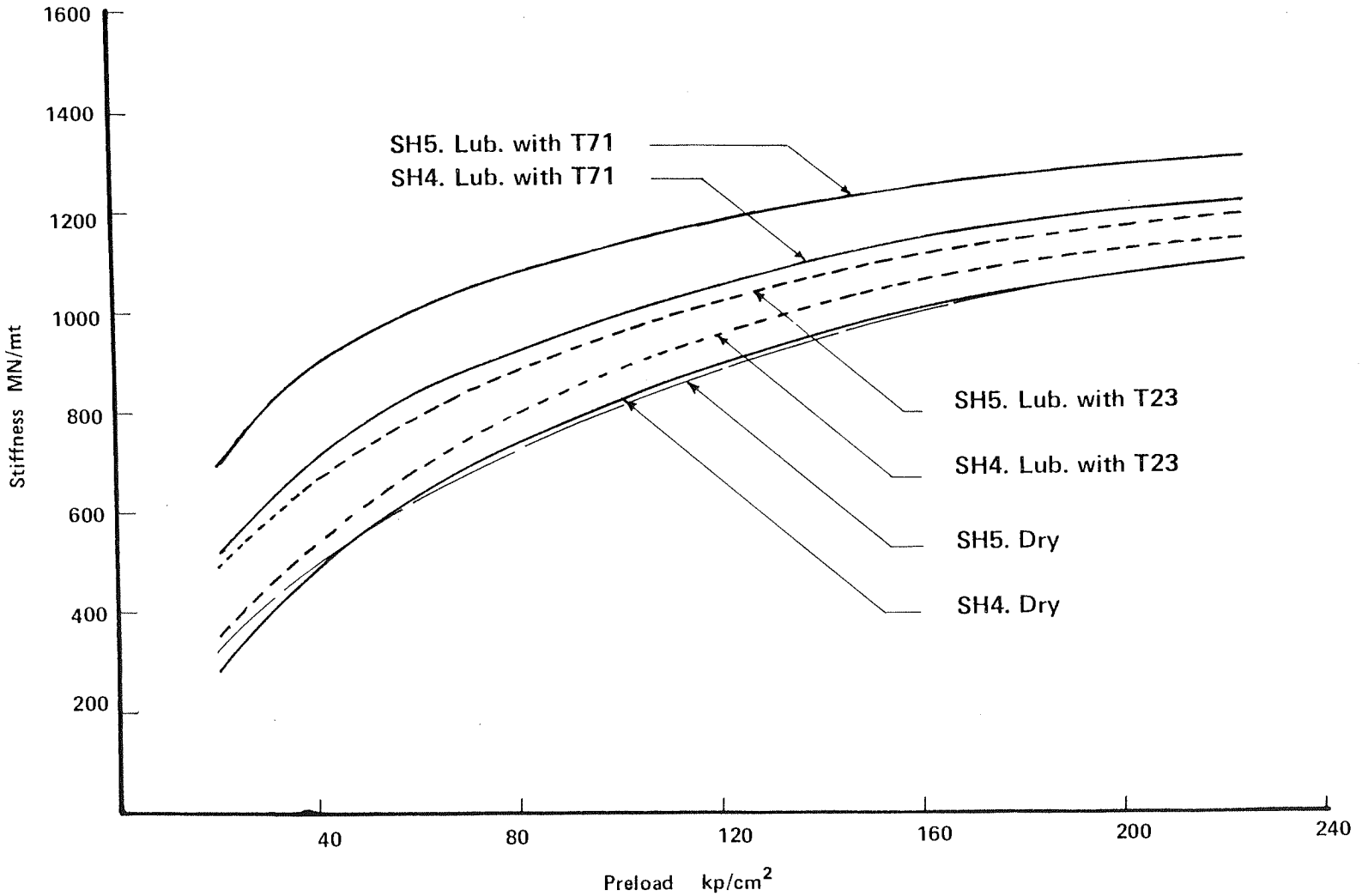

Fig. 73 Comparison between the dynamic stiffness of SH4 and SH5

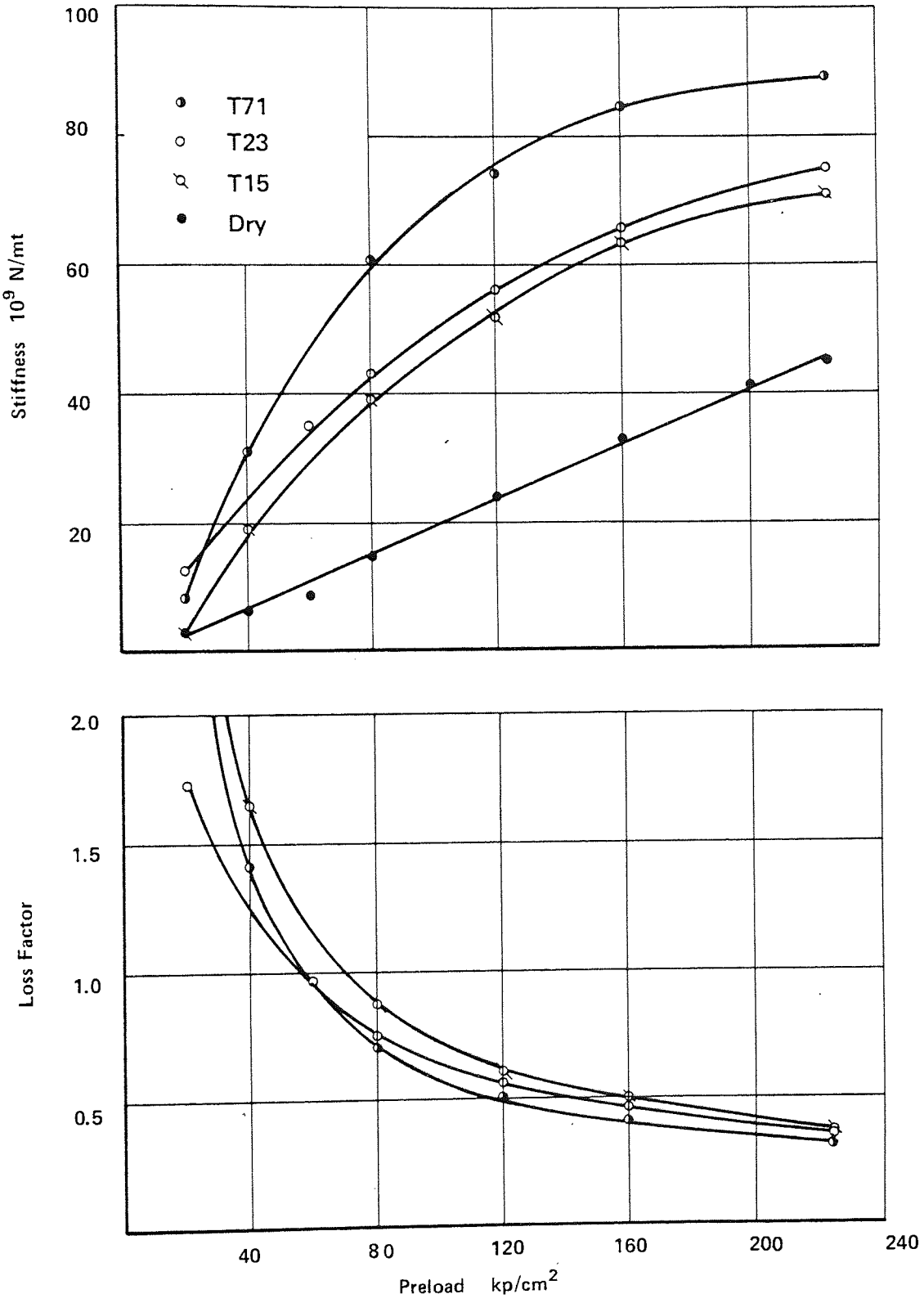

Fig. 74 Dynamic stiffness and loss factor of ML1 joint

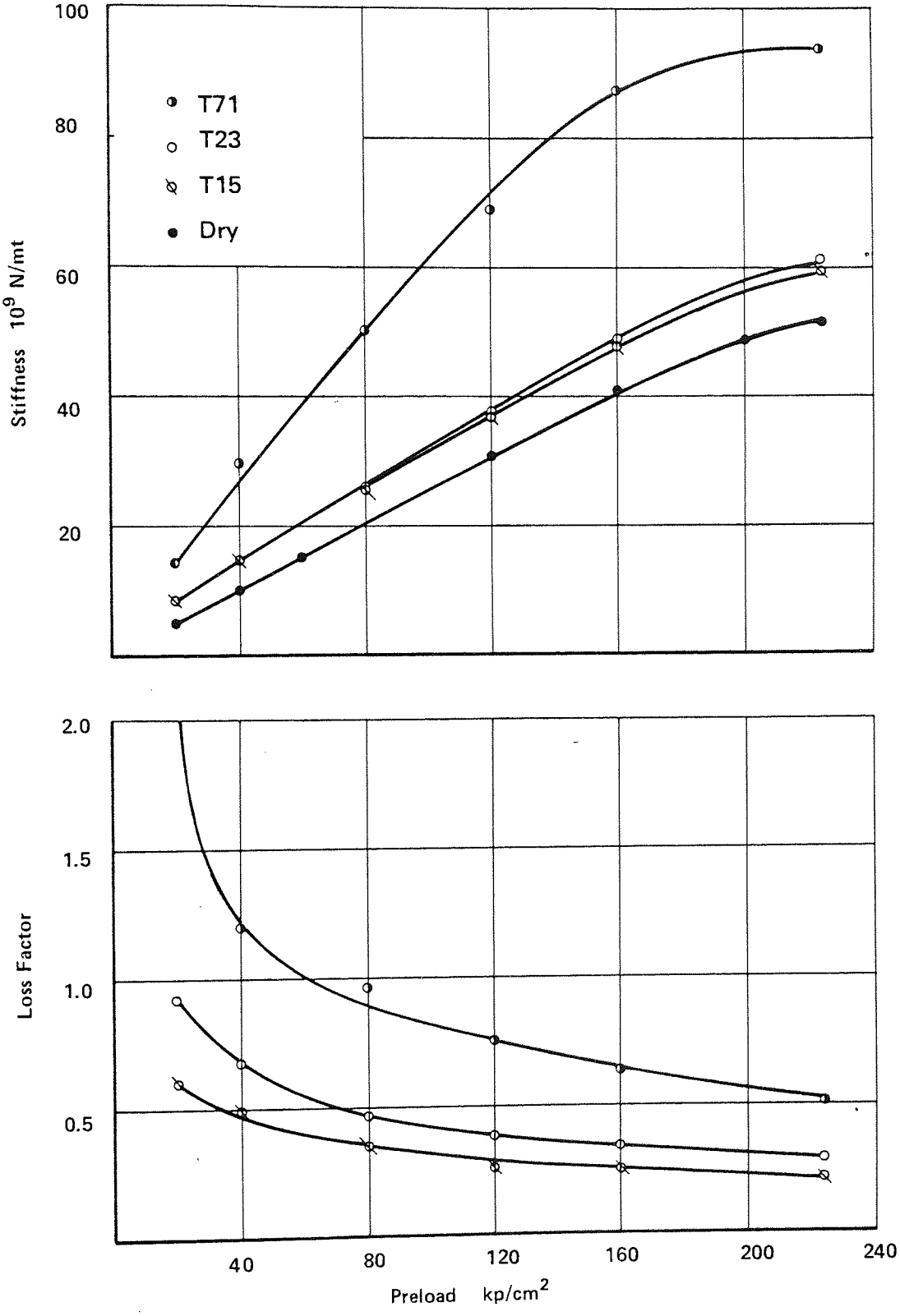

Fig. 75 Dynamic stiffness and loss factor of ML2 joint

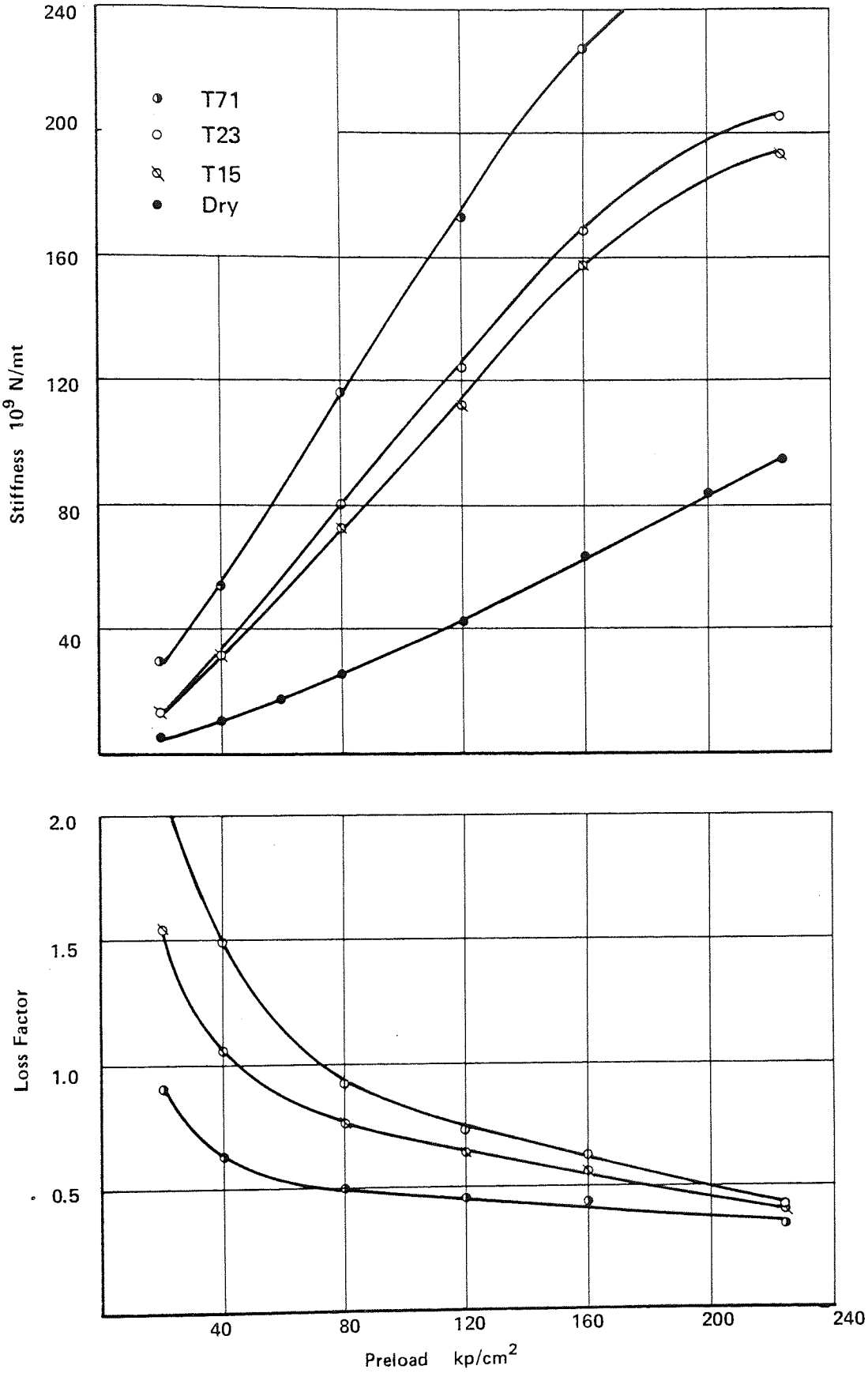

Fig. 76 Dynamic stiffness and loss factor of ML3 joint

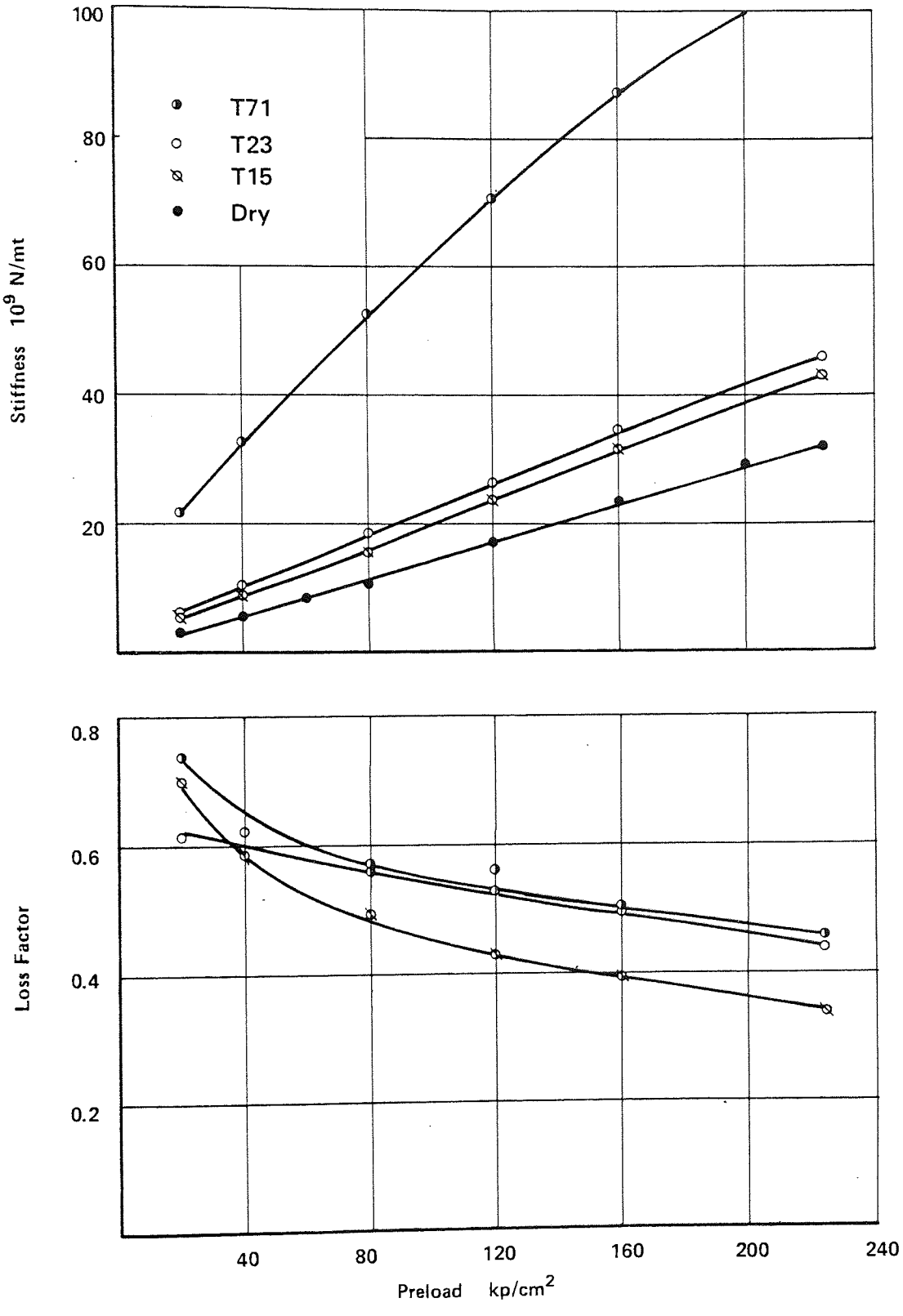

Fig. 77 Dynamic stiffness and loss factor of ML4 joint

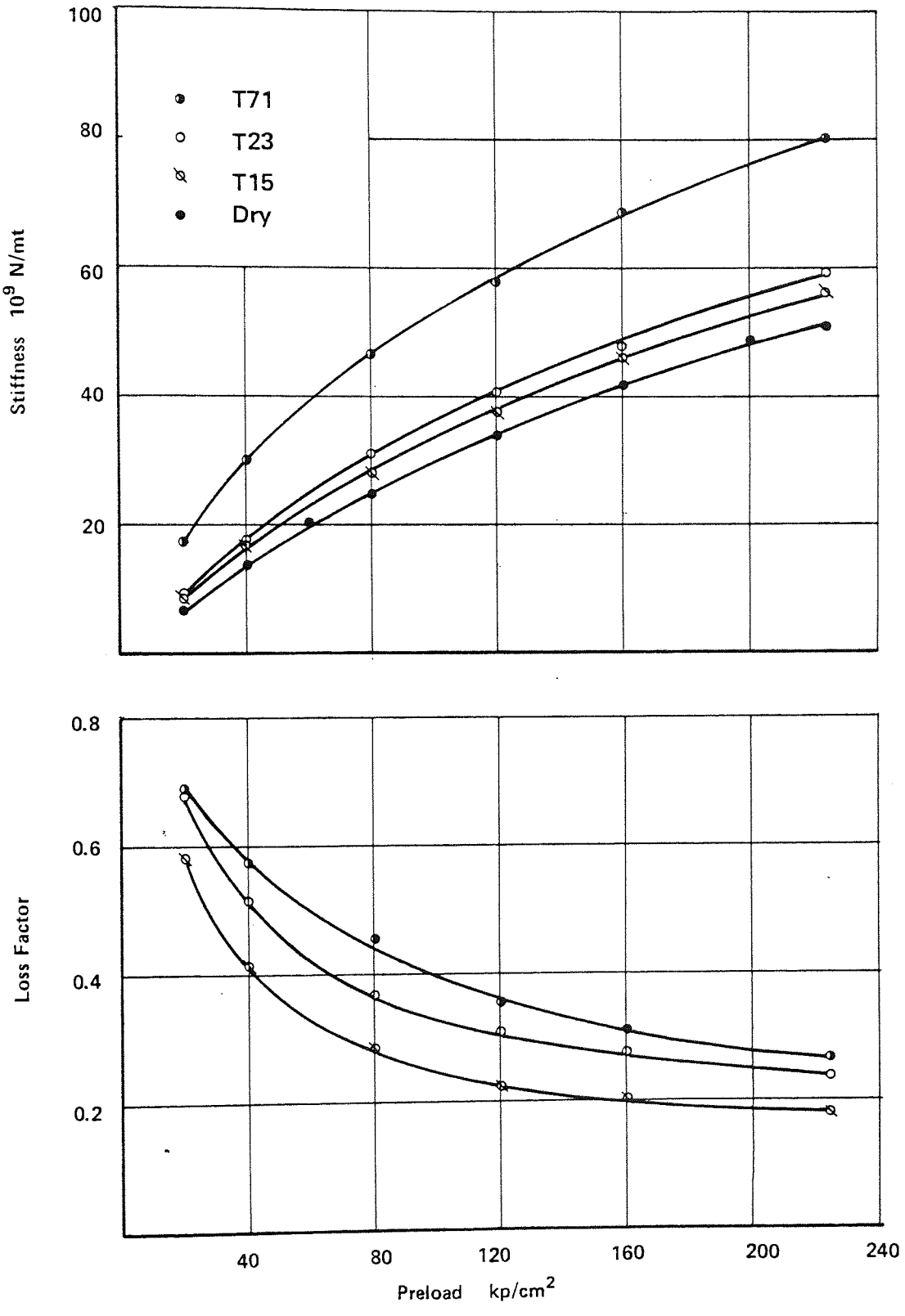

Fig. 78 Dynamic stiffness and loss factor of SH1 joint

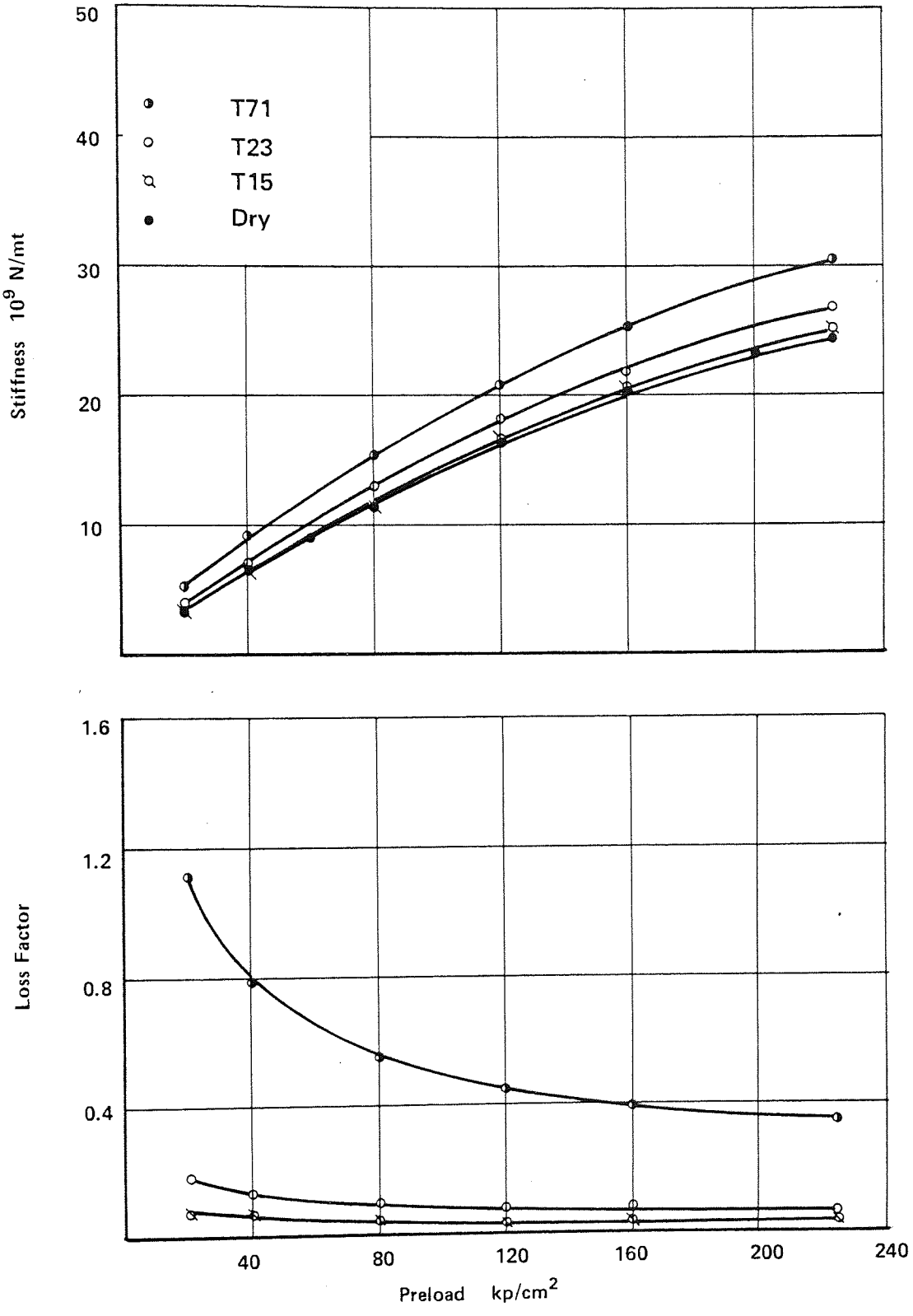

Fig. 79 Dynamic stiffness and loss factor of SH2 joint

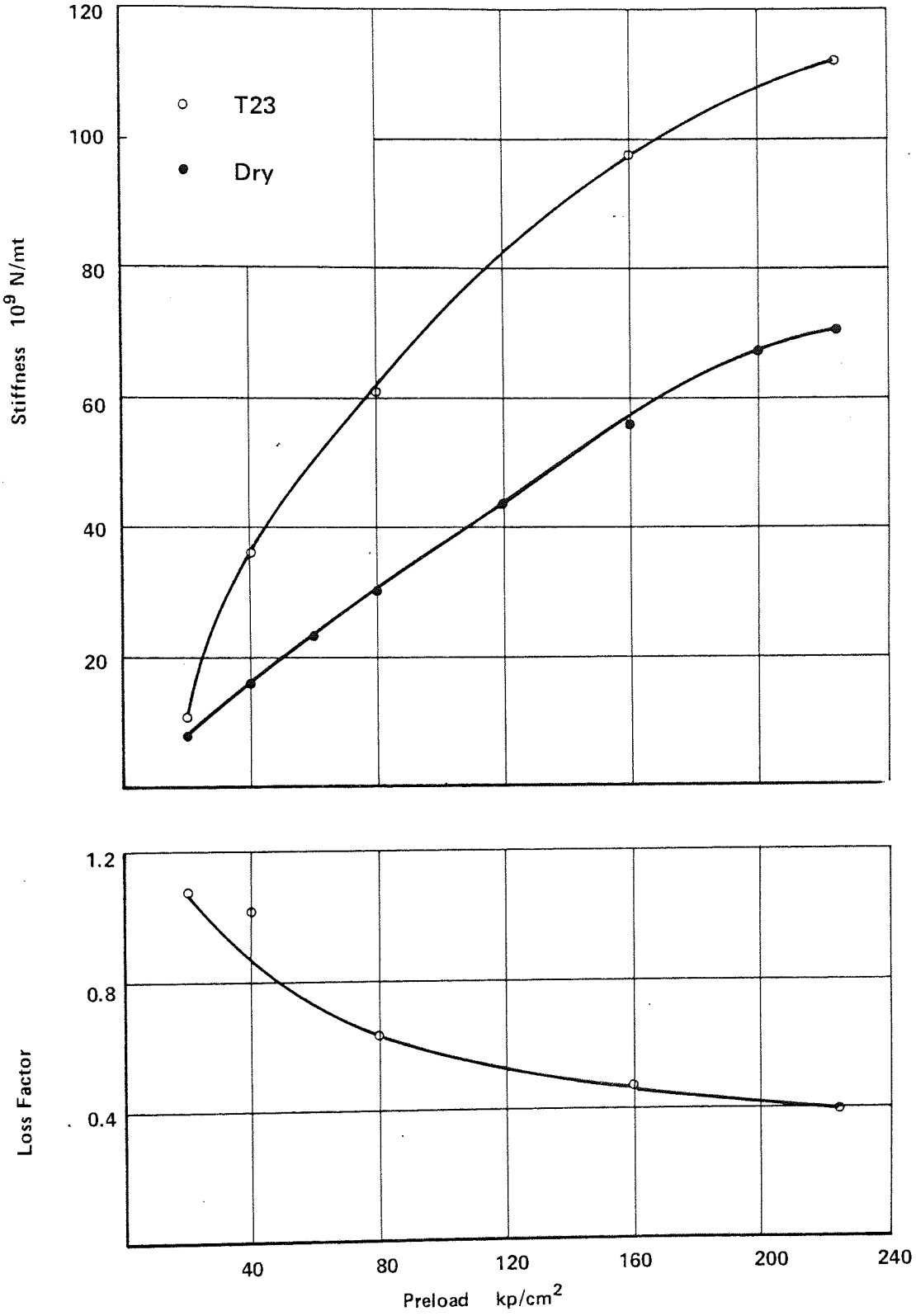

Fig. 80 Dynamic stiffness and loss factor of SH3 joint

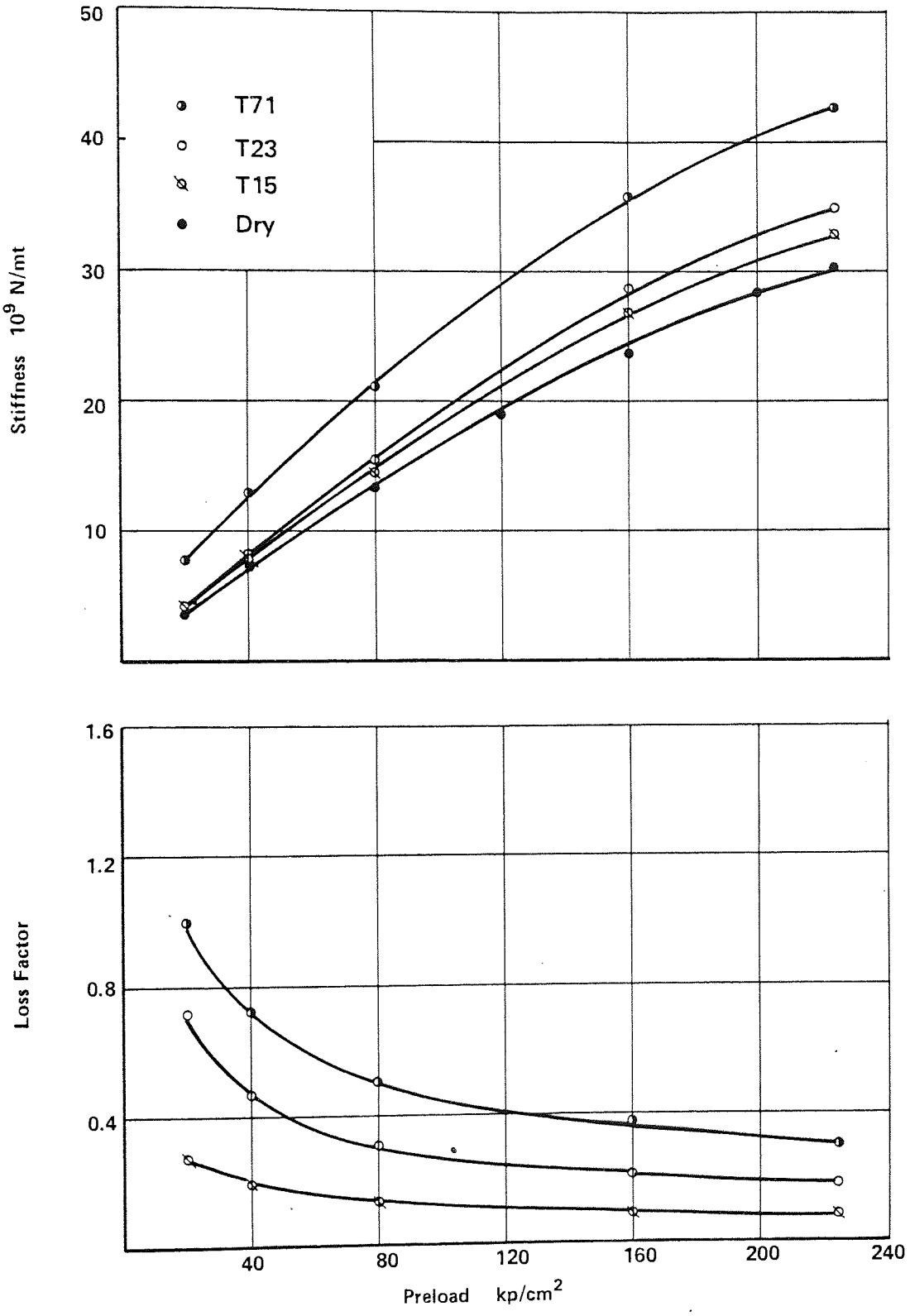

Fig. 81 Dynamic stiffness and loss factor of SH4 joint

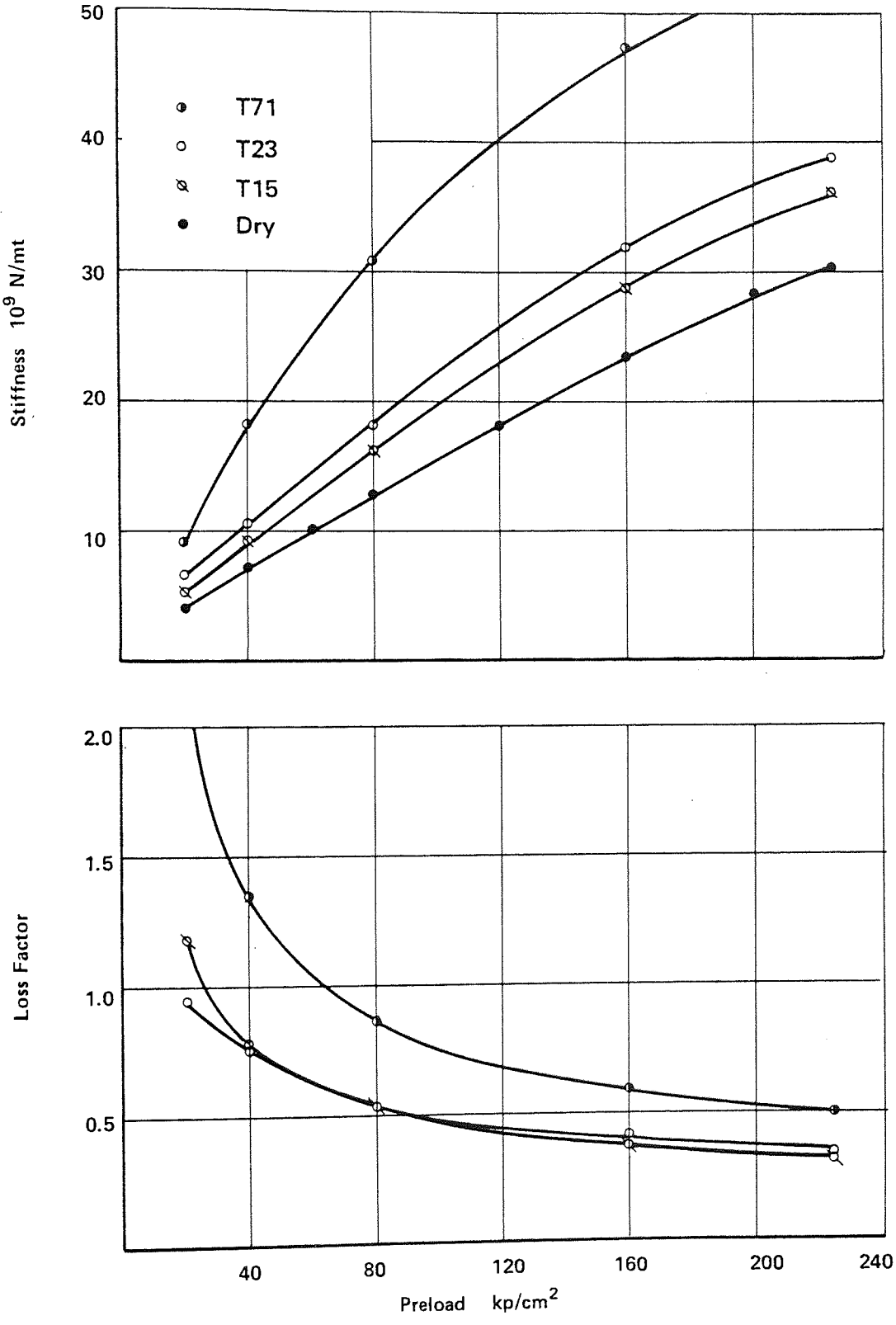

Fig. 82 Dynamic stiffness and loss factor of SH5 joint

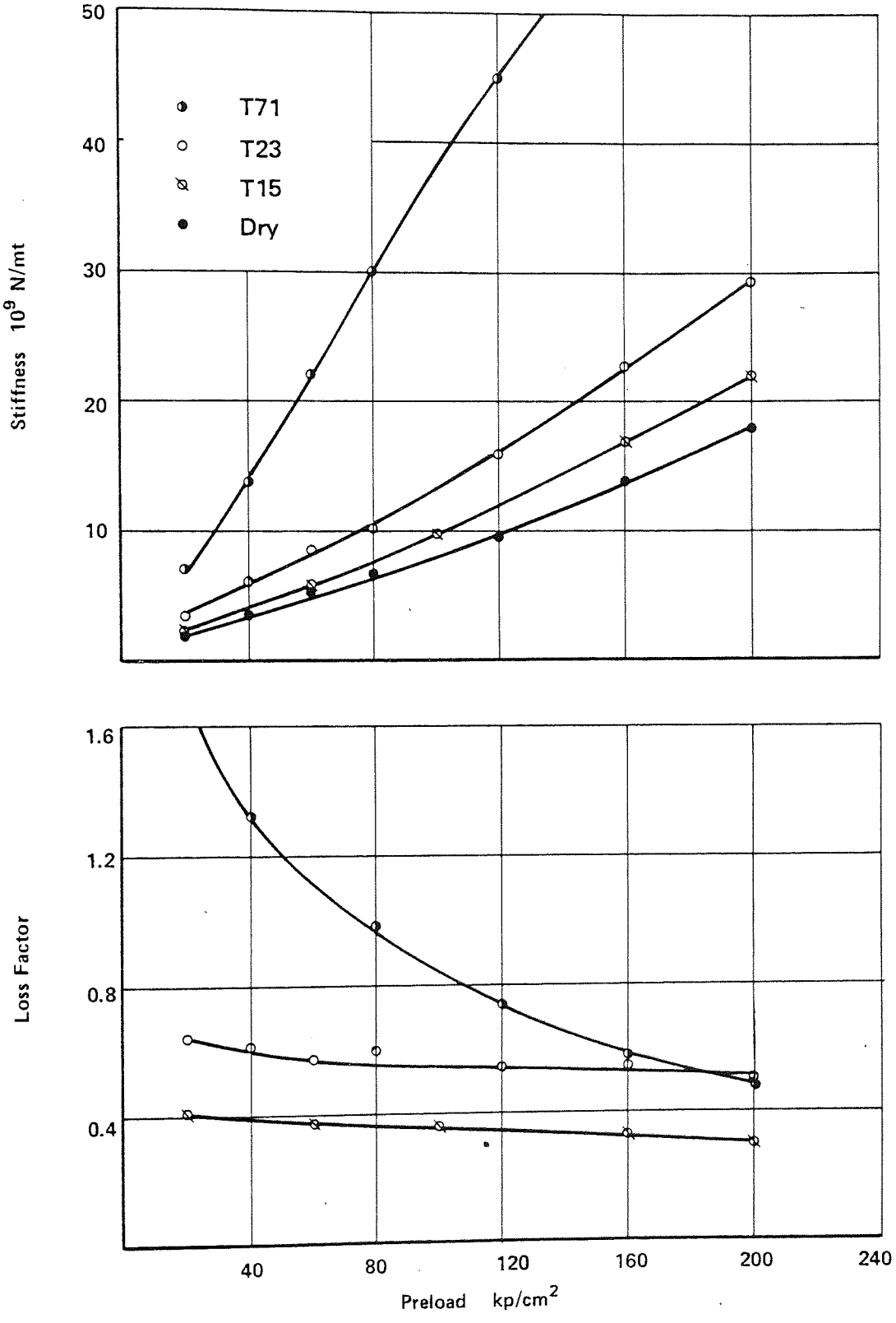

Fig. 83 Dynamic stiffness and loss factor of TN1 joint

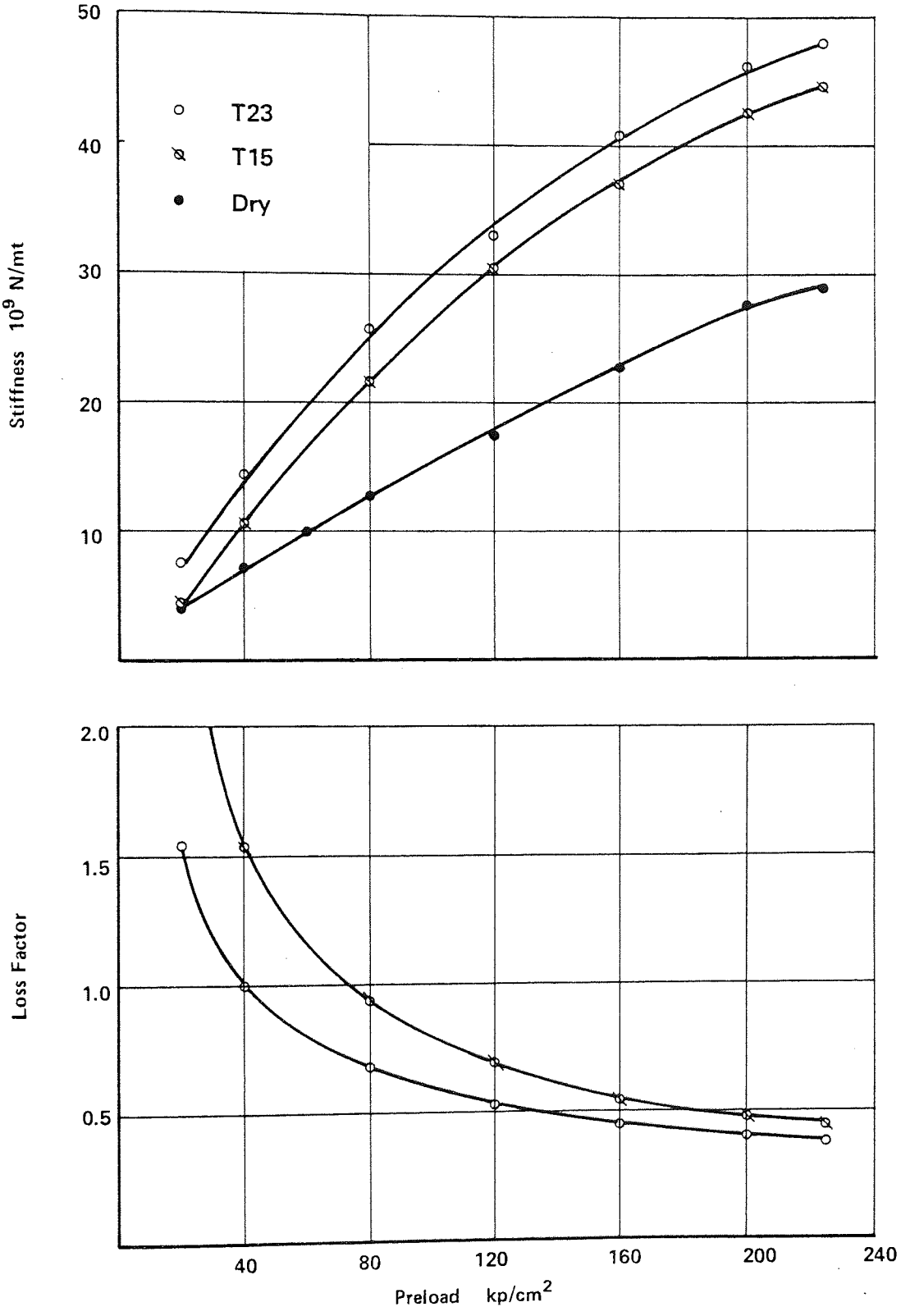

Fig. 84 Dynamic stiffness and loss factor of TN2 joint

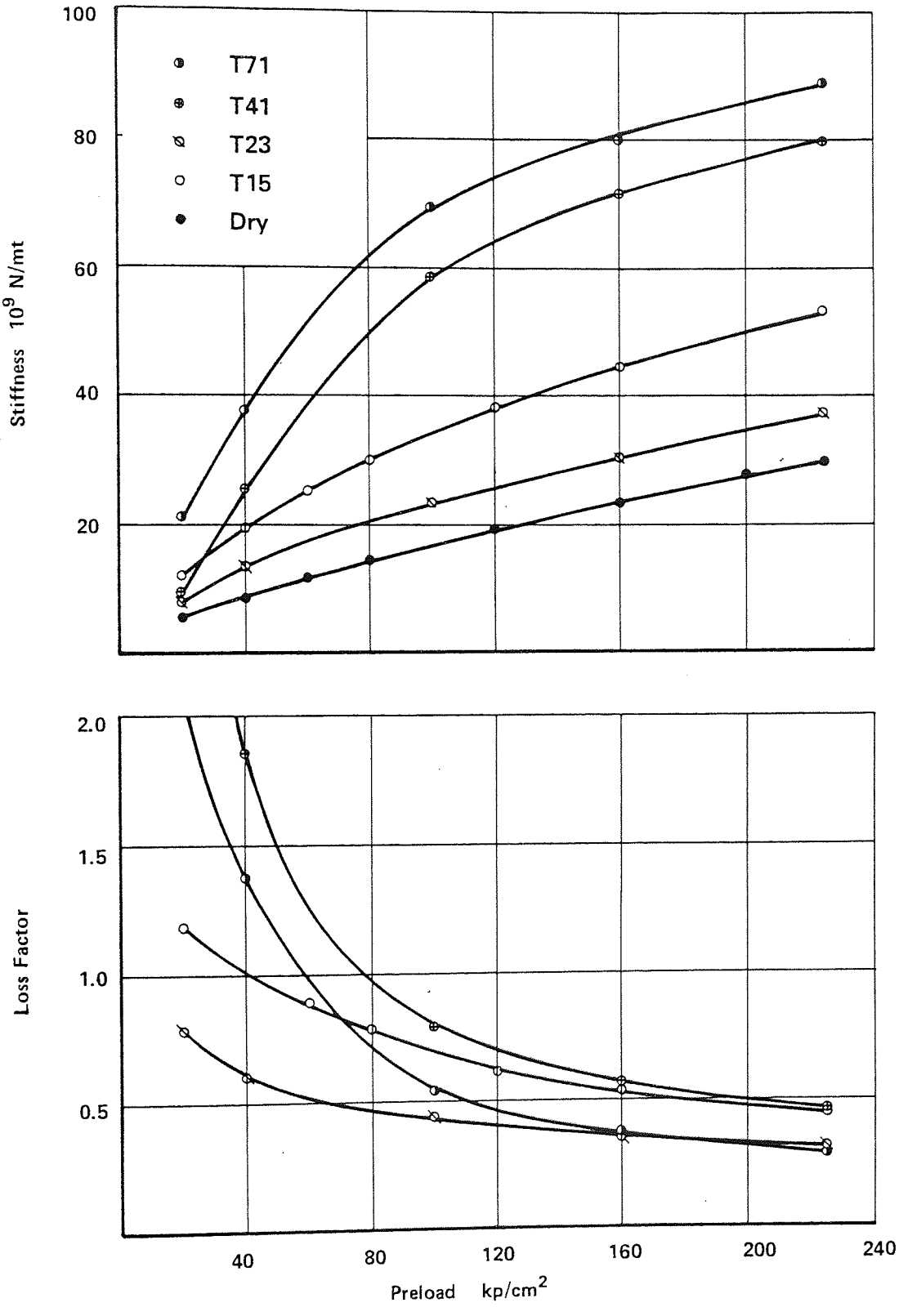

Fig. 85 Dynamic stiffness and loss factor of TN3 joint

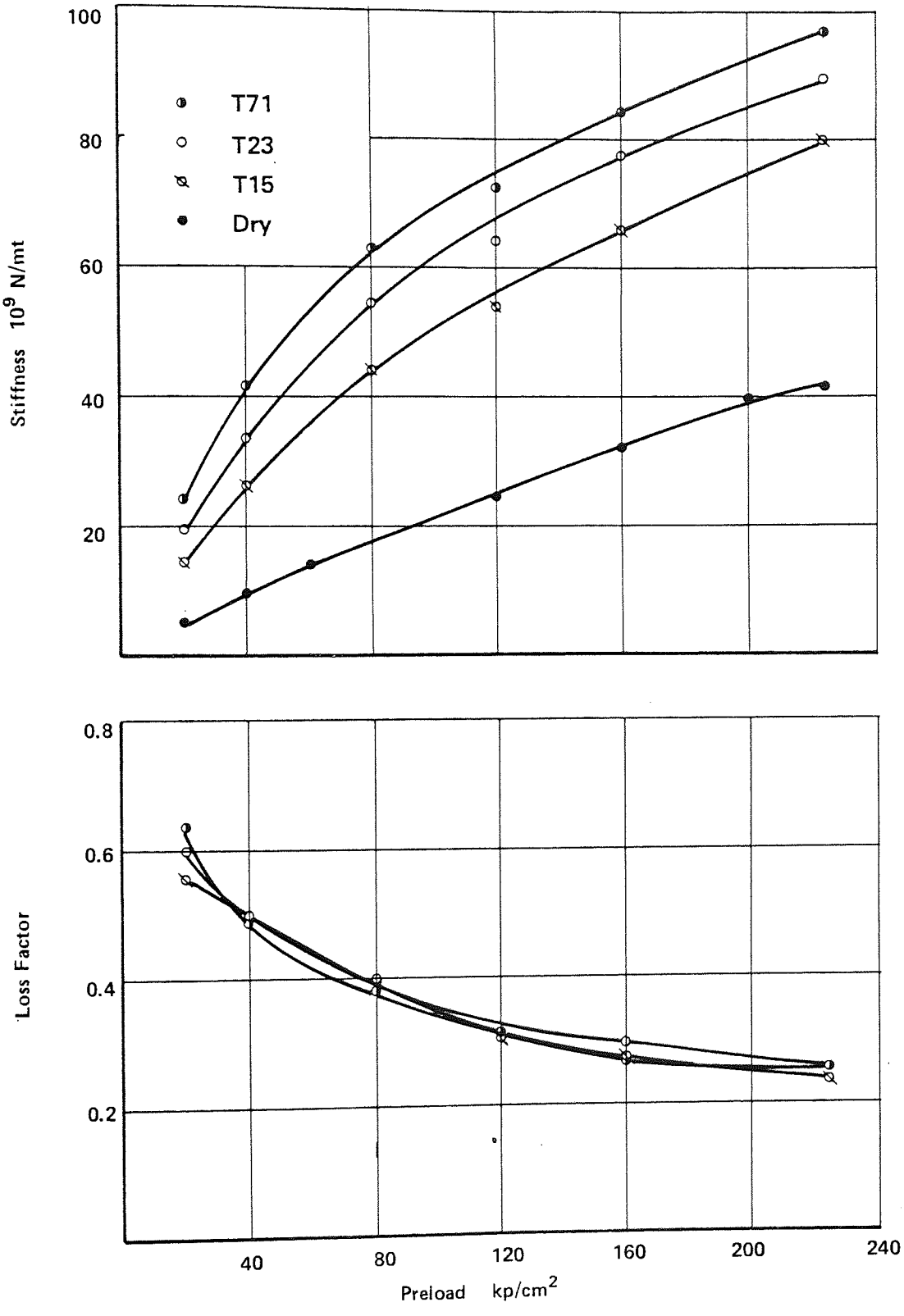

Fig. 86 Dynamic stiffness and loss factor of TN4 joint

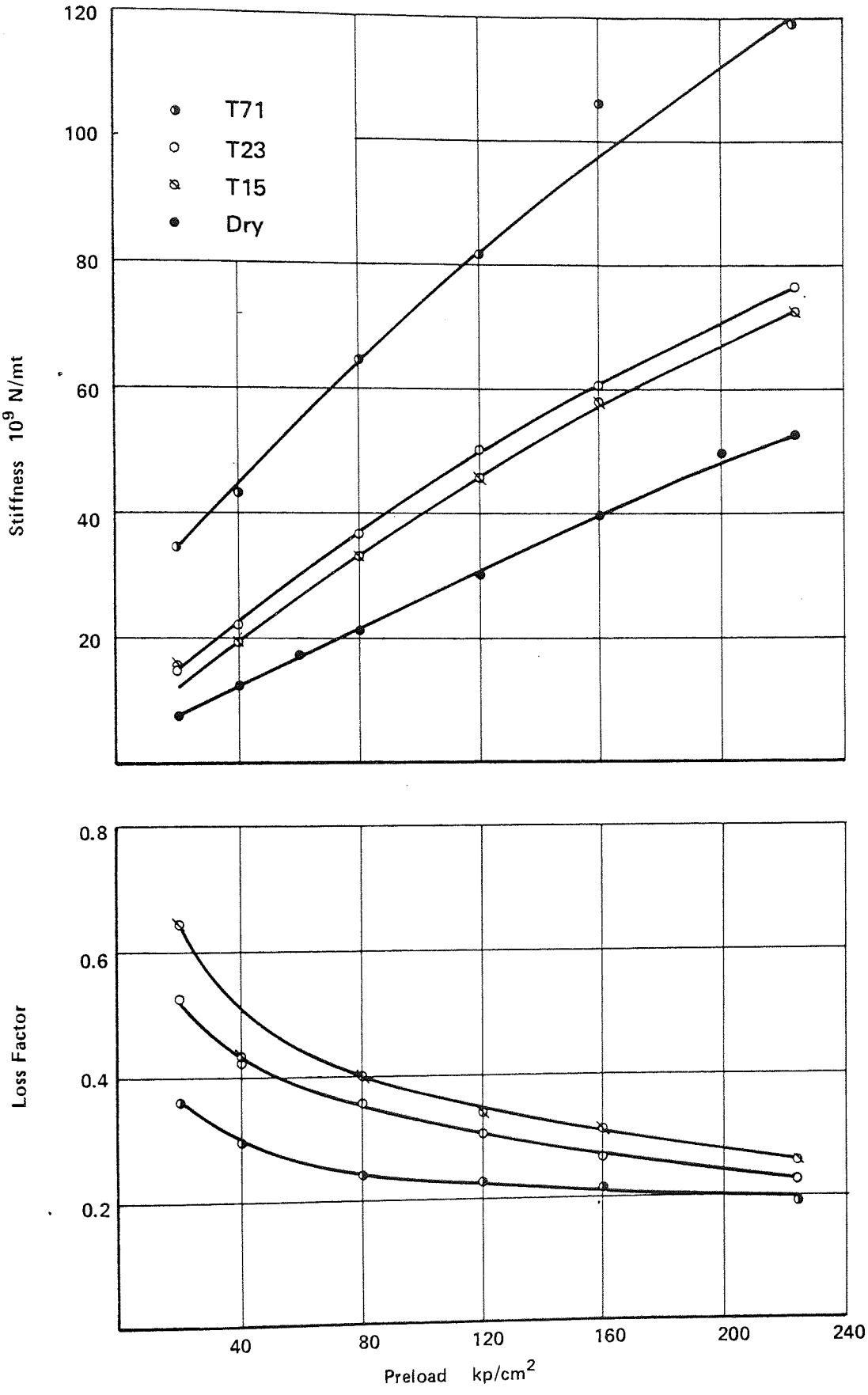

Fig. 87 Dynamic stiffness and loss factor of GN1 joint

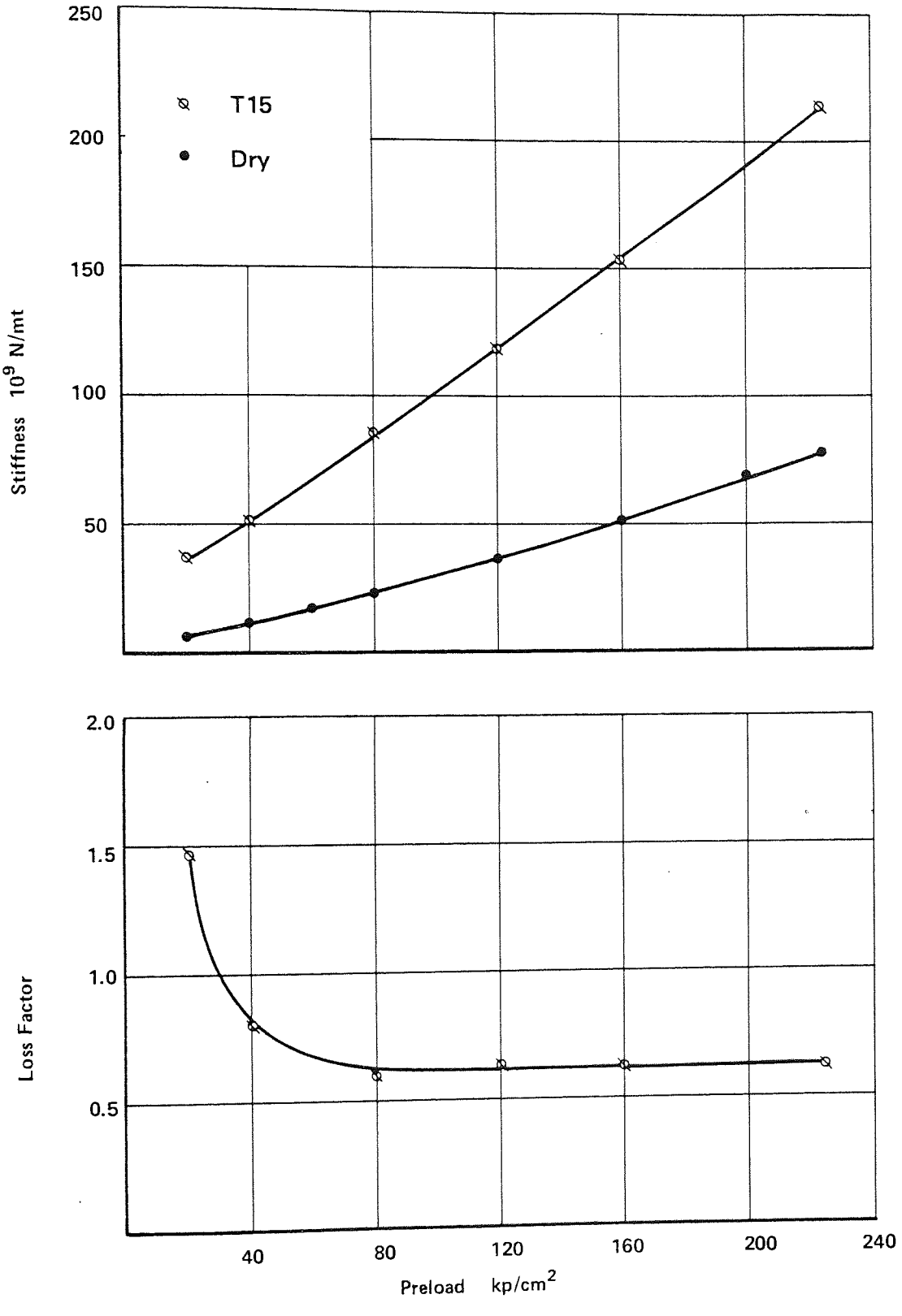

Fig. 88 Dynamic stiffness and loss factor of GN2 joint

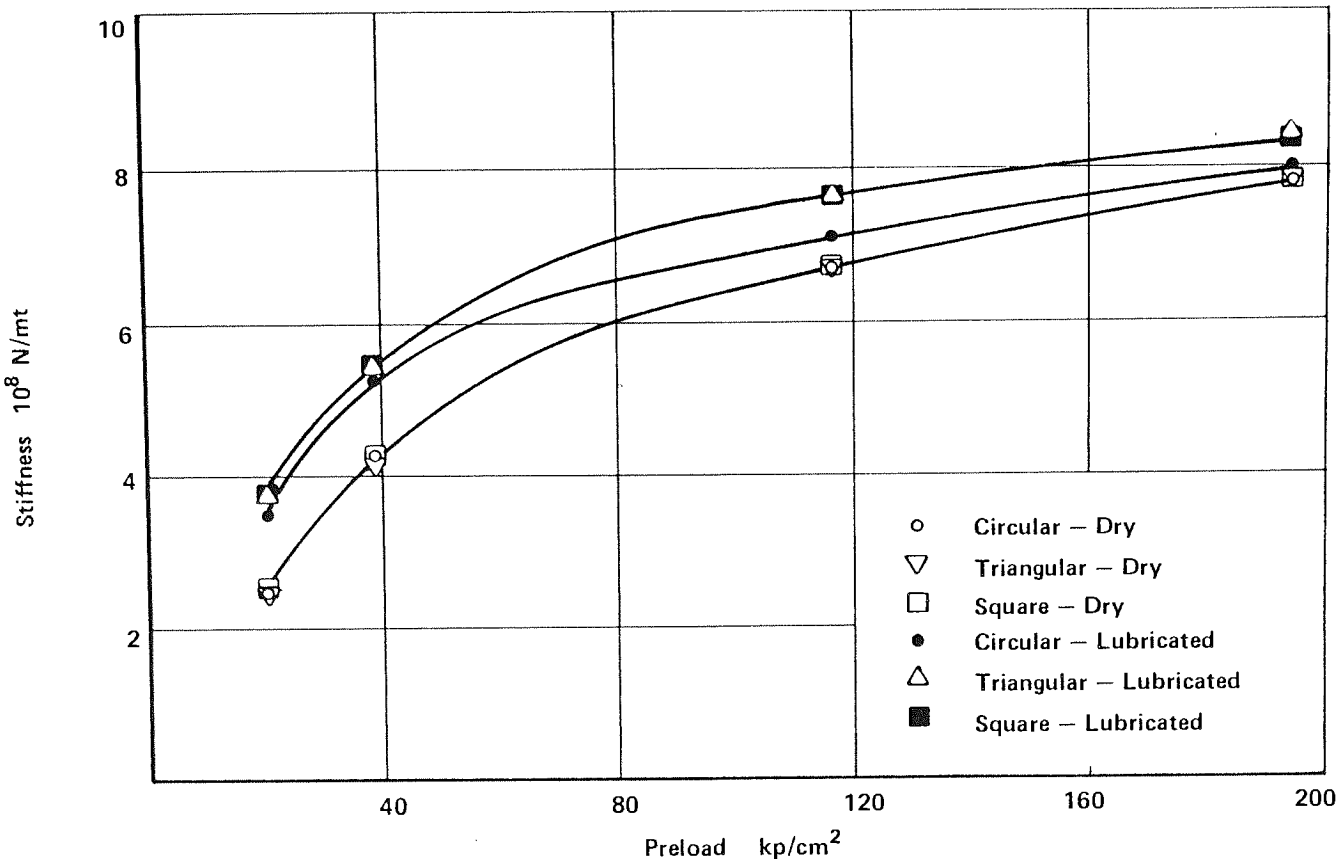

Fig. 89 Effect of planform shapes on the dynamic stiffness of jointed columns

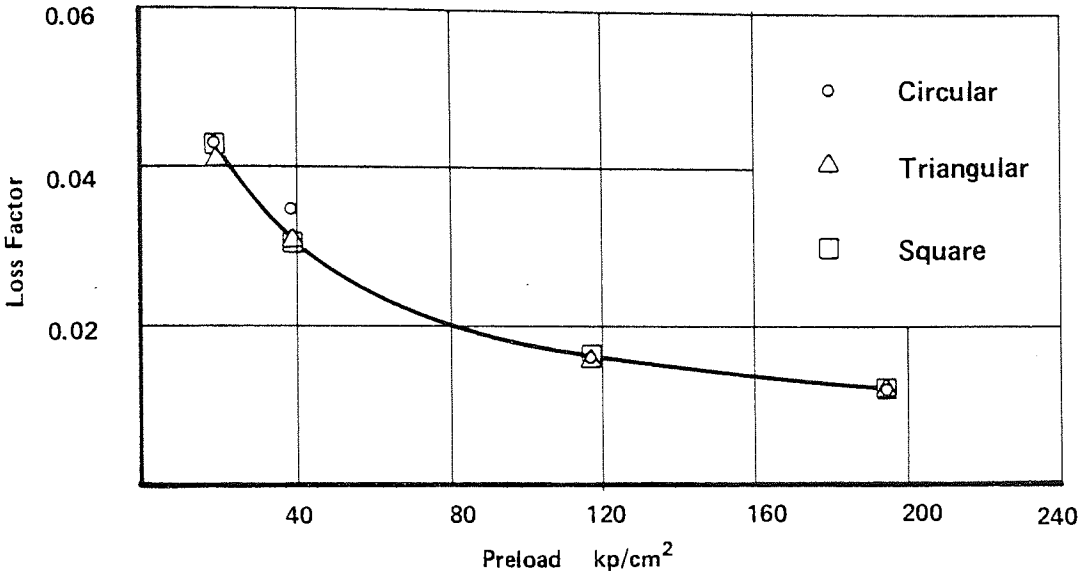

Fig. 90 Effect of planform shapes on the loss factor of dry jointed columns

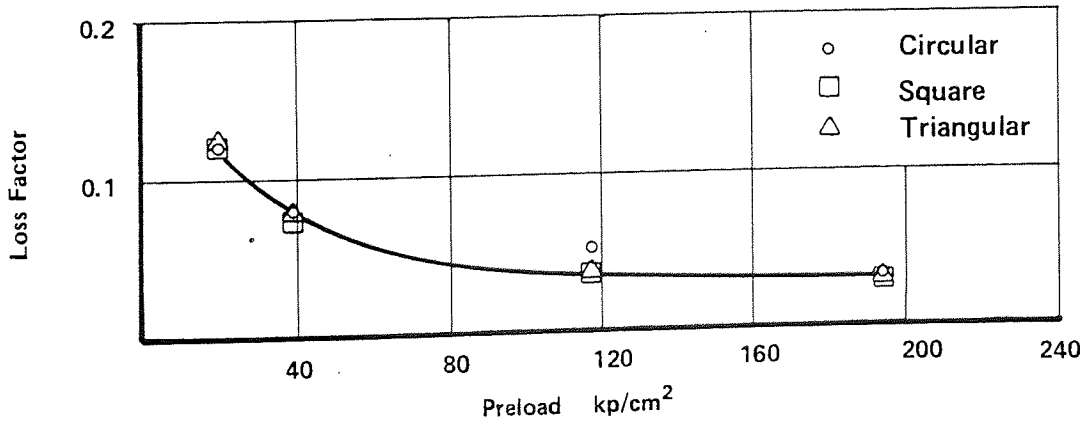

Fig. 91 Effect of planform shapes on the loss factor of lubricated joints

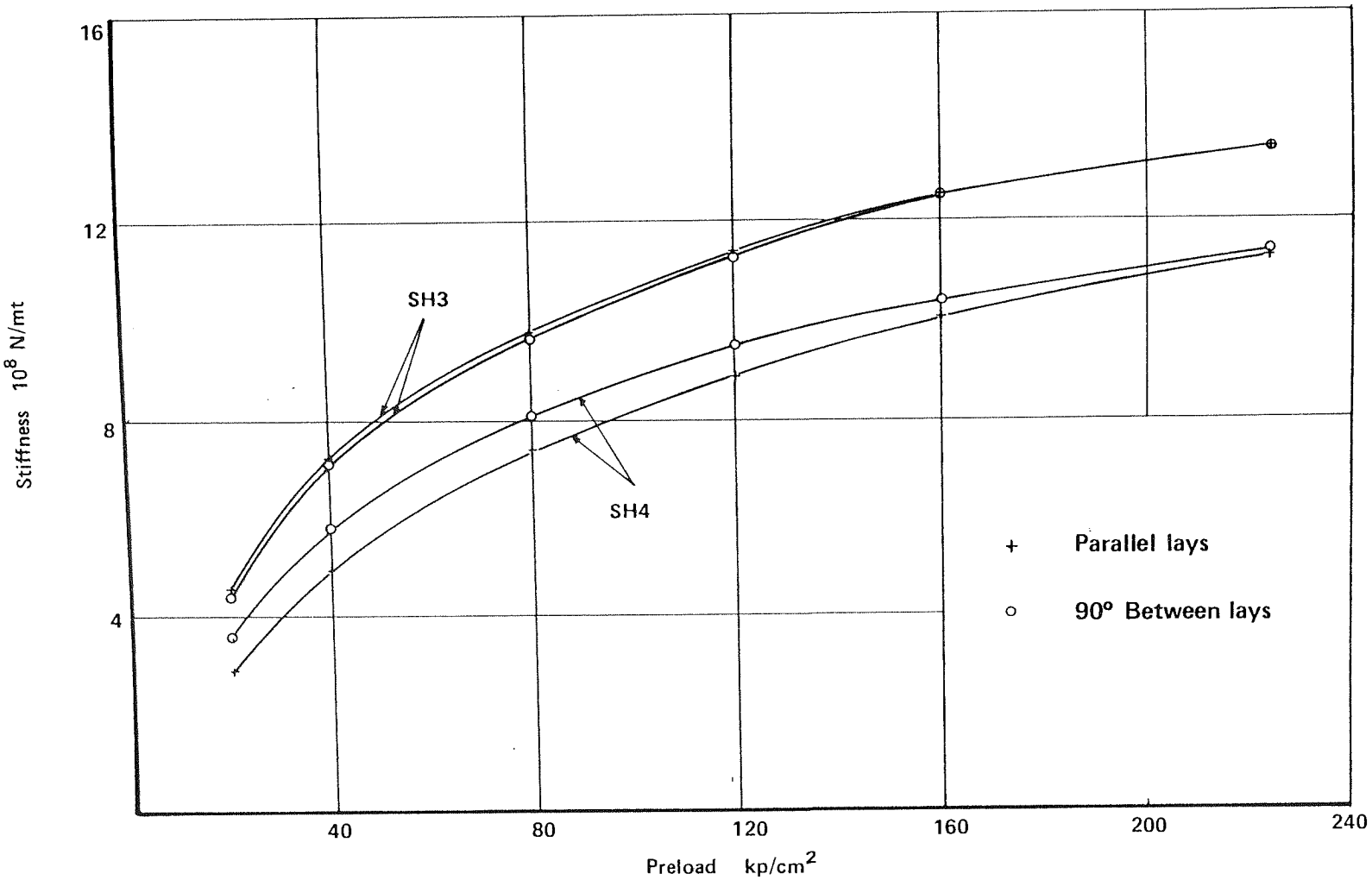

Fig. 92 Influence of direction of lays

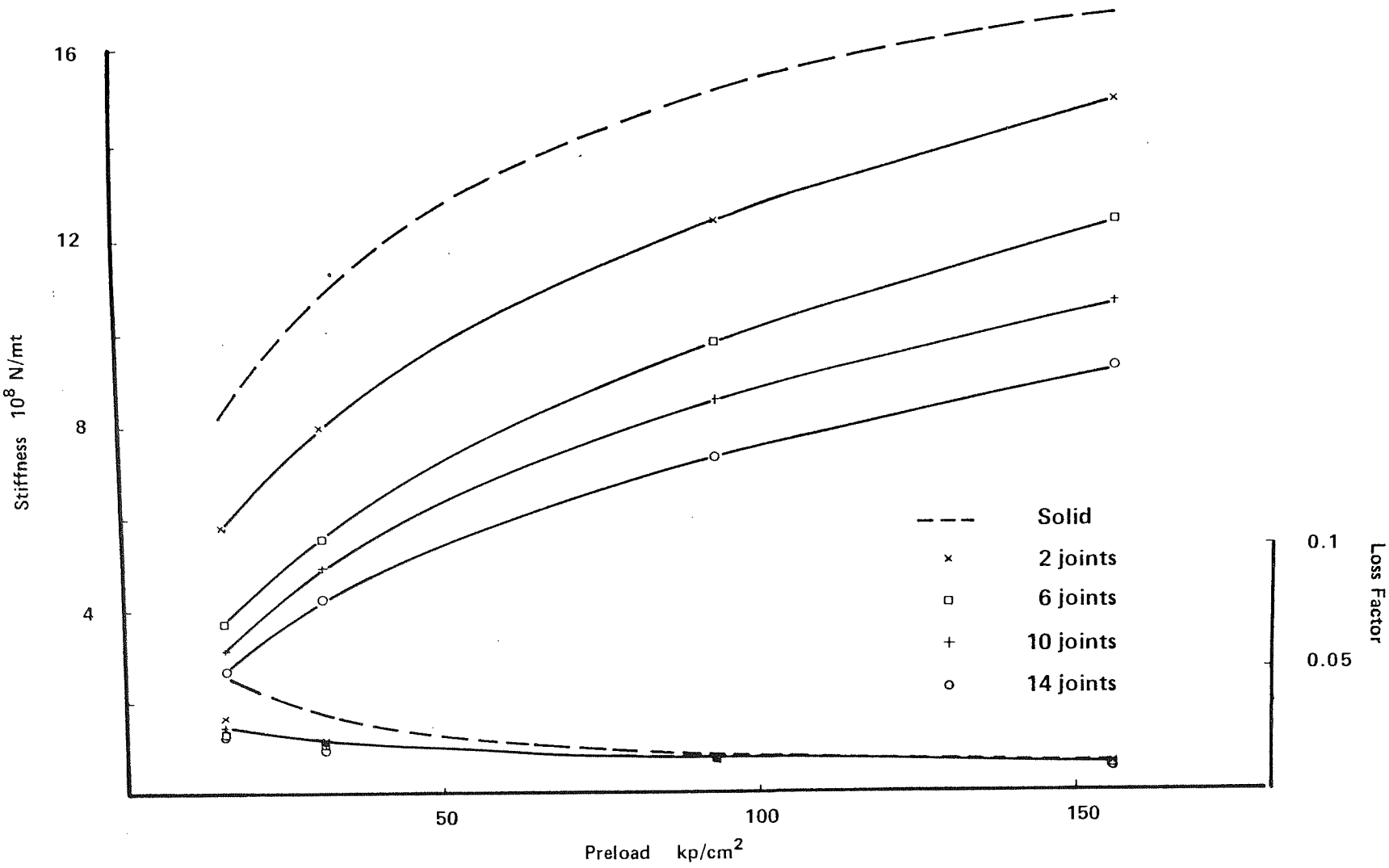

Fig. 93 Effect of number of joints in a fixed jointed column length

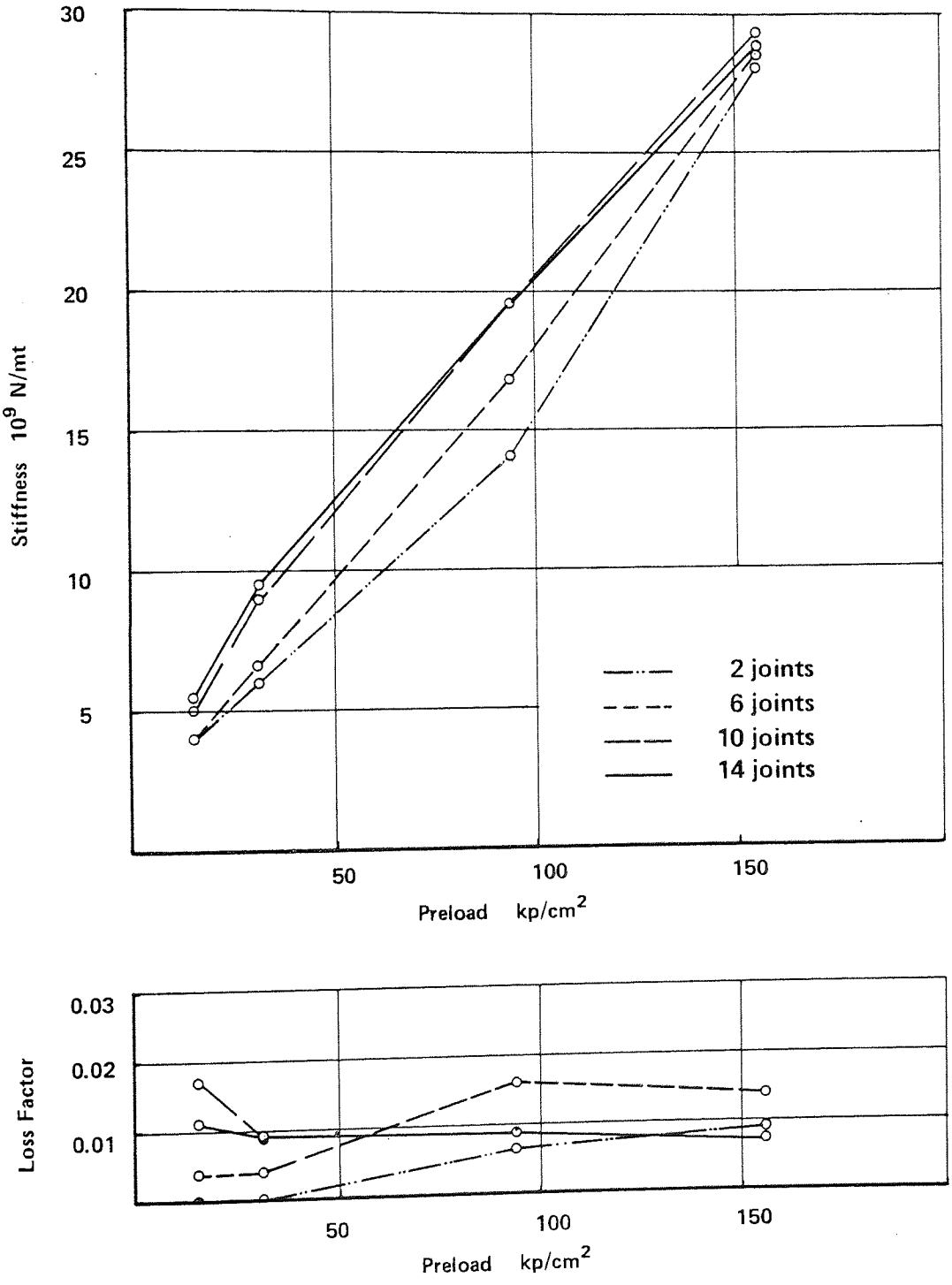

Fig. 94 The stiffness and loss factor of a single joint as the number of joints tested varies

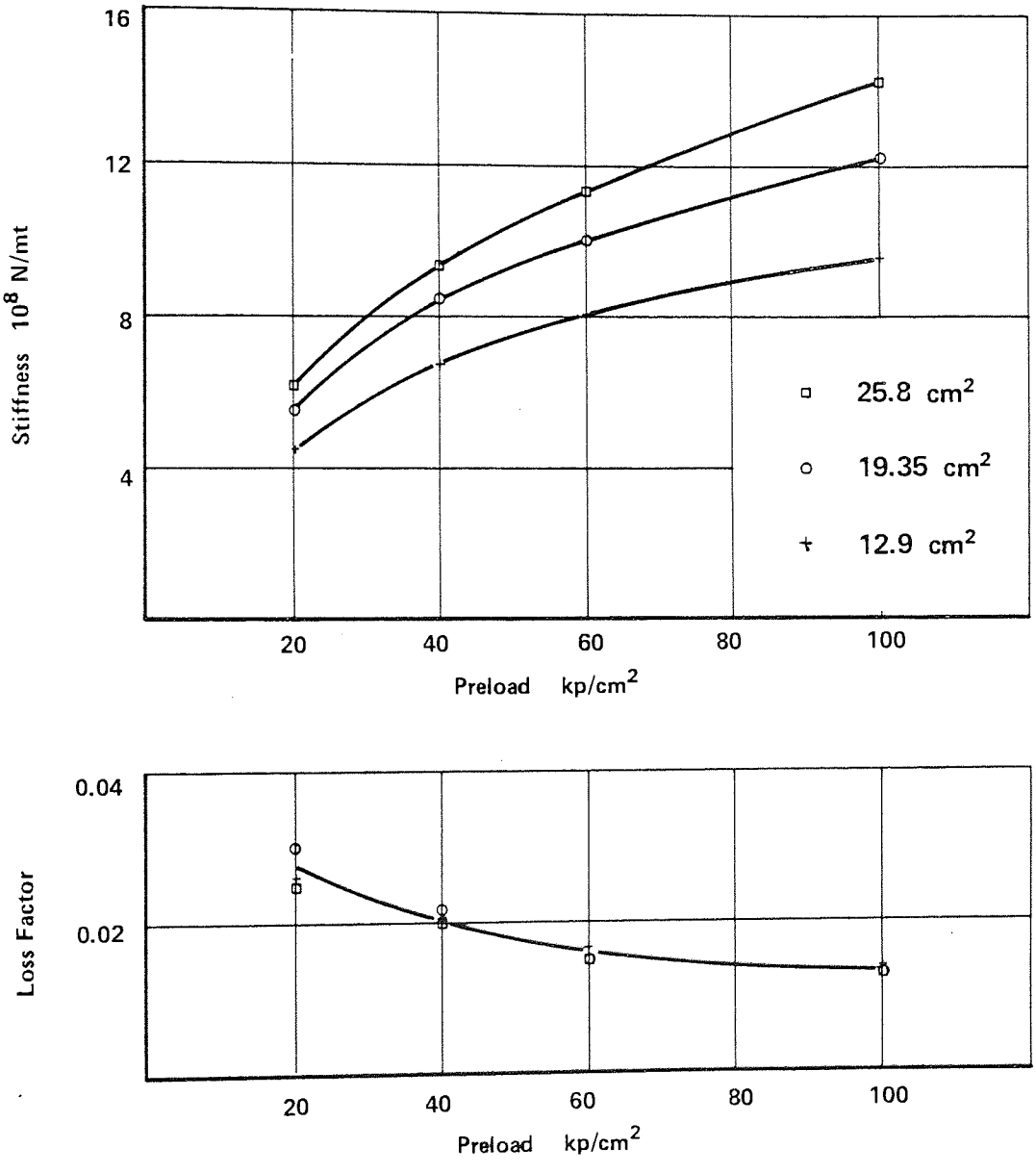

Fig. 95 Stiffness and loss factor of jointed columns (effect of the apparent area of contact)

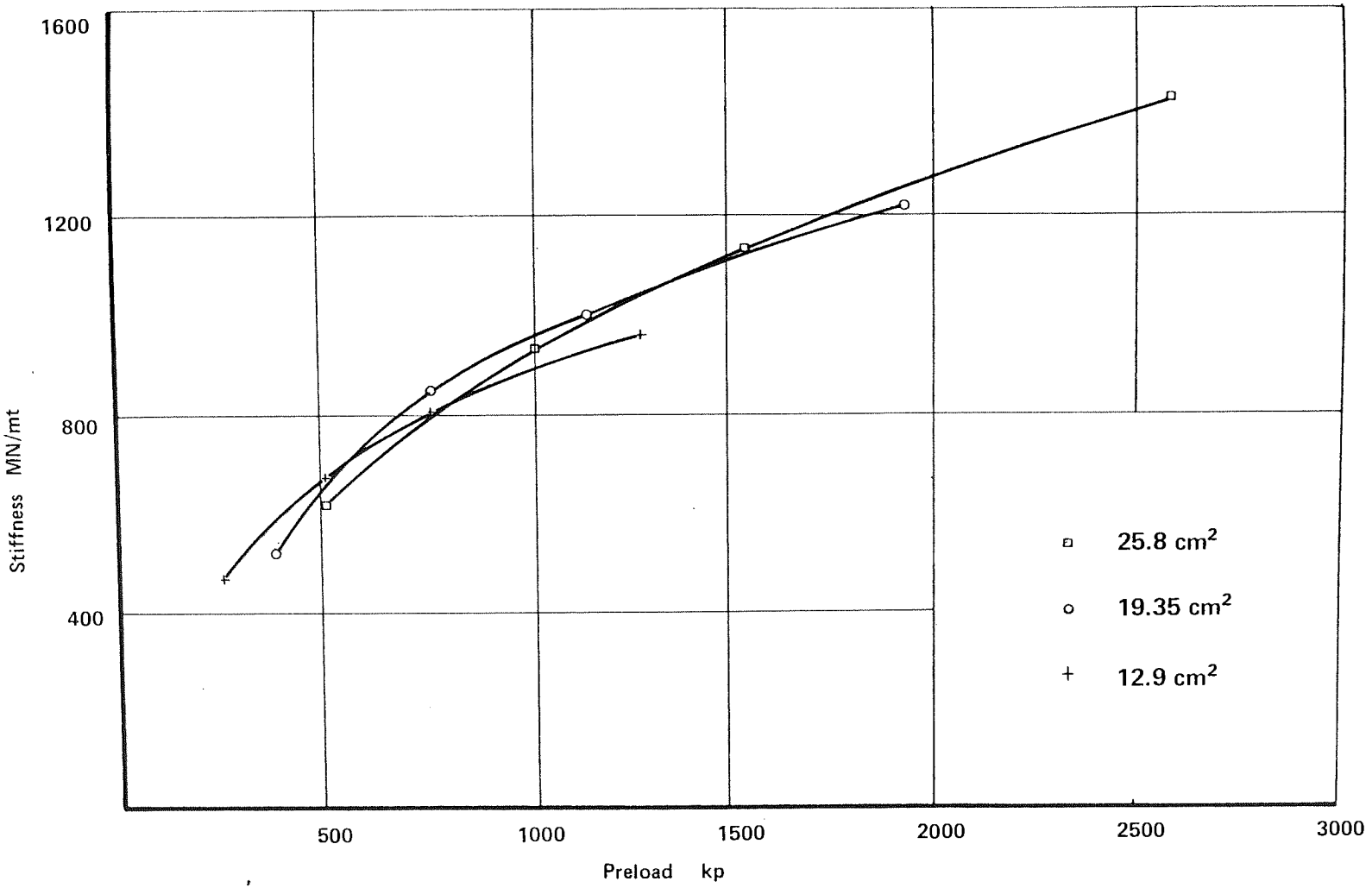

Fig. 96 Stiffness of jointed column versus preload in kp
(effect of the apparent area of contact)

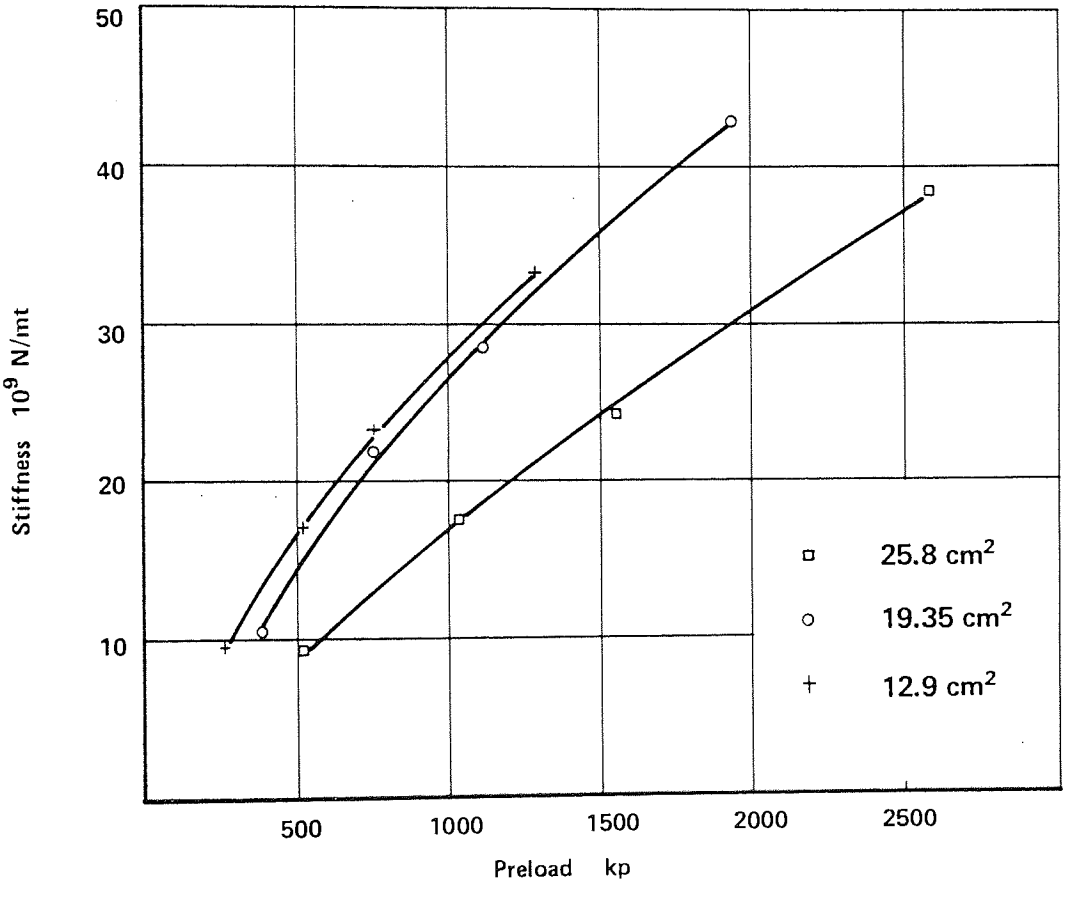

Fig. 97 Effect of apparent area of contact on the dynamic stiffness of joints

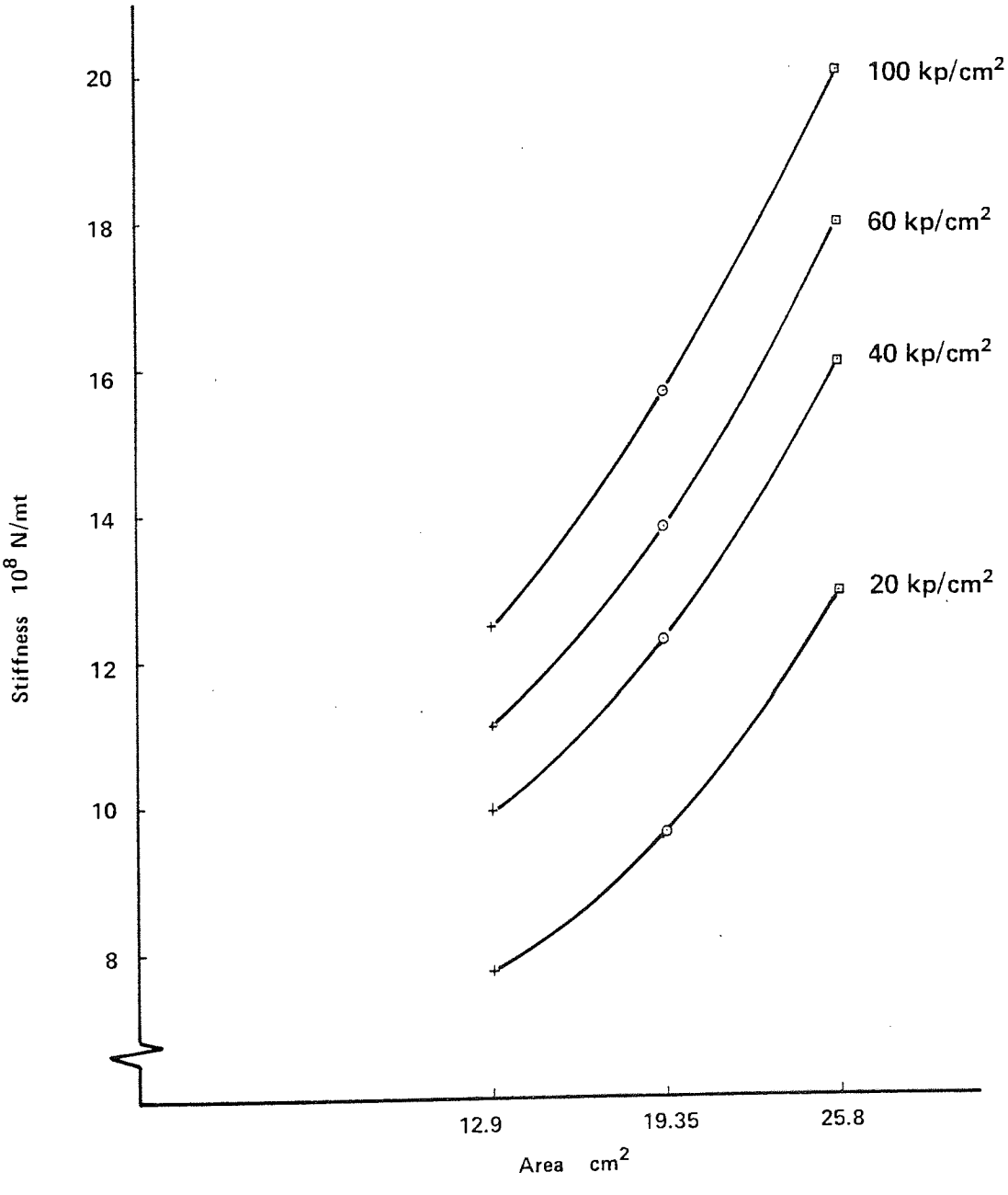

Fig. 98 Stiffness of equivalent solid columns versus area

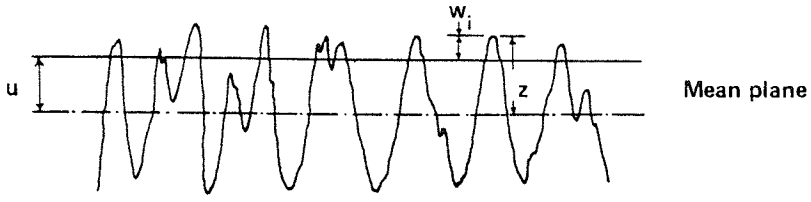

Fig. 99 Contact between a rough surface and a plane

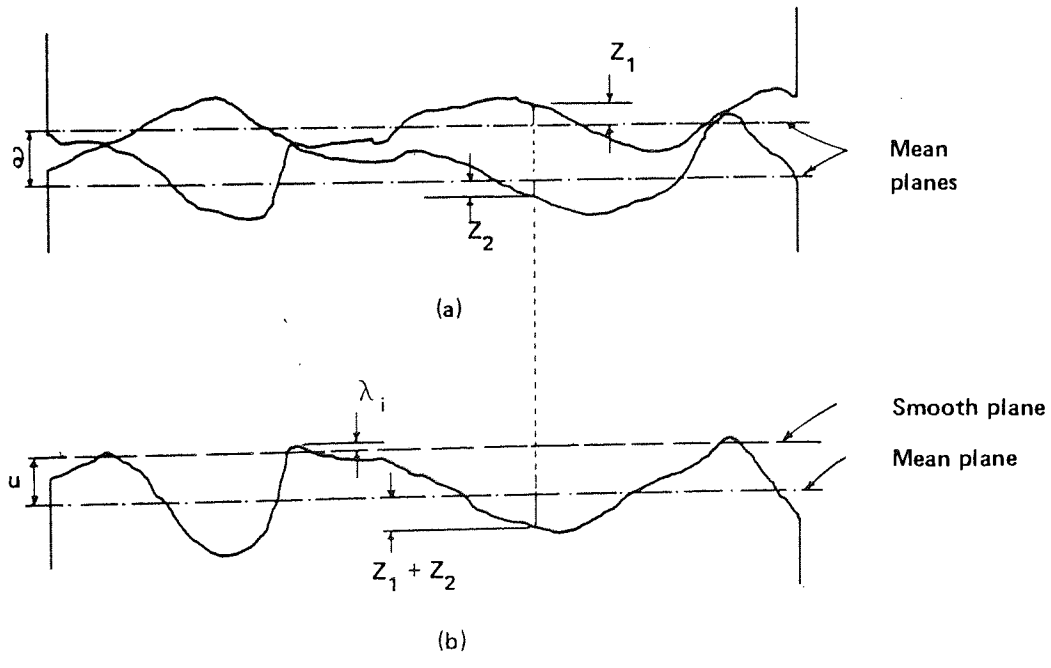

Fig. 100 Contact between unflat surfaces
a. Two unflat surfaces in contact
b. Equivalent contact for the sufaces in (a)

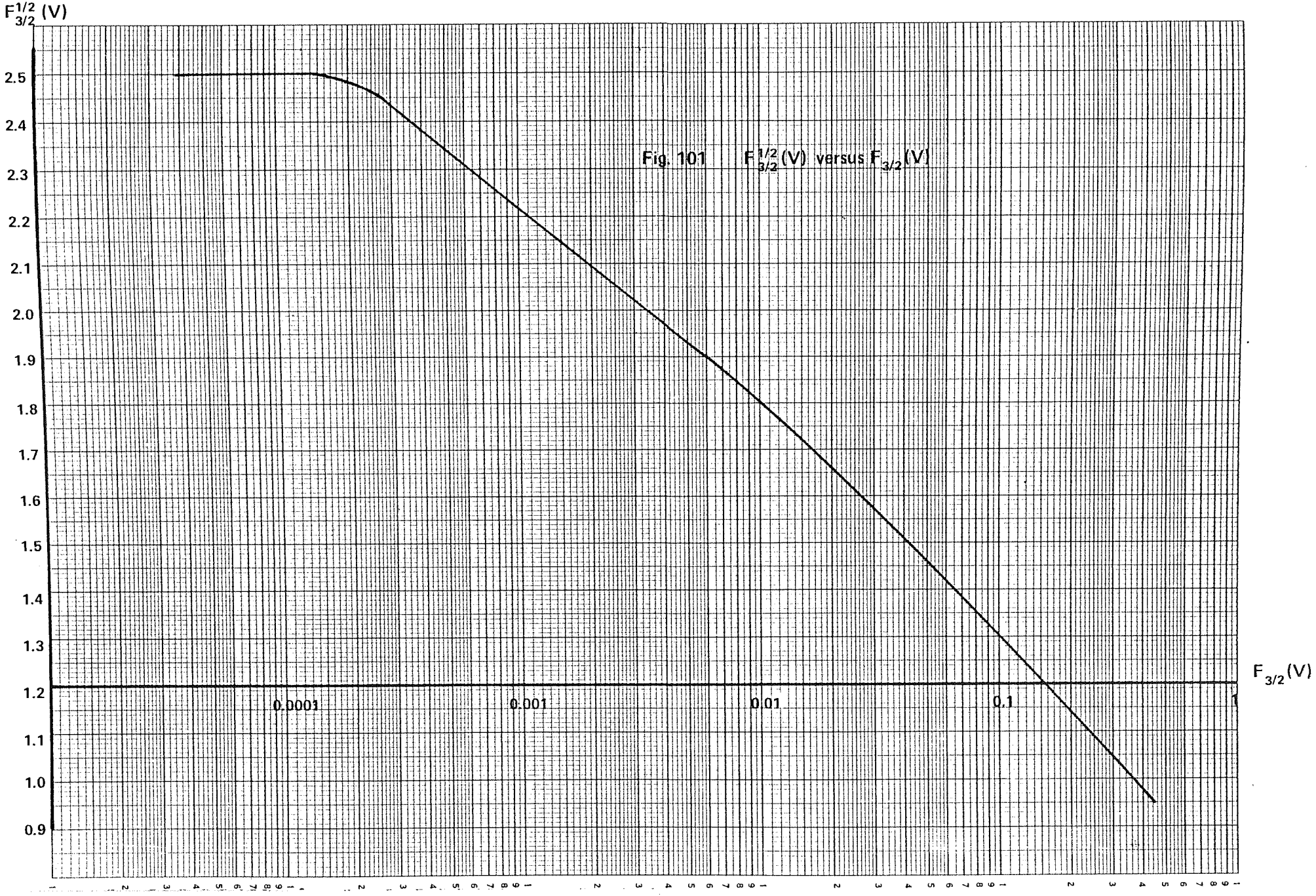

Fig. 101 $F^{1/2}_{3/2}$(V) versus $F_{3/2}$(V)

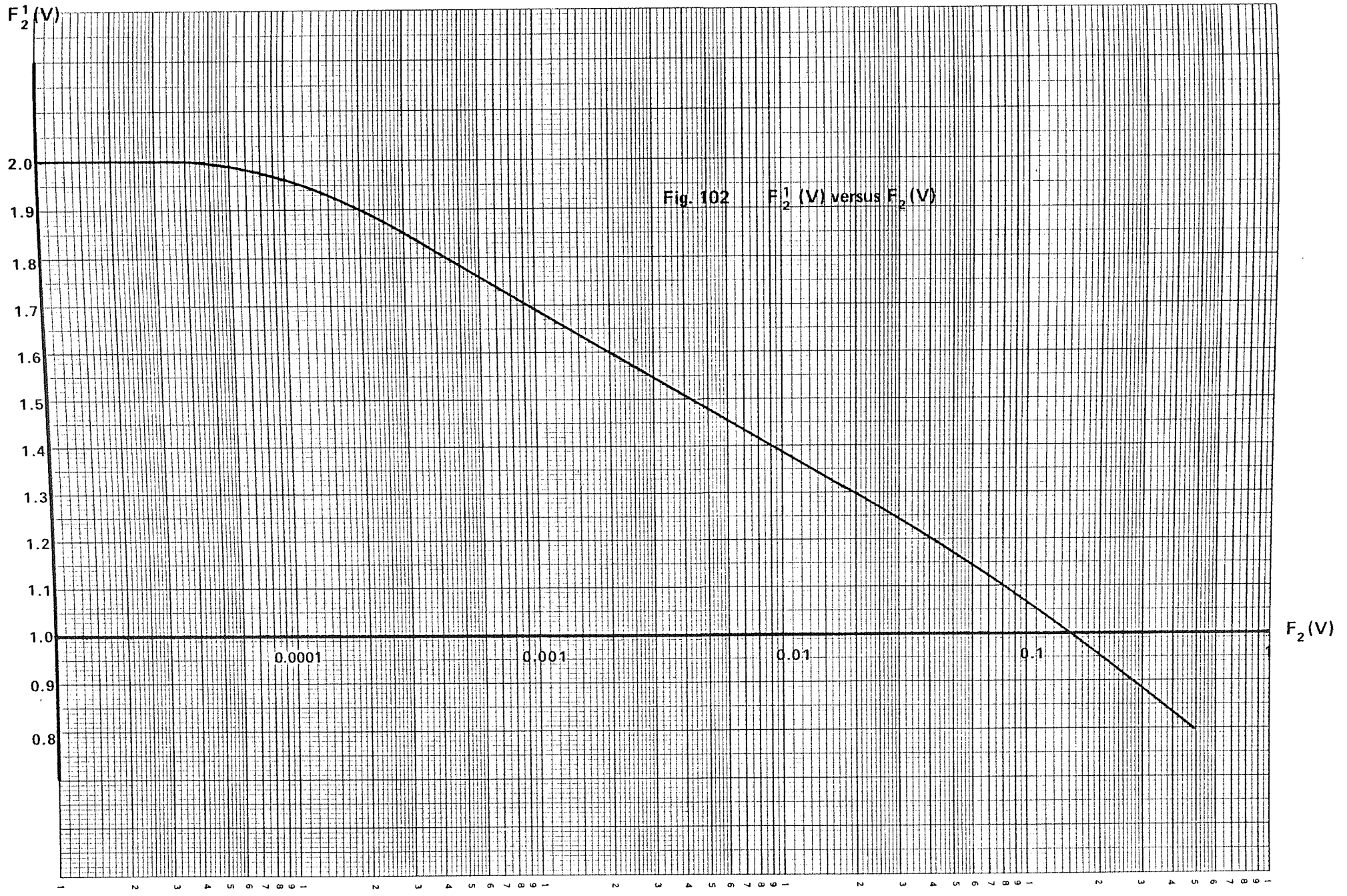

Fig. 102 F_2^1 (V) versus F_2 (V)

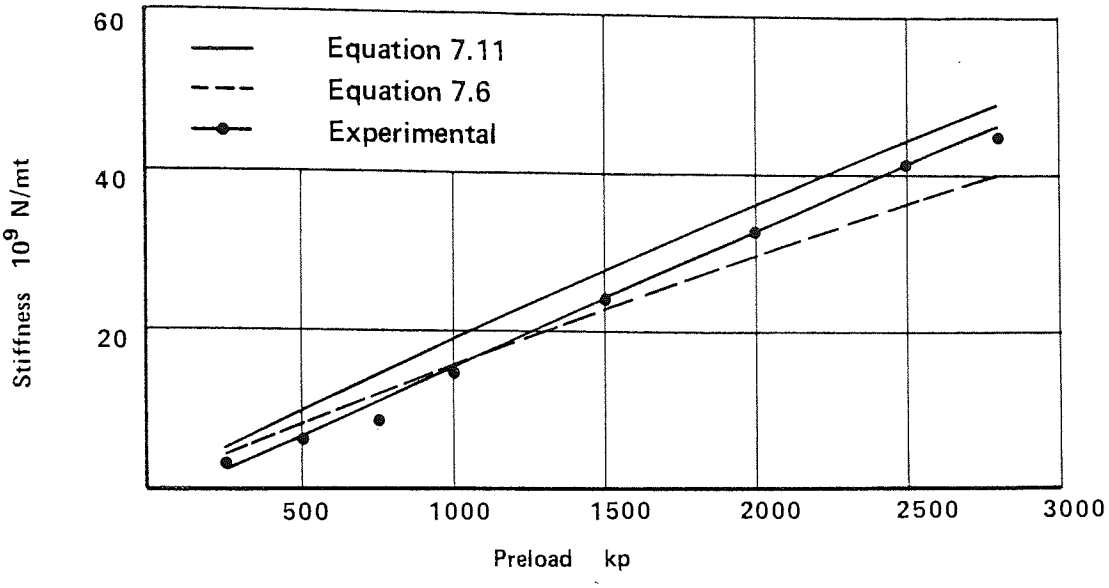

Fig. 103 Experimental and theoretical stiffness of ML1 joint

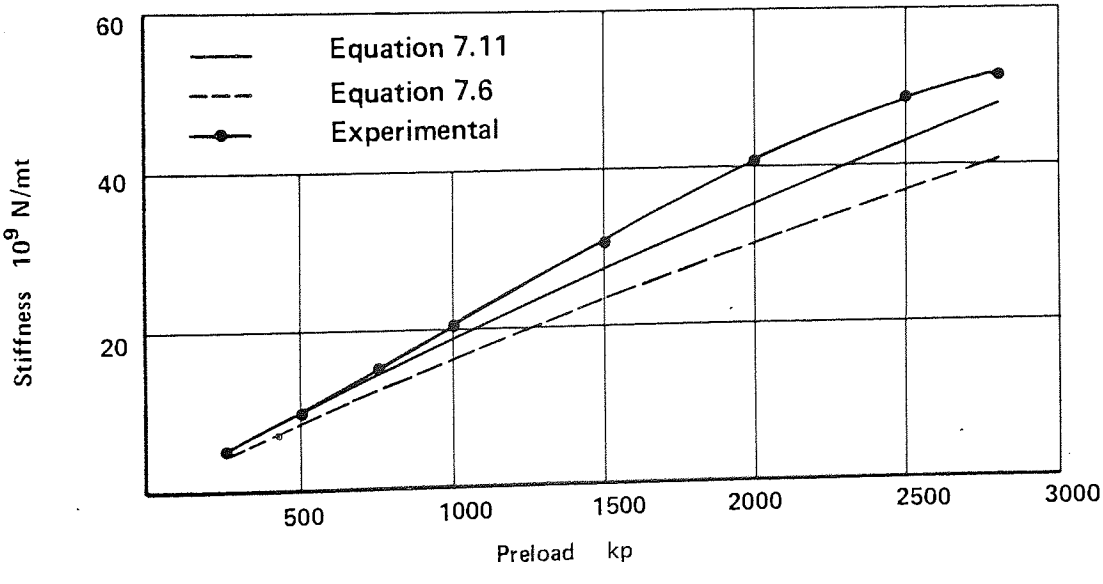

Fig. 104 Experimental and theoretical stiffness of ML2 joint

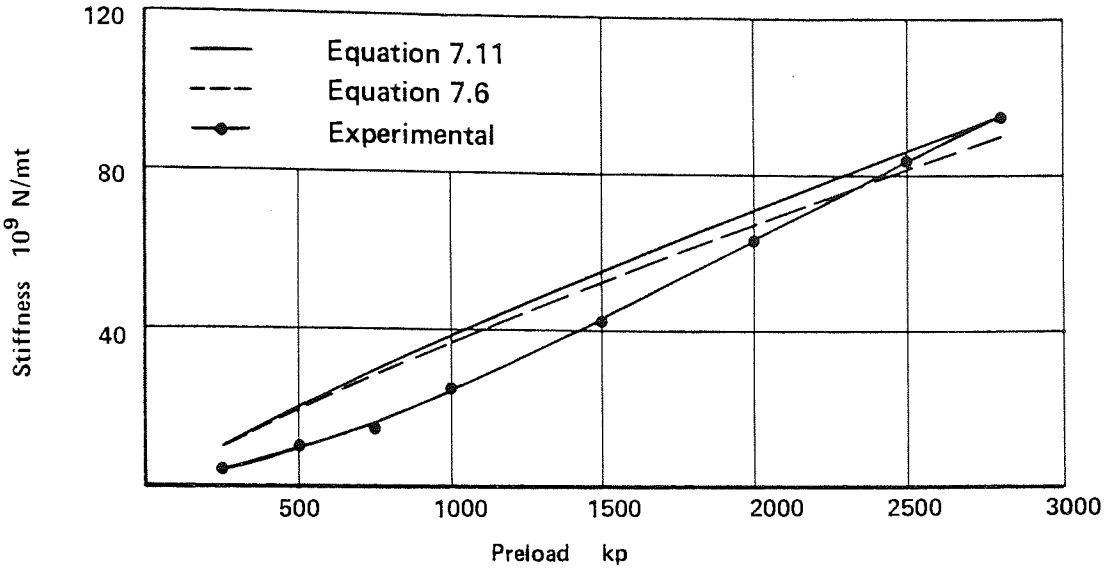

Fig. 105 Experimental and theoretical stiffness of ML3 joint

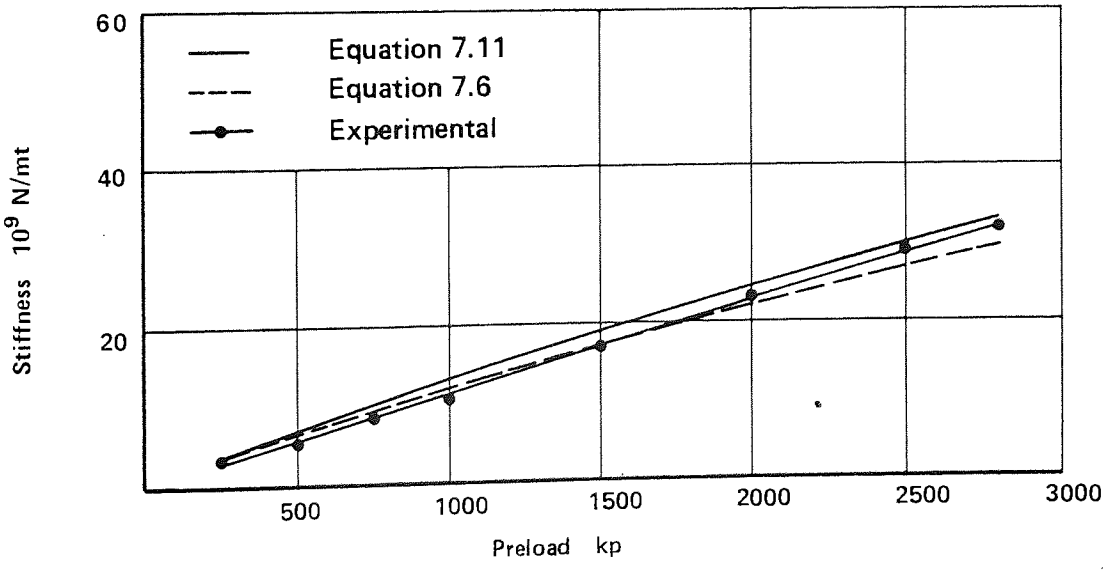

Fig. 106 Experimental and theoretical stiffness of ML4 joint

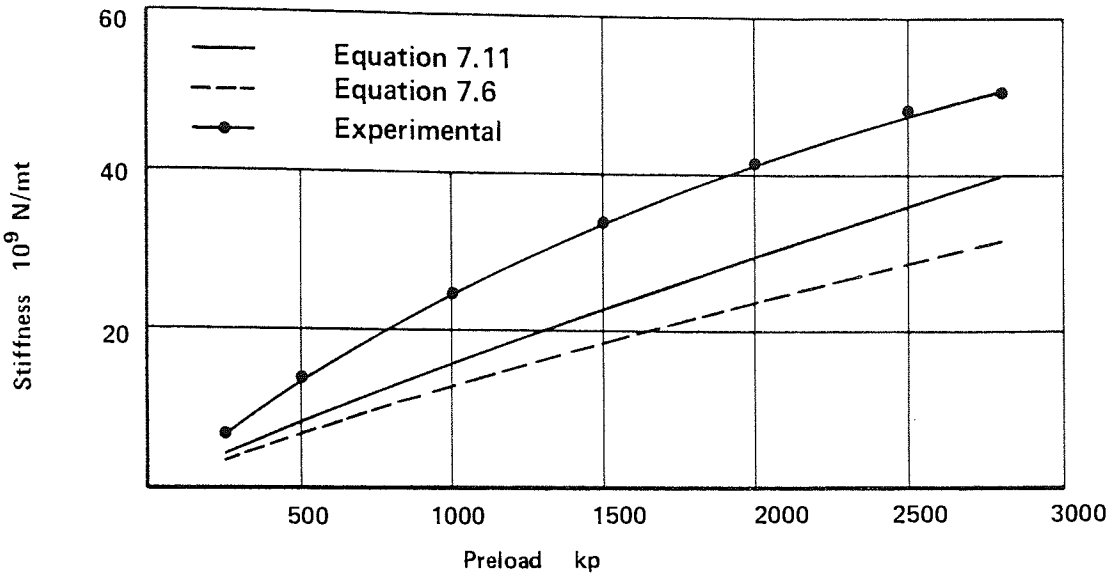

Fig. 107 Experimental and theoretical stiffness of SH1 joint

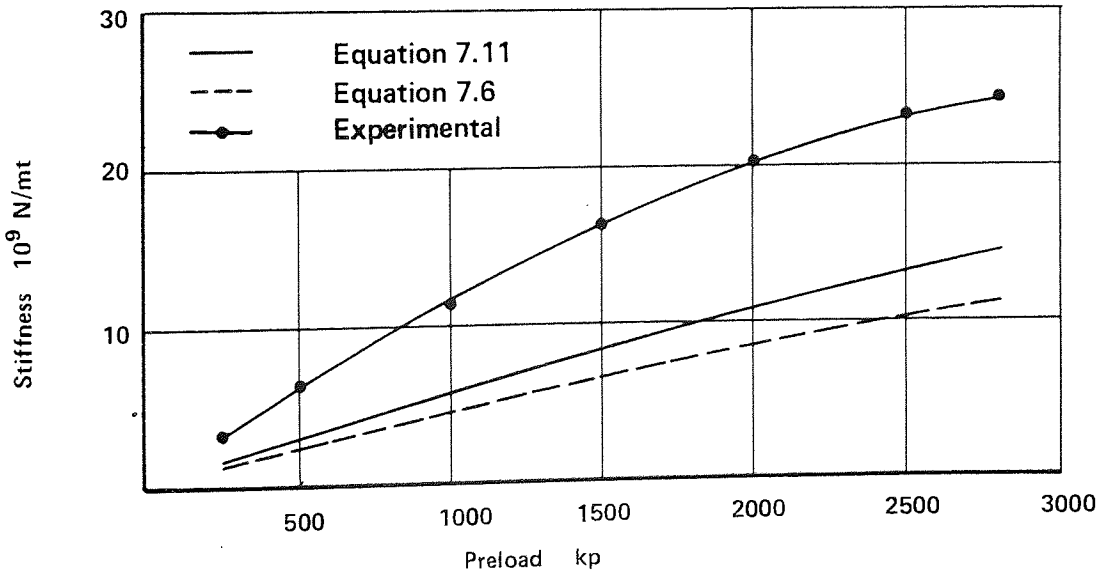

Fig. 108 Experimental and theoretical stiffness of SH2 joint

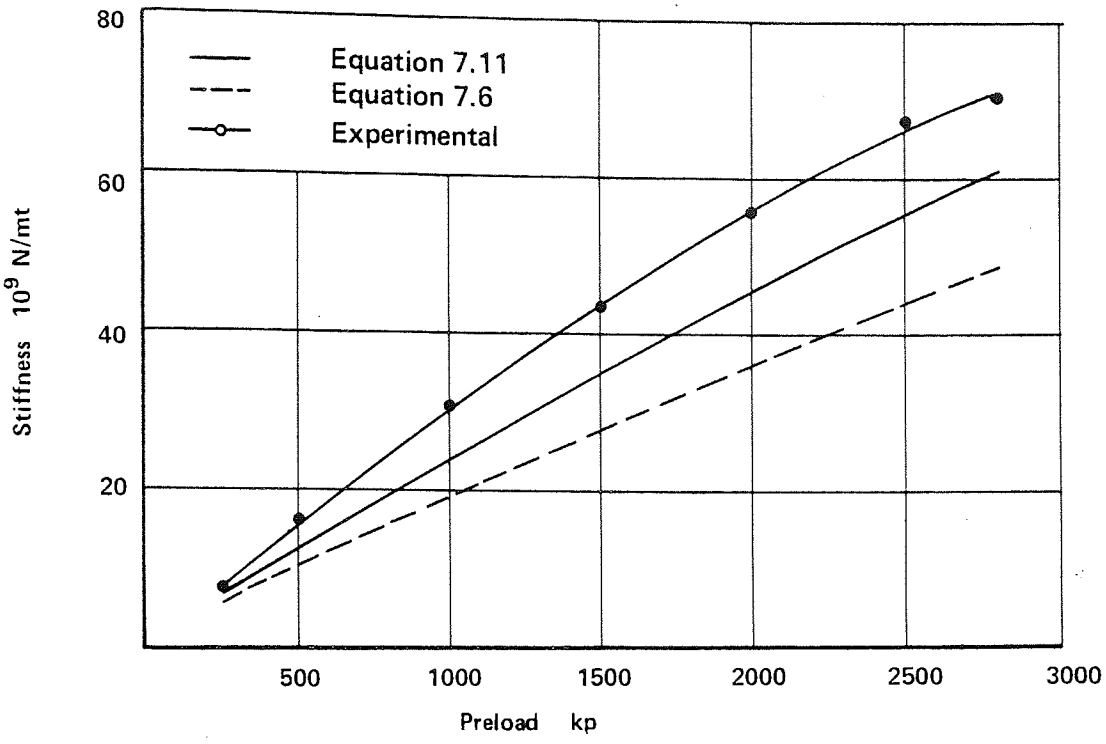

Fig. 109 Experimental and theoretical stiffness of SH3 joint

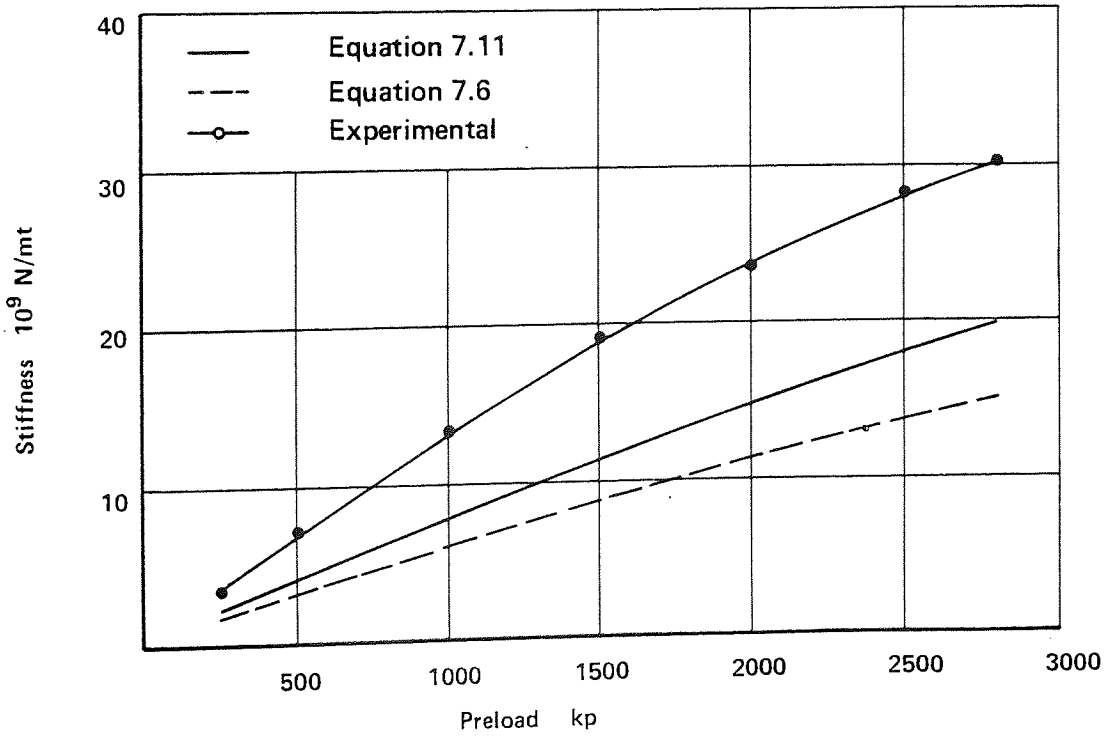

Fig. 110 Experimental and theoretical stiffness of SH4 joint

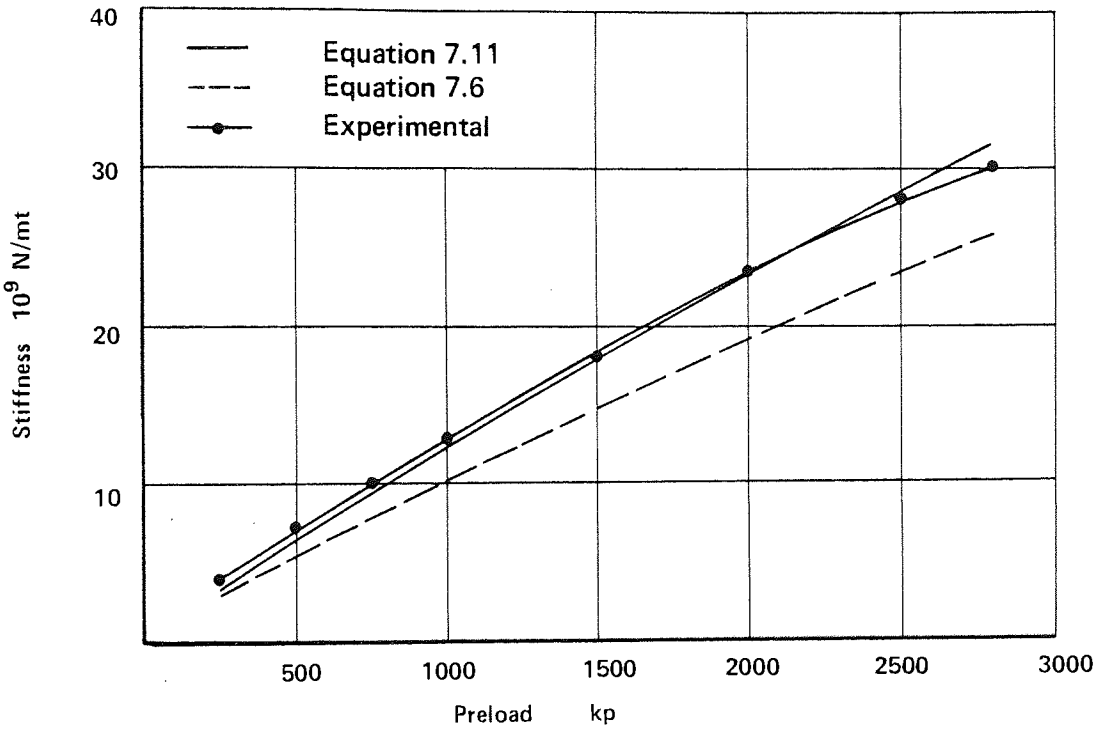

Fig. 111 Experimental and theoretical stiffness of SH5 joint

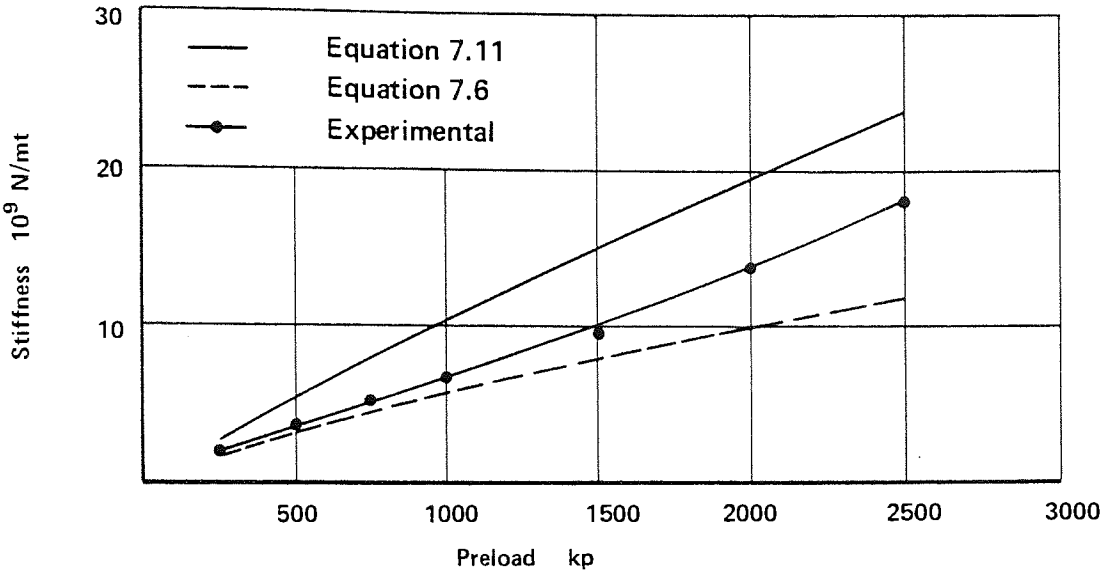

Fig. 112 Experimental and theoretical stiffness of TN1 joint

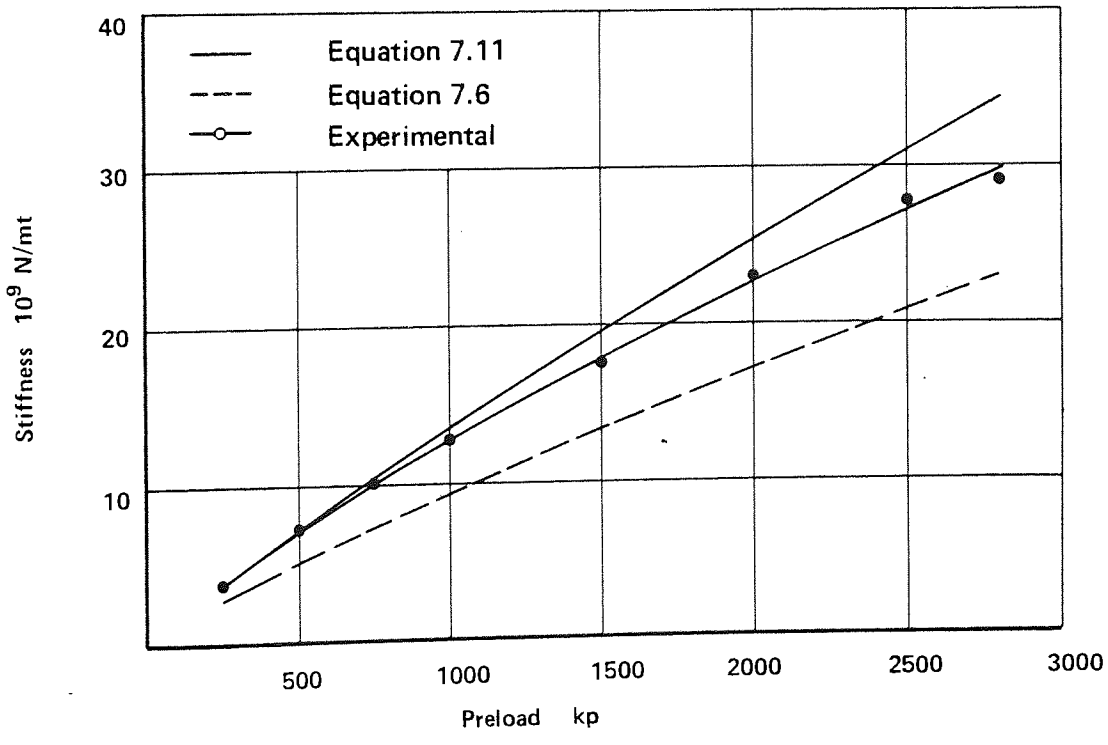

Fig. 113 Experimental and theoretical stiffness of TN2 joint

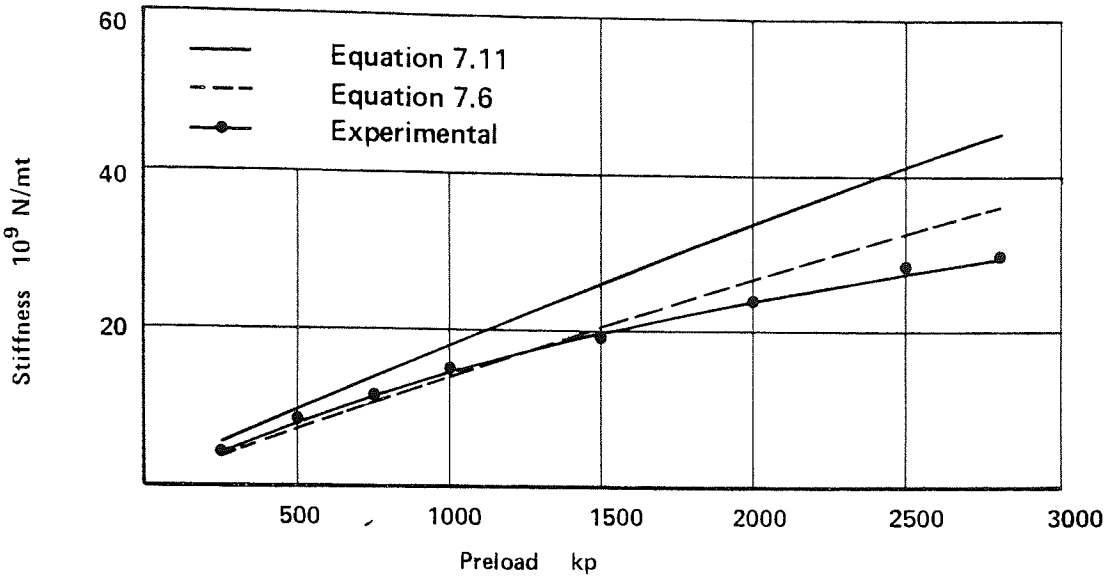

Fig. 114 Experimental and theoretical stiffness of TN3 joint

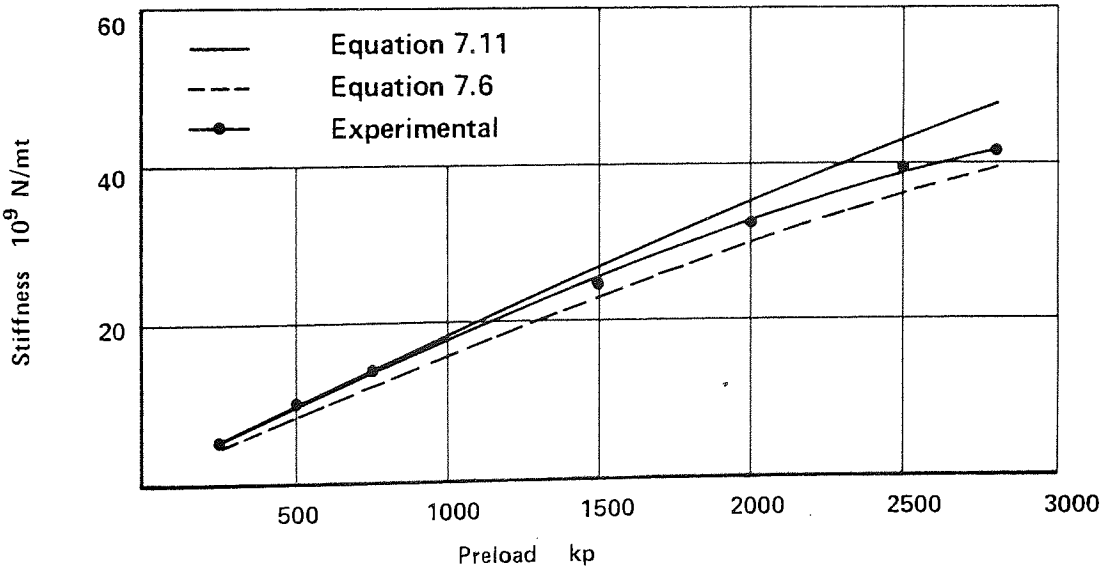

Fig. 115 Experimental and theoretical stiffness of TN4 joint

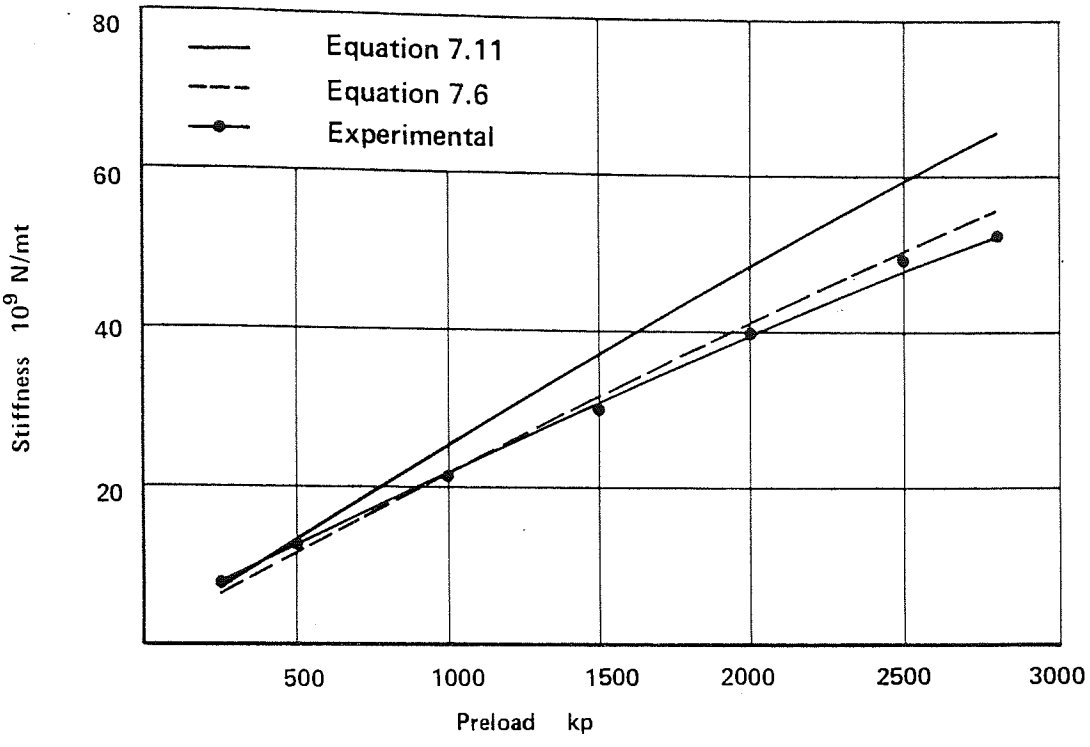

Fig. 116 Experimental and theoretical stiffness of GN1 joint

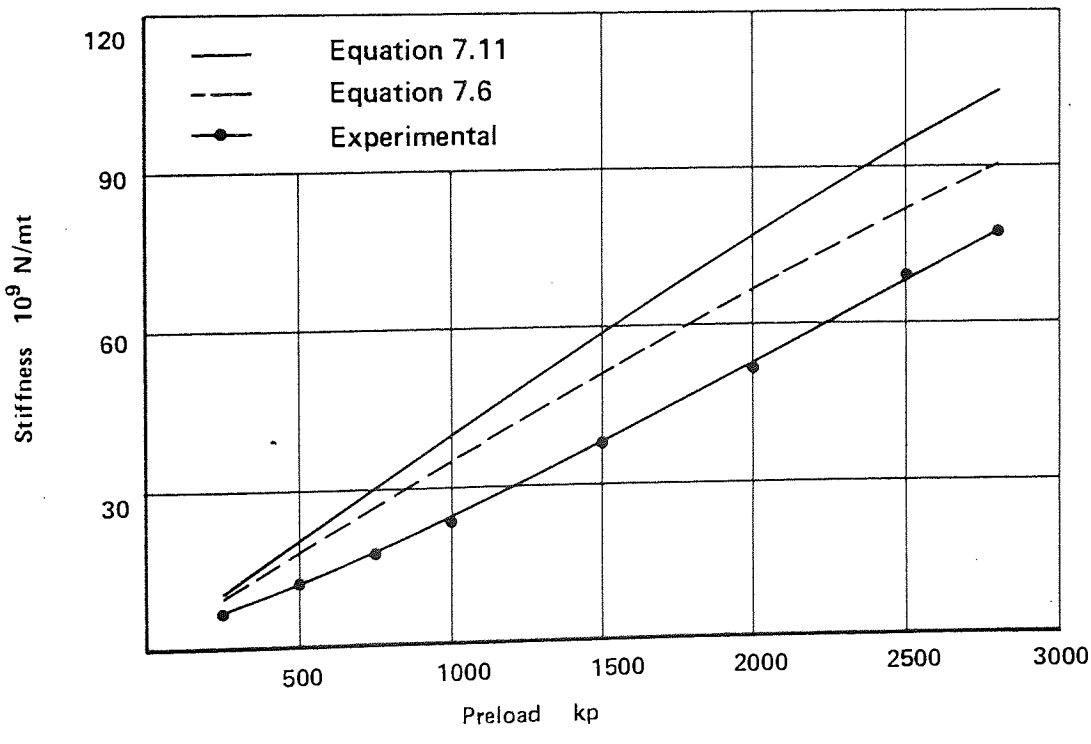

Fig. 117 Experimental and theoretical stiffness of GN2 joint

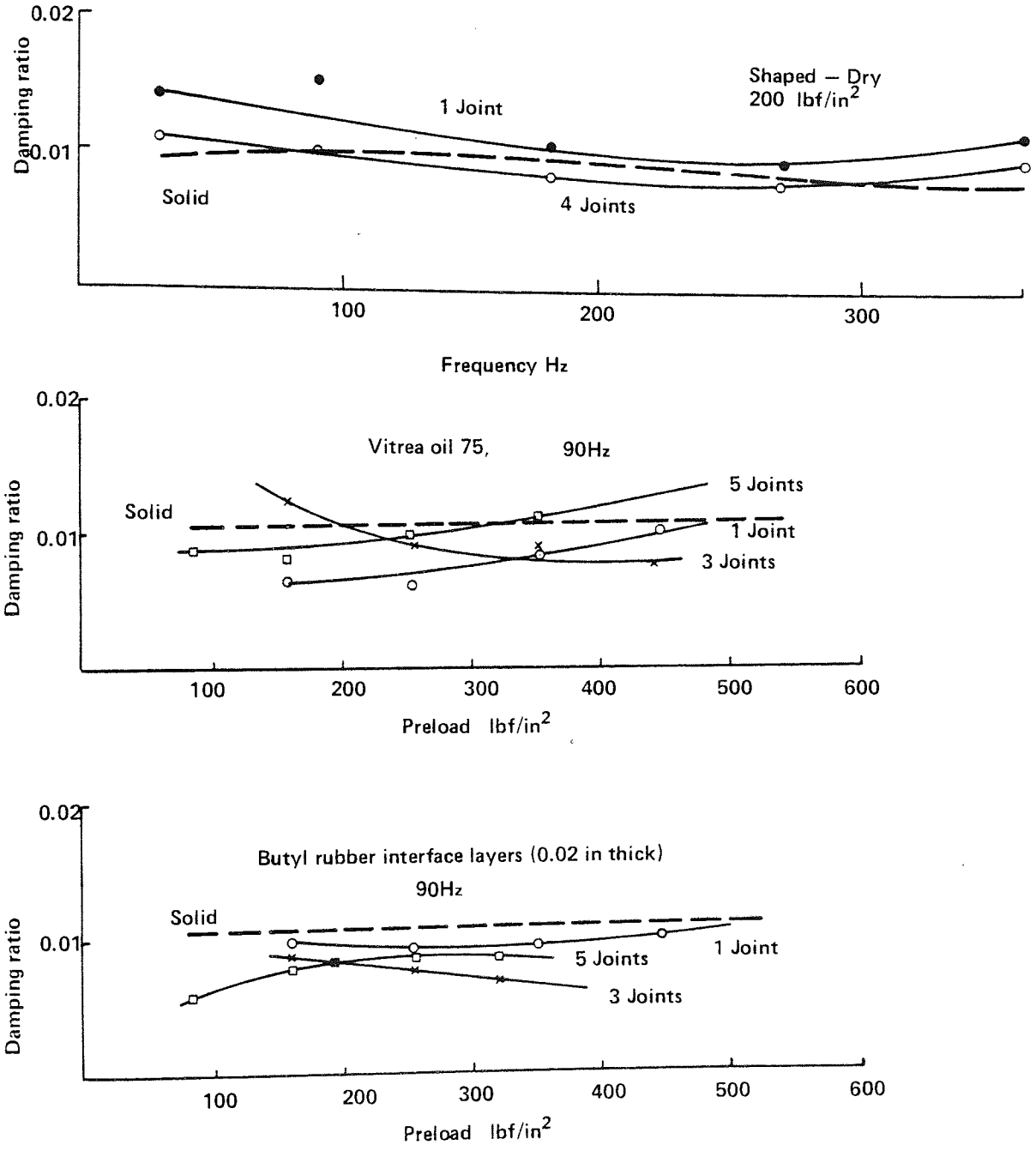

Fig. 118 Some results from reference (28)

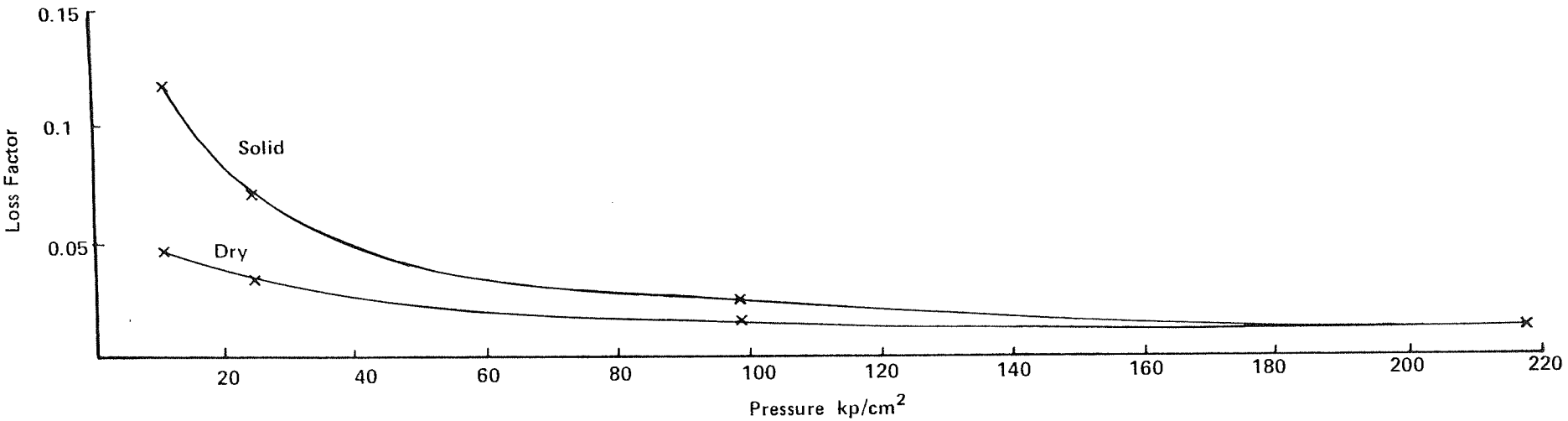

Fig. 119 Mean of loss factors of solid and dry jointed columns
[Khoyi's results (41)]

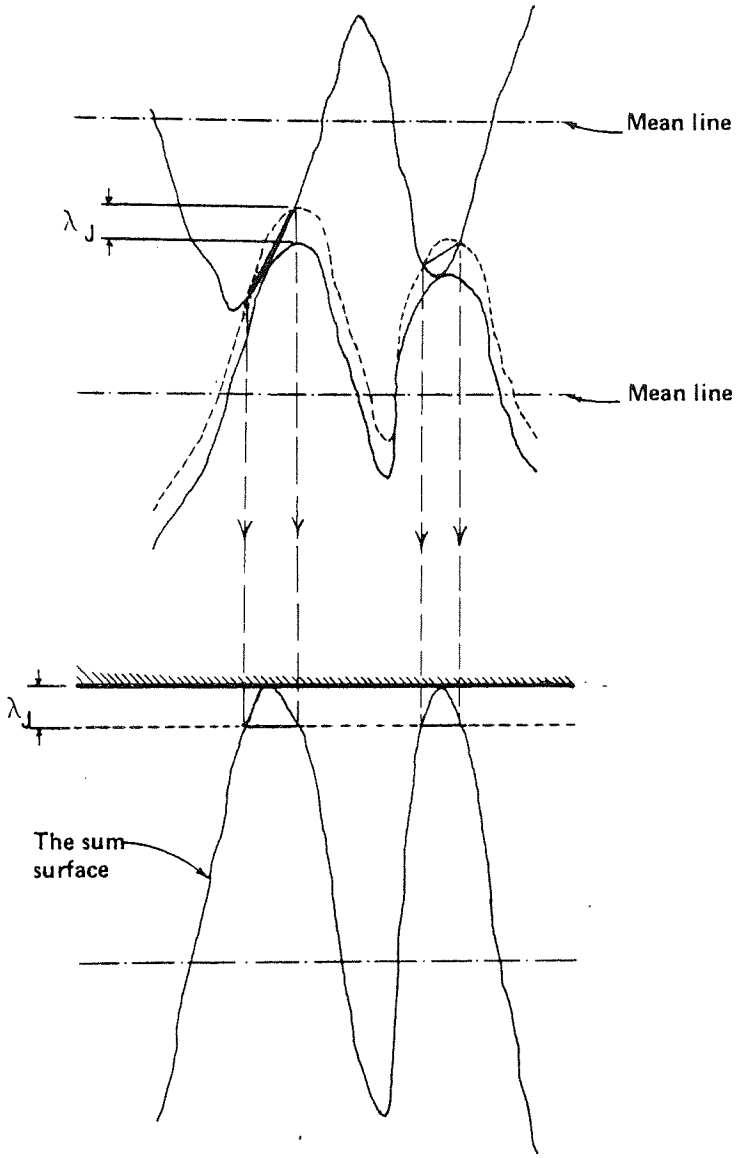

Fig. 120 Simulation of contact between roughness asperities

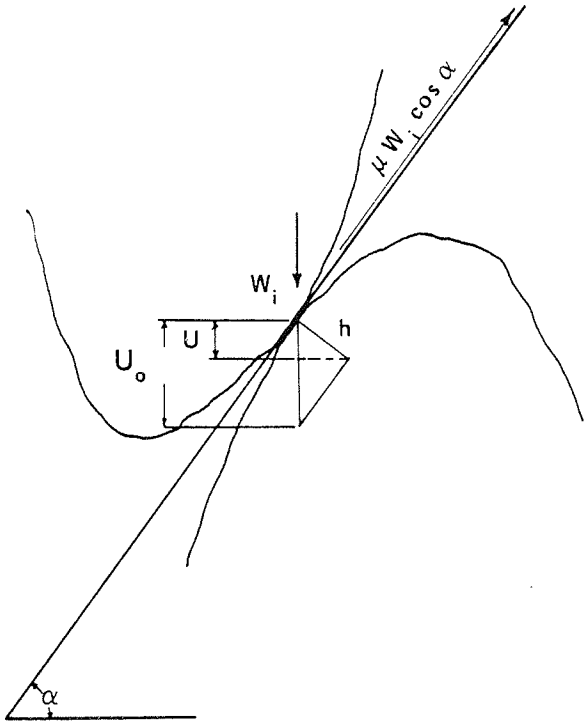

Fig. 121 Contact between two surface roughness asperities

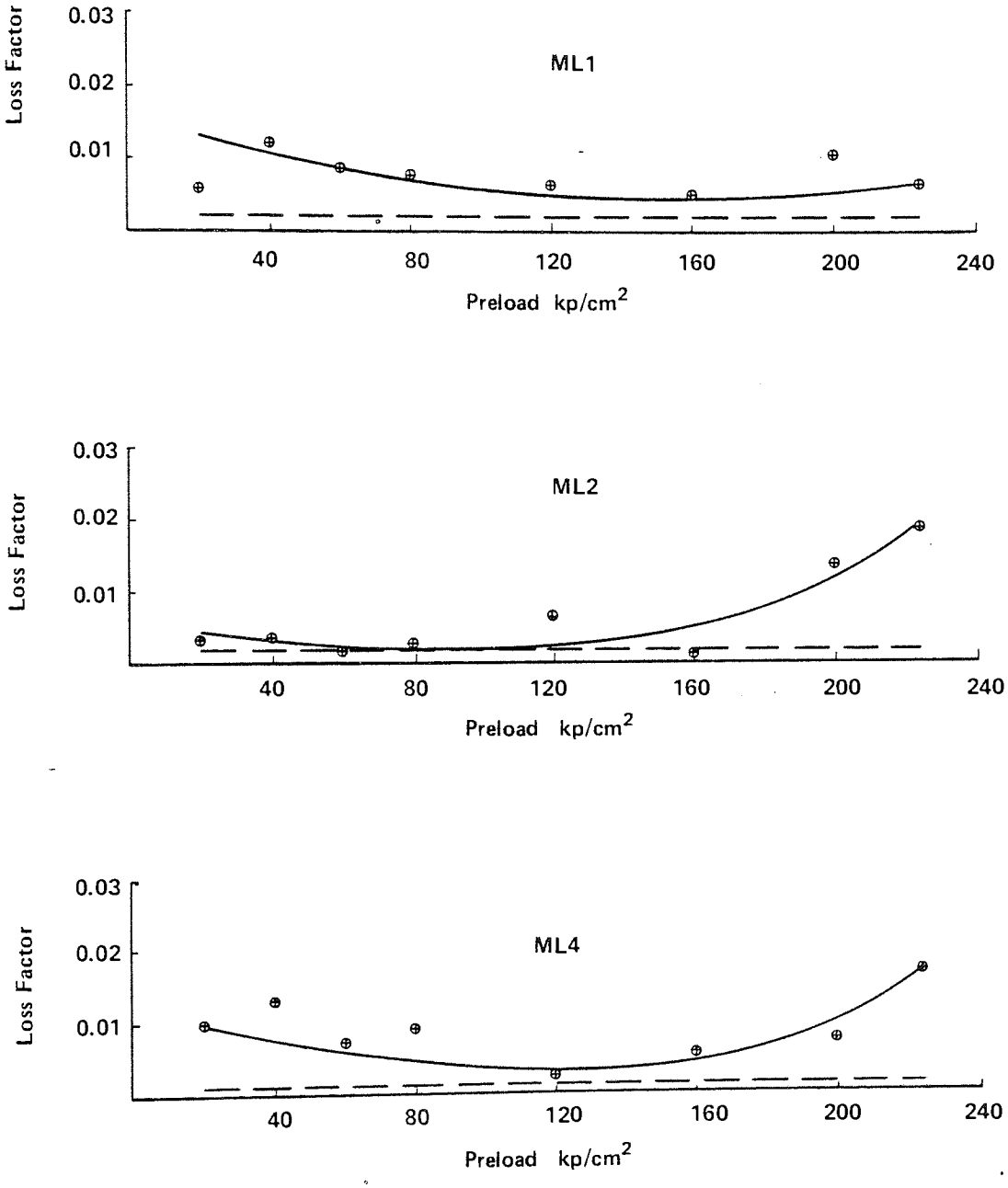

Fig. 122 Theoretical and experimental loss factor for milled joints

—⊕— Experimental

— — Theoretical

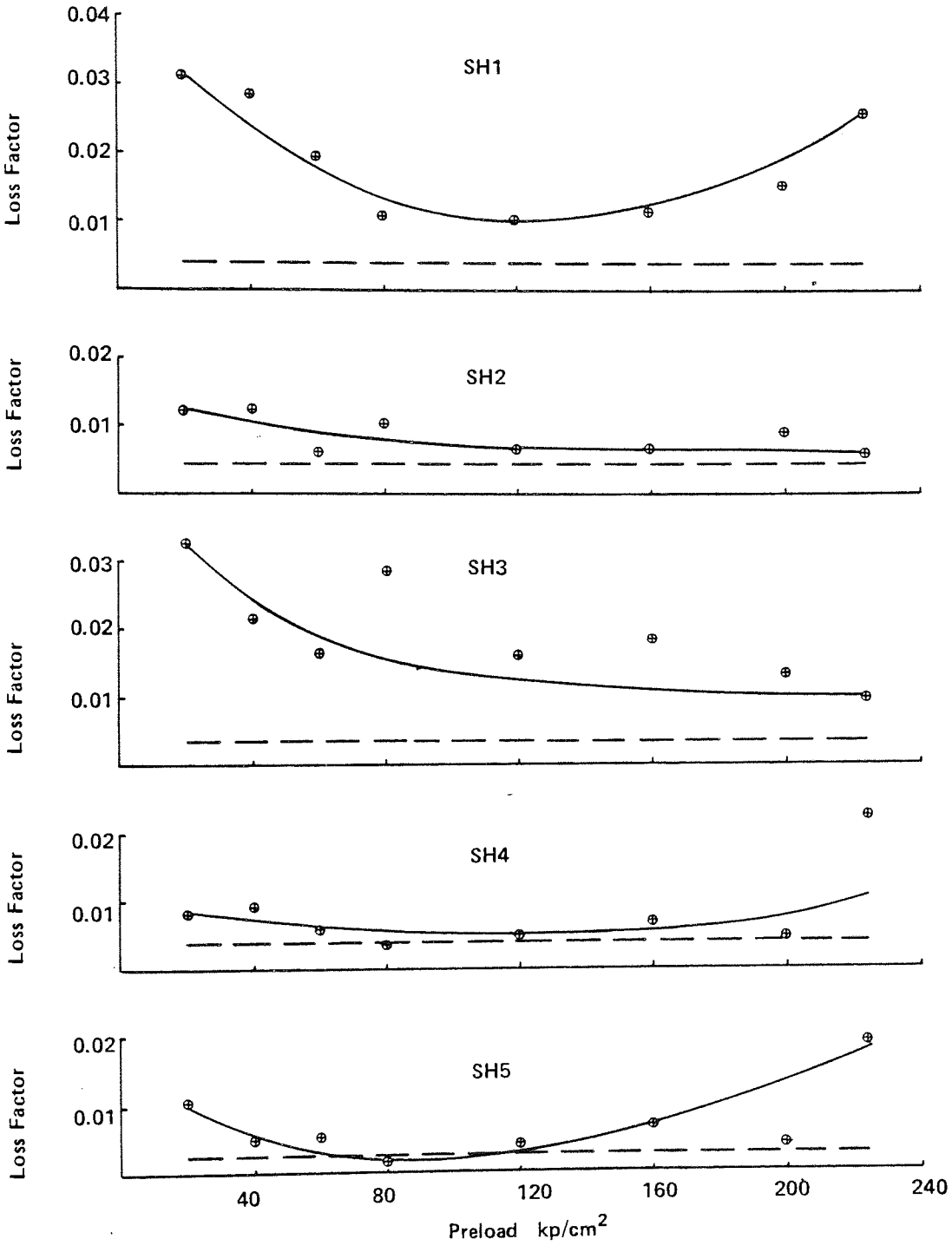

Fig. 123 Theoretical and experimental loss factor for shaped joints

—⊕— Experimental

— — Theoretical

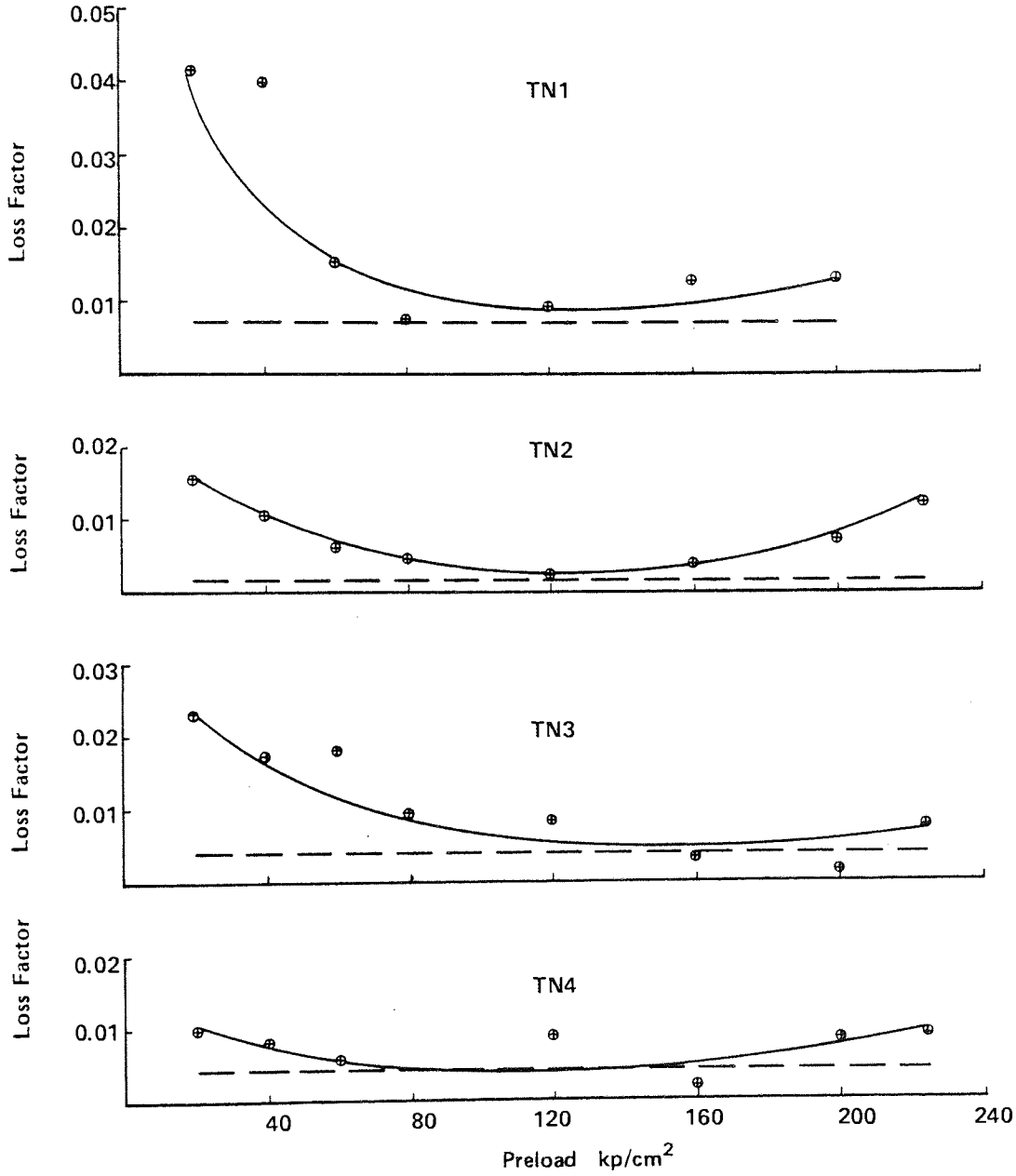

Fig. 124 Theoretical and experimental loss factor for turned joints

—⊕— Experimental

— — Theoretical

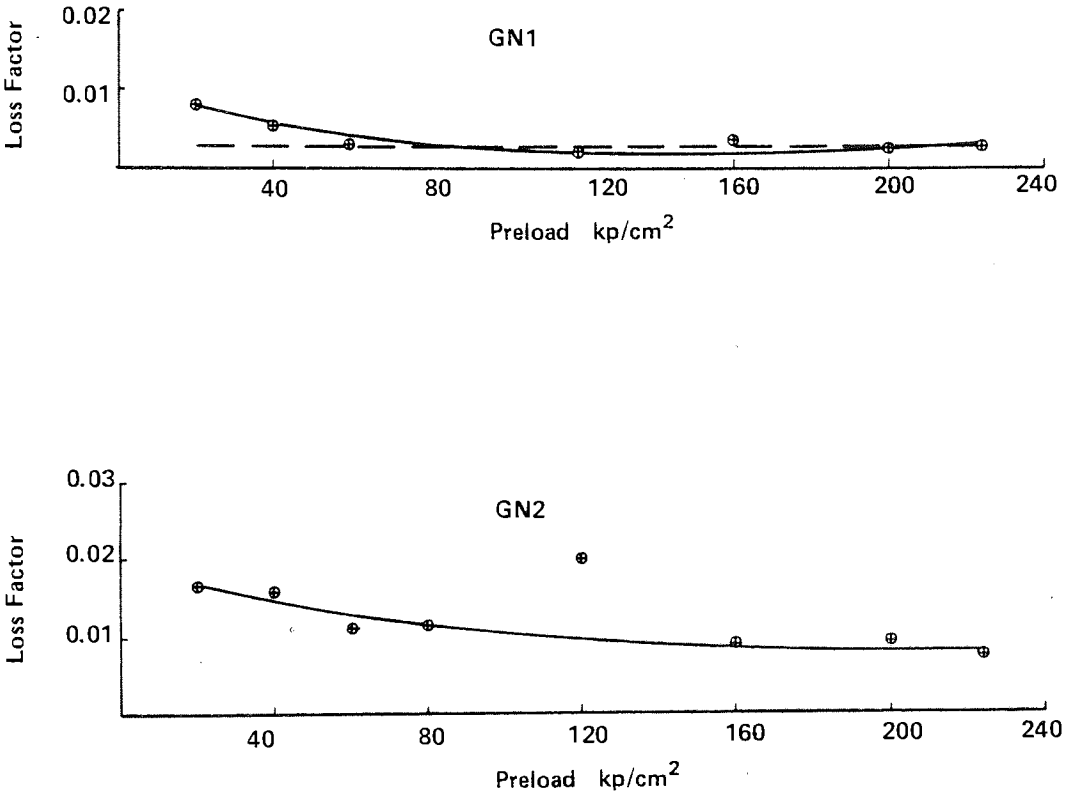

Fig. 125 Theoretical and experimental loss factor for ground joints

—⊕— Experimental

— — Theoretical

Aston University

Content has been removed for copyright reasons

Fig. 126 **Machined surfaces**
(a, b and d are reproduced from reference 92)

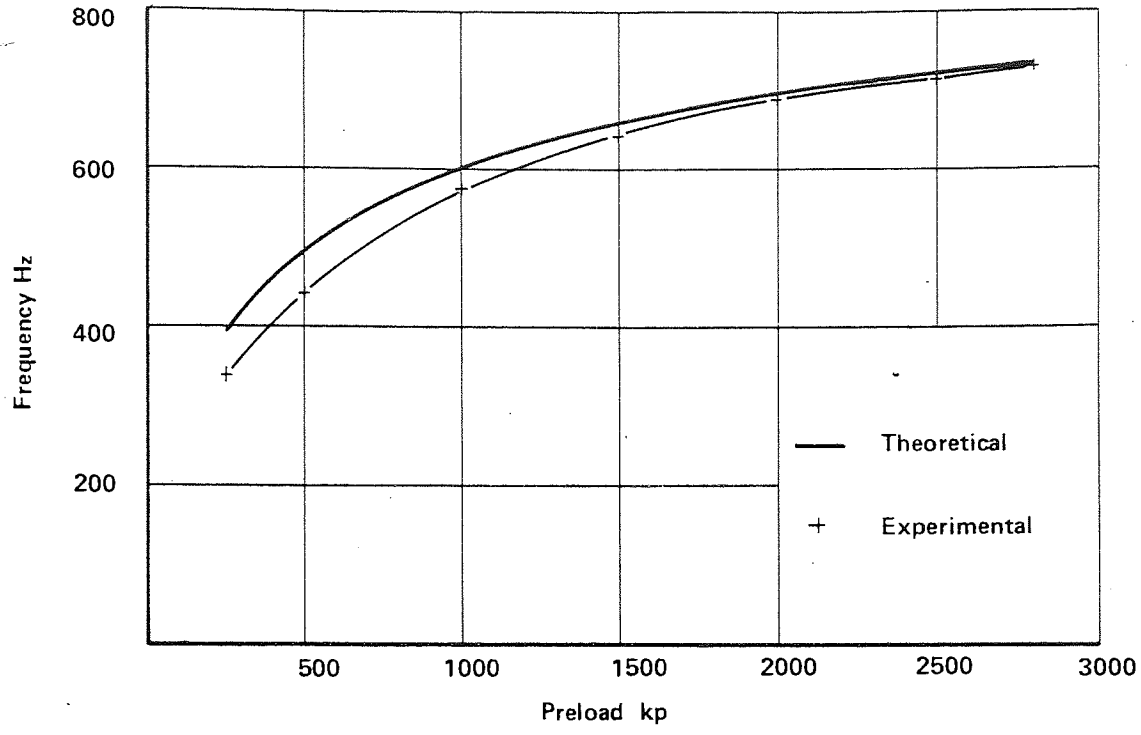

Fig. 127 Natural frequency of the test rig with ML1 jointed column

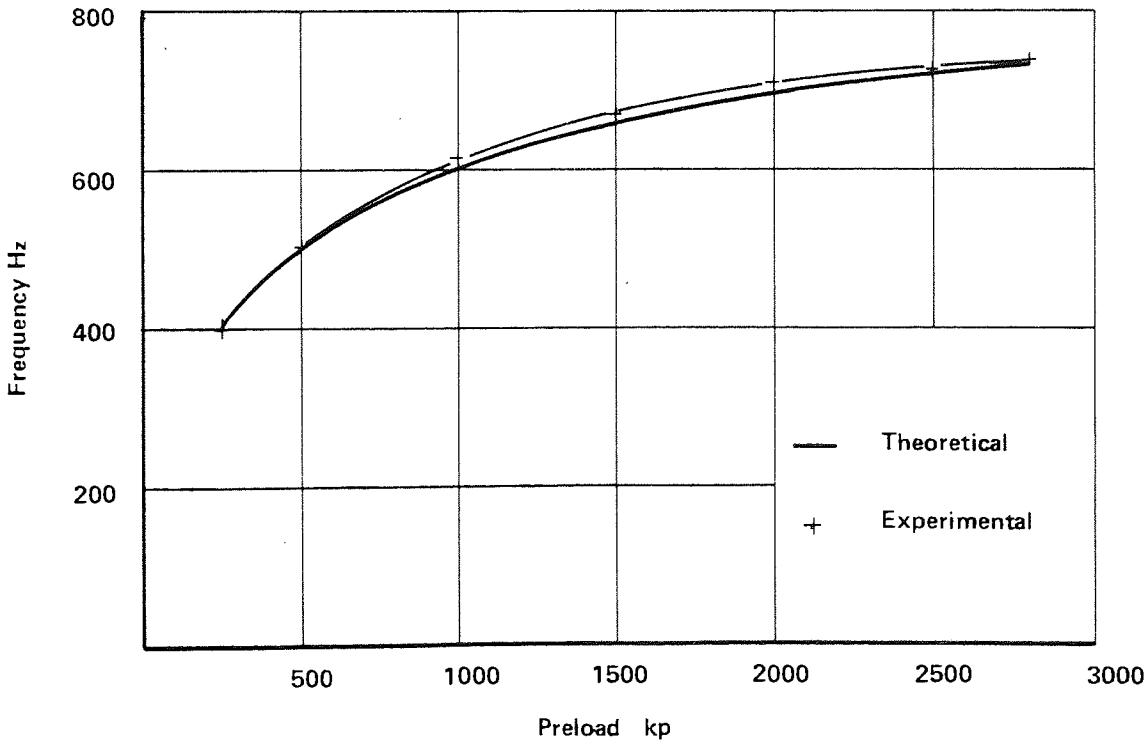

Fig. 128 Natural frequency of the test rig with ML2 jointed column

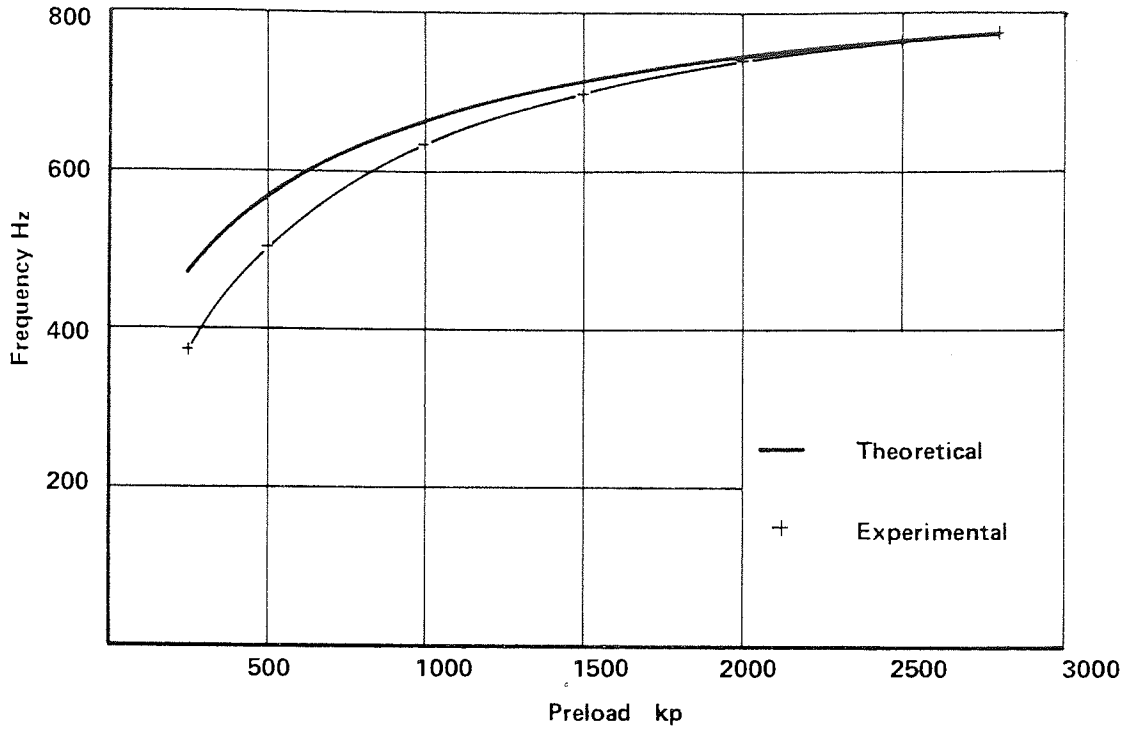

Fig. 129 Natural frequency of the test rig with ML3 jointed column

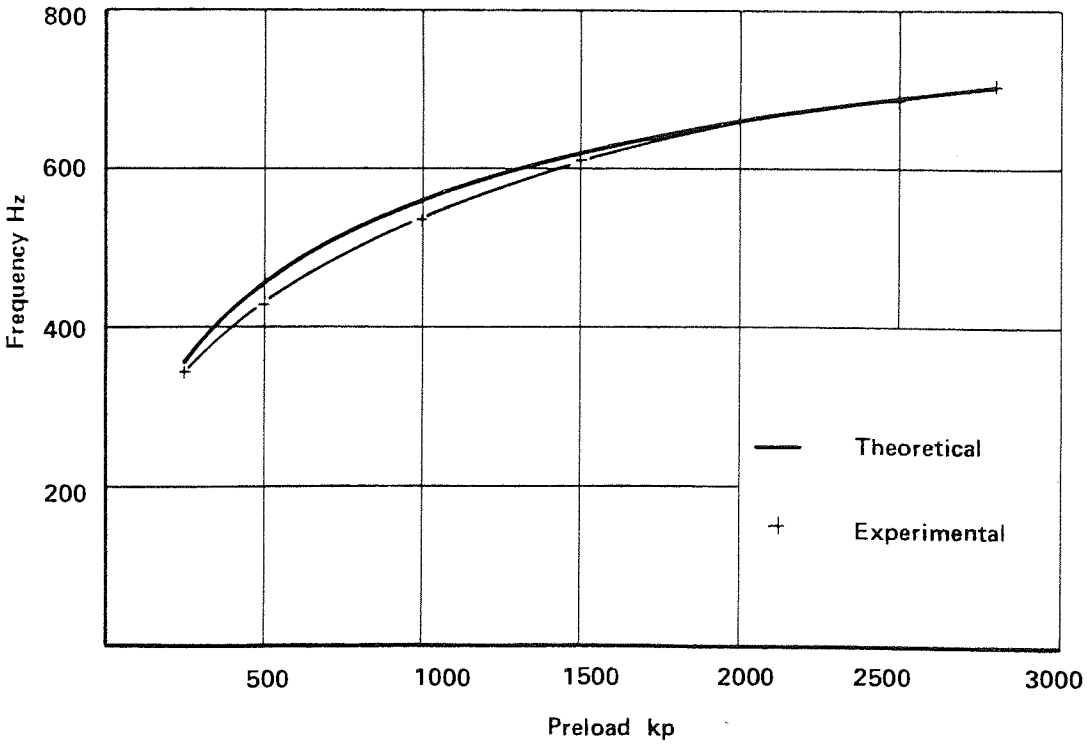

Fig. 130 Natural frequency of the test rig with ML4 jointed column

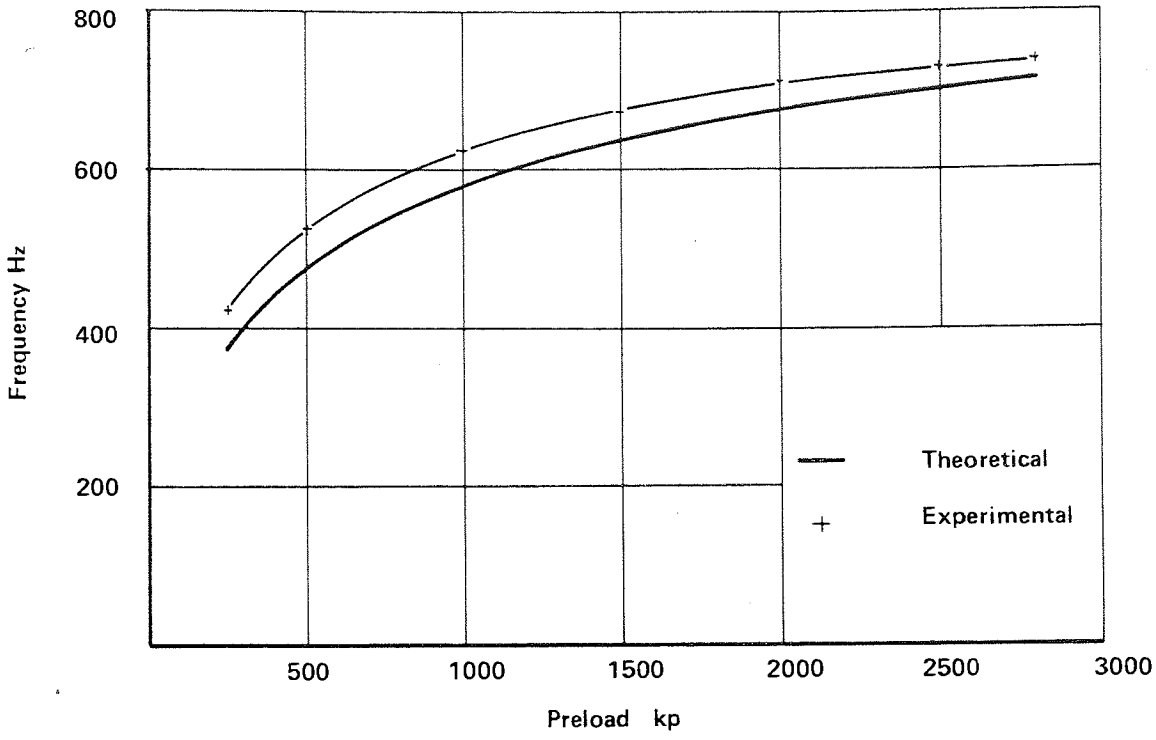

Fig. 131 Natural frequency of the test rig with SH1 jointed column

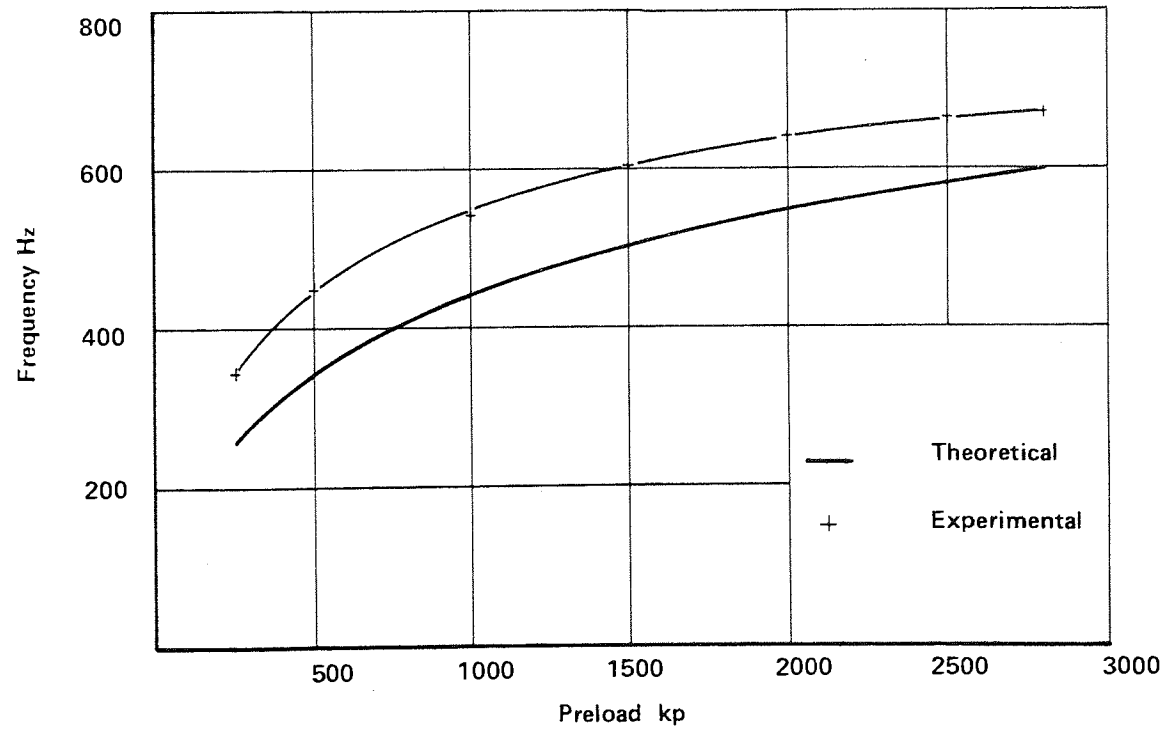

Fig. 132 Natural frequency of the test rig with SH2 jointed column

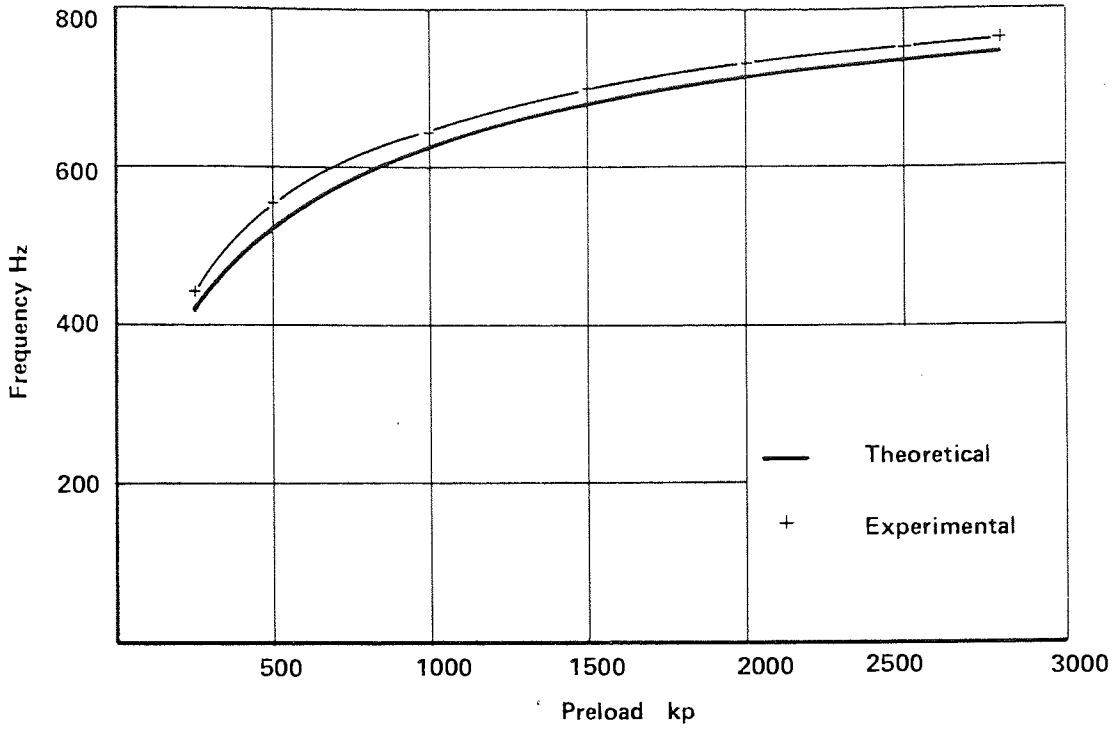

Fig. 133 Natural frequency of the test rig with SH3 jointed column

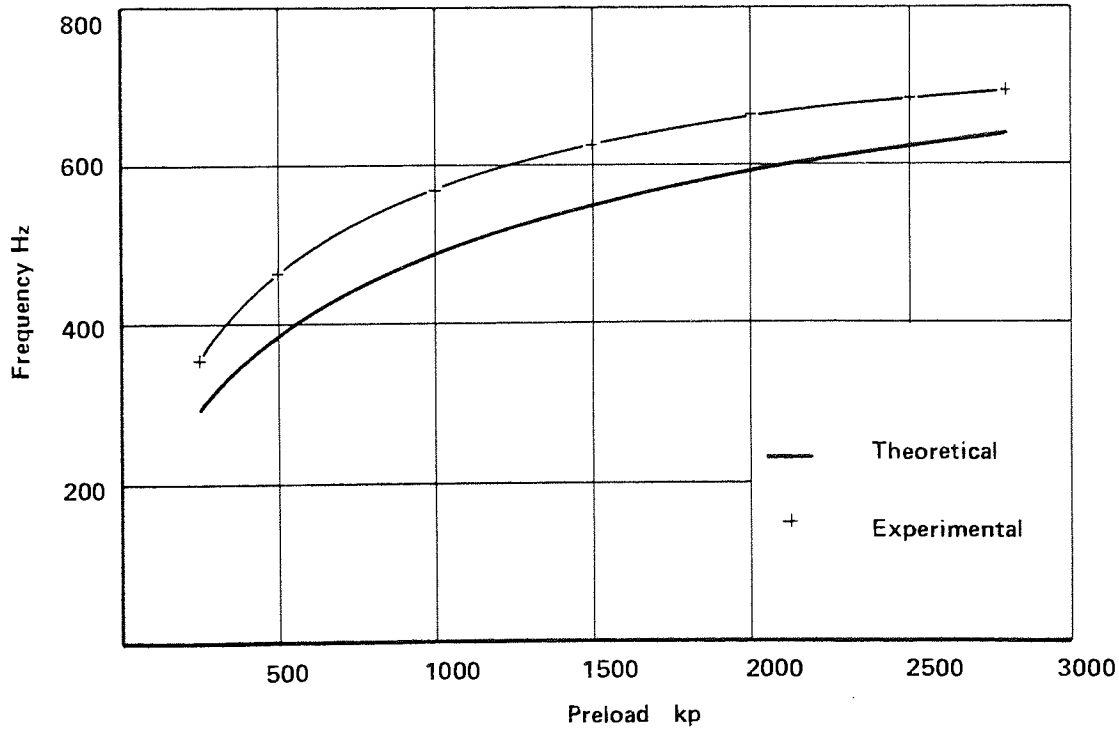

Fig. 134 Natural frequency of the test rig with SH4 jointed column

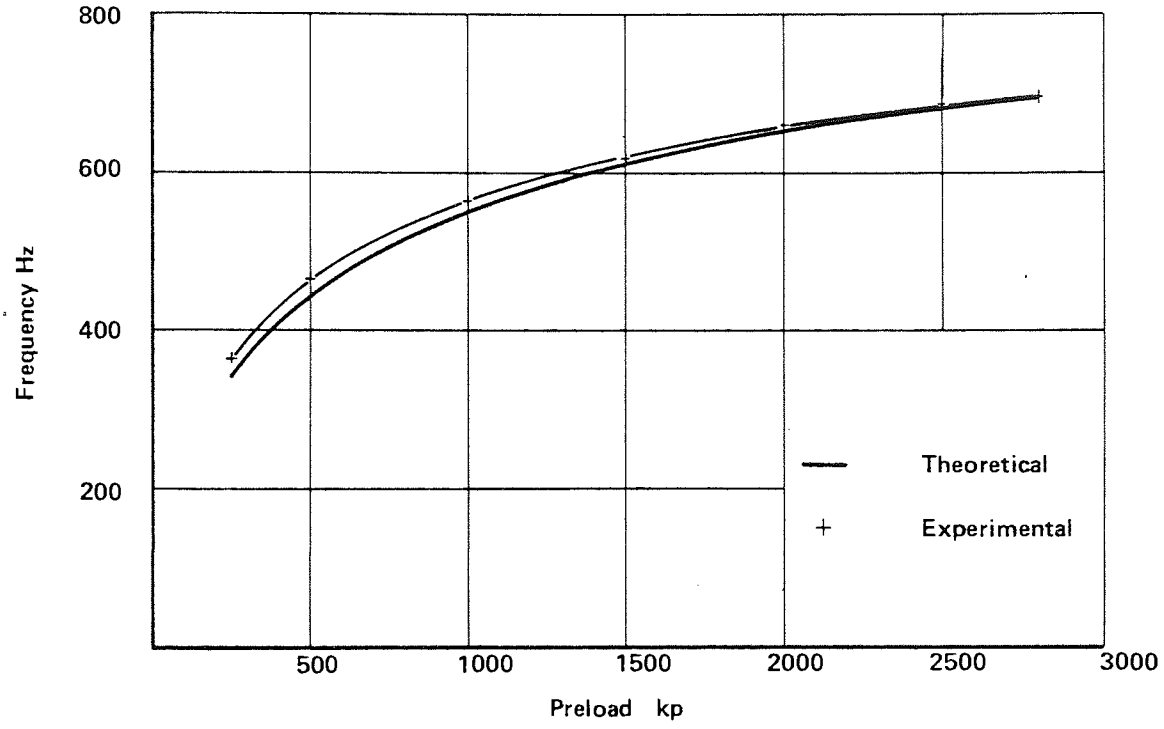

Fig. 135 Natural frequency of the test rig with SH5 jointed column

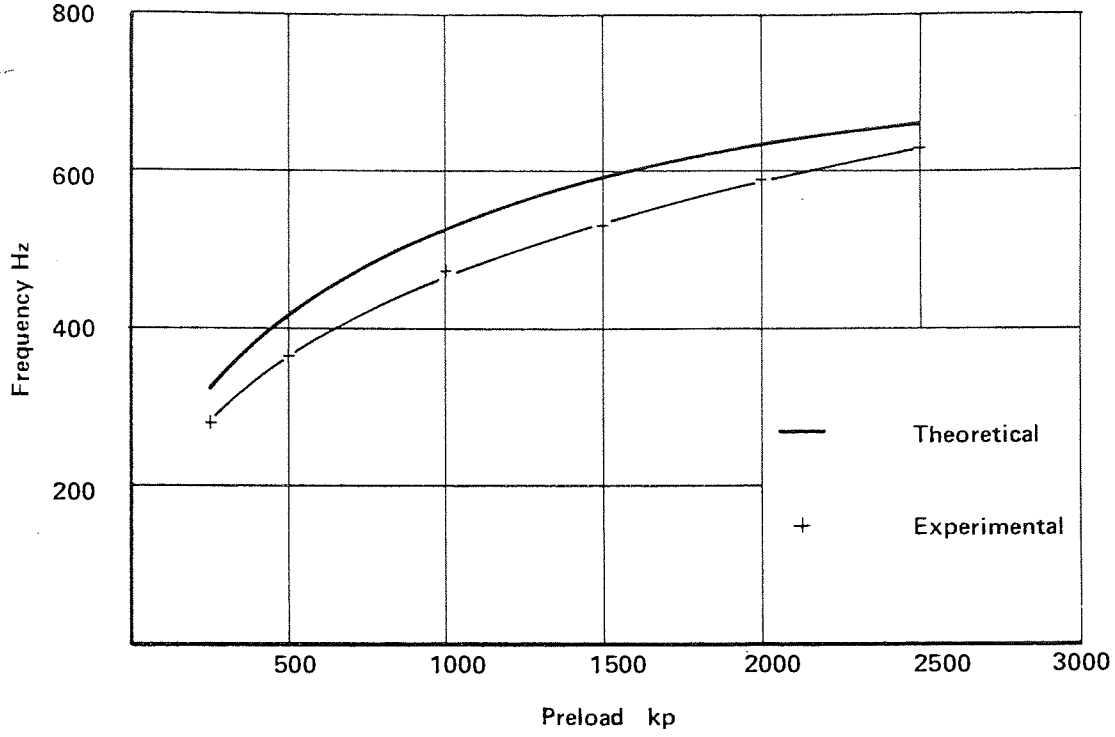

Fig. 136 Natural frequency of the test rig with TN1 jointed column

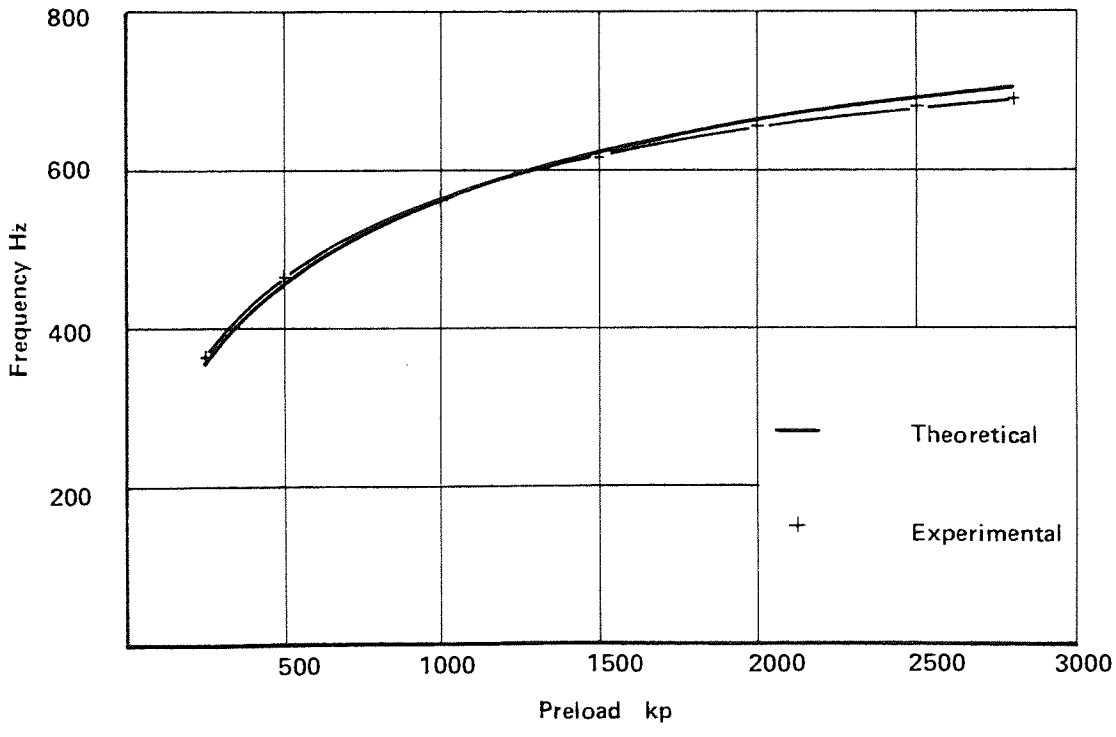

Fig. 137 Natural frequency of the test rig with TN2 jointed column

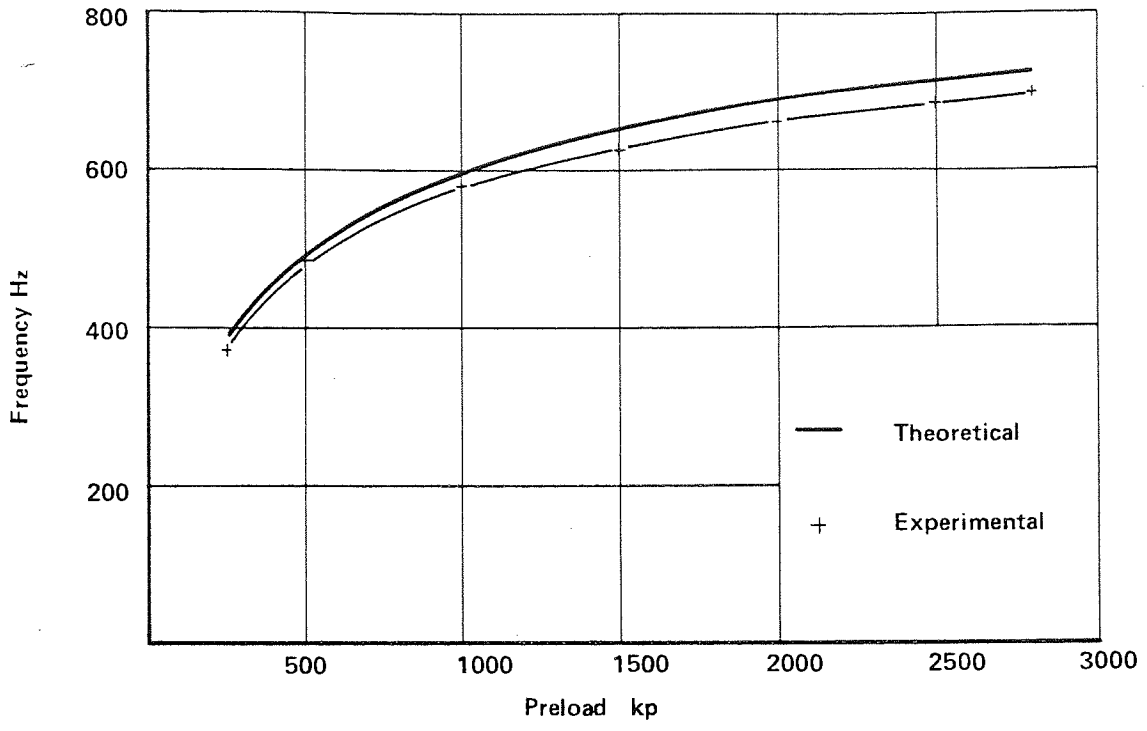

Fig. 138 Natural frequency of the test rig with TN3 jointed column

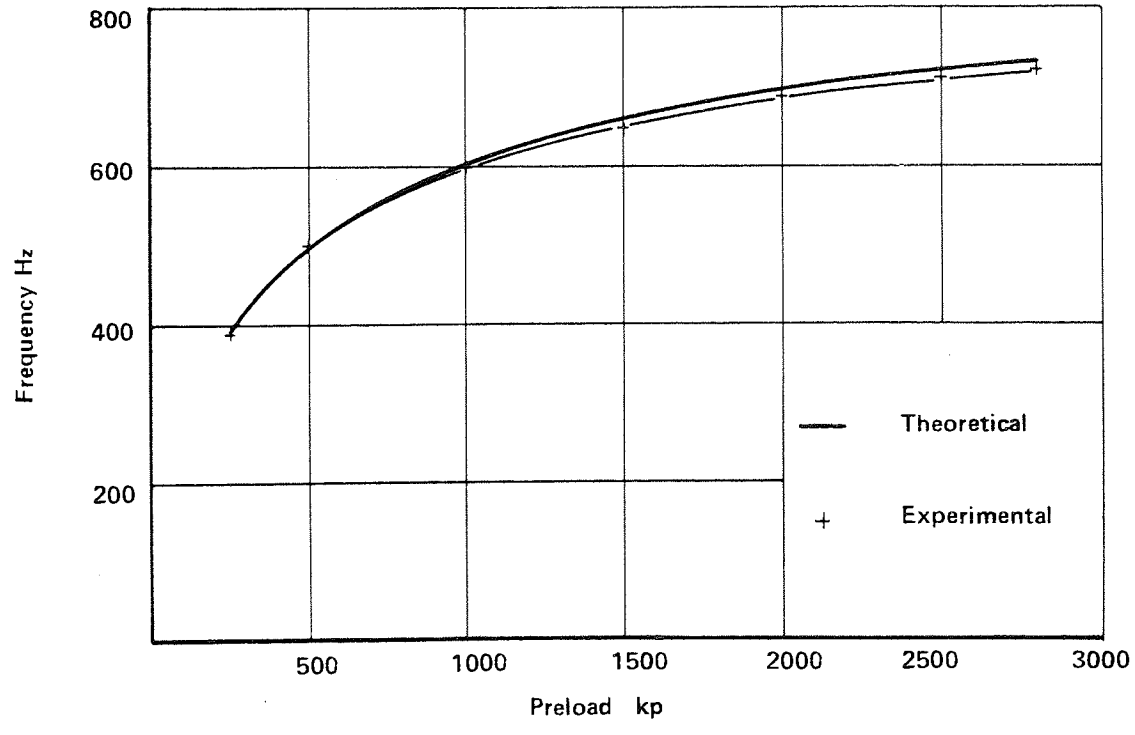

Fig. 139 Natural frequency of the test rig with TN4 jointed column

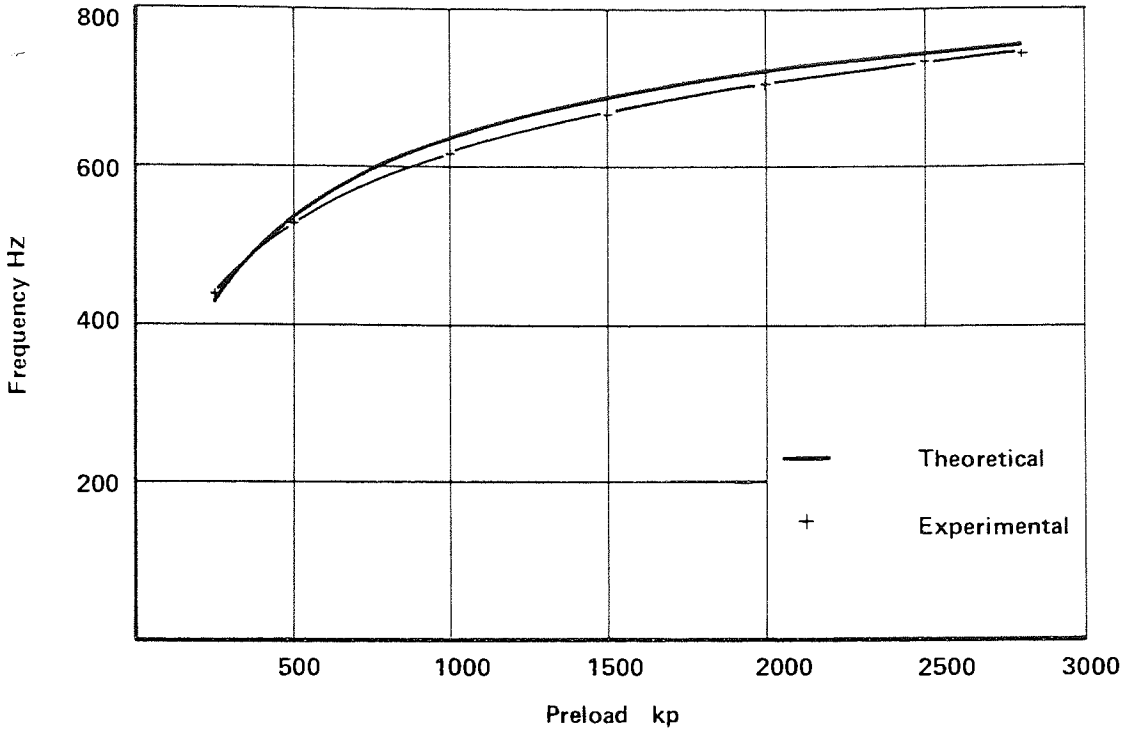

Fig. 140 Natural frequency of the test rig with GN1 jointed column

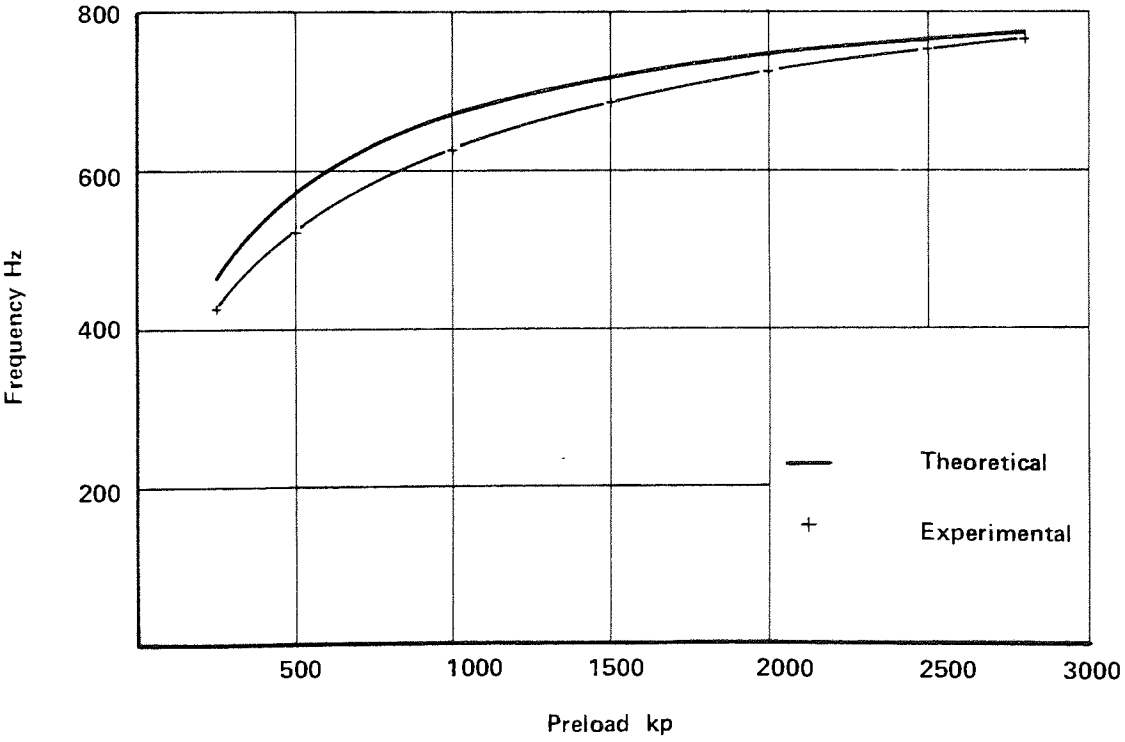

Fig. 141 Natural frequency of the test rig with GN2 jointed column

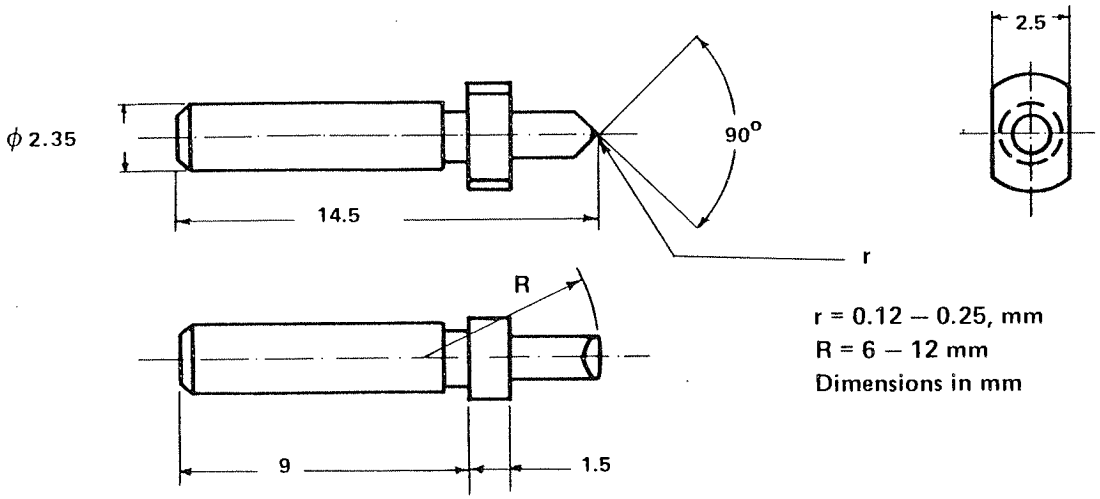

Fig. 142 Dimensions of the stylus used for the repeated measurements of waviness [93]

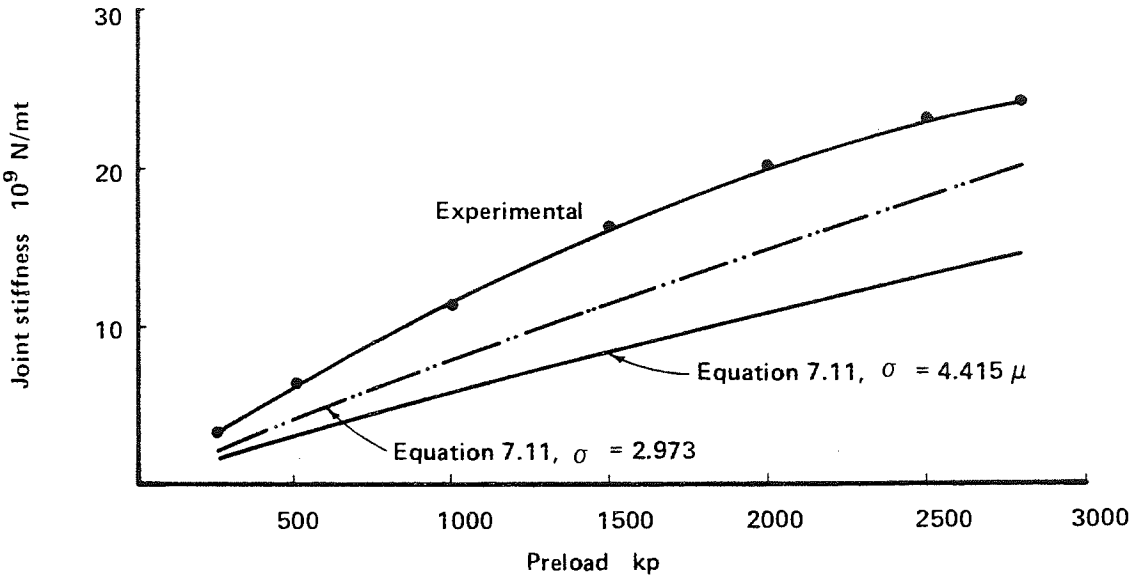

Fig. 143 Experimental and theoretical stiffness of SH2 joint after repeating the measurement of its flatness

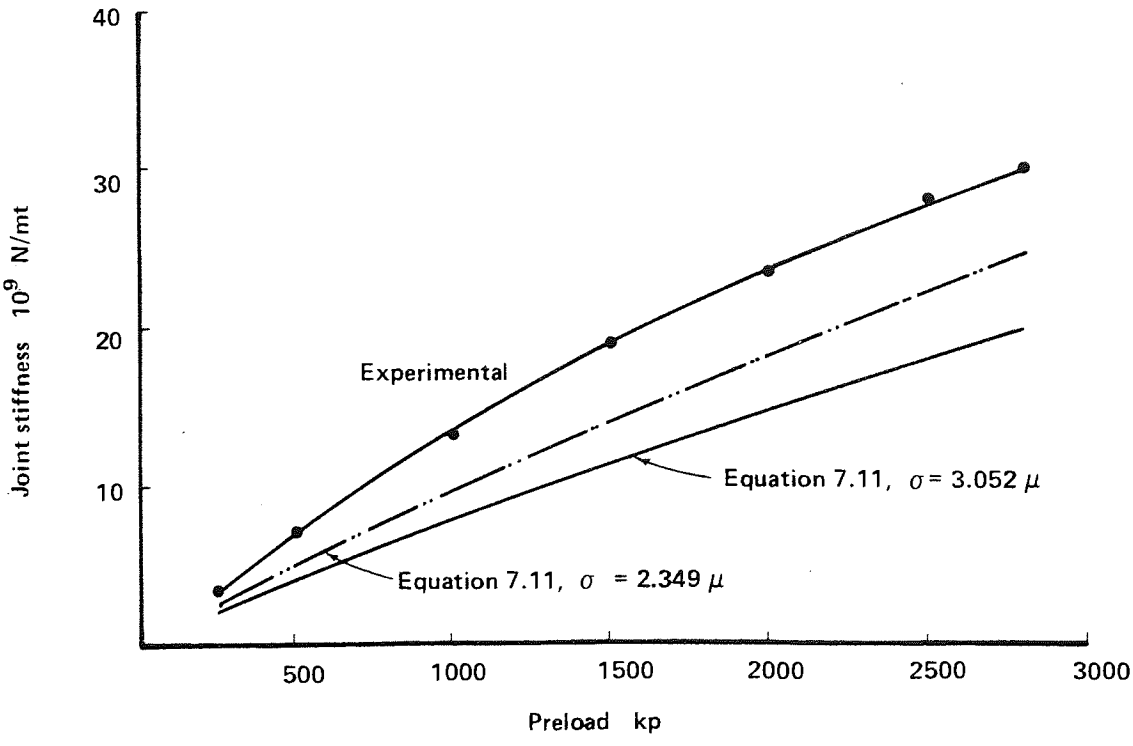

Fig. 144 Experimental and theoretical stiffness of SH4 joint after repeating the measurement of its flatness